Enhancement of Reinforced Soil Wall Performance under Dynamic Loading

Binod Shrestha

A thesis submitted in fulfilment
of the requirements for the degree of
Doctor of Philosophy

Faculty of Engineering and Information technology
University of Technology, Sydney

January 2013

Certificate of Authorship/Originality

I certify that the work in this thesis has not previously been submitted for a degree nor has it been submitted as part of requirements for a degree except as fully acknowledged within the text.

I also certify that the thesis has been written by me. Any help that I have received in my research work and the preparation of the thesis itself has been acknowledged. In addition, I certify that all information sources and literature used are indicated in the thesis.

Binod Shrestha

January 2013

Acknowledgements

First, I would like to sincerely thank my supervisor, Associate Professor Hadi Khabbaz for his guidance, support and friendship during my Ph.D. study. He advised me in various ways and inspired my future career development with suggestions for work-family balanced life. His encouragement and motivation have always inspired me.

I also owe special thanks to my co-supervisor, Dr. Behzad Fatahi, for his valuable guidance and contribution during this study.

I would also like to express my gratitude to Professor Bijan Samali and Associate Professor Jinachun Li for serving in my doctoral assessment and providing valuable suggestions on how to use the shake table facilities.

Staff members of the shake table facility, Peter Brown and Rami Haddad, as well as the soil laboratory technicians at UTS provided great support and assistance with the experimental part of this research. Their help is greatly appreciated. Administrative support from the staff of the School of Civil and Environmental Engineering and the University Graduate School at UTS is also deeply appreciated.

I am also grateful to my long term friend Rudra Pun, for his assistance during the research, particularly with constructing the model and conducting the shake table tests. I would also like to thank my close friends Behnam Fatahi and Ali Parsapajouh, for their help and support, and for making life more fun and easy.

I am grateful to the Australian Government, and the Department of Industry, Innovation, Science, Research and Tertiary Education (DIISRTE) for funding the

Australian Postgraduate Awards (APA), and am thankful to UTS for awarding me this reputable scholarship.

I am forever indebted to my parents for their understanding, and endless patience and support. I can imagine how happy and proud they are at this accomplishment. This work is a small dedication to them for their love, encouragement, and support. I would also like to thank my brothers, and relatives and friends for their moral support. Special thank goes to Muna, my wife and best friend, for her great love, kind patience and priceless company during every single step of our life. I am eternally indebted and grateful to her.

Finally, thanks are due to my son Binam and daughter Manvi, for their forbearance and affection during four years of my study at UTS.

Dedicated to my ancestors

Abstract

Reinforced soils have been widely used in a variety of applications because of their satisfactory performance and cost effectiveness. A number of investigations to determine the seismic deformation modes of reinforced soil walls with conventional horizontal inclusions have already been conducted, but only limited investigations with the partial inclusion of vertical elements have been conducted, and then they did not consider the performance of reinforced soil walls under dynamic loading.

This research presents a new concept of soil reinforcement using vertical fortification designed to connect layers of conventional horizontal reinforcement together. For this proposed system, as with conventional reinforced soil, the selected granular material is compacted over the horizontal reinforcement up to a given height, and then subsequent layers of horizontal reinforcement are laid down. Afterwards, reinforcements are inserted vertically or at an inclined angle, as per the design requirements. Each layer is then tied to another so that it acts as one integrated system, reducing the total force at the back of the facing panels.

This concept is modelled numerically using PLAXIS 2D version 9.0 using the Kobe earthquake loading. The convincing results from this numerical analysis encouraged me to conduct an experimental program that included shake table tests. The selections of materials were then tested to determine which materials were readily available on the market. Four reduced scale physical models, with and without vertical reinforcement, with angled reinforcement towards the facing and against the facing were tested on a shake table under stepped-up sinusoidal acceleration input. The results of the four models tested were then compared to evaluate the performance enhancement of a soil

wall with vertical reinforcement. The results showed that the wall with vertical reinforcement improved its performance under dynamic loading remarkably.

Finite element models based on the same parameters used in the shake table experiments and with a PLAXIS 2D program were developed, from which the numerical outcomes generated similar patterns of better performance when vertical fortification was included. Those results are matched against the experimental outcomes, and the results show a reasonable agreement between the measured and calculated displacements, backfill surface settlements and accelerations, albeit there were some discrepancies. These slight dissimilarities could be the result of implementing, to some extent, different physical properties in the numerical model and their variability within the measured data. An array of parametric studies with varying design parameters was also carried out, with the results indicating that the magnitude of dynamic response increases with a decreasing angle of friction and the extent of dynamic response decrease with an increasing Young's modulus. It is also found that the vertical reinforcement with very close spacing (less than three times the spacing of horizontal reinforcement), adds no extra benefit for the wall system.

According to the findings of this study, the proposed inclusion of vertical components to reinforced soil walls enhances the stability of the walls compare to the conventional reinforced soil systems under earthquake loading. The vertical components increase the integrity of the reinforced wall and create blocking actions, which reduce deformations at both facing wall and backfill surface. These outcomes point out the potential benefits of inserting vertical elements into a conventional soil reinforcement system under dynamic loads.

Contents

List of Figures

List of Tables

List of Symbols

1. Latin Notations

A	Area of the shear surface
A_{vr}	Area of the shear surface of vertical reinforcement
c	Cohesion
c_{inter}	Cohesion of the interface
c_{soil}	Cohesion of the surrounding soil
C	Damping matrix
D	Damping ratio
D_{max}	Maximum damping ratio
E	Young's modulus
F	Load vector
g	Gravity acceleration (9.8 m/s^2)
G	Shear modulus
G_{max}	Maximum shear modulus
h	Height of the specimen
H	Height of the wall
H_i	Height of vertical reinforcements at each layer
K	Stiffness matrix
K_{AE}	Total earth pressure coefficient
k_h	Horizontal seismic coefficient
k_v	Vertical seismic coefficient
L_a	Length of the anchorage
L_{vr}	Length of vertical reinforcement in anchorage zone
m	Shear distortion ratio
M	Mass matrix

M_D	Driving moment
M_R	Moment resistance due to the shear strength of the soil
N	Number of reinforcement layers
P_l	Horizontal force
P_{AE}	Total active earth force
$P_{AE\text{-}HOR}$	Horizontal component of total active thrust
$q_{u(R)}$	Total bearing capacity after the reinforcement
$q_{u(UR)}$	Bearing capacity of the unreinforced soil foundation
r	Radius of specimen
R_{inter}	Interface reduction factor
R_T	Tensile strength of the reinforcing materials per unit length
S	Shear force
S_Z	Spacing of reinforcements
T_i	Tensile force in the i^{th} layer of reinforcement
T_r	Tensile force
T_{vr}	Tensile strength of the vertical reinforcement
u	Depth of reinforcement location
u	Displacement vector
$\dot{u}$	Velocity
$\ddot{u}$	Acceleration
V_l	Vertical force
V_p	Compression wave velocity
W	Weight of the wedge
W_A	Weight of the static internal failure wedge

2. Greek Notations

β	Angle of the back slope
γ	Unit weight of the retained soil

γ_r	Reference strain
δ	Mobilised interface friction angle between the back of the facing wall and the backfill soil
ΔM_R	Increase in moment resistance due to the reinforcement
ΔP_{dyn}	Dynamic earth force
ΔT_{dyn}	Dynamic tensile reinforcement load increment
$\Delta T_{dyn\ i}$	Dynamic tensile reinforcement increment
ΔT_{vi}	Increased tensile force due to the vertical reinforcement
θ	Angle of inclination of the inside face of the wall to the vertical
λ	Inter-wedge shear mobilisation ratio
μ_v	Vertical reinforcing ratio
ν	Poisson's ratio
σ_1	Vertical stress
τ	Shear stress
τ_{max}	Maximum shear stress
ϕ	Friction angle of the retained soil
ϕ_f	Factored soil friction angle
ϕ_{inter}	Friction angle of the interface
ϕ_{soil}	Friction angle of the surrounding soil
ψ	Angle of seismic inertia
ψ	Dilatancy angle

Chapter 1

1. Introduction

1.1 General

Reinforced soil walls have been built over the past several decades. Their growing acceptance over its conventional counterparts is mainly due to its cost effectiveness, which includes low material cost, short construction period, and ease of construction. Moreover, its acceptance has also been triggered by a number of technical factors, including aesthetics, reliability, simple construction techniques, good seismic performance, and the ability to tolerate large deformation without structural distress. The construction of geosynthetic reinforced soil (GRS) walls in Australia started in the mid-eighties while the construction of GRS walls for roads and rails commenced in 1991 (Lo 2003). The key components of reinforced soil walls are shown in Figure 1.1. Case histories have indicated that properly built GRS walls performed better than traditional retaining walls during the previous large earthquakes (Hoe & Dov 2005). Indeed, the satisfactory seismic performances of GRS walls may have contributed to the conservatism implemented in the latest practical design and analysis of these structures.

The seismic responses can be examined by means of physical model tests or numerical modelling studies. Since it is uneconomical and impractical to examine the seismic response of a GRS wall via a series of full scale tests using different types of soils and reinforcements under various seismic loads, a much more cost effective and practical approach is to conduct a reduced scale test followed by numerical modelling where the

numerical tool must be validated based on physical model tests under controlled conditions.

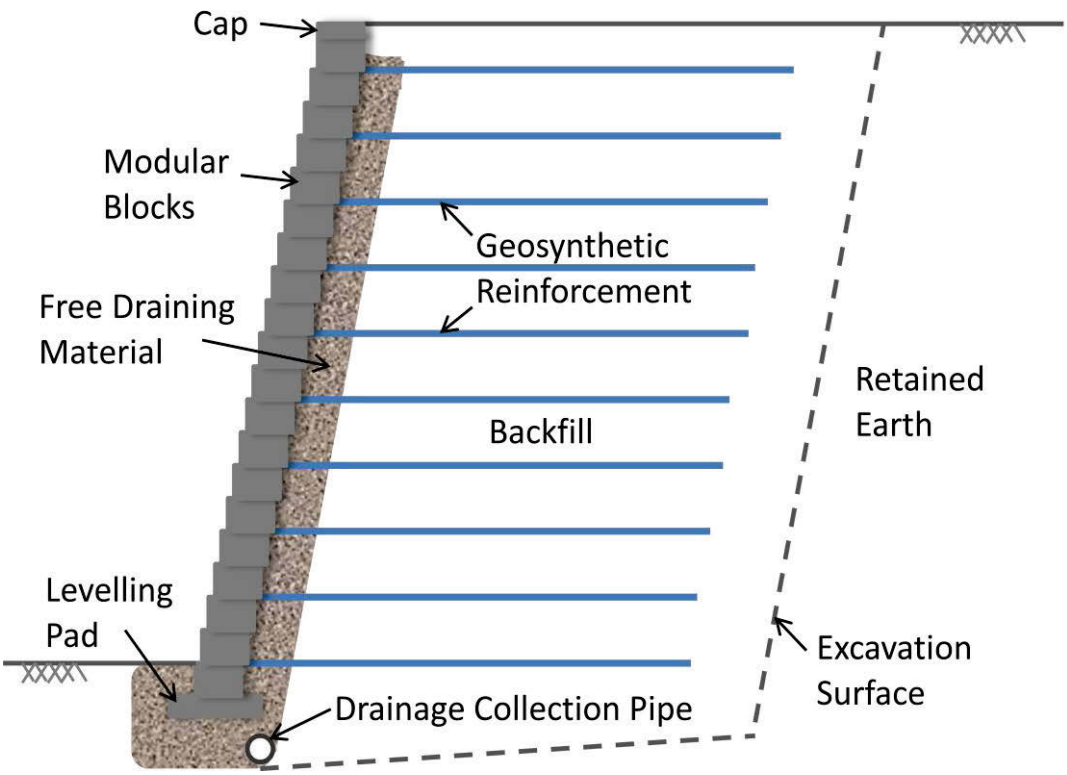

Figure 1.1 A schematic cross section of a GRS wall

The conventional methods of soil reinforcement consist of using continuous planar inclusions (e.g. metallic strips, geogrids, or geotextiles) within the earth structures. This research introduces a new method, called the inclusion of 'Vertical Reinforcement,' which is a composite material inserted into the soil between two consecutive layers of horizontal reinforcement. Since vertical reinforcement provides an isotropic increase in the strength of the soil composite without introducing continuous planes of weakness, vertical reinforcement is a novel technique for improving the strength of the soil over conventional reinforcement.

1.2 Scope and Objectives of the Study

Reinforced soils have been used in a wide variety and range of applications. Many studies, examining the reinforcement of soil, mainly focused on soils reinforced with conventional horizontal inclusions (Zhang et al. 2008), although some did investigate the strength of soil reinforced with multi-layer horizontal-vertical orthogonal elements (Zhang, Javadi & Min 2006; Zhang et al. 2008), and the pull out response for cellular reinforcement (Khedkar & Mandal 2009; Wesseloo, Visser & Rust 2009). A three dimensional cellular reinforcement can be used instead of horizontally placed reinforcement in conventional, two-dimensional reinforcement in reinforced retaining walls (Khedkar & Mandal 2009). Here the longitudinal members are connected perpendicular to the transverse members of equal height. The addition of reinforcement in the form of height over two dimensional reinforcements makes the cellular reinforcement stiffer and allows for the use of low modulus materials for manufacturing purposes. Zhang, Javadi & Min (2006) suggested using three dimensional reinforcing elements for reinforced soil applications. They demonstrated the adequacy and enhanced performance of three dimensional reinforcement over planar reinforcement based on an array of triaxial tests, but these studies on the partial inclusion of vertical elements did not consider the performance of reinforced soil walls under dynamic loading.

The study of GRS walls after the previous large earthquakes provided useful knowledge on the seismic performance, and analysis and design of GRS wall structures, and helped to identify deficiencies in current design practice and areas of future research. The recognised malfunctions of GRS walls confirm that there is an enormous scope for

improving existing technologies (Koseki et al. 2006), so this research fills the gap by enhancing the current seismic performance of reinforced soil.

This research presents a new system of soil reinforcement using vertical fortifications designed to connect layers of conventional horizontal reinforcement to each other. The primary difference between general practice and the insertion of vertical reinforcement is that the latter not only provides passive resistance against shearing, it also keeps all the layers intact, which increases the strength and stability of the reinforced soil. The idea of asserting the effect of vertical acceleration by strengthening the interaction between the soil and reinforcement, and installing vertical or inclined reinforcements are discoursed. Moreover, this study investigates the improvement in the behaviour of reinforced soil after the inclusion of vertical reinforcement and its constructive role, in order to address the possible modes of failure.

The main goal of this study is to investigate the enhanced performance of reinforced soil by inserting vertical fortification under dynamic loading. In addition to this, the specific objectives are:

1. Presenting the theoretical development of vertical reinforcement and potential construction techniques
2. Conducting comparative studies on factors affecting the performance of reinforced soil with and without the inclusion of vertical reinforcement
3. Carrying out an experimental program that includes shake table dynamic tests, and developing different types of models for evaluating the performance of walls after the insertion of vertical reinforcement.

4. Analysing the behaviour of the walls using finite element analysis to validate the numerical procedure
5. Conducting parametric studies of reinforced soil walls based on numerical analysis

1.3 Research Methodology

To achieve the research objectives, the following procedures were adopted:

1. Conducting an extensive literature review on the performance of GRS walls under seismic loads that comprises the case histories of post earthquake investigations, physical model tests, and numerical modelling of GRS walls to derive the tasks to be performed in this study
2. Development of the concept of vertical reinforcement based on soil mechanics theories and analysing potential field construction procedures.
3. Pre-verification of the concept of vertical reinforcement using the PLAXIS 2D version 9.0 program, before commencing extensive laboratory experiments to evaluate the enhancement of reinforced soil with vertical reinforcement.
4. Development of the methodology used for constructing physical models, materials selection, and the instrumentation and input parameters for the shake table experiments.
5. Carrying out shake table tests and analysing the results of four different models including, (i) a horizontally reinforced wall without vertical reinforcement, (ii) with vertical reinforcement, (iii) with reinforcement inclined towards the facing and (iv) with reinforcement inclined against the facing.

6. Analysing the behaviour of the wall with the finite element method using PLAXIS software to compare the results against measurements obtained from the experimental tests.
7. Conducting parametric studies by varying the essential design parameters such as the soil friction angle, the reinforcement spacing, and stiffness of the backfill soil.

1.4 Organisation of this Dissertation

This dissertation is organised into eight chapters, the highlights of which are as follows:

Chapter 1 - Introduction: This chapter gives a general background of reinforced soil walls, including the scope and objectives of the study, and the research methodology.

Chapter 2 - Literature review: This chapter contains critical reviews of past studies pertinent to the present research. The major focus of this chapter is to compile existing knowledge and findings in the area of reinforced soil walls and identify the gaps that must be bridged to achieve the objectives of the present study.

Chapter 3 - Theoretical consideration of vertical reinforcement: This chapter presents the theoretical development of vertical reinforcement inclusion into conventional horizontal reinforcement. It also summarises the current analytical approaches for seismic analysis and design, and discusses the possible improvement of reinforced soil walls over various failure modes.

Chapter 4 – Concept verification using numerical modelling: This chapter demonstrates the verification of the concept of vertical reinforcement using the PLAXIS 2D program under Kobe earthquake loading. The results of the numerical analysis indicate the possible performance of reinforced soil walls with vertical reinforcement.

Chapter 5 – Experimental program: This chapter describes the properties of all materials used in physical models, the test equipment and construction procedures of all four models, namely, without vertical reinforcement (Model 1), with vertical reinforcement (Model 2), with angled reinforcement towards the facing (Model 3), and with angled reinforcement against the facing, (Model 4). In addition, the similitude rule for a proper scale down of the model and base excitation acceleration are conferred in this chapter.

Chapter 6 – Test results and discussion: This chapter provides the results obtained from shake table experiments under stepped-up sinusoidal loading. Comparisons of these results are then carried out on the four models to evaluate the enhanced performance of reinforced soil walls after inserting vertical fortification.

Chapter 7 – Numerical verification and parametric studies: This chapter comprises the analysis of the behaviour of reinforced walls with the same parameters used in the shake table experiments, using the PLAXIS 2D program. The numerical outcomes are compared among the models and these results are then matched up with the experimental outcomes. The results of the parametric studies are also included in this chapter.

Chapter 8 - Conclusions and recommendations: This chapter provides the final conclusions from this study and some recommendations for future work.

Chapter 2

2. Performance of Reinforced Soil: A Literature Review

2.1 Introduction

This chapter provides a thorough and critical review of the performance of reinforced soil based on previously published studies. It incorporates many case histories of post earthquake investigations into the field performance of geosynthetic reinforced soil (GRS) retaining structures, physical model tests in the laboratory and the numerical modelling of GRS walls. This integration assesses the influential factors used to enhance the seismic performance of retaining walls. The research study of three dimensional reinforced soil and the advantage of GRS walls over conventional walls is also evaluated in detail. The outcomes of investigations conducted by other scholars and researchers on this topic have been used to refine the experimental and numerical tasks that will be performed in this study.

2.2 Performance of Reinforced Soil in Past Earthquakes: Case Histories

Studying the seismic performance of reinforced soil structures has, since the 1995 Kobe earthquake, attracted a great deal of attention, and more especially after the failure reported during the 1999 Ji-Ji earthquake in Taiwan. In recent years various research groups at academic institutions and government agencies have started research projects

on this issue, and seismic issues related to GRS walls have been addressed in many reports and keynote lectures at conferences on geosynthetics. For instance, the Kobe case histories have been described in detail by Tatsuoka, Koseki & Tateyama (1997, 1996), case histories from the 1994 Northridge earthquake, USA, were studied by White & Holtz (1997), Bathurst & Alfaro (1997) and Bathurst, Hatami & Alfaro (2002) provided an extensive review of the seismic design, analysis, and performance of GRS walls, Tatsuoka et al. (1998) investigated the stability of GRS walls against high seismic loads, Murata (2003) reported further progress on research and development in Japan related to GRS walls, and Koseki et al. (2006) reviewed the knowledge of the seismic performance, analysis and design of GRS wall structures and then pointed out the deficiencies in current design practice and areas for future research. Those case histories have helped to advance the state of the art in this field, while the documented failures of GRS wall showed plenty of room for improvement in existing technologies. Therefore, the lessons learned from past earthquakes, and knowledge about ongoing achievements in this field are summarised to identify the strengths and weaknesses of GRS walls under seismic loads, and uncover better design and construction solutions.

2.2.1 1994 Northridge earthquake

The performances of soil structures reinforced with geosynthetics were reported by Sandri (1997) through a survey of reinforced segmental (modular block) retaining walls in the Los Angeles area with heights greater than 4.5 m, area immediately after the Northridge earthquake. The 1994 Northridge earthquake had a local Richter magnitude of 6.7 with strong motion that lasted 10 to 15 seconds. Unlike most other earthquakes, the vertical acceleration of the Northridge earthquake was as strong as the horizontal acceleration, which is why this earthquake was so destructive. The survey showed no

evidence of visual damage to 9 out of 11 structures located within 23 to 113 km of the earthquake epicentre. Two structures (Valencia and Gould walls) showed tension cracks within and behind the reinforced soil mass that were clearly attributable to seismic loading. The photograph taken after 1994 Northridge earthquake showing cracks at the back of shortened lengths of reinforcement at the top of a Valencia wall is shown in Figure 2.1.

Figure 2.1 Valencia wall, USA (Bathurst & Cai 1995)

Bathurst & Cai (1995) analysed both structures and showed that the location of these cracks could be reasonably well predicted using conventional pseudo-static (Mononobe-Okabe) wedge analyses. A similar survey of three GRS walls by White & Holtz (1997) after the same earthquake revealed no visual indications of distress, and a survey by Stewart et al. (1994) highlighted that some cracks had developed in unreinforced crib

walls and unreinforced segmented walls. They concluded that concrete crib walls may not perform as well as more flexible GRS retaining wall systems under seismic loading.

2.2.2 1995 Hyogoken-Nanbu (Kobe) earthquake

The performances of reinforced soil structures subjected to the 1995 Hyogo-Ken Nanbu earthquake in Japan were reported by Tatsuoka, Koseki & Tateyama (1997, 1996). The 1995 Hyogo-Ken Nanbu earthquake had a Richter local magnitude of 7.2. Many retaining structures were located in the severely affected areas, where they were used to support the railway tracks.

Figure 2.2 Tanata GRS wall after 1995 Kobe earthquake (Tatsuoka, Tateyama & Koseki 1996)

A comparison between the gravity and cantilever reinforced concrete walls and soil walls reinforced with geosynthetics and full height rigid facing showed they performed well and suffered only slight damage (e.g. a limited amount of displacement). For

instance, according to the report by Tatsuoka, Tateyama & Koseki (1996), a GRS wall at Tanata with a full height rigid facing survived the 1995 Kobe earthquake, and only experienced some minor damage. A residual lateral displacement of about 200 mm was recorded at the top and 100 mm at the bottom, with respect to the adjacent box culvert, as shown in Figure 2.2.

2.2.3 1999 Chi-Chi earthquake

The devastating 1999 Chi-Chi earthquake in Taiwan had a magnitude of 7.3 on the Richter scale. The frequency of the shake ranged from 1.0 to 4.0 Hz and one of the recorded peak horizontal ground accelerations was as high as 1.0 g. Several GRS walls were damaged during the 1999 Chi-Chi earthquake (Huang 2000; Koseki & Hayano 2000; Ling & Leshchinsky 2003).

a) Photograph of the damaged structure

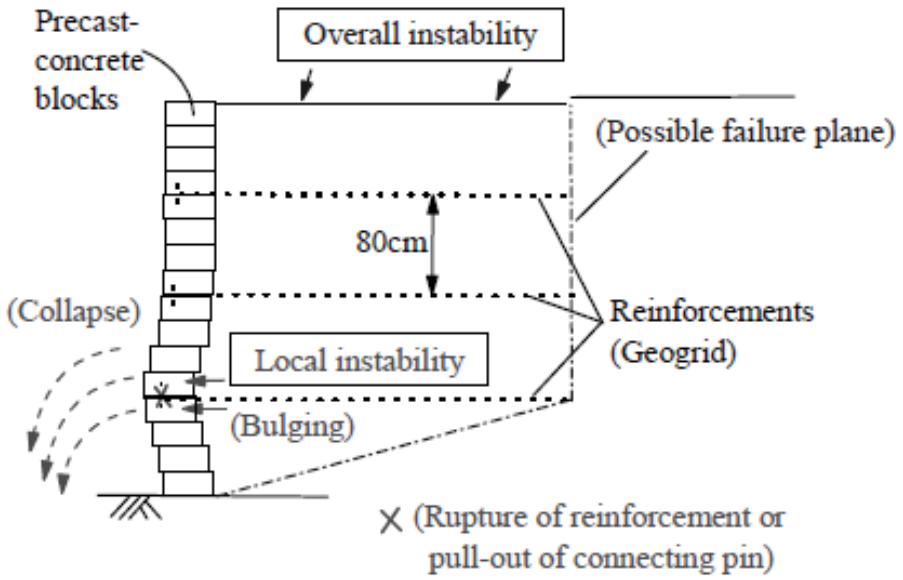

b) Cross section of the failed wall

Figure 2.3 An example of a failed segmented GRS wall after the 1999 Chi-Chi earthquake (Koseki & Hayano 2000)

An example of a segmented wall using concrete masonry blocks and poor quality backfill is illustrated in Figure 2.3. The vertical spacing may have been too large to prevent excessive deformation of the facing. In addition, there was evidence that the reinforcement ruptured at the connections and pulled out the connecting pins between the courses as the facing opened up (bulged) during failure. However, it is difficult to conclude that these post earthquake observations of the wall is evidence that the facing triggered the collapse or the facing failed as part of a larger kinematic mechanism. However, it was noted from a series of segmental GRS walls during the same earthquake that the magnitude of damage diminished as the spacing between the reinforcement decreased. In contrast to observations made during the Kobe earthquake, close to the collapsed wall, a reinforced concrete cantilever retaining wall was undamaged (Koseki et al. 2006).

2.2.4 2001 El Salvador earthquake

A magnitude 7.6 earthquake occurred on 13 January 2001, 60 km off the coast of El Salvador. A large number of retaining walls were damaged. At the time of the earthquake, there were 25,000 m^2 modular block (segmental) retaining walls in place (Race & Del Cid 2001). A survey of those structures provided an opportunity to identify why some structures behaved well and others did not. All the structures were constructed on hillsides to extend property fills. The walls were up to 8 m in height. Two walls that failed were examined in detail and revealed that the use of masonry privacy fences attached to the top of the walls were contributing factors in that they developed additional overturning loads at the top.

Figure 2.4 Wall failures in El Salvador due to 1.7 m high unreinforced section at top of wall added by the owner after original construction (Koseki et al. 2006)

A second major cause of failure was the extension of the top unreinforced (gravity) portion of the walls added by the owners after construction (Figure 2.4), or the cutting

of reinforcement behind the walls to install sub-surface utilities. According to site observations (Bathurst 1998), all the walls that were designed and built in compliance with the National Concrete Masonry Association (NCMA) seismic design guidelines survived the earthquake without any severe damage.

2.2.5 2004 Niigataken-Chuetsu earthquake

During the 2004 Niigataken-Chuetsu earthquake in Japan, many embankments for roads, railways, and hillside widening were damaged (JSCE 2006). Figure 2.5 shows another case history where a national highway and a railway embankment were severely damaged by the same slide during the Chuetsu earthquake. The highway embankment was repaired using a GRS wall with segmental facing panels (Figure 2.6).

Figure 2.5 Failure of highway and adjacent railway embankment resulting from 2004 Chuetsu earthquake (JSCE 2006)

Figure 2.6 Repair of highway embankment as a result of 2004 Chuetsu earthquake (JSCE 2006)

In this construction technique, the facing panels are not in contact with the reinforced soil backfill during fill placement because the backfill can be well compacted without disturbing the facing. The soil was contained by an internal wrapped face and a metal mesh form

2.2.6 2007 Niigataken-Chuetsu-Oki earthquake

Figure 2.7 shows damage to the retaining wall of a municipal road constructed on a slope, caused by the July 16, 2007 Niigataken-Chuetsu-Oki earthquake. By way of contrast, an RSW with segmental facing panels made of metal mesh located at the foot of the slope survived the earthquake, as shown in Figure 2.8.

Figure 2.7 Failure of RW for municipal road at Agewa caused by 2007 Niigataken-Chuetsu-Oki earthquake (Koseki 2012)

Figure 2.8 RSW with at Agewa with segmental facing panels made of metal mesh (Koseki 2012)

2.2.7 2008 Iwate-Miyagi-Nairiku earthquake

2008 Iwate- Miyagi-Nairiku earthquake had a Richter local magnitude of 7.2.

Figure 2.9 Failure of anchor tendons for cut-slope at construction site of Isawa dam caused by 2008 Iwate-Miyagi-Nairiku earthquake (Koseki 2012)

Figure 2.10 RSW with segmented facing panels made of metal mesh at construction site of Isawa dam (Koseki 2012)

Figure 2.9 shows an anchored cut-slope at a dam construction site. The anchors were 20 to 40 metres long and had been installed as a countermeasure against landslide movement. By the time of the June 14, 2008 Iwate- Miyagi-Nairiku earthquake, most of the tendons were broken at their free sections, and the upper parts of the broken tendons had been ejected. On the other hand, an RSW with segmental facing panels made of metal mesh located on the other side of the slope survived the earthquake undamaged, as shown in Figure 2.10.

2.3 Physical Model Tests

Physical model shake table tests were conducted to investigate the seismic performance of soil structures reinforced with geosynthetics. Both the reduced scale and full scale models seated on laboratory shake tables have been reported. Reduced scale model testing using shake tables is the most common approach used to gain qualitative and quantitative insights into the seismic behaviour of reinforced soil wall systems. In some instances shake tables mounted on a centrifuge have been used (Izawa, Kuwano & Takahashi 2002; 2004), and in very rare instances, full scale tests have been performed. One disadvantage of reduced scale tests is that the response of the model may be influenced by low confining pressure, far end boundary conditions of the shake table strong box, and improperly scaled mechanical properties of the reinforcement. Nevertheless, qualitative insights are possible using this experimental approach. Furthermore, the models can be used to develop and validate numerical codes that can be used in lieu of investigating the wall at a prototype scale. A review of shake table tests reported in the literature prior to 2002 was reported by Bathurst et al. (2002). Table 2.1 summarises the main aspects of the past and recent shake table laboratory model tests.

Table 2.1 Summary of shake table model tests

Reference	Height	Facing type	Reinforcement	Reinf. length	Reinf. spacing	Backfill	Input base motion	Critical acceleration	Failure mode
	mm			mm	mm			(g)	
Sabernahani et al. (2009)	1000	Wrapped-around wall facing	Knitted textile; non-woven textile; geogrid	500; 700; 900	100; 200	SP (D_{10} = 0.16 mm; D_r = 47% &84%)	Sinusoidal horizontal (0.6, 1.5, 2.4,, and 3.34 Hz)	Not reported	Bulging ad overturning
Krishna and Latha (2007); Latha and Krishna (2008)	600	Wrap-faced; rigid-faced	Woven polypropylene (PP) geotextile	420	150; 200; 300	Poorly graded sand (D_r = 37 to 87%)	Sinusoidal horizontal (1 to 3 Hz)	Not reported	Not reported
Ling et al. (2005)	2800	Concrete blocks (12° batter)	Polyster (PET) and polyvinyl alcohol (PVA) geogrids	2050; 1680 mix with 2520	600; 400	Tsujuba sand (D_r = 52-56%)	Irregular vertical and horizontal	Not reported	Not failed
Lo Grasso et al. (2005)	350	Aluminum L-shaped section with slope = 70°	Bi-axial polypropylene (PP) geogrid	350	Varied from 25 to 50	Dry silica sand (D_r = 70%)	Sinusoidal (4, 5 & 7 Hz) and irregular horizontal	Not reported	Two-wedge
Perez and Holtz (2004)	1219	Wrapped faced at slope = 63°	Pellon nonwoven fabric	Varied from 305 to 610	Varied from 61 to 203	Silica sand (D_r = 91%)	Sinusoidal horizontal (5 Hz)	Varied from 0.15 to 0.29	Two-wedge
Safronie et al. (2001)	900	Rigid facing	High density polyethylene 9HDPE) geogrid	360; 540	150	Leighton Buzzard sand	Sinusoidal horizontal and irregular horizontal	Not reported	Tilting of facing

Table 2.1 Cont'd.

Reference	Height	Facing type	Reinforcement	Reinf. length	Reinf. spacing	Backfill	Input base motion	Critical acceleration	Failure mode
	mm			mm	mm			(g)	
Matsuo et al. (1998)	Varied from 1000 to 1400	Varied from discrete panel to continuous panel	Geogrid reinforcement (Tult = 19.4 kN/m)	Varied from 400 to 700	200	Air-dried Toyoura sand	Sinusoidal horizontal (5 Hz); irregular horizontal	Varied from 0.38 to 0.59	Two-wedge
Ramakrishnan et al. (1998)	900	Wrapped faced; segmental block	Woven polypropylene (PP) geotextile	500	150	Dry silica sand	Sinusoidal horizontal (3 Hz)	0.25; 0.45	Not reported
Sakaguchi (1996)	1500	Cement coated foam bloack	Geogrid	Not reported	300	Standard laboratory silica sand No. 4	Sinusoidal horizontal (4 Hz)	0.33	Not reported
Sugimoto et al. (1994)	700 - 1050	Wrapped faced at slopes varied from 24° to 79°	Tensar SS-1	Not reported	Not reported	Niigata sand	Sinusoidal horizontal	Not reported	Excessive crest settlement
Murata et al. (1994)	2480	Full-height igid facing	Geogrid reinforcement (Tult = 19.4 kN/m)	1000	150	Inagi sand	Sinusoidal horizontal (3.4 Hz); irregular horizontal	Stable at 0.51 g	Not reported

Table 2.1 Cont'd.

Reference	Height	Facing type	Reinforcement	Reinf. length	Reinf. spacing	Backfill	Input base motion	Critical acceleration	Failure mode
	mm			mm	mm			(g)	
Wolfe et al. (1978)	600	Discrete panel	Mylar tape strips; fiberglass screen strips	Varied from 305 to 762	38	Uniform fine dry quartz sand	Sinusoidal horizontal & vertical; irregular horizontal & vertical	Not reported	Not reported
Richardon and Lee (1975)	300; 380	25 mm curved aluminum sheet; 38 mm flat aluminum sheet	3.8 mm wide aluminum foil strips; 6 mm wide mylar tape strips	Varied from 76 to 150	38	Sand	Sinusoidal horizontal (11.6 Hz)	Not reported	Not reported

2.3.1 GRS walls with full-height rigid facing

In order to investigate the reasons for the relatively satisfactory performance reported for GRS walls with full height rigid facings during the 1995 Kobe earthquake, a series of 1g model shake table tests were carried out by Watanabe et al. (2003). The model walls were about 500 mm high with a level backfill. They were seated on a horizontal soil foundation and uniformly surcharge loaded of 1 kPa. The foundation and backfill were modelled by very dense dry sand layers. The models were subjected to several sequential base excitation records by scaling the Kobe earthquake in 0.1g increments (see also Koseki et al. 2003).

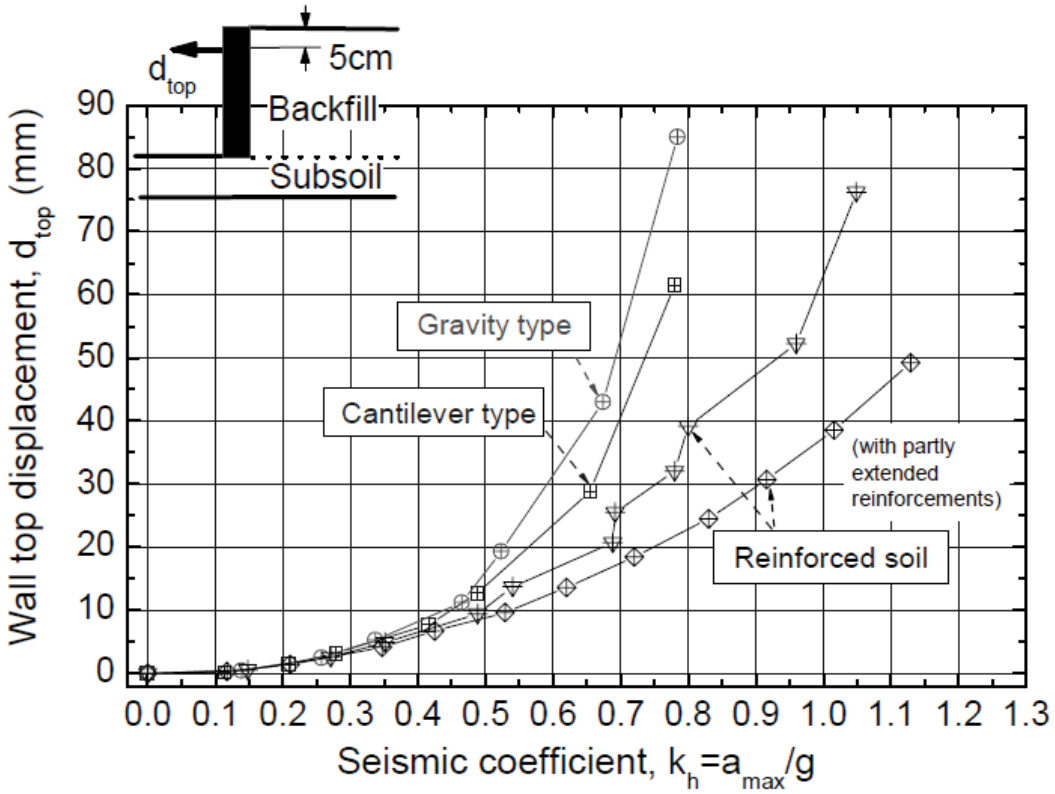

Figure 2.11 Permanent displacements at top of wall versus peak horizontal ground acceleration coefficient (Watanabe et al. 2003)

Figure 2.11 shows the cumulative permanent horizontal displacements near the top of each GRS model and a conventional type of wall. There was no significant difference

up to a seismic coefficient value of about 0.5, but under higher seismic loads the residual wall displacements of conventional retaining walls accumulated rapidly, whereas the GRS structures exhibited more ductile behaviour; particularly the wall with extended layers of reinforcement.

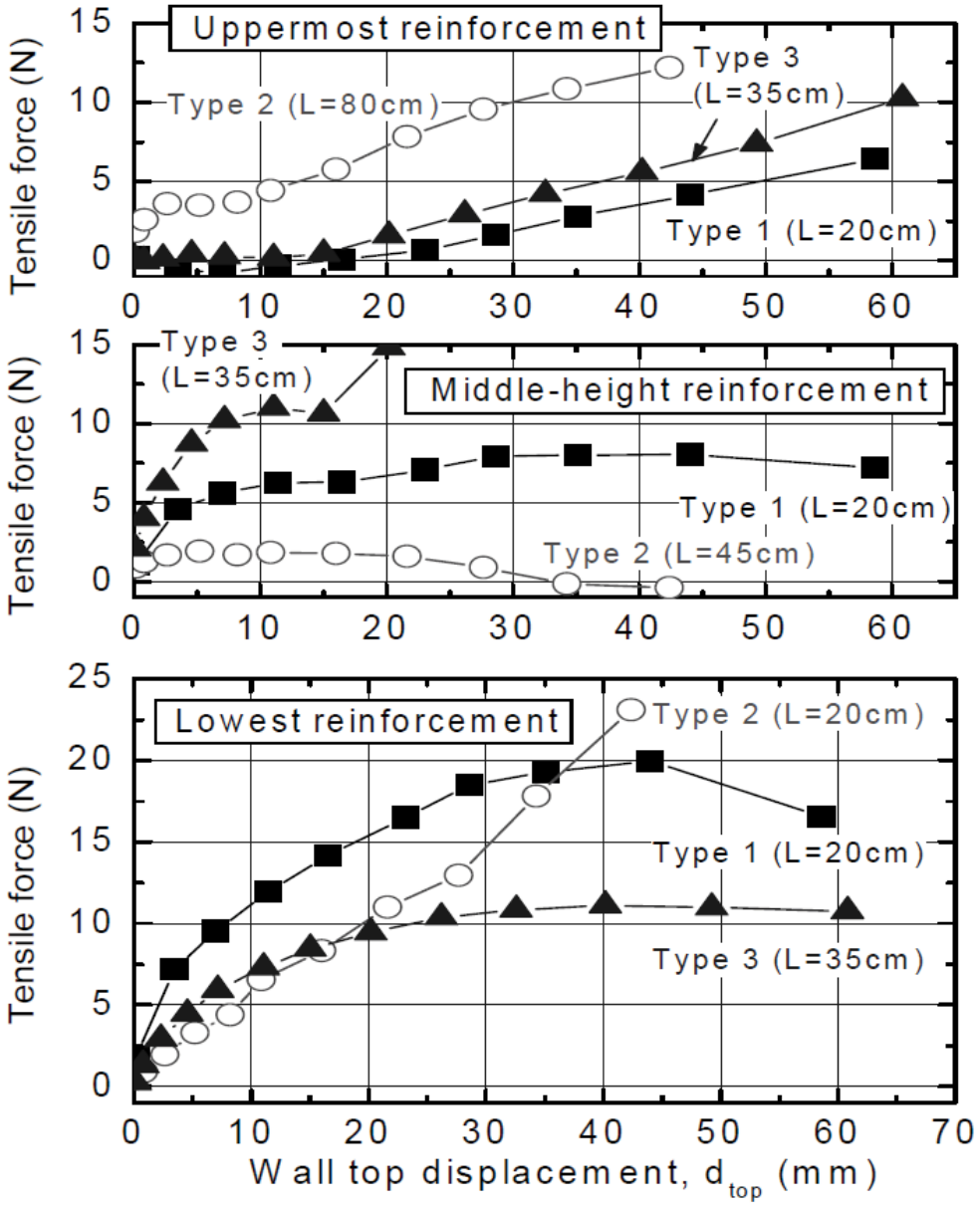

Figure 2.12 Reinforcement loads during base shake of GRS wall structures (Watanabe et al. 2003)

Figure 2.12 shows the accumulation of tensile loads in layers of reinforcement at three different heights. The acceptable performance of GRS walls was related to the

stabilising influence of layers of reinforcement on the wall facing deformation. For example, the largest tensile load was generated in the uppermost extended layer of reinforcement of the Type 2 wall, which increased its resistance to the facing overturning. This highlights the observation by others that the distribution of reinforcement loads may be higher at the top of the wall under earthquake loading, which is opposite to the trend typically assumed for walls under static loading conditions.

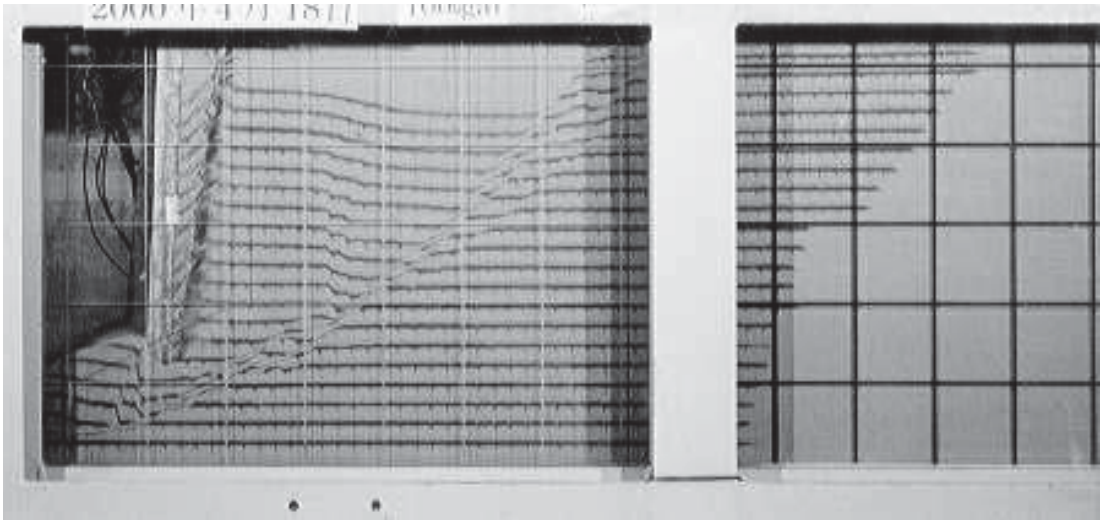

Figure 2.13 Development of a global instability mechanism during shaking of a GRS model wall (Kato et al. 2002)

Figure 2.13 shows a global failure mechanism developed behind and below a GRS model wall constructed with a sloped toe. This highlights the influence of the foundation and toe conditions on the ultimate failure mechanism in these structures, and can result in a failure pattern that was not predicted by conventional limited equilibrium models that assume horizontal sliding at the base of a reinforced soil mass. The histories of the sum of the reinforcement loads generated in identical walls, one constructed with a slope at the toe and the other with a level foundation, are plotted in Figure 2.14. The data shows that reinforcement loads peaked and then softened as deformation in the

wall accumulated in the structure with a slope, while the structure with a level foundation accumulated a reinforcement load monotonically with increasing wall deformation.

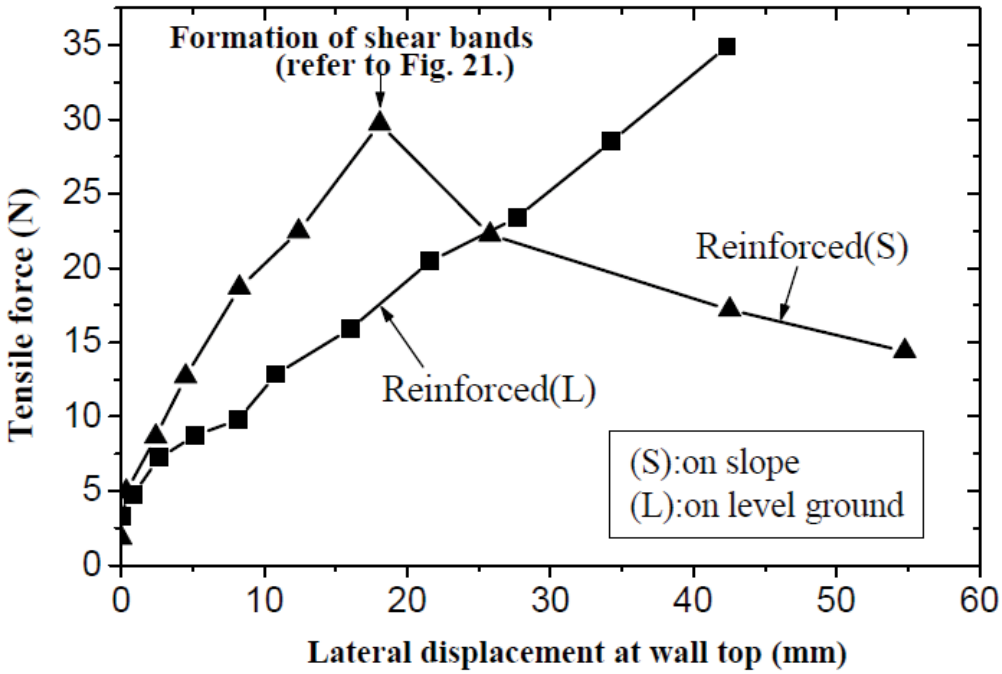

Figure 2.14 Sum of tensile loads in reinforcement layers for GRS walls with a sloped foundation toe (S) and level ground (L) (Kato et al. 2002)

El-Emam and Bathurst (2004, 2005) investigated the influence of a toe constraint using a series of 1 m high shake table tests constructed with a rigid facing panel (Figure 2.15a). The horizontally restrained toe in the reduced scale models attracted approximately 40% to 60% of the total peak horizontal earth load during base excitation, showing that under simulated earthquake loading, a stiff facing column plays an important role in resisting dynamic forces. The inability of current design methodologies to account for the portion of lateral earth force resisted by the restrained toe at the base of a structural facing column leads to an under estimation of wall's load capacity.

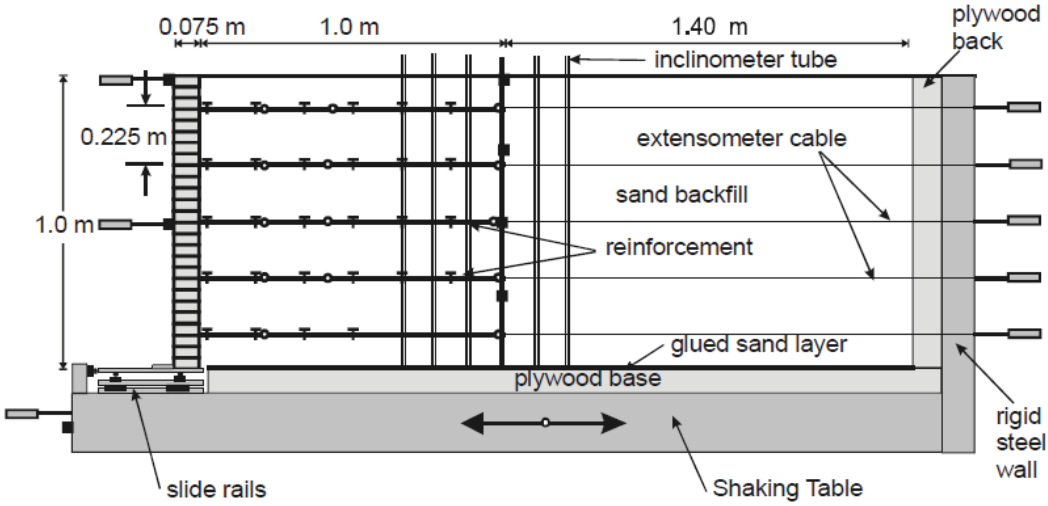

(a) Shake table model

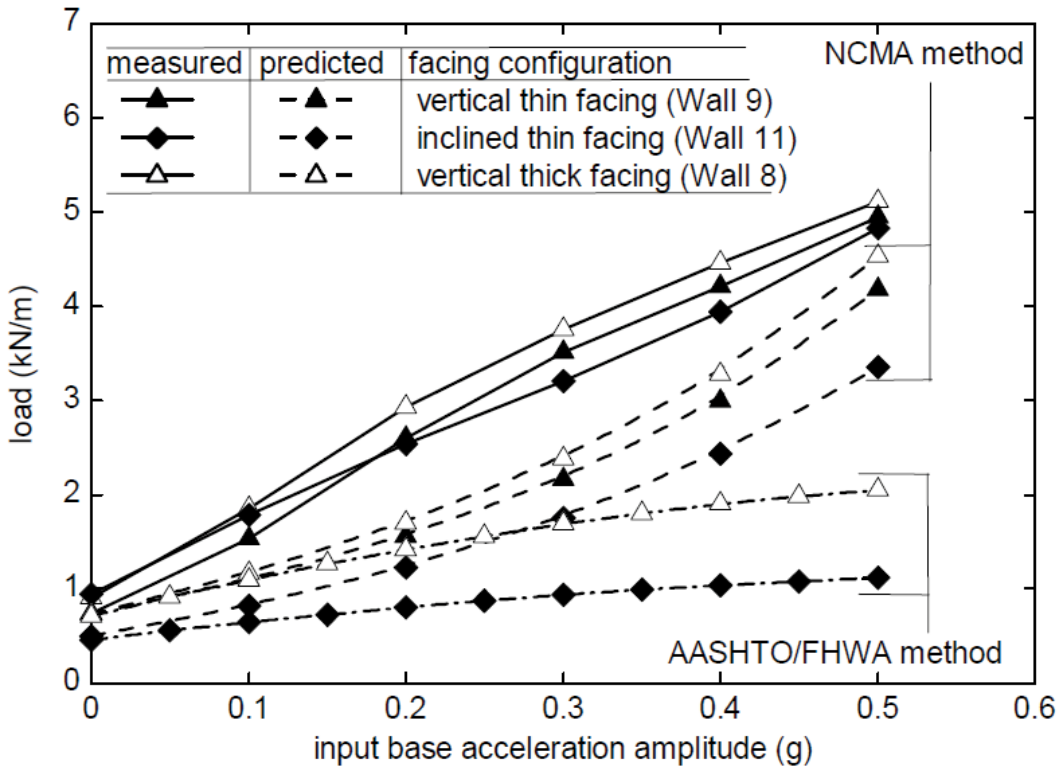

(b) Computed and measured horizontal loads in layers of reinforcement versus the level of peak base excitation acceleration

Figure 2.15 Reduced scale models of rigid panel walls with a hinged toe (El-Emam & Bathurst 2005)

They also recorded that a vertical force developed at the base of the model walls during base shake and showed that down drag forces developed at the connections which resulted in vertical toe loads that were significantly higher than the self weight of the facing panel. Limit equilibrium based methods of design were shown to consistently under estimate the total load carried by the reinforcement and horizontal toe in their models, which is not conservative for design (Figure 2.15b), although the pseudo-static NCMA method (Bathurst 1998) proved to be less conservative than the AASHTO (2002) method.

2.3.2 GRS walls with segmented facing

Bathurst et al. (2002) reported the results of a series of shake table tests that examined the seismic resistance of 1 m high models of walls reinforced with vertical and inclined facings constructed with segmented blocks, vertical incremental panels, and rigid full height panels. The tests focused on the influence of the interface shear properties on the stability of the facing column (Figure 2.16). The influence of the shear capacity of the interface and facing batter can be seen in Figure 2.17. The vertical wall (Test 4) with a fixed construction interface (equivalent to a rigid panel wall) required the greatest input acceleration to generate large displacements during staged shaking.

The vertical wall with no shear connections between the layers of segmented blocks performed worst (Test 1), although its resistance to displacement improved greatly for the weakest interface condition by simply increasing the wall batter to 8 degrees from the vertical (Test 3). The vertical wall with an incremental panel facing (i.e. the segmented layers were rigidly connected between the layers of geosynthetics) (Test 2) gave a displacement response that fell between the results of walls 1 and 4.

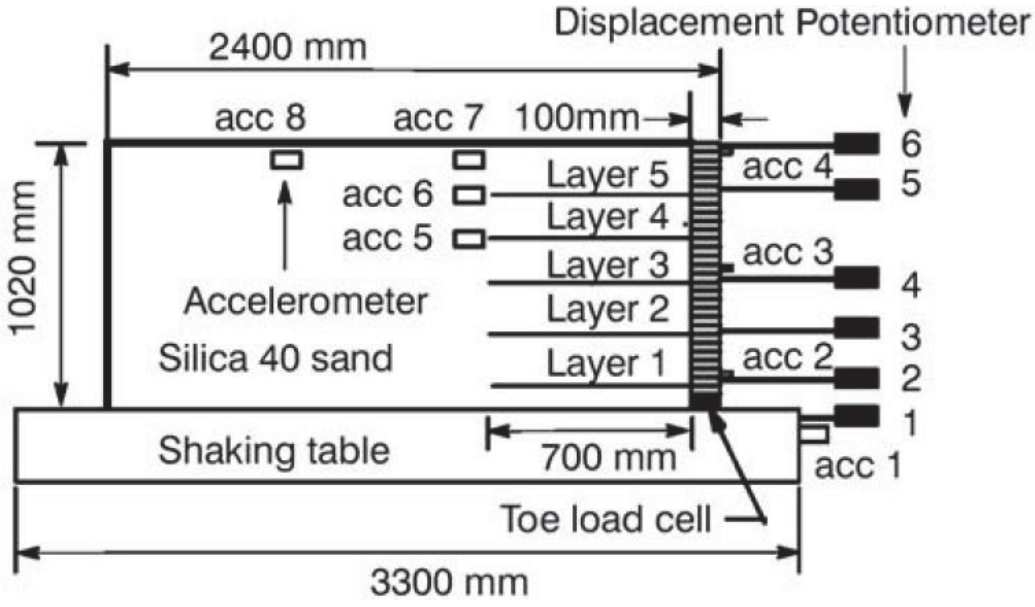

Figure 2.16 Shake table test arrangement for 1 m high GRS model wall (Bathurst, Hatami & Alfaro 2002)

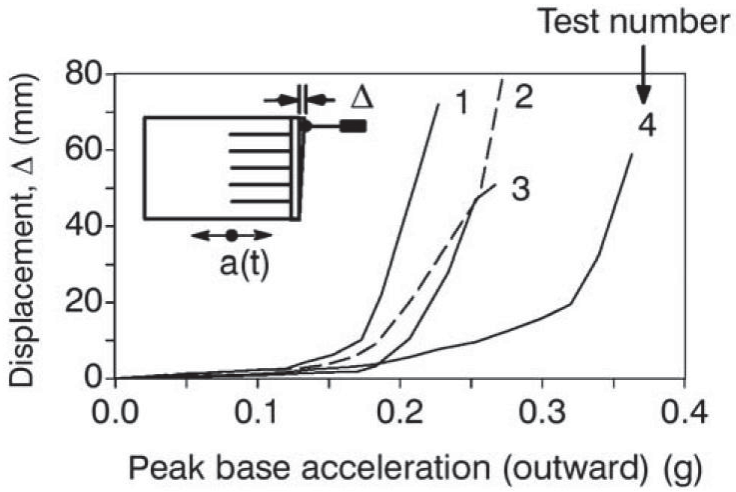

Figure 2.17 Wall displacements versus peak base acceleration for model walls with different facing types (Bathurst, Hatami & Alfaro 2002)

Ling et al. (2005) reported the only experimental program to date in which full scale model (2.8 m high) shake table tests were carried out on GRS segmental retaining walls (Figure 2.18). The walls were subjected to both vertical and horizontal components of the Kobe earthquake acceleration. The test walls showed maximum deformations at the crest that were very small at a scaled peak horizontal acceleration of 0.4g. The walls

showed less than 100 mm of maximum deformation under a more severe acceleration scaled to 0.86g. The tests showed that increasing the length of the reinforcement at the crest of the wall and reducing the space between the reinforcement improved the seismic response of the structures.

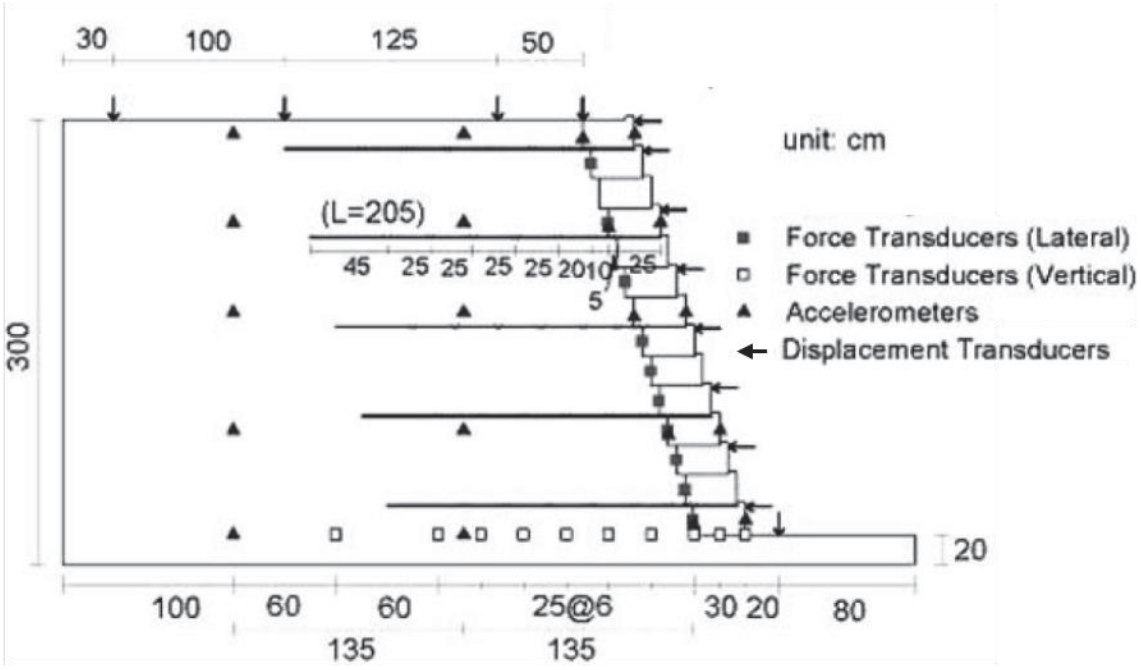

Figure 2.18 Full scale shake table test of segmented retaining wall (Ling et al. 2005)

Krishna & Latha (2007) conducted shake table tests on a wrap face of 0.6 m high GRS walls to understand the influence of the relative density of the backfill soil on the seismic response of reinforced soil wall models (Figure 2.19). The response of reinforced soil wall models constructed at different relative density backfill and subjected to base excitation, was compared in terms of the lateral displacement of the facing, and acceleration of the lateral earth pressures on the facing. Wrap and rigid faced model reinforced soil retaining walls 750 × 500 mm in plan and 600 mm deep were constructed and tested under a sinusoidal motion using a uni-axial shake table. The typical rigid faced configuration of the wall, and the instrumentation, is as shown in Figure 2.20.

Figure 2.19 Laminar box mounted on a shake table (Krishna & Latha 2007)

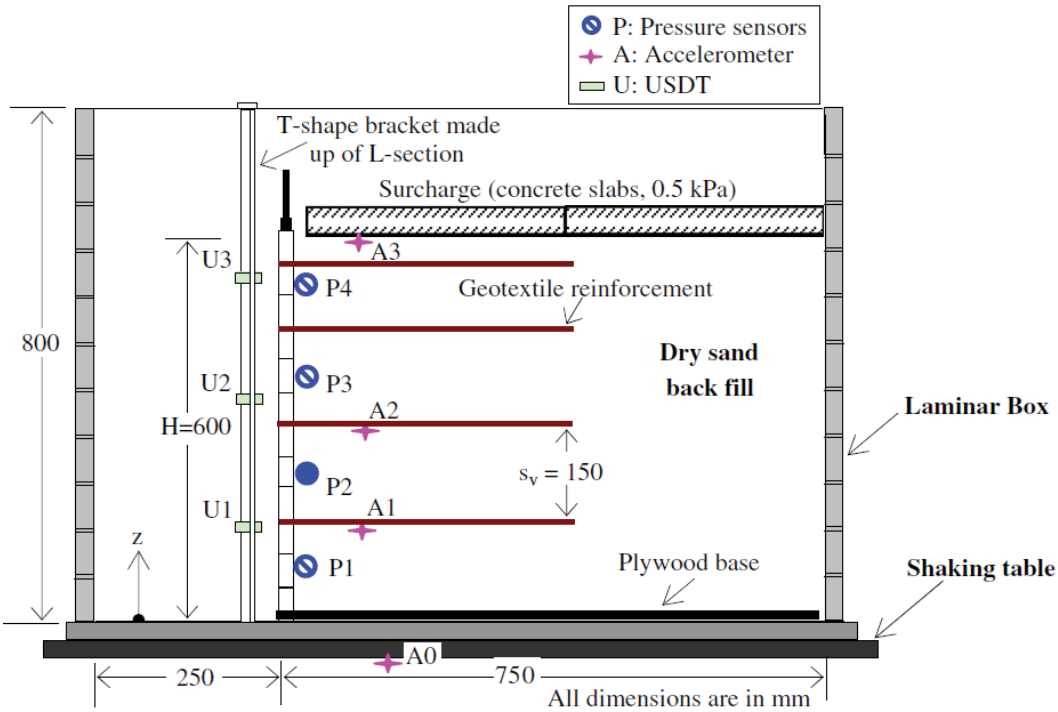

Figure 2.20 A schematic diagram of a typical rigid-faced wall configuration and instrumentation (Krishna & Latha 2007)

It was observed from these tests that the effect of the backfill density on the seismic performance of reinforced retaining walls was pronounced only at very low relative density and at a higher base excitation. The walls constructed with higher relative density backfill showed less face deformation and more amplified acceleration when tested at higher base excitation, than the walls constructed at lower densities. The response of wrap and rigid faced retaining walls was not affected very much by the relative density of the backfill when tested at lower base excitation. Displacement in the wrap faced walls was many times higher than the rigid faced walls.

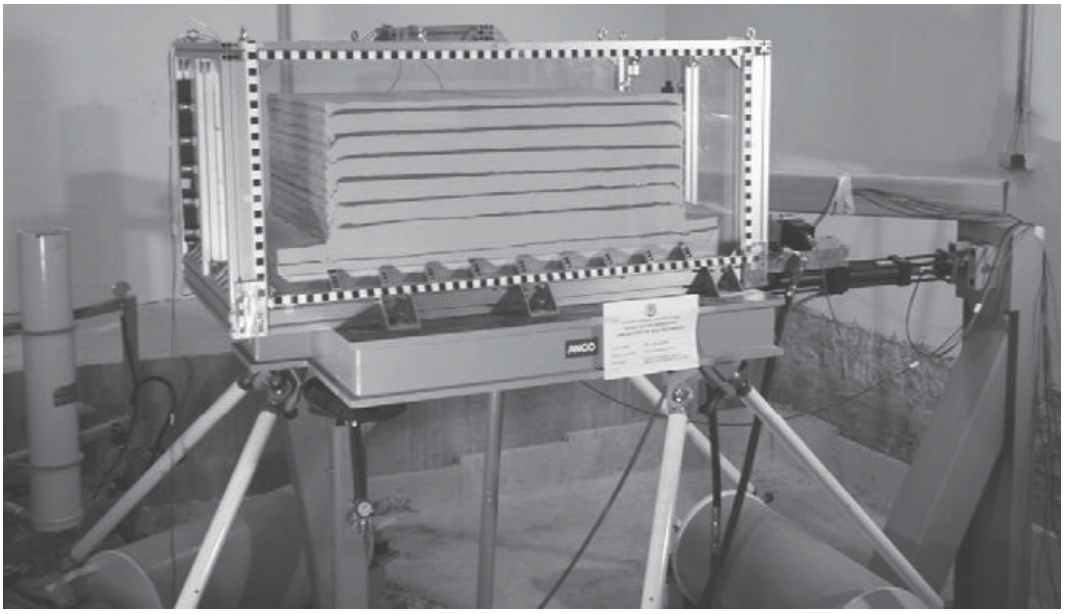

Figure 2.21 Reinforced earth retaining wall models (Model-1) inside the rigid sandbox, installed on the NTUA shake table (Anastasopoulos et al. 2010).

Anastasopoulos et al. (2010) investigated the seismic performance of a typical bar mat retaining wall 7.5 m high, positioned back to back, and with 21.4 m distance supporting a dry granular backfill. The performance of the bar mat reinforced soil walls was found to be totally acceptable for realistic levels of seismic excitation. The model retaining walls were placed inside a rigid 1.6 × 0.9 × 0.75 m (length × width × height) sand boxes, which consisted of an aluminium space frame, covered with 16mm thick

plexiglass panels to allow observation of the deformed specimen as shown in Figure 2.21.

The latter consisted of an aluminium space frame (ASF) covered with 15 mm thick plexiglass panels to allow the deformed specimen to be observed. It was concluded that the seismic performance of the bar mat reinforced soil walls was quite acceptable for realistic levels of seismic excitation.

2.3.3 Other new applications

Kato et al. (2002) reported the beneficial effects of installing soil nails below the base of the facing in order to improve the seismic performance of GRS walls constructed on slopes. This technique resulted in a potential failure mechanism that allowed a larger tensile load to be carried by the layers of reinforcement (Figure 2.22). It should be noted that in the case without nails, the tensile load was reduced after a global failure mechanism had been formed. Reinforcement load softening was prevented by using soil nails below the base of the wall facing.

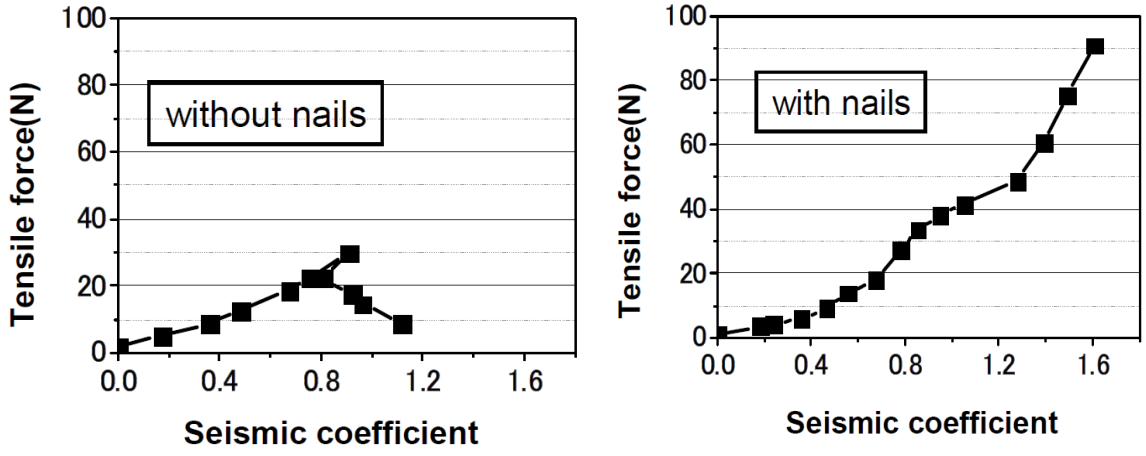

Figure 2.22 Influence of soil nails on the sum of tensile loads in layers of reinforcement (Kato et al. 2002)

Another technique involves improving the mechanical properties of onsite soils by the addition of cement. Examples of this technique are described in this section.

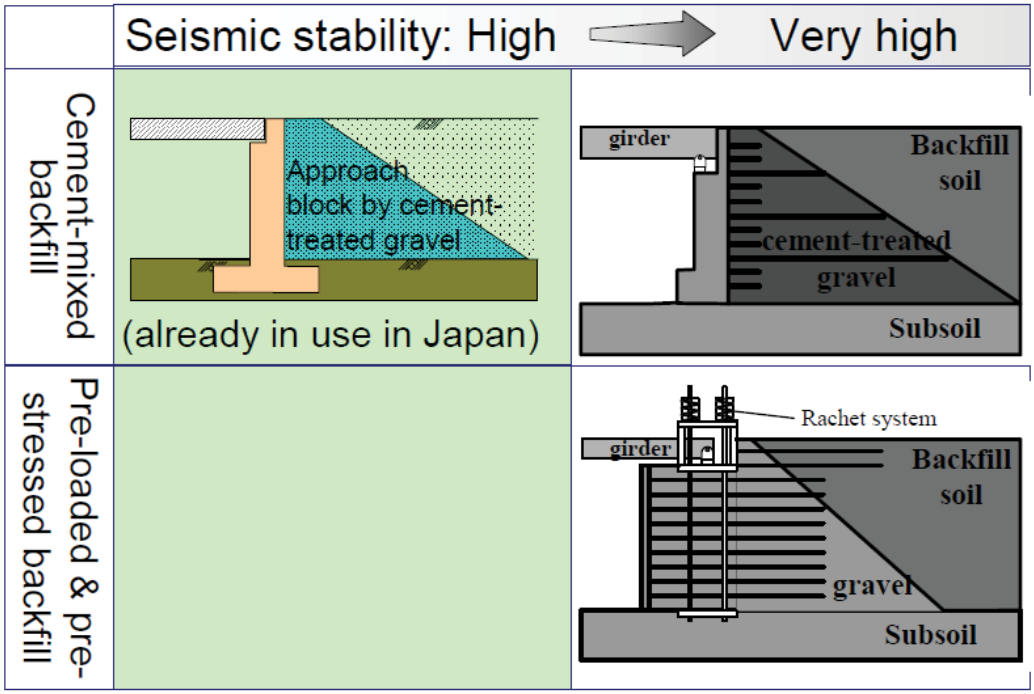

Figure 2.23 Example of methods used to improve the seismic stability of bridge abutments in Japan (Aoki et al. 2003)

GRS structures have also been studied to improve the seismic stability of abutments supporting bridge decks. Aoki et al. (2003) carried out shake table tests on conventional and GRS bridge abutment models using backfill treated with cement and pre-loaded and pre-stressed GRS walls with gravel backfill and full height rigid facings (Figure 2.23). The seismic stability of abutments treated with cement increased significantly compared to the structures treated with cement but without geosynthetic reinforcement that are currently in use in Japan. This construction technique resulted in a 20% saving compared to the conventional solution without the combination of backfill treated with cement and geosynthetic reinforcement. Saito et al. (2006) carried out a series of 1g shake table tests that showed that sandy backfill soils treated with cement and combined with geosynthetic reinforcement could also improve its seismic performance.

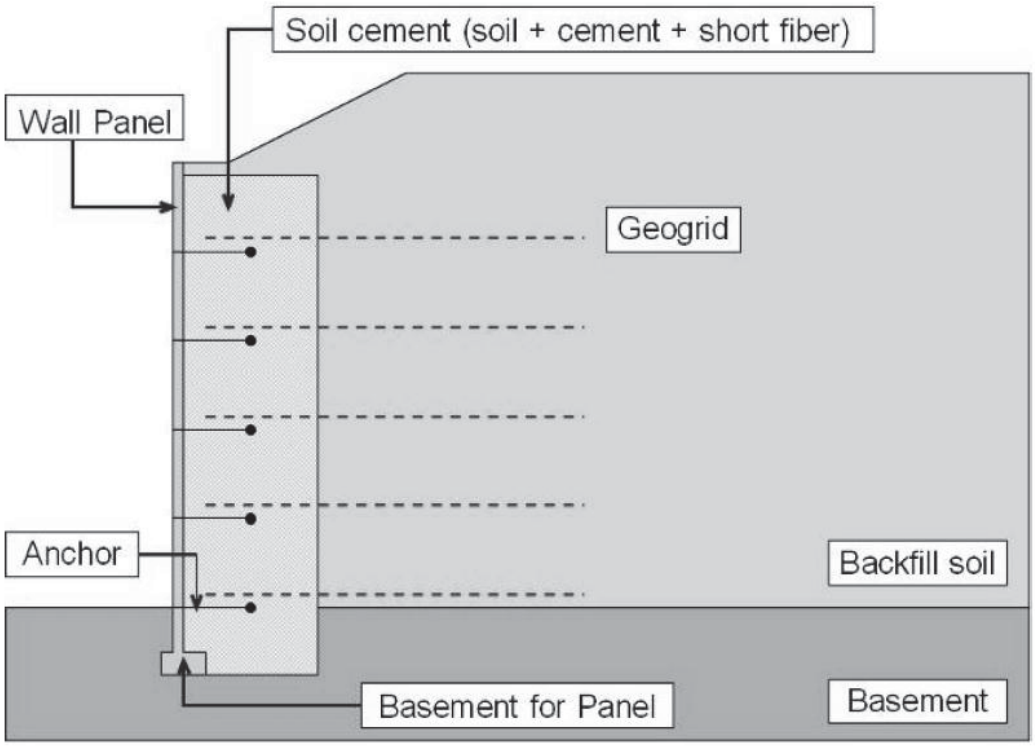

Figure 2.24 An example of a highway embankment project with combined cement-treated backfill and geosynthetic reinforcement (Ito et al. 2006)

A variation of the combined backfill treated with cement and geosynthetic reinforcement technique reported by Ito et al. (2006), was used to construct an embankment for a national highway in Japan (Figure 2.24).

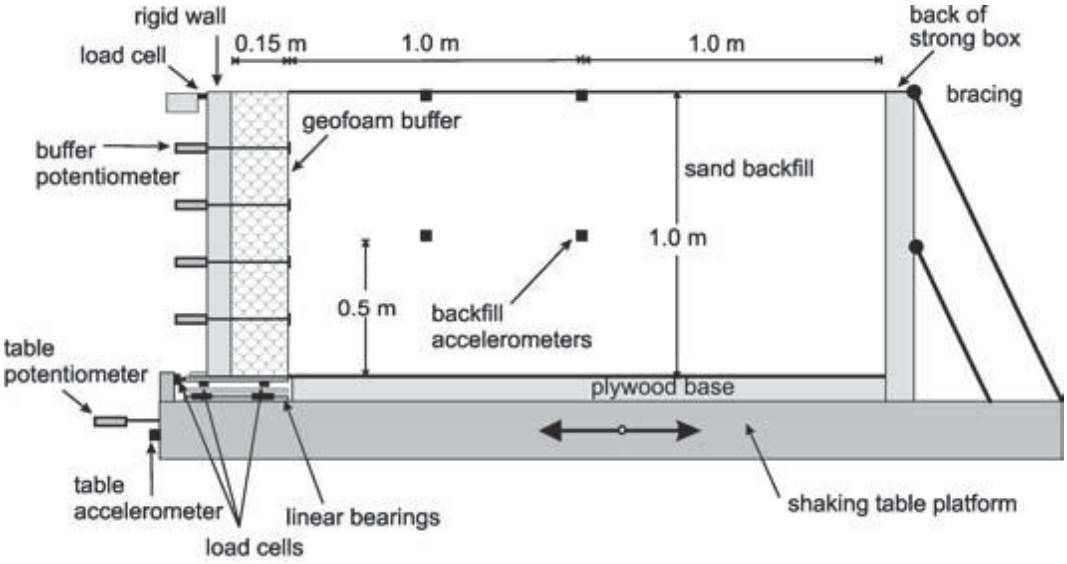

(a) Shake table test with geofoam EPS buffer

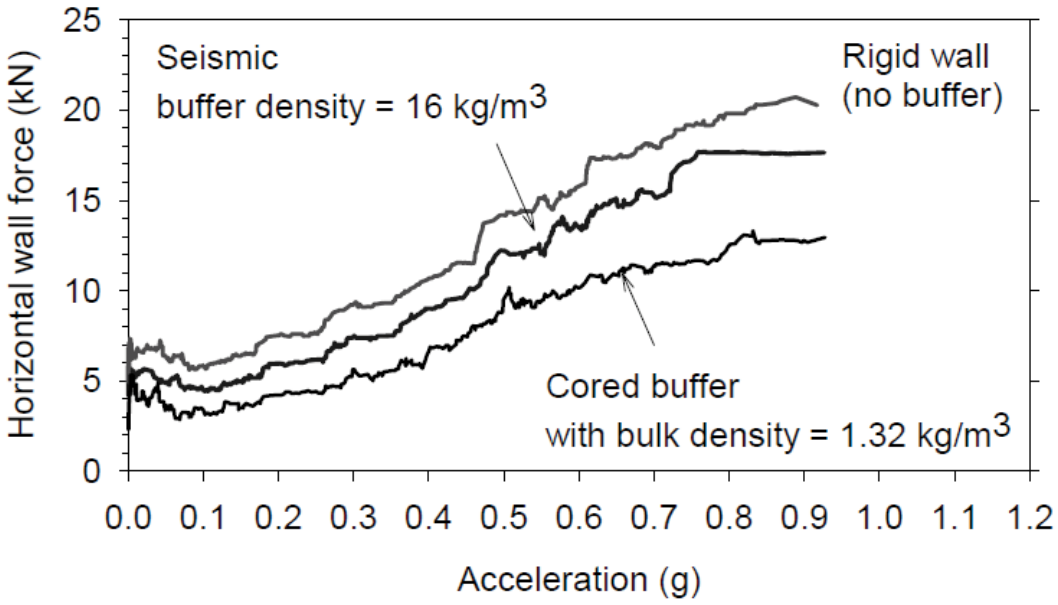

(b) Horizontal wall force

Figure 2.25 Shake table tests demonstrating reduction in seismic forces against rigid walls using geofoam EPS seismic buffers (Zarnani, Bathurst & Gaskin 2005)

Another technology was the use of expanded polystyrene (EPS) as a geofoam seismic buffer for rigid wall structures. The first use of this approach to attenuate seismically induced dynamic forces against basement walls was reported by Inglis et al. (1996). Proof of concept has been demonstrated by Zarnani, Bathurst & Gaskin (2005) who reported the results of a series of 1 m high shake table tests with a 150 mm thick EPS seismic buffer (Figure 2.25a). The tests showed that the total earth force under a simulated seismic load was reduced by 15% using a standard EPS material and 40% with a hollow core material (Figure 2.25b).

2.4 Numerical Modelling

A numerical investigation on the seismic response of a GRS wall is more economical than conducting physical model tests, although it does suffer from an extreme idealism which is not encountered in a physical model test. Nevertheless, finite element

numerical solutions are much more rigorous than the conventional limit equilibrium approach because they satisfy the force and equilibrium condition, the strain and compatibility condition, and the constitutive material laws. Indeed, both qualitative and quantitative performances could be obtained from numerical investigations. For example, the influence of boundary conditions and base acceleration records on the seismic response of a GRS wall were examined by Bathurst and Hatami (1998) and Vieira et al. (2006). The effect of the design parameters on the natural frequency of a GRS structure was investigated by Hatami & Bathurst (2000). GRS walls with complex geometry such as tiered walls and bridge abutments under seismic loads, have been analysed numerically by Guler & Bakalci (2004) and Fakharian & Attar (2007). Other seismic design parameters such as the properties of the soil and layout of the reinforcement were considered by Ling, Liu & Mohri (2005a), whereas numerical modelling performed by Rowe & Ho (1998) suggested that the tensile stiffness of the reinforcement had a significant effect on the deformation of GRS walls.

The conclusions drawn from numerical investigations could either be implemented or served as supplements to the design guidelines. It can be noted that in North America, the conventional seismic design of GRS structures follows the guidelines put forth by Elias, Christopher & Berg (2001) and Bathurst (1998), where the design methodologies are based on a pseudo-static limited equilibrium approach. Other design methodologies have been summarised by Zornberg & Leshchinsky (2003) and Koseki et al. (2006). As expressed by Cai & Bathurst (1995b), properly conceived numerical models can be used to gather both qualitative insights and quantitative data for the performance of GRS walls under seismic loading and to guide the development of design methodologies.

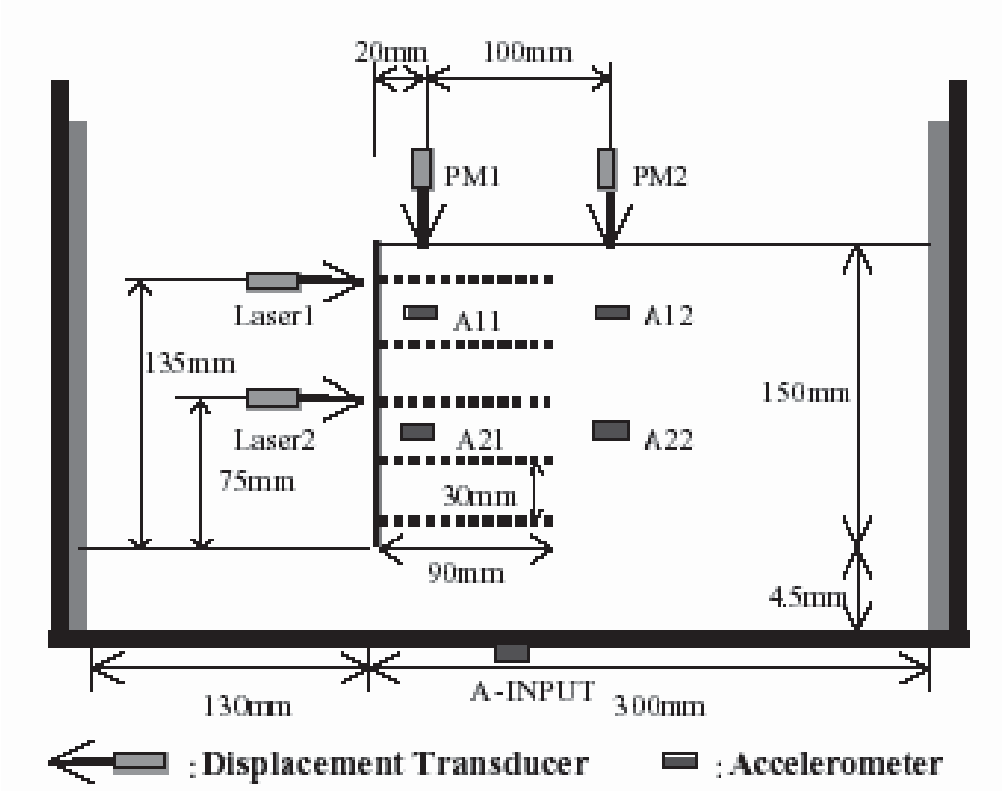

(a) Shake table model mounted on a centrifuge

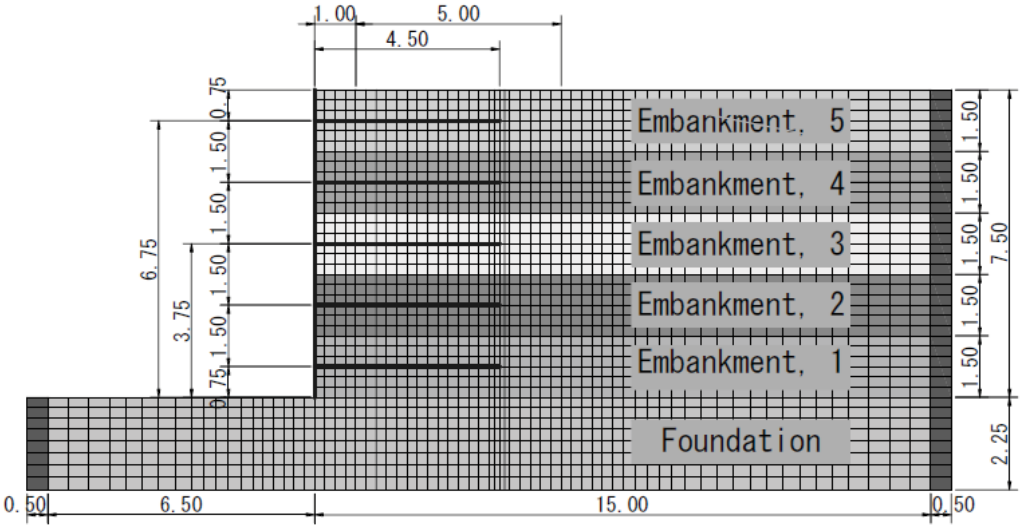

(b) Finite element model (dimensions on the centrifuge model test)

Figure 2.26 Numerical modelling of a centrifuge test of a segmental GRS wall (Fujii et al. 2006)

Fujii et al. (2006) carried out a numerical study aimed at simulating the results from a series of dynamic centrifuge tests on GRS segmental walls (Figure 2.26). They conducted 2-D finite element (FE) analyses using the program FLIP. The foundation soil and backfill were modelled using a multi-spring approach (Iai, Matsunaga & Kameoka 1992). The layers of reinforcement and facings were modelled by linear and beam elements, and the interfaces with the backfill were modelled by joint elements. Figure 2.27a shows a typical comparison between the measured and computed time histories of acceleration in the unreinforced backfill at prototype scale. In total, thirteen test cases with different input wave forms and amplitudes were analysed.

Figure 2.27b summarises a comparison between the measured and computed maximum accelerations. In general, reasonable agreement was obtained up to an acceleration of 0.6g, with a tendency for the numerical model to slightly overestimate the response of the physical test. The largest deviations could be the result of failure planes forming in the backfill, which was not properly modelled in the numerical code.

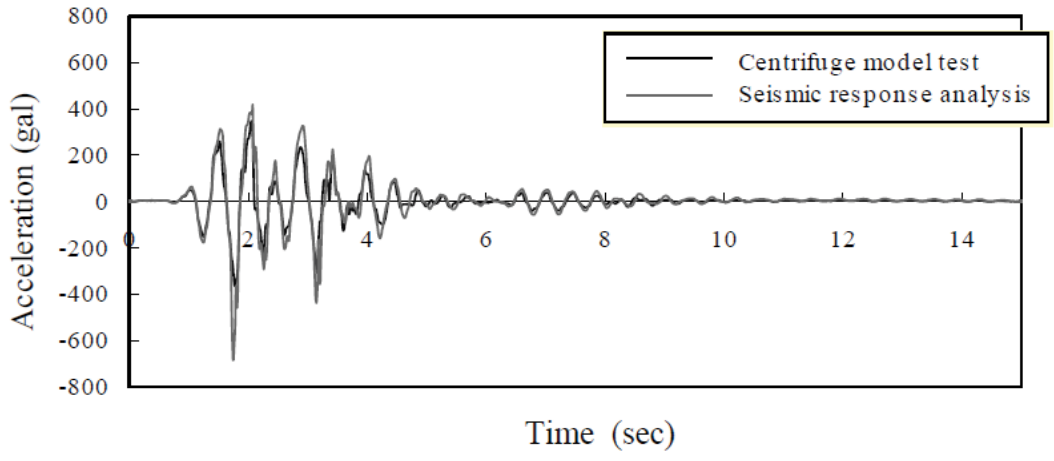

(a) Example comparison of measured acceleration response in physical rest and computed response

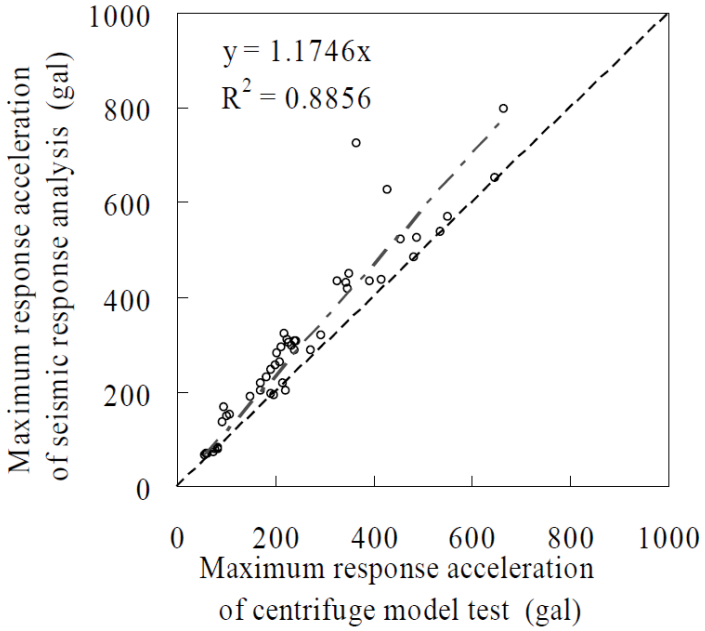

(b) Peak acceleration

Figure 2.27 Comparison of physical test results and computed acceleration responses of centrifuge tests of segmental GRS walls (Fujii et al. 2006)

The lateral displacement of the facing between the measured and computed data is shown in Figure 2.28. The accumulation of lateral displacement was simulated reasonably well although a phase lag was sometimes observed between the measured and computed responses.

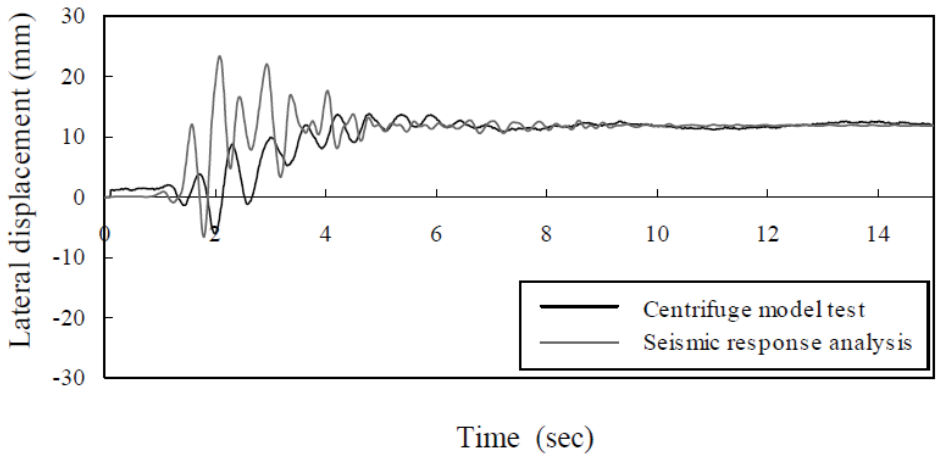

(a) An example for comparison of the measured lateral wall response in a physical test and the computed response

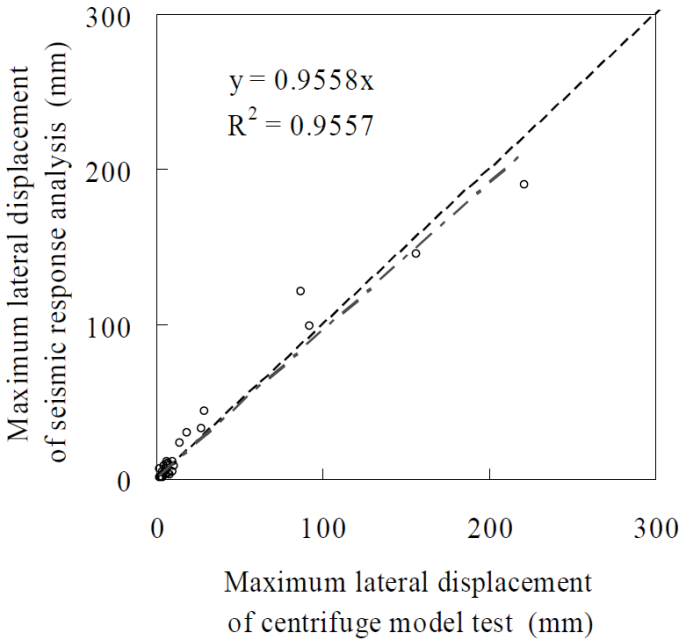

(b) Lateral displacement

Figure 2.28 Comparison between physical test and computed lateral displacement response of centrifuge tests of segmental GRS walls (Fujii et al. 2006)

El-Emam & Bathurst (2004) reported the numerical modelling of 1 m high shake table tests that investigated full height panel face GRS walls with different toe boundary conditions (i.e. hinged, and free to rotate and slide). They used the finite difference based program FLAC (Figure 2.29a). The numerical models were found to give reasonably accurate predictions of the experimental results (wall facing displacements, reinforcement loads, and measured toe loads) despite the complexity of the physical models under investigation. A constant stiffness of reinforcement was shown to be a reasonable assumption for numerically modelling the polyester geogrid reinforcement used in the physical tests. However, slip in the soil and reinforcement of layers with a shallow overburden was not considered in the numerical simulations and this is thought to have led to some discrepancies in the response to the reinforcement load close to the top of the wall. Both numerical and physical models showed that conditions at the boundary of the toe had a large influence on the performance and stability of the wall

under static and simulated seismic loading conditions. Finally, both the numerical and experimental models showed that current pseudo-static seismic design methods may underestimate the size of the soil failure zone behind the wall facing, particularly under large input base acceleration amplitudes, as illustrated in Figures 2.29b and 2.29c. It can be noted that the dark shading in the figure indicates large shear strains and these analytical methods are unable to explicitly account for the influence of the toe boundary on response of the wall.

Rowe & Skinner (2001) reported a field case investigation of a full scale test wall constructed at the Public Works Research Institute (PWRI) (Nakajima et al. 1996; Ochiai & Fukuda 1996; Public Works Research Institute (PWRI) 1997; Tsukada et al. 1998) in the Kanto region of Japan. The 8m high wall had a concrete block facing and was reinforced with 11 layers of geosynthetic grid reinforcement 6 m long (see Figure 2.30). A version of the finite element program AFENA (Carter & Balaam 1990), modified to account for modelling reinforced soil walls, was used to conduct the numerical analysis.

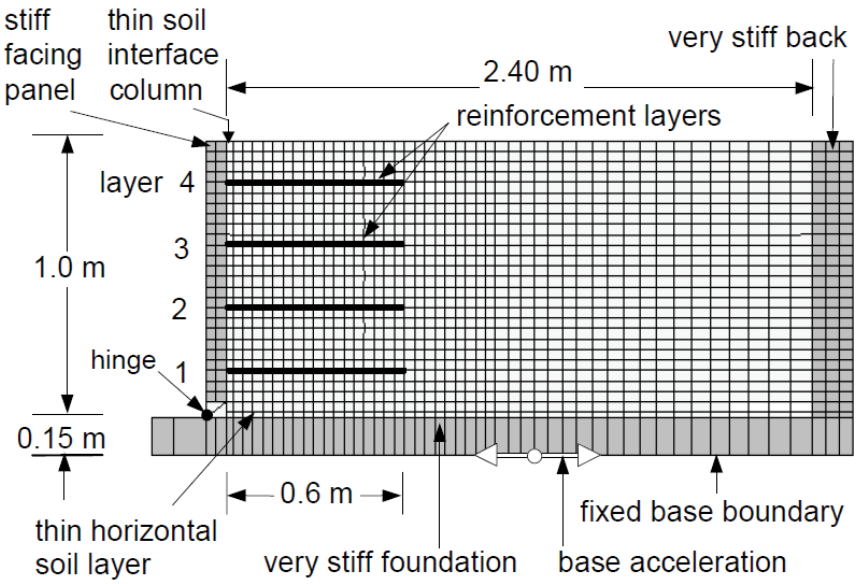

(a) FLAC numerical grid

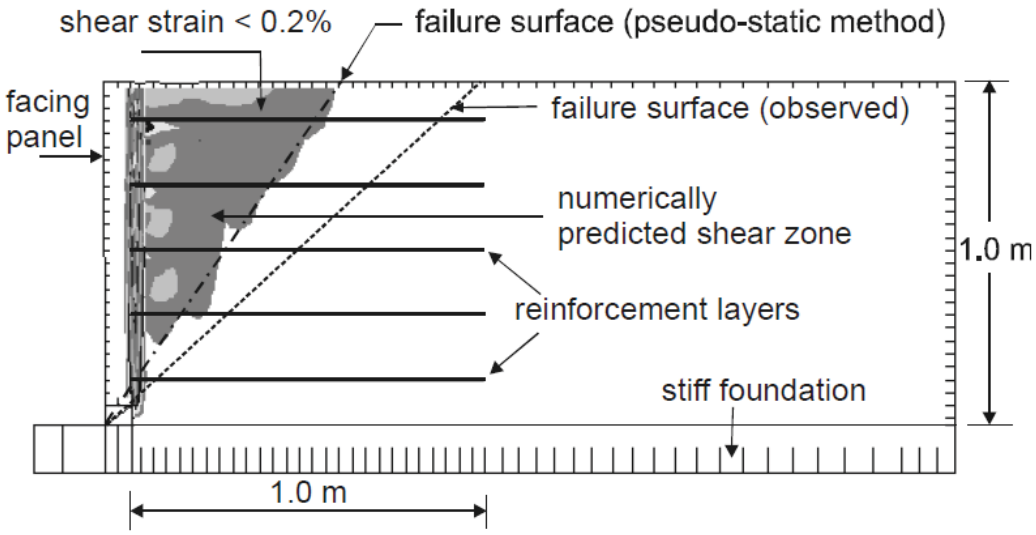

(b) Acceleration amplitude = 0.15g

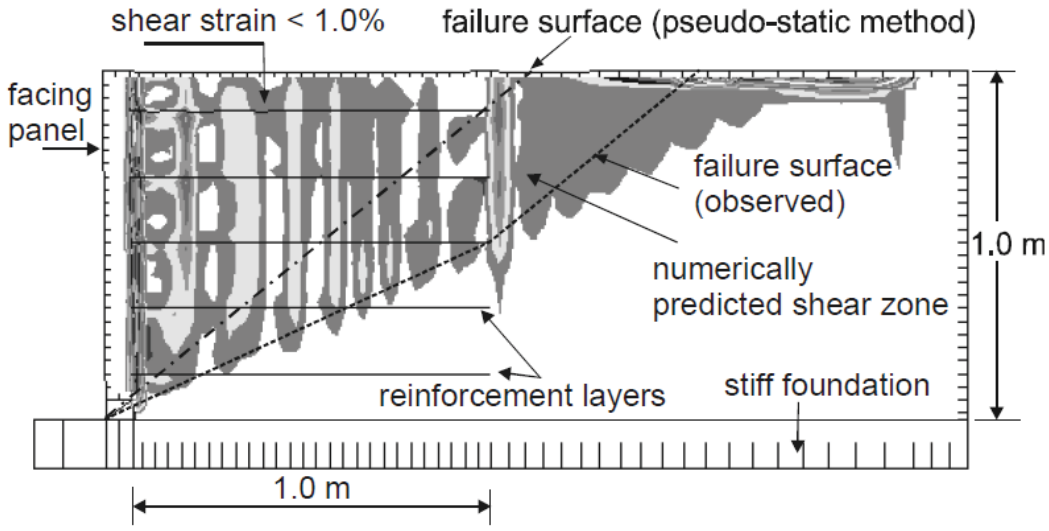

(c) Acceleration amplitude = 0.5g

Figure 2.29 Predicted and observed failure surfaces from hinged toe model wall (5 layers ofreinforcement and L/H = 1.0) at different input base acceleration amplitudes (El-Emam & Bathurst 2004)

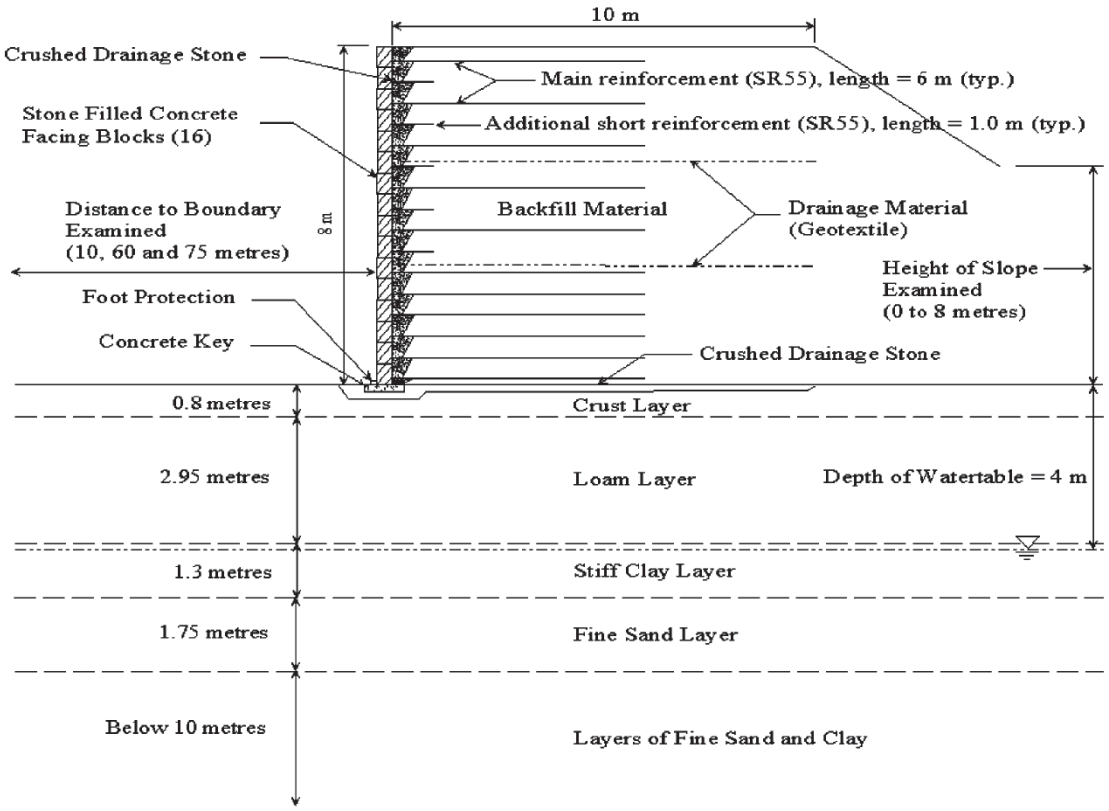

Figure 2.30 Cross section of wall (Public Works Research Institute (PWRI) 1997)

The deformation at the face and along the base of the wall, the stress along the base of the wall and behind the facing blocks and the strains in various layers of reinforcement, were all calculated and compared. The calculated and observed deformations at the front of the facing showed very encouraging agreement, although the deformation was slightly over predicted at the top and bottom of the wall, as shown in Figure 2.31.

A parametric study was conducted to investigate the effect of different characteristics of soft loam material in the foundation strata. The study was conducted by varying one loam parameter at a time while keeping all the other values constant. In general, the behaviour of the wall was consistent with expectations, with respect to the load distribution, deformation and stress at the toe, horizontal pressure against the wall face, and observed strains in the reinforcement. It was shown that for the soil wall reinforced with geosynthetic constructed on a yielding foundation, the stiffness and strength of the

foundation could have a significant effect on its behaviour; indeed a highly compressible and weak foundation layer could significantly increase deformation at the face and base, place strain into the layers of reinforcement, and to a lesser extent, the vertical stresses at the toe of the wall, compared to a rigid foundation.

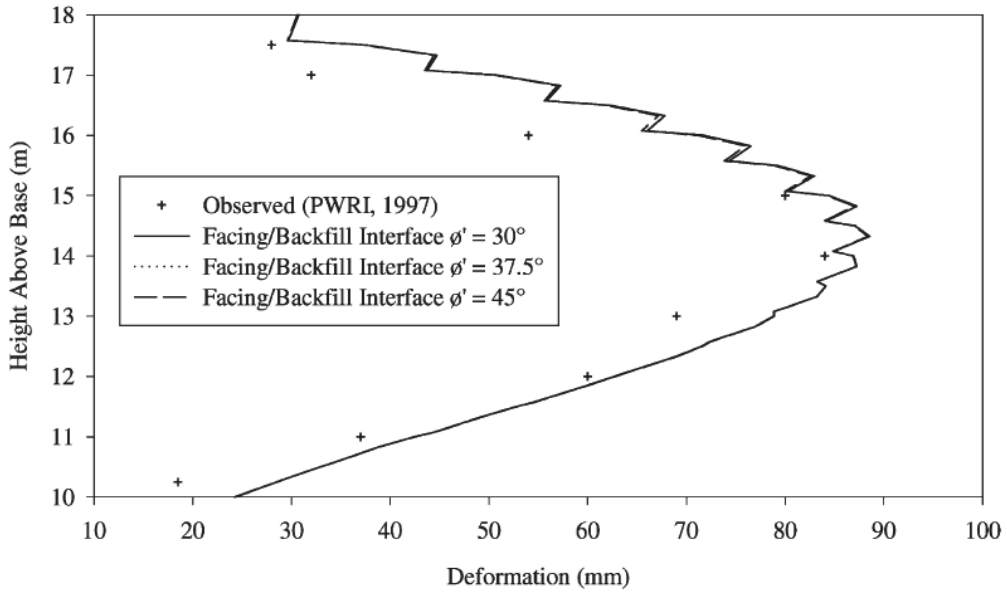

Figure 2.31 Comparison of observed and calculated lateral facing deformation (Rowe & Skinner 2001)

Bathurst & Hatami (1998) reported the results of a numerical parametric study of an idealised 6 m high GRS wall with a full height rigid facing and six layers of reinforcement. They showed that the magnitude and distribution of reinforced loads were sensitive to the stiffness of the reinforcement materials used.

Lee, Chang & Ko (2010) carried out a numerical simulation of shake table tests conducted by Ling et al. (2005) and Burke (2004) for the validation of this study because they are full scale models with detailed descriptions of backfill, reinforcement, and interface properties. The three shake table test walls had segmental block facing, and the backfill was reinforced with geogrids. The geometry and instrumentation of the test walls are as shown in Figure 2.32. All three test walls had a height of 2.8 m. Three

full scale GRS walls loaded by a shake table were simulated by the finite element program LS-DYNA.

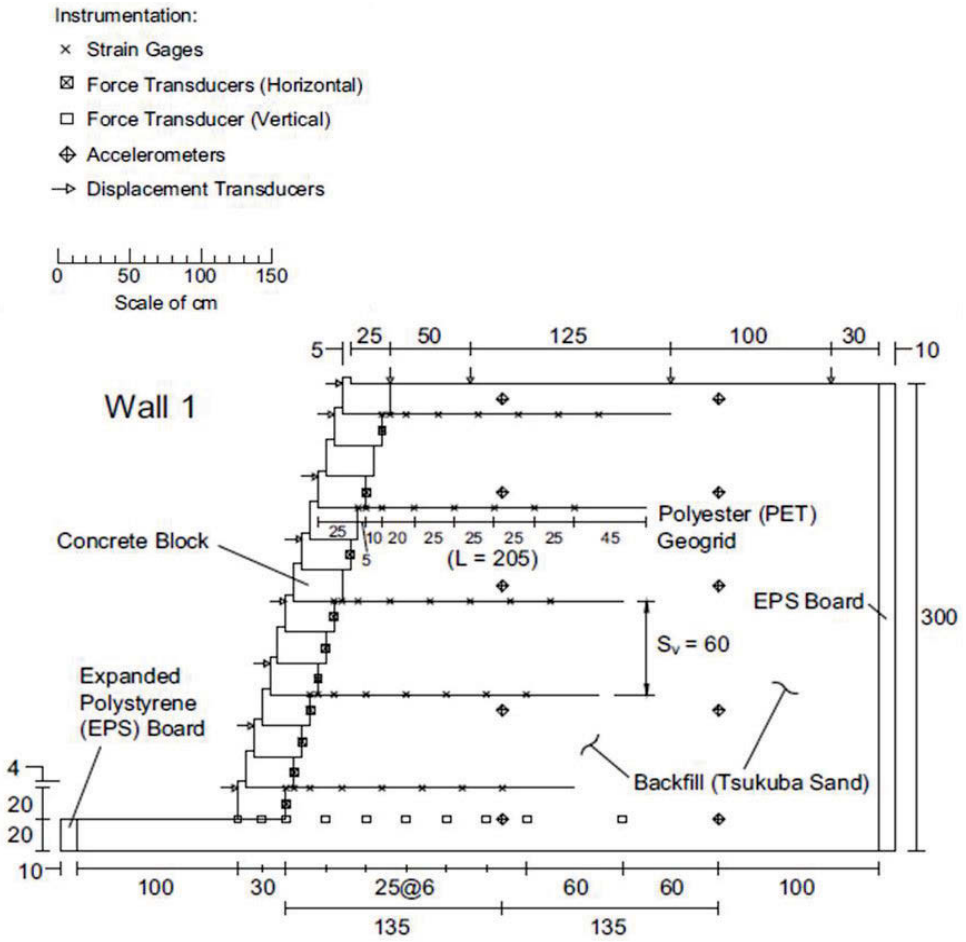

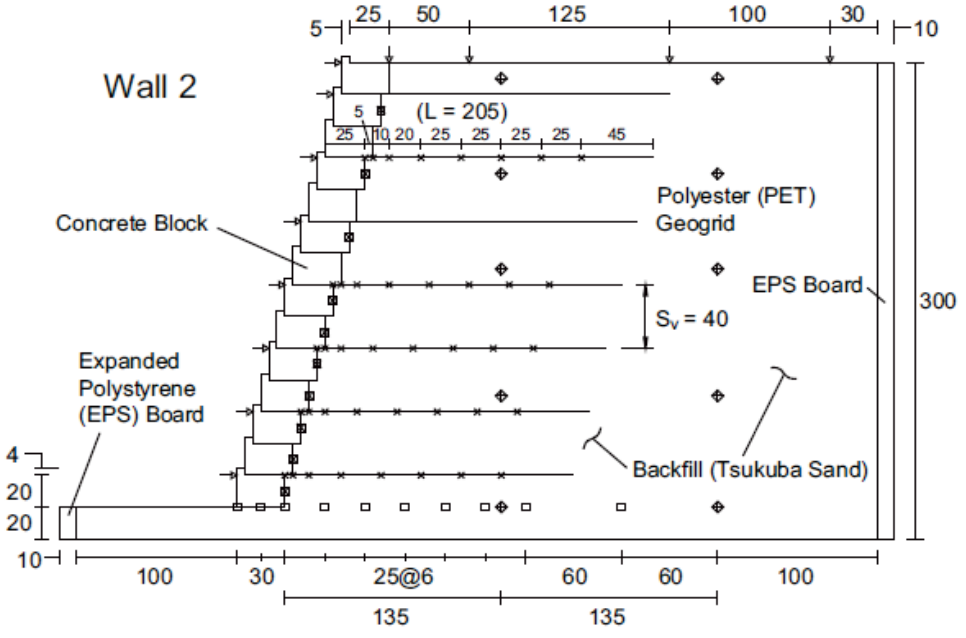

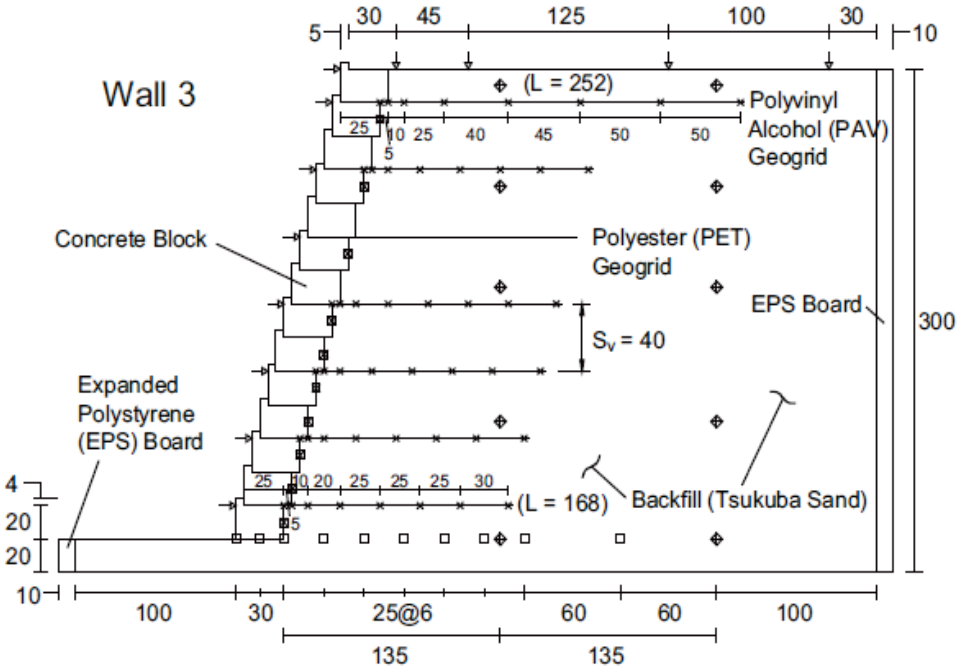

Figure 2.32 Dimensions and instrumentation of Walls 1, 2, and 3 (Ling et al. 2005)

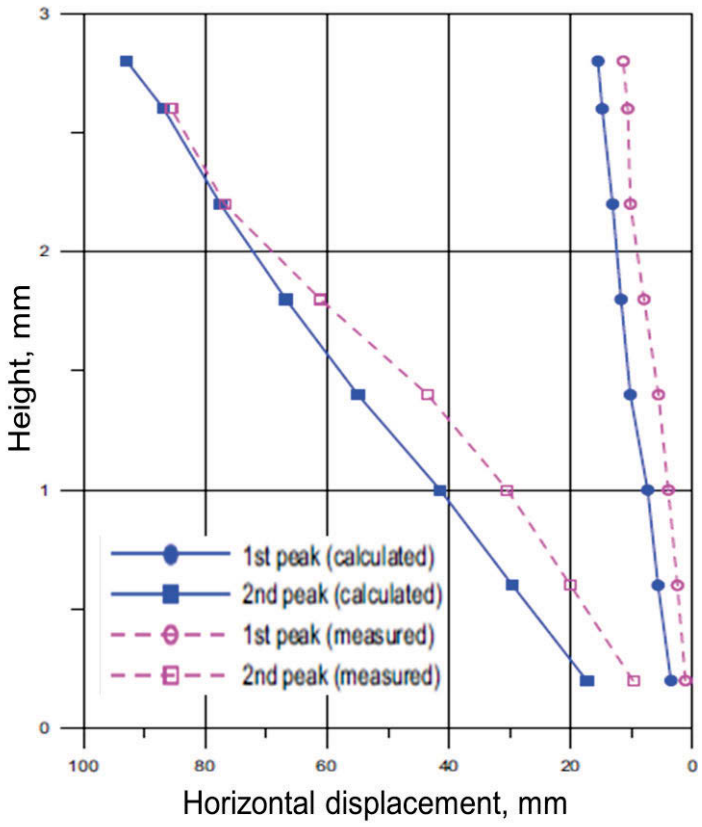

(a) Wall 1

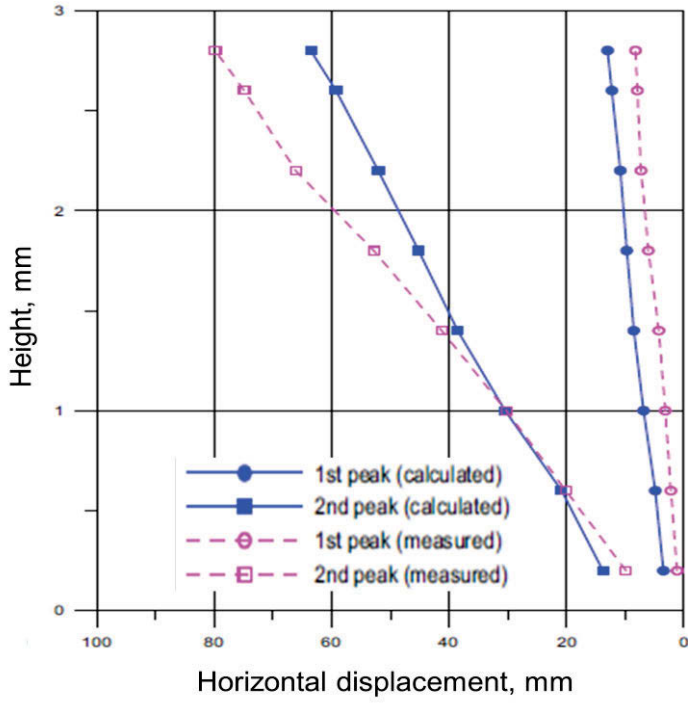

(c) Wall 2

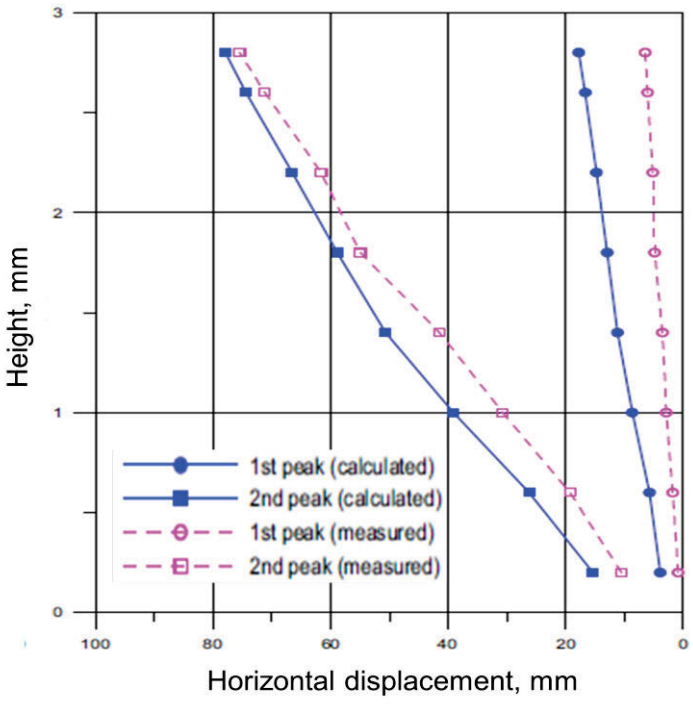

(c) Wall 3

Figure 2.33 Wall face peak horizontal displacement comparison between the calculated and the measured data (Ling et al. 2005)

The results of the numerical simulations were compared to the measured performances reported by both Ling et al. (2005) and Burke (2004), and a comparison of the calculated and measured wall face peak horizontal displacement for the three test walls is shown in Figure 2.33. Wall facing displacement increases with increasing seismic loads, although in the first simulated shake there was a general over estimation of displacement in the wall, but the prediction in the second shake was much better.

A comparison of the calculated and measured settlement of the backfill surface of the three walls is presented in Figure 2.34. As with the prediction of wall face displacement, simulation of the first shake over estimated the permanent settlement, although the calculated and the measured results from the first shake showed a similar settlement profile, where more settlement occurred close to the wall facing and less towards the back of the wall.

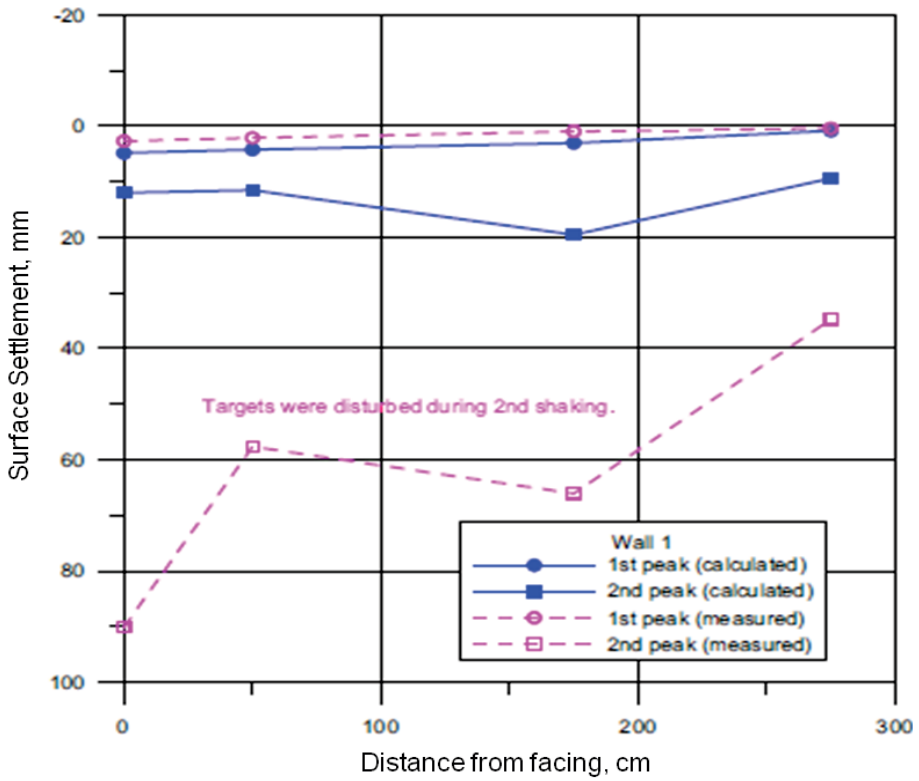

(a) Wall 1

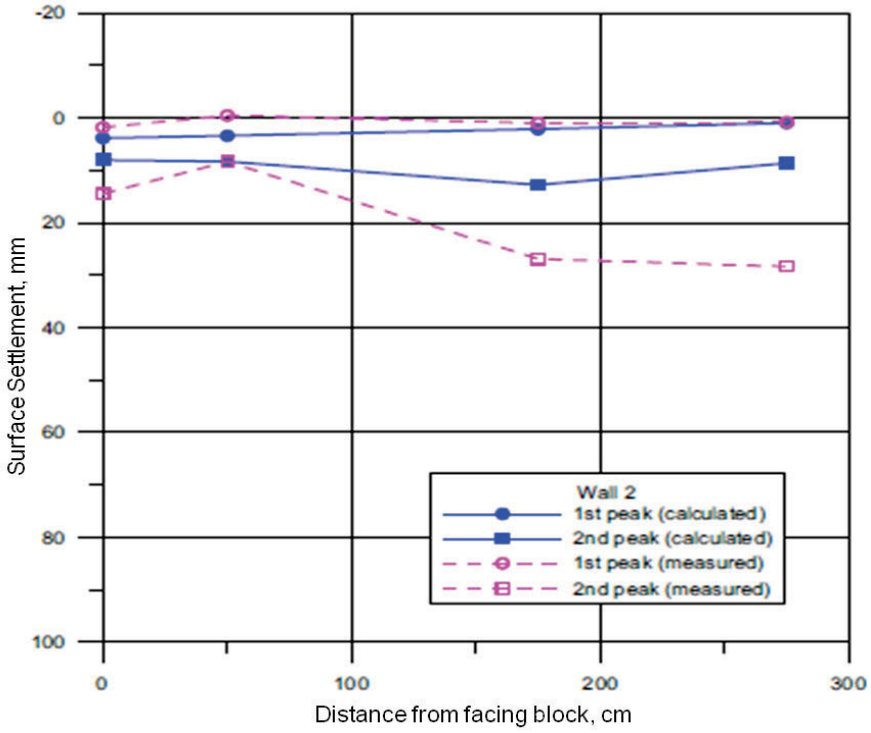

(b) Wall 2

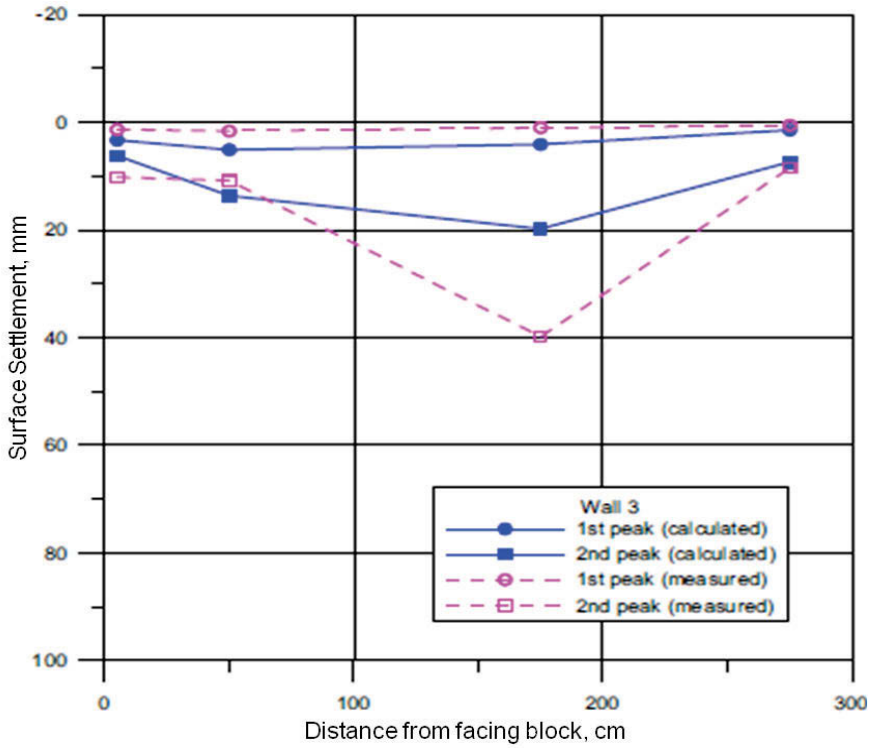

(c) Wall 3

Figure 2.34 Comparison of backfill surface settlement (Ling et al. 2005)

The numerical analyses concluded that the seismic wall displacement decreased as the spacing between the reinforcement decreased.

GRS walls with complex geometry such as tiered walls and bridge abutments under seismic loads were analysed numerically by Guler & Bakalci (2004) and Fakharian & Attar (2007). The computer program PLAXIS was used in the parametric study performed by Guler & Bakalci (2004) for the tiered wall where the parameters analysed included the height of the wall (i.e., 4 m and 6 m), the ratio of the length of geosynthetic reinforcement to the height of the upper and lower walls, the ratio of the distance between two walls to the their height, and the vertical spacing, and stiffness, of the geosynthetics (i.e., 0.25 m and 0.5 m). The soil and geosynthetic reinforcements were simulated by the elastic-plastic Mohr-Coulomb model and linear elastic model, respectively. It was found that deformation of the wall was significantly influenced by the ratio of the distance between two walls to their height, and a bigger berm reduced the amount of deformation. It was also found that the length of reinforcement in the lower wall caused more deformation than the length of reinforcement in the upper wall. A list of numerical simulations specifically for GRS structures subjected to dynamic shake down by different researchers is summarised in Table 2.2.

2.5 Key Elements in Enhancing Seismic Performance of Retaining Walls

The key factors improving the seismic performance of reinforced soil walls are facing rigidity, arrangements of reinforcements, properties of reinforcement, and backfill and subsoil conditions, which are explained in details below.

Table 2.2 Summary of numerical simulation on seismic performance of GRS structures

Reference	**Code (method)**	**Facing model (element)**	**Reinforcement model (element)**	**Backfill model (element)**	**Interface model (element)**	**Input motion**	**Validation test**	**Performance examined**
Liu et al. (2011)	ABAQUS (finite element)	Linear elastic	Elastoplastic viscoplastic bounding surface (1-D bar element)	Drucker-Prager creep model	Mohr-Coulomb (thin layer element)	Kobe record	Dynamic centrifuge	Acc.; disp.; crest settlement; reinf. strain
Fujii et al. (2006)	FLIP (finite element)	Elastic (linear-beam element)	Elastic (linear- beam element)	Multi-spring	Joint element	Kobe record	Dynamic centrifuge	Acceleration; displacement; earth pressure
Ling et al. (2004)	DIANA-SWANDYNE II (finite element)	Linear elastic	Bounding surface	Generalized plasticity soil	Elastic perfectly plastic interface element	Sinusoidal record	Dynamic centrifuge	Acceleration; displacement; vertical and lateral pressures
Burke (2004)	DIANA-SWANDYNE II (finite element)	Linear elastic (8- & 6-node element)	1-D bounding surface (3-node bar element)	Pastor-Zienkiewicz III (8- & 6-node element)	Slip element	Kobe record	Full-scale shake table	Acceleration; displacement; vertical and lateral pressures; reinforcement load
Helwany et al. (2001)	DYNA3D (finite element)	Not given	Linear elastic (shell element)	Ramberg-Osgood (solid element)	Penalty based Interface	Sinusoidal record	Full-scale shake table	Acceleration; displacement; interface load
El-Emam et al. (2001)	FLAC (finite difference)	Not given	Elastic-plastic (2-node cable element)	Mohr–Coulomb elastic-plastic strain softening	Not given	Sinusoidal record (5 Hz)	Reduced-scale shake table	Displacement; reinforcement load; acceleration; toe condition

2.5.1 Facing rigidity

The effects of the facing rigidity on the stability of GRS walls were investigated and discussed in detail by Tatsuoka (1993). Basically, as the facing becomes more rigid, the pressure of earth acting on the back of the facing increases such that deformation decreases but the ultimate stability of the wall actually increases. This means that a large degree of flexibility is not necessarily a preferable property for a completed GRS wall, although it was required to accommodate any possible large deformation of the subsoil, so that a deep foundation becomes unnecessary. One possible compromise was that walls should be as flexible as possible during construction, but be stiff enough before they are open to service.

Koseki & Hayano (2000) conducted a study on a failed segmental GRS wall after the 1999 Chi-Chi earthquake. It was noted that an insufficient number of reinforcements could have been subjected to excessive tensile force, causing local rupture where they connected to the facing, and/or the overall rigidity of the facing may not have been enough to resist the earthquake loads, causing excessive deformation of the stacked facings and of the connecting pins to be pulled out.

2.5.2 Arrangement of reinforcements

Another important factor for enhancing the performance of a reinforced soil wall is how the reinforcement is arranged. For instance, the study by Watanabe et al. (2003) discussed the effect of various arrangements of reinforcement on wall displacement, as shown in Figure 2.37:

- R1 or type1 having relatively short reinforcement of equal lengths,
- R2 or type 2 having partially extended reinforcements, and
- R3 or type 3 having relatively long reinforcement of equal lengths.

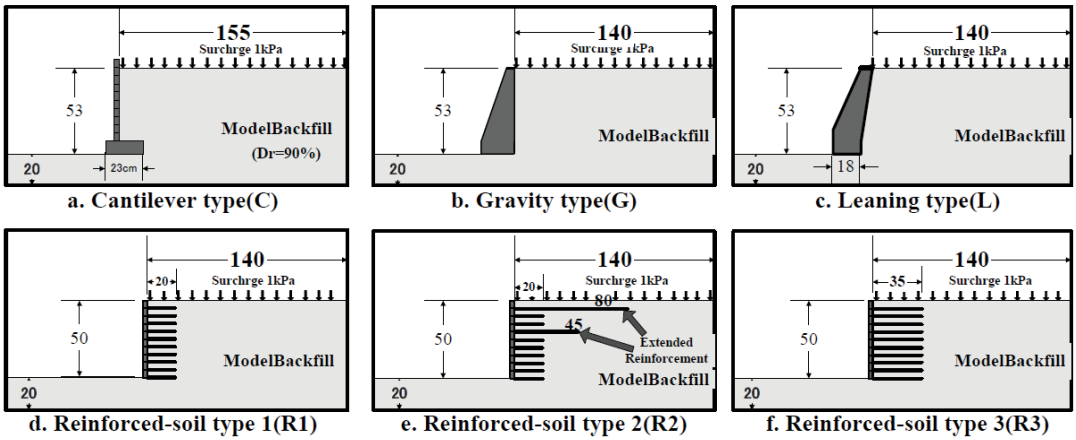

Figure 2.35 GRS wall models on level ground (Watanabe et al. 2003)(note: all dimensions are in cm)

Of these three types, as can be seen in Figure 2.35, the wall type 3 exhibited the smallest amount of residual displacement at the top of the wall. In addition, although the total length of reinforcement of wall type 2 was about 80 % as large as for wall type 3, their seismic performance in terms of displacement of the top of the wall, was similar. The performance of wall type 2 confirmed that a partial extension of upper reinforcement can significantly improve its seismic stability because the upper reinforcement can resist the overturning mode of failure more effectively.

In turn, the tensile force mobilised in the reinforcement concentrated into the extended uppermost reinforcement of wall type 2 implies that this reinforcement was the key to its superior performance. It was also important to note that with walls type 2 and 3, the calculated values of the critical seismic coefficient to induce a factor of safety equal to unity in a pseudo-static limited equilibrium stability analysis against overturning failure were different from each other (0.55 and 0.70, respectively) refer to Watanabe et al. (2003) for the detailed conditions of this calculation. In spite of this difference, the seismic performance of these two walls was similar. This was possibly affected by the shear deformation of reinforced backfill, which was not considered when evaluating the critical seismic coefficients listed above.

2.5.3 Properties of reinforcement

The properties of the reinforcement also play a key role in enhancing the response of GRS walls to the earthquake. To evaluate their seismic performance, another series of 1 g model shake tests was conducted by Nakajima et al. (2007) as an extension of the model tests presented previously (Figure 2.35), while considering two models of geosynthetic reinforcement, as shown in Figure 2.36.

Table 2.3 Properties of model reinforcements (after Nakajima et al. 2007)

Property	Secant tensile stiffness		Ultimate pull-out resistance
Unit	Per single strip (kN/ε/strip)	Per unit width (kN/ε/strip)	Per unit width for buried length of 0.5 m (kN/m)
Phosphor bronze (PB)	3.5 - 5.7	41 - 66	2.96
Polyester (PE)	0.31 - .36	105 - 121	4.48

As summarised in Table 2.3, the tensile stiffness of the geosynthetics per single strip that was evaluated in direct tension tests was higher with the Phosphor Bronze (PB) model, although their tensile stiffness per unit width of the grid was higher with the PE model because it consisted of many more strips than the PB model.

Despite these differences in the properties of reinforcement, the cumulative tilting angles and base sliding displacements of the GRS wall models (type 2, Figure 2.35e) using two types of reinforcement were generally similar to each other. It can be noted that in these model tests, the peak base acceleration was 0.9 g in the first shake step, which was increased in 0.3 g and 0.4 g increments in the second and third shake steps, respectively, while the fourth shake step was conducted using the same base acceleration as the third one.

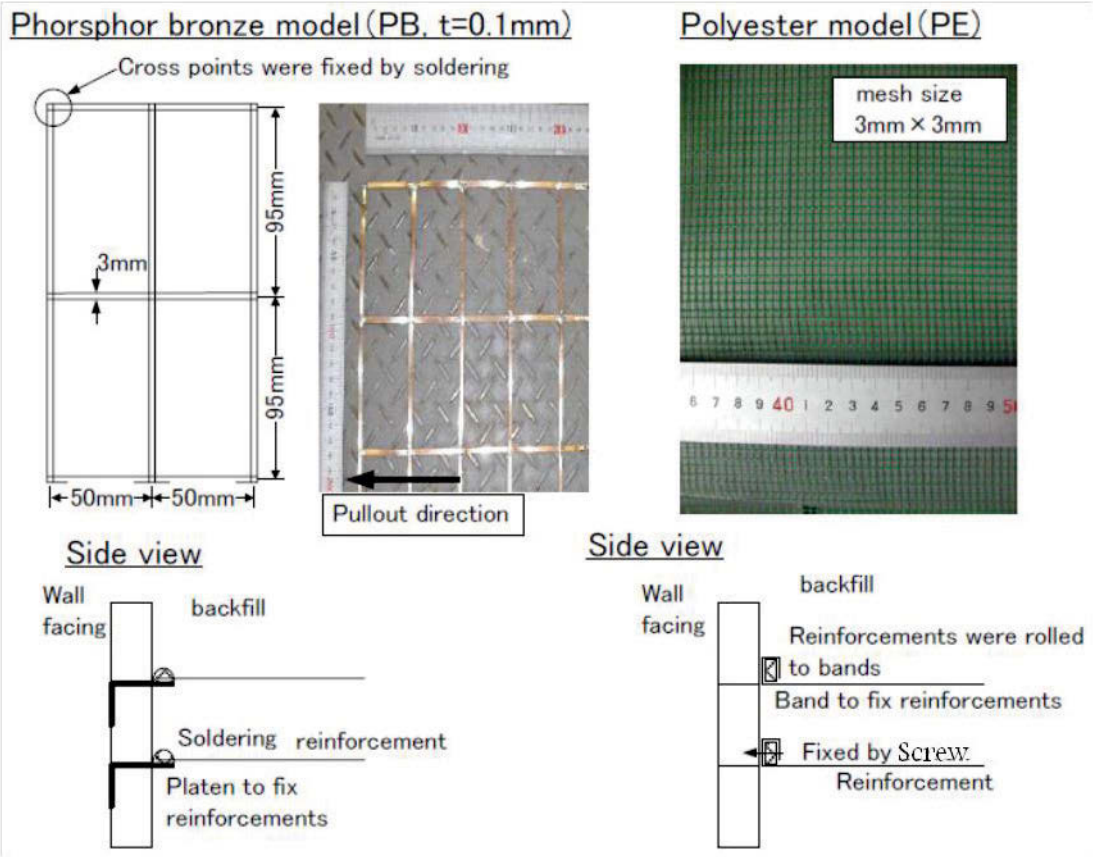

Figure 2.36 Geosynthetic reinforcement models (Nakajima et al. 2007)

The influential factor affecting the tilting behaviour of GRS walls observed in the present model tests, would be the resistance to pull out mobilised at small levels of displacement. As mentioned above, it was larger with the PB model than the PE model, although the ultimate resistance was vice versa. Since there was no rupture or pullout failure of the reinforcement, these properties would not have affected the tilting behaviour in the model tests.

2.5.4 Backfill and subsoil conditions

The seismic performance of GRS retaining walls also depends on the backfill and subsoil conditions. For example, backfill soils that are not well compacted may not mobilise enough resistance to stop the reinforcement from being pulled out, regardless of whether the reinforcement is stiff enough or strong enough, and they may also suffer excessive settlement during service prior to earthquakes, causing the reinforcement to

fail locally where they connect to the facing. And once pull out or local failure of the reinforcement occurs, GRS walls become unstable during earthquakes as well as under working load conditions (Koseki 2012).

Moreover, in comparison to backfilling working without reinforcement as was used for conventional type reinforced walls, backfill soil with reinforcement can be compacted more effectively because, the reinforcement confines any lateral deformation during compaction. On this basis, due attention should be paid when constructing GRS walls to ensure that the backfill soil has been compacted sufficiently (Koseki et al. 2006).

This confinement of lateral deformation in the backfill soil would in turn mobilise tensile forces in the reinforcement which would also restrict the facing from becoming displaced.

2.6 Overview of Failure Modes

The modes of failure for the design of reinforced soil walls can be divided into three categories in the current guidelines and specifications, as shown in Figure 2.37. They are: external, internal, and facing elements failures (CFEM 2006). External stability considers the reinforced soil mass as a rigid body subjected to lateral earth pressure from backfill soil and supplementary loads, but in design instability in the walls consists of base sliding, overturning, bearing capacity, excessive settlement, and global (deep seated) failures.

The bearing capacity and modes of settlement failure depend on each other. Settlement can be limited if the walls are designed properly and their bearing capacity and failure modes are considered. Internal stability considers the position and strength of reinforcement within the reinforced soil mass, and comprises the tensile over stressed, pull out, and internal sliding failures of reinforcement. This means that the length,

position, and strength of the reinforcement must be such that the wall will satisfy all the failure modes and with minimum safety factors given in the specifications. The facing elements failure, which is considered to be a local stability criterion in design, was related to the connections of the reinforcement and facing units, column shear failure, and toppling.

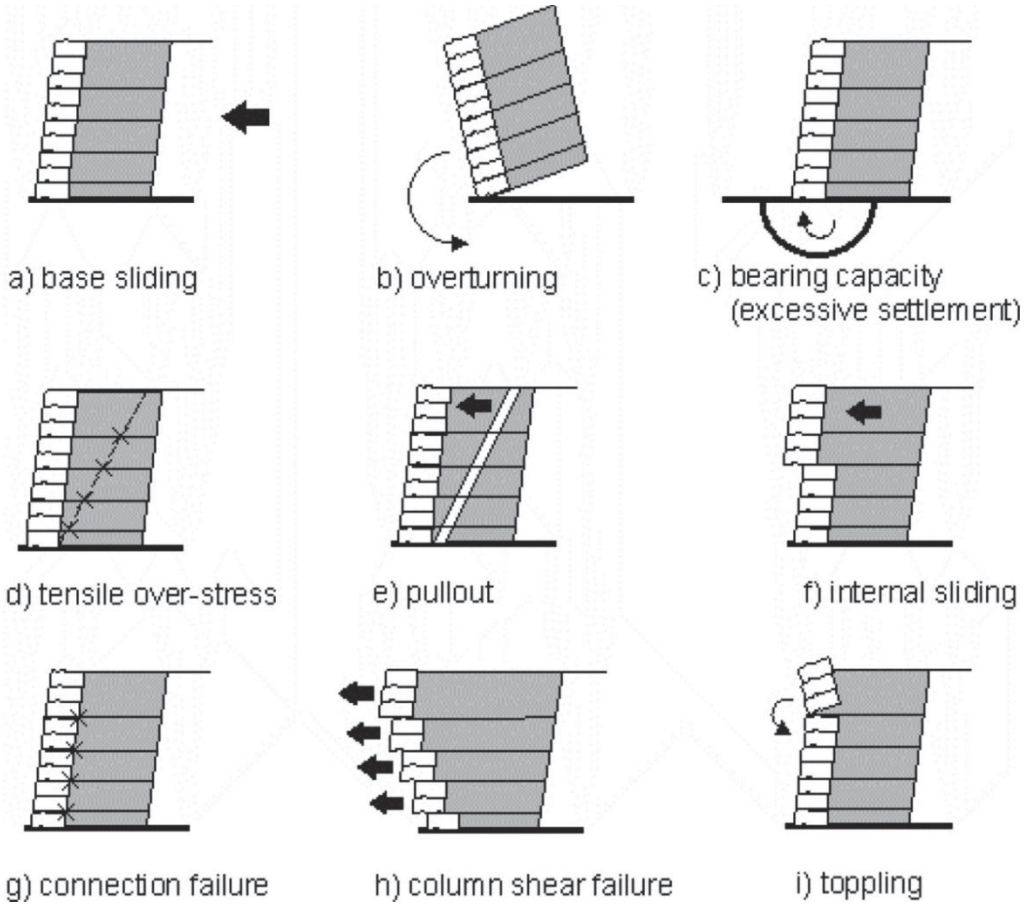

Figure 2.37 Modes of failure for reinforced soil walls (CFEM 2006)

Further instability modes should also be considered in certain conditions, such as those governed by seismic or cyclic loading. Sabermahani, Ghalandarzadeh & Fakher (2009) investigated two main seismic deformation modes, overturning (maximum displacement at the top) and bulging (maximum displacement at mid-height) of the facing, together with an additional base sliding mode that occurred at the same time as the other two modes.

Overturning Mode: According to Sabermahani, Ghalandarzadeh & Fakher (2009), in an overturning mode, the top of the wall faced maximum lateral displacement, causing the reinforced zone to rotate outwards like a rigid block. This outwards movement caused a gap to form in front of the backfill parallel multi-line failure surfaces to develop. The maximum ground surface settlement over the wall occurred on top of the gap. Moreover, multi-line failure surfaces occurred at the rear part of the reinforced zone in the backfill but there was no internal failure in the reinforced zone. Figure 2.28 shows details of the failure mechanism and deformation mode in the reinforced zone and backfill. This figure depicts a stepped shape formation on the ground surface caused by a discontinuity that appeared in the ground settlement profile. Furthermore, the ends of the layers of reinforcement had settled downwards due to a drag down force behind the reinforced zone.

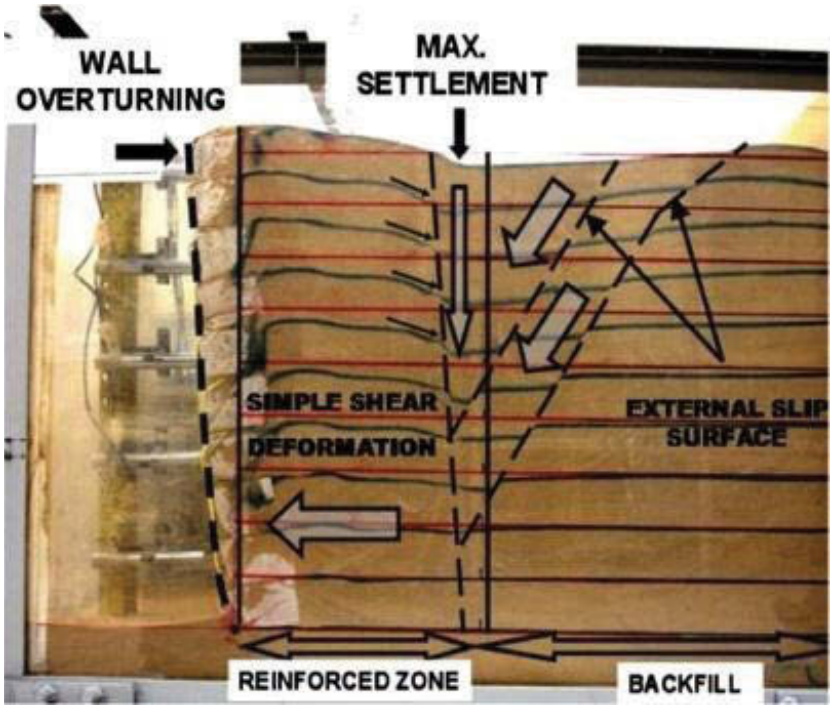

Figure 2.38 Details of the overturning mode and the failure mechanism (Sabermahani, Ghalandarzadeh & Fakher 2009)

This behaviour was based on some limited assumptions of equilibrium as it was not exactly to the same as the overturning or base sliding of a rigid body. Sabermahani, Ghalandarzadeh & Fakher (2009) mentioned that the rotation of the reinforced zone around the toe of the wall, presumed to be rigid, caused the first layer of reinforcement to excavate the layer of foundation soil.

Bulging Mode: Generally, the failure mechanism in walls with bulging deformation was not the same as the overturning mode where there was no external failure surface. Instead, there was an internal single failure surface in the reinforced zone where maximum displacement occurred in the middle of the wall facing (Sabermahani, Ghalandarzadeh & Fakher 2009).

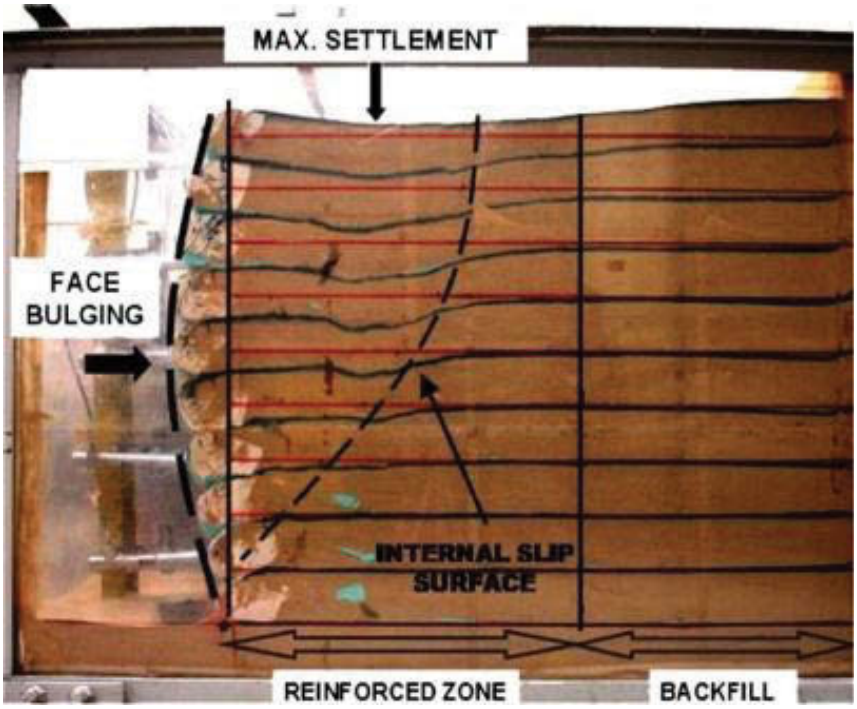

Figure 2.39 Details of the bulging mode and the failure mechanism (Sabermahani, Ghalandarzadeh & Fakher 2009)

Figure 2.39 shows details of the position of the slip surface, and the internal failure mechanism and maximum settlement in the bulging mode. As there was no large lateral movement in the reinforced body, uniform small settlement in the backfill was seen in

the ground surface profile. The face bulging in a convex shape caused a concave shaped settlement profile that developed maximum settlement at the middle of the reinforced zone. This behaviour was considered to be a flexible medium and this flexibility of the reinforced zone helped the toe of the wall not to excavate the foundation layer.

2.7 Three Dimensional Soil Reinforcement

2.7.1 Introduction

A number of recent studies have been carried out on reinforced soil retaining walls with planar reinforcement such as geotextiles and geogrids (e.g.Chen 2007; Chen & Chiu 2008; Shekarian, Ghanbari & Farhadi 2008; Won & Kim 2007; Yoo & Kim 2008). However, the scarcity of space and elevated height requirements in urban areas have encouraged researchers to consistently introduce new kinds of reinforcing materials with different shapes and sizes, along with better external and internal design strategies for reinforced soil structures. A different type of reinforcement geometry for a reinforced soil wall was proposed by Zhang et al. (2008) and Khedkar & Mandal (2008). Pull out test behaviour has been studied by several researchers to understand the various factors affecting the pull out response of reinforcement, i.e., the size of the box, the size of the sample, the length of the sleeve, as well as conditions at the front and the side wall, and the test speed, etc. (Farrag, Acar & Juran 1993; Moraci & Recalcati 2006; Palmeira 2004; Sobhi & Wu 1996; Sugimoto, Alagiyawanna & Kadoguchi 2001; Teixeira, Bueno & Zornberg 2007). Bergado et al. (2003) and Khedkar & Mandal (2007) in particular, simulated the pull out tests using the finite element method based on PLAXIS software. Many researchers (Bergado, Bukkanasuta & Balasubramaniam 1987; Nernheim 2005; Palmeira & Milligan 1989) made it clear that the geometry of the reinforcement was one of the important factors in pull out study. In particular, Bergado, Bukkanasuta & Balasubramaniam (1987) found that bamboo grids have a generally

higher pull out resistance than geogrids, provided that each one has the same plan area. The reason for this was that bamboo reinforcement has a thicker transverse member than geogrid reinforcement. Recently, Racana, Grediac & Gourves (2003) studied the geometric arrangement of reinforcements, i.e., horizontal, vertical, and corrugated steel strips, in order to achieve a shorter length anchorage. They found that a corrugated geometry was better than the other two reinforcement geometries and from a practical point of view, suggested corrugated strips as the reinforcement, forming a network of geocells filled in with compacted soil. Xie (2003) presented a reinforcing ring, whose mechanical function was to turn the lateral earth pressure to the stress within the reinforcing ring. Zhang, Javadi & Min (2006) suggested using three dimensional reinforcing elements for reinforced soil to enhance its performance. They demonstrated the acceptability and better performance of three dimensional reinforcement over two dimensional, planar reinforcement on the basis of triaxial tests. However, testing procedures under plane strain conditions are preferred because they are the most practical approaches to studying the behaviour of reinforced soil walls.

2.7.2 Cellular reinforcement

Khedkar & Mandal (2009) proposed a three dimensional cellular reinforcement for reinforced soil applications. Their experimental study, as well as the finite element analysis for the pull out response of cellular reinforcements under low normal pressures indicated that cellular reinforcement performed better than the planar arrangement. Yet, in order to incorporate the advantages of upcoming cellular types of reinforcement in reinforced soil retaining walls, a systematic study of cellular reinforcement for its pull out characteristics under working surcharge pressures was a prerequisite. Their study aimed at understanding the interaction between soil and cellular reinforcement under working surcharge pressures. Laboratory pull out tests with different heights of cellular

reinforcements were conducted under normal pressures of 75 kPa and 100 kPa. A dimension optimisation analysis for cellular reinforcement was carried out. The laboratory test results were compared with the results from the finite element method with help from the computer software program 'PLAXIS V8'. A theoretical analysis with respect to the ultimate pull out resistance for cellular reinforcement was presented by introducing a reduction factor.

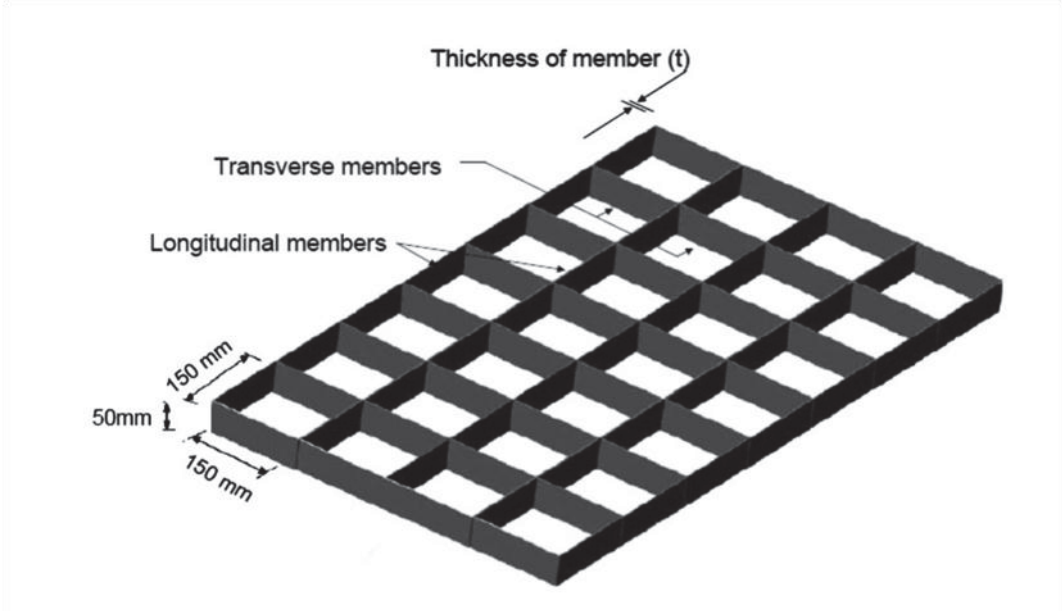

Figure 2.40 Cellular reinforcement (Khedkar & Mandal 2009)

A three dimensional cellular reinforcement can be used instead of a conventional, horizontal two dimensional reinforcement into a reinforced soil retaining wall. Figure 2.40 shows a typical cellular reinforcement where the longitudinal members are connected perpendicular to transverse members of equal height. Various materials such as steel, polypropylene, and high density polyethylene, etc. can be used to manufacture such reinforcement. Compared to planar reinforcement, a new dimension in the form of the height of reinforcement makes cellular reinforcement stiffer, allowing low modulus materials to be used for manufacturing purposes. Depending upon their longitudinal

spacing, the increased height of transverse members anticipates good bearing resistance in pull out situations of cellular reinforcement (Khedkar & Mandal 2009).

The results of the pull out test were analysed in terms of load displacement curves for all seven types of reinforcements under normal pressures. In order to account for the pull out resistance offered by inserted grips and soil, pull out tests were conducted with grips alone, i.e., without any reinforcement and under the same normal pressures of 75 kPa and 100 kPa. The pull out forces due to grips, were measured at each level of displacement and then subtracted from the pull out force measured in the test with sheet reinforcement and cellular reinforcements at the same displacement. This procedure was analogous to accounting for the grip resistance in an internal clamping system, and was used by Moraci and Recalcati (2006).

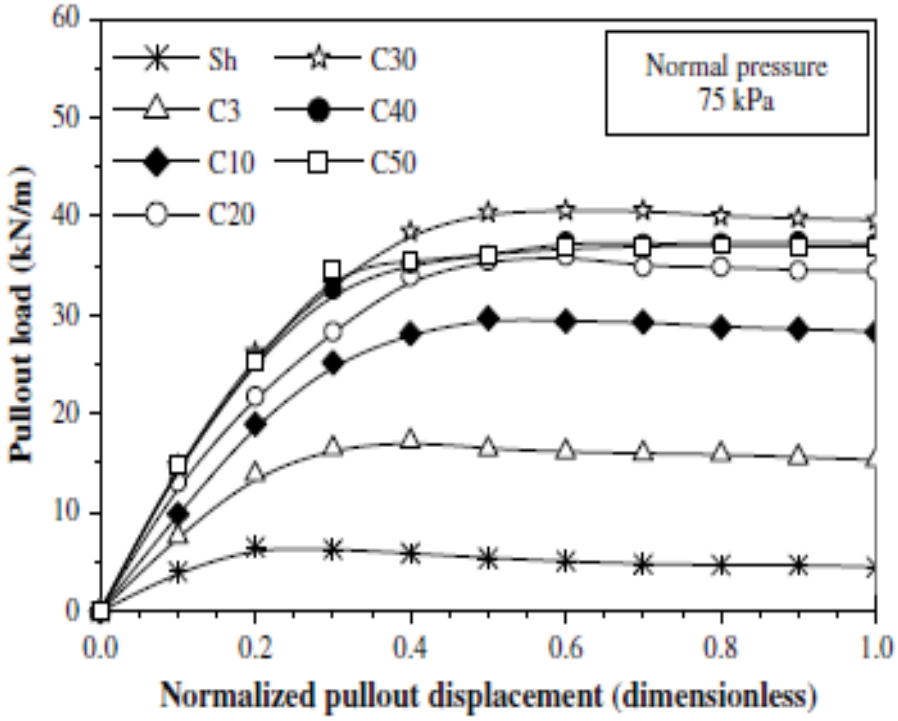

(a) 75 kPa normal pressure

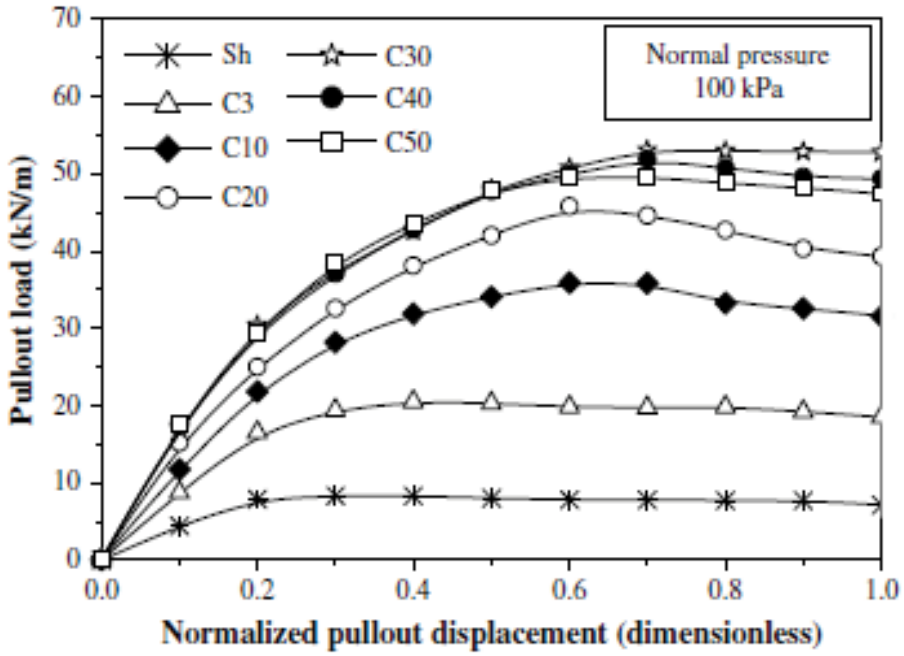

(b) 100 kPa normal pressure

Figure 2.41 Pullout load versus displacement curve comparison for various reinforcement heights (Khedkar & Mandal 2009)

Figure 2.41 represents the variation of load versus normalised displacement for various heights of reinforcement under normal pressures of 75 kPa and 100 kPa. Pull out displacement was normalised with the dimension of the longitudinal cell. In case of tests conducted at 75 kPa of normal pressure for all the reinforcement, it was observed that the pull out load increases initially with an increase in normalised pull out displacement to a particular normalised displacement (0.2 - 0.7), after which the pull out load decreased with an increase in displacement. The sheet reinforcement showed the minimum ultimate load amongst all the reinforcements whereas the 30 mm high cellular reinforcement showed a maximum ultimate load. The pull out load displacement curves for 3 mm high reinforcement (C3) performed better than sheet reinforcement (Sh), but its pull out performance was less when the reinforcements were 10 mm high and above. The pull out load displacement curves for C30, C40, and C50 were close to each other. Whereas C40 showed less ultimate resistance than C30, C50 had the least ultimate

resistance of the three. These results were quite different from those expected before the test; where it was expected that an increase in the height of cellular reinforcement would increase the ultimate resistance. The cause might be attributed to interference by the transverse members because of their increased height. Similar observations were found for the case of pull out load displacement curves at 100 kPa normal pressure (Figure 2.41b). Moreover, the ultimate pull out load increased for all seven types of reinforcement tested at 100 kPa normal pressure compared to 75 kPa normal pressure. Cellular type geometry reinforcement performed better in pull out behaviour than the planar, two dimensional reinforcement used under normal pressures of 75 kPa and 100 kPa. For further details refer to Khedkar & Mandal (2009).

2.7.3 Multi-layer horizontal–vertical orthogonal elements

A new concept of soil reinforcement with specific types of horizontal–vertical (H–V) orthogonal reinforcing elements, as one specific example of 3D inclusions, was proposed by Zhang, Javadi & Min (2006, 2008). Typical soil structures reinforced with H–V orthogonal reinforcing inclusions for in situ applications are shown in Figure 2.42a. Most of reinforced soil structures were built under (or close to) plane strain conditions. However, a triaxial test under axi-symmetric conditions was one of the important methods used to investigate the effects of H–V orthogonal reinforcing inclusions on the mechanical behaviour of reinforced sand. Therefore, 52 series of triaxial tests were carried out by Zhang, Javadi & Min (2006) on sand reinforced with two-layers H–V orthogonal inclusions and vertical elements. A comparison was made between the shear strength of soil reinforced with horizontal reinforcements and with H–V orthogonal inclusions. Based on the experimental results, the interaction of H–V orthogonal reinforcing elements with soil has been analysed. Using the limit equilibrium theory, a strength model has been developed for soil reinforced with multi-layer H–V

orthogonal inclusions. The results of a prediction by the proposed model have been compared with those obtained from the triaxial tests. It has been shown that the results of an analytical solution have been in good agreement with results from the triaxial tests.

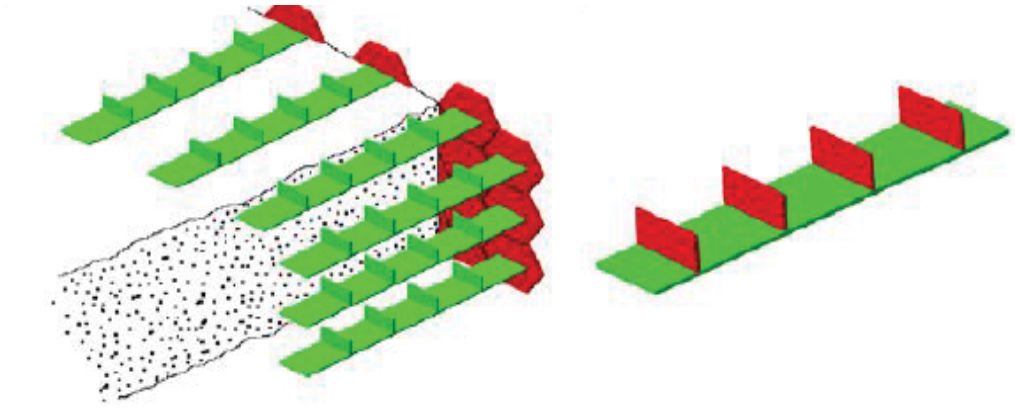

(a) Reinforced soil structure (b) Single-sided

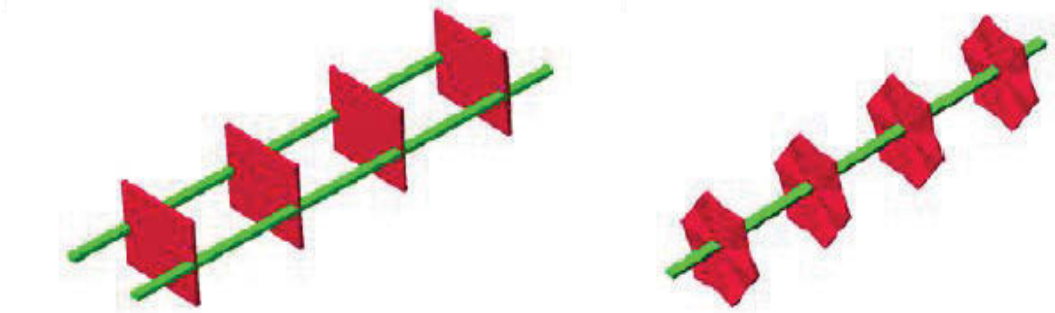

(c) Vertical reinforcements (d) Axial denti-hexagonal reinforcements

Figure 2.42 Typical horizontal–vertical orthogonal reinforcing elements (Zhang et al. 2008)

As reported by Zhang et al. (2008), in soils reinforced with H–V orthogonal reinforcing inclusions as well as conventional horizontal reinforcement, vertical reinforcing elements were also laid in the soil. The main configurations of H–V reinforcements were divided into three categories:

(1) Vertical reinforcements were laid upon conventional horizontal reinforcements in the soil; these were typically rectangular or hexagonal in shape, as shown in Fig. 2.42b.

(2) Vertical inclusions were laid in soil without any horizontal reinforcements; these were grid and ring shape reinforcements. Geocell was one special example of this type of H–V reinforcement. These vertical inclusions can be connected to each other by a series of rigid bars, as shown in Figure 2.42c.

(3) Axial denti-reinforcements were laid in soil, as shown in Figure 2.42d; these were typically rectangular or hexagonal in shape. The influence of denti-reinforcements was different from conventional ribbed inclusions. Apart from the frictional resistance, the former will provide passive resistance against shearing that will increase the strength and stability of the reinforced soil, while the latter mainly enlarges frictional resistance. Typical stress-strain curves for sand reinforced with H‑V orthogonal inclusions were presented in Figure 2.43. These figures indicate that the maximum deviator stress increases with increasing the vertical reinforcing ratio (μ_v), which is expressed by percent as follows:

$$\mu_v = \frac{r_0 \sum_{i=1}^{n} H_i}{rh} \times 100\% \tag{2.1}$$

where, n is the number of reinforcing layers; H_i is the height of vertical reinforcements at each layer; r_0 is the radius of vertical reinforcements; h is the height of specimen; r is the radius of specimen.

The peak strength for most specimens occurred at an axial strain of about 1.5‑3%.

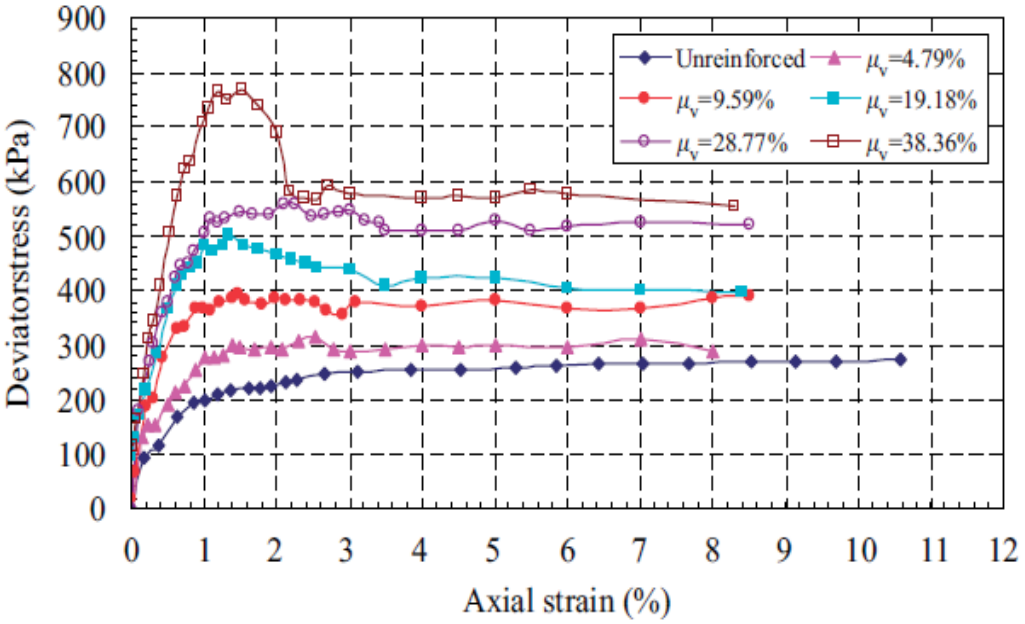

(a) Vertically reinforced ($\sigma_3 = 100\ kPa$)

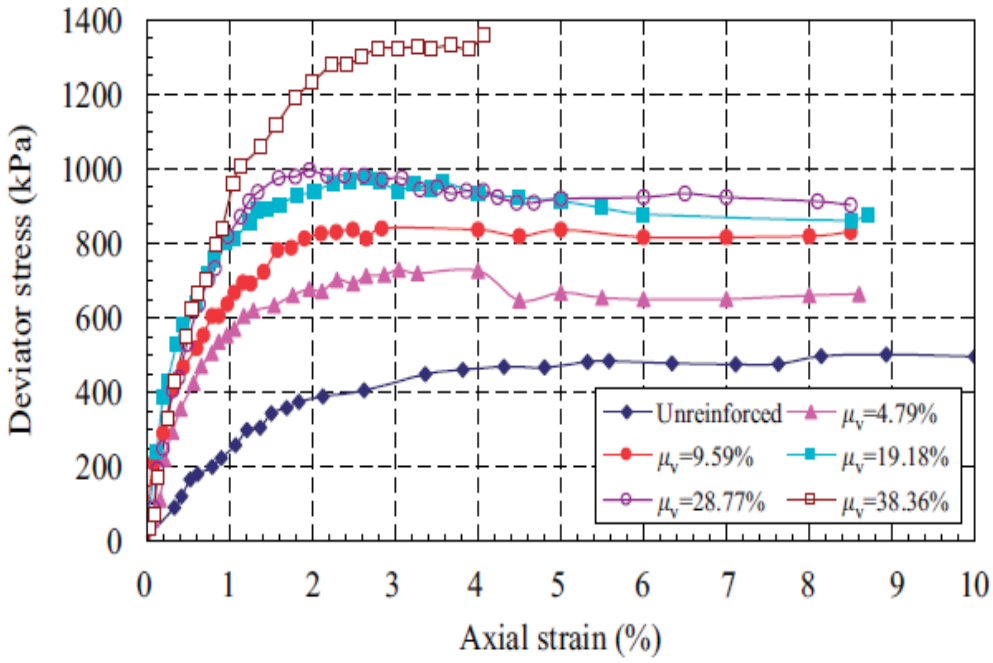

(b) Vertically reinforced ($\sigma_3 = 200\ kPa$)

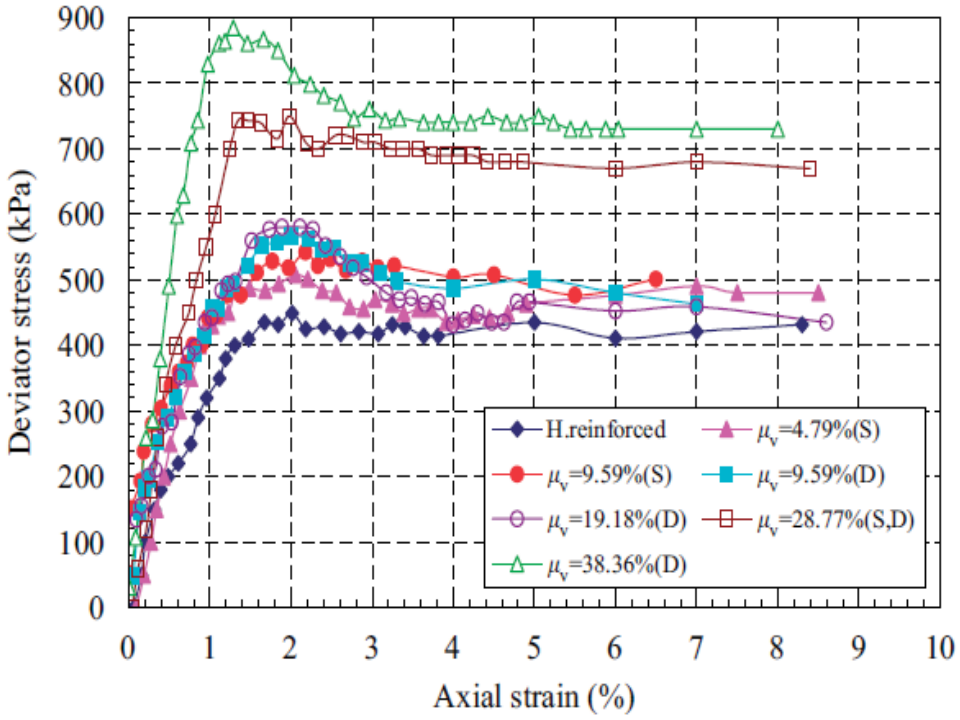

(c) H–V reinforced ($\sigma_3 = 100\ kPa$)

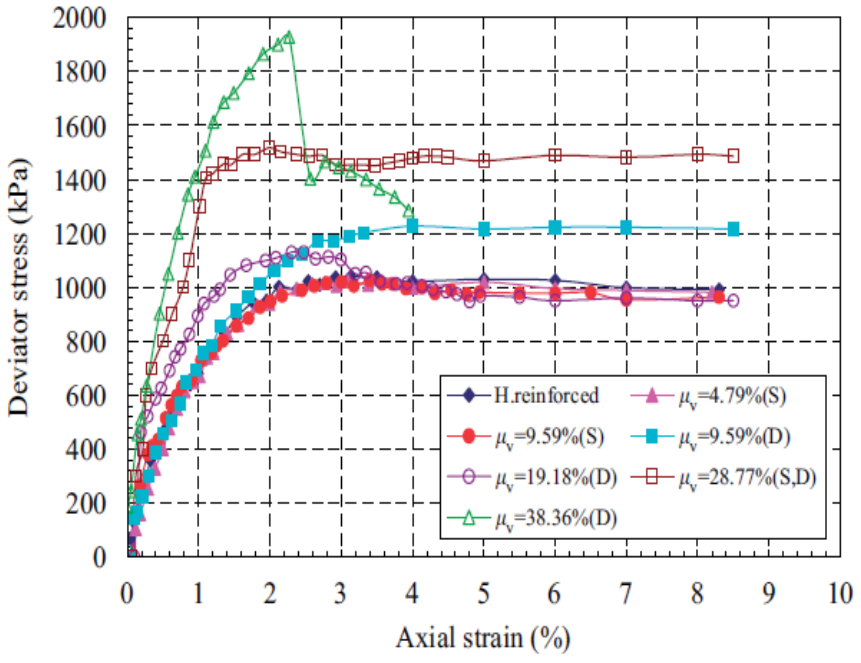

(d) H–V reinforced ($\sigma_3 = 200\ kPa$)

Figure 2.43 Deviator stress–axial strain curves for sand reinforced with vertical and H–V reinforcing elements with different reinforcement ratios and confining pressures (Note: S-single-sided and D-double-sided) (Zhang et al. 2008)

As mentioned by Zhang et al. (2008), the following conclusions were drawn from the results:

(1) The experimental results indicated that the inclusion of H-V orthogonal reinforcing elements (especially the double sided H-V elements) led to an increase in the angle of internal friction of the soil as well as a slight increase in the apparent cohesion.

(2) The strength of sand reinforced with H-V orthogonal elements increased with an increasing height of the vertical reinforcements.

(3) For sand reinforced with H-V orthogonal elements and with the same vertical height, double sided H-V orthogonal elements would result in a greater increase in strength than single sided ones.

(4) It was shown that the results of analytical predictions by the proposed strength model for soil reinforced with H-V orthogonal elements were in good agreement with the results of triaxial tests.

2.8 Summary

This chapter has outlined recent studies comprising the case histories of post earthquake investigations on the field performance of GRS retaining structures, shake table experiments, and numerical modelling of GRS walls. The key elements of GRS wall to improve seismic performance have been summarised followed by the research in the three dimensional reinforcement.

Well documented case histories on the seismic performances of GRS retaining structures in the field is extremely limited due to insufficient information regarding input ground motion, material properties, boundary conditions, construction details, and pre-earthquake static performances. However, GRS retaining walls performed well

during the 1989 Loma Prieta earthquake, 1994 Northridge earthquake, and 1995 Hyogo-Ken Nanbu, Japan earthquake. The high seismic stability of GRS retaining walls observed in the USA and Japan may be due to the conservation built into the design procedure. However, the failure of GRS retaining walls reported in 1999 Chi-Chi, Taiwan earthquake, 2001 El Salvador earthquake, and 2001 Nisqually earthquake indicated that inadequate design considerations and poor construction quality control can render GRS structures vulnerable to severe ground motions. Some probable causes of failure include: (1) insufficient compaction of the backfill, (2) weak foundation material, (3) large spaces between the reinforcement, and (4) additional overturning load from the add-on structures.

Shake table experiments, both reduced scale and full -scale models seated on laboratory shake tables, have been reported to investigate the seismic performance of soil structures reinforced with geosysnthetics. Reduced scale model testing using shake tables is the most common approach used to gain qualitative and quantitative insights into the seismic behaviour of reinforced soil wall systems. To better simulate the stress conditions experienced by the full scale prototype, other researchers have used dynamic centrifuge tests to examine the seismic performance of reinforced soil walls and embankments. It can be noted that a full scale model is preferred over a reduced scale model because it is not necessary to be concerned about the similitude model and boundary effects that are often encountered in reduced scale models and centrifuge testing. The implications resulting from the shake table test and centrifuge test to the seismic design and analysis of reinforced soil structures have been summarised. Furthermore, the models can be used to develop and validate numerical codes that can in turn be used to investigate the response of walls at a prototype scale.

Numerical investigation on the seismic performance of a GRS wall is more economical than physical model tests. In addition, finite element numerical methods were much more rigorous than a conventional limit equilibrium approach because they satisfy the force-equilibrium condition, the strain-compatibility condition, and the constitutive material laws. The conclusions drawn from numerical investigations could either be implemented or served as supplements to the design guidelines. Both qualitative and quantitative performances could be obtained from numerical investigations. The influence of the length and stiffness of reinforcement on the seismic response of GRS walls were examined using several computer programs such as FLAC and PLAXIS.

The major factors for improving the behaviour of reinforced soil in earthquake loading have also been discussed in this chapter. The discussion has focused on facing rigidity, the arrangement and properties of reinforcement, conditions of the backfill and subsoil, and an overview of failure modes.

The research carried out using the three dimensional reinforcement has also been synopsised. The results of proposed strength model are compared with those obtained from the triaxial tests. It is shown that the results of prediction were in good agreement with those of the triaxial tests. However, these studies have been based on the partial inclusion of vertical elements and have not considered the performance of reinforced soil walls under dynamic loading.

The study of GRS walls after the previous large earthquakes recognised malfunctions of GRS walls and demands more research for the enhancement. In addition, due to limited lands in urban areas, researchers are consistently trying to introduce new kinds of reinforcing materials with different shapes and sizes, as well as better external and internal design strategies for reinforced soil structures. This research presents a new system of soil reinforcement using vertical elements to connect layers of conventional

horizontal reinforcement to each other for the improvement of the seismic performance behaviour of reinforced soil walls.

Chapter 3

3. Theoretical Consideration of Vertical Reinforcement

3.1 Introduction

The technique of reinforcing soil is a thousand year old concept where many different types of reinforcing materials have been used, from bamboo to steel strips, and from tree branches to geogrids. Several research have been carried out on the performance of reinforced soil, such as investigations into variations of the planar surface of geogrids and the use of fibre as reinforcement. The behaviour of soils reinforced with fibre has been studied widely, particularly the consideration of reinforcement embedded perpendicularly or inclined to the shear zone in a shear box, in order to study the behaviour of dry sand reinforced with different types of fibres (Kumar, Walia & Mohan 2006; Michalowski & Cermak 2003; Prabakar & Sridhar 2002; Yetimoglu & Salbas 2003). Gray & Ohashi (1983) considered reinforcement embedded perpendicularly or at an inclination to the shear zone in a shear box. A series of laboratory investigations were carried out by Arenicz & Choudhury (1988) to study the effects of different types of randomly distributed reinforcing elements on the strength of the soil.

Besides the study of conventional reinforced soil where the reinforcement is placed horizontally, Zhang, Javadi & Min (2006) carried out a series of triaxial tests to study the behaviour of sand reinforced with a single layer three dimensional inclusion. From these tests the effects of the height of the vertical reinforcement, the stiffness of the

reinforcing materials and the confining pressure on strength of the reinforced sand were discussed. The three dimensional inclusions consisted of conventional horizontal reinforcing stripes and vertical reinforcing elements (rectangular or triangular shapes), and are shown in Figure 3.1 for in situ applications.

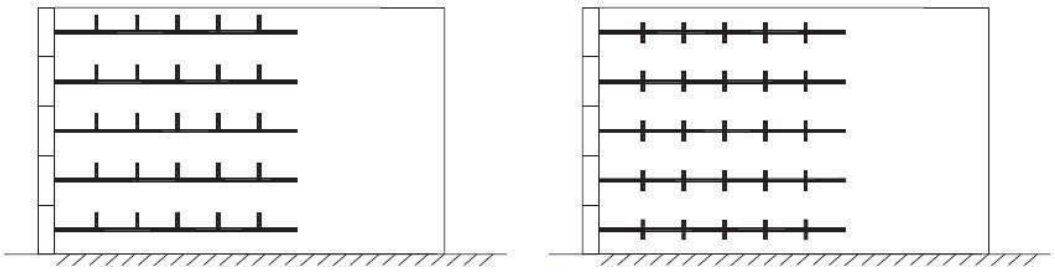

(a) Horizontal and single-vertical (b) Horizontal and double-vertical

Figure 3.1 Typical 3D reinforced soil structures (after Zhang, Javadi & Min 2006)

This chapter provides a novel concept of vertical reinforcement and its theoretical development for vertical reinforcement for building retaining walls. This section presents the current analytical approaches used for seismic analysis and design, followed by possible improvement on the behaviour of reinforced soil to strengthen it against different modes of failures. In addition, the probable field construction techniques used to insert the vertical reinforcements are discussed.

3.2 Current Analytical Approaches for Seismic Analysis and Design

The first analytical study on the influence of seismic induced forces on the stability of earth retaining structures can be traced to the work of Sabro Okabe in his milestone paper (Okabe 1924). In this seminal work, there was significant of research on the development of analytical methods that considered the potentially large forces that exert additional destabilising forces on earth retaining walls, slopes, dams and embankments

during earthquakes. The vast majority of this work focused on conventional earth structures, but with the growing use of geosynthetics in reinforced soil walls, slopes and embankments, the need to extend current methods of analysis for conventional structures under seismic loading to geosynthetic reinforced systems in similar environments has been taken into consideration. In this section the advantages of the inclusion of vertical reinforcement together with horizontal reinforcement is discussed. Different approaches are considered, such as extending the conventional limit equilibrium methods of analysis for earth structures, to including destabilising body forces related to the assumed horizontal and vertical components of ground acceleration.

3.2.1 Mononobe-Okabe approach

The magnitude of the dynamic force increment due to shaking can be evaluated using the Mononobe-Okabe approach (Mononobe & Matsuo 1929; Okabe 1924) in the external seismic stability analysis, which is an extension to the conventional Coulomb sliding wedge theory, where the effects of lateral inertia forces on the retained soil mass are integrated. As in the static case, the soil at the rear is considered to be in limit equilibrium exerting a horizontal force onto the reinforced soil block. Because the soil block is a monolithic unit, this external force is simply applied to the reinforced block and the conditions regarding external stability are calculated. With an internal design, the sideways inertial force applied onto the potentially sliding block (active zone) is estimated from the seismic coefficient (k_h). Under static forces and this additional dynamic force, pull out and rupture are checked.

In earthquake engineering practice, the Mononobe-Okabe approach is common, since the Coulomb wedge analysis is extended to include horizontal and vertical inertial forces due to the ground shaking. The geometry and force diagram associated with this method is shown in Figure 3.2. The backfill retained by the wall is assumed to be in an

active mode of failure under its own weight and inertial forces due to ground acceleration. Both the retaining structure and the retained backfill act as rigid bodies with maximum shear stress along the potential sliding surface.

According to Whitman (1990), the dynamic pressures on earth retaining structures are a complex problem of interaction between soil and structure, so he suggested that peak dynamic stresses should be a main concern in design. The Mononobe-Okabe approach fails to represent the actual dynamic behaviour, but it is a scheme to relate dynamic earth pressures to a possible state of failure.

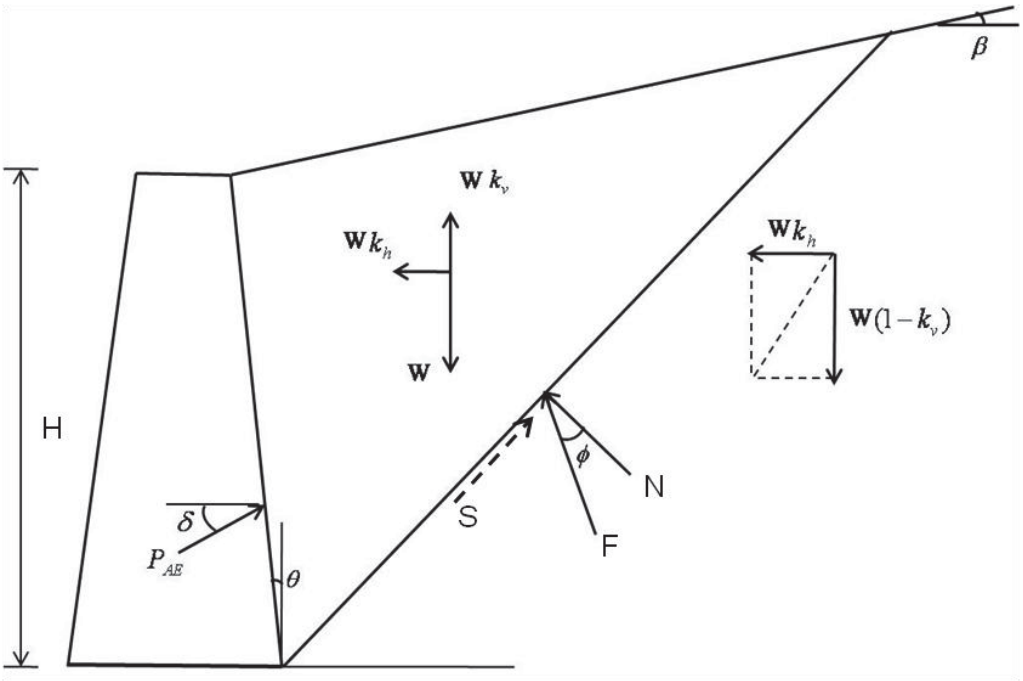

Figure 3.2 Mononobe-Okabe approach (Note: W = weight of the wedge, S and N = shear and normal forces, F = resultant of S and N)

The magnitude of the dynamic earth force is correlated to the static earth pressure by a coefficient k_h which is based on the maximum ground acceleration. In the Mononobe-Okabe method the total active earth force (P_{AE}) is calculated by:

$$P_{AE} = \frac{1}{2}\gamma H^2[(1 \pm k_v)K_{AE}] \quad (3.1)$$

where γ is the unit weight of the retained soil and H is the height of the wall, and K_{AE} is the total earth pressure coefficient. The vertical acceleration coefficient k_v will have a plus sign when acting downwards and a minus sign when acting upwards. In most cases, the vertical ground acceleration is taken as acting upwards, thus reducing the total active earth pressure, while in some cases it is ignored completely. The same sign convention is applied to the total earth pressure coefficient formula. The total earth pressure coefficient for a cohesionless dry backfill can be calculated using Equation 3.2.

$$K_{AE} = \frac{\cos^2(\phi-\psi-\theta)/\cos\psi\cos\psi^2\theta\cos(\psi+\theta+\delta)}{\left[1+\sqrt{\frac{\sin(\phi+\delta)\sin(\phi-\psi-\beta)}{\cos(\beta-\theta)\cos(\psi+\theta+\delta)}}\right]^2} \quad (3.2)$$

where,

ϕ = the friction angle of the retained soil

δ = the mobilised interface friction angle between the back of the facing wall and the backfill soil (or the mobilised interface friction angle between the back of the reinforced soil zone and the retained soil, in case the reinforced earth wall system is treated as a monolithic structure)

θ = the angle of inclination of the inside face of the wall to the vertical (or batter angle of the back of the MSE wall)

β = the angle of the back slope

ψ = the angle of seismic inertia given by

$$\psi = \tan^{-1}\left(\frac{k_h}{(1-k_v)}\right)$$

The horizontal component of total active thrust is ($P_{AE\text{-}HOR}$):

$$P_{AE-HOR} = \frac{1}{2}\gamma H^2[(1-k_v)K_{AE}]\cos(\delta+\theta) \quad (3.3)$$

The parameters k_h and k_v are the horizontal and vertical seismic coefficients, respectively. These parameters are expressed as a fraction of the gravitational acceleration g.

3.2.2 Parameters of the dynamic behaviour of reinforced soil walls

When the layers of soil are vibrating due to an earthquake, the stress-strain hysteresis loop may be obtained based on a non-linear elastic curve, as shown in Figure 3.3.

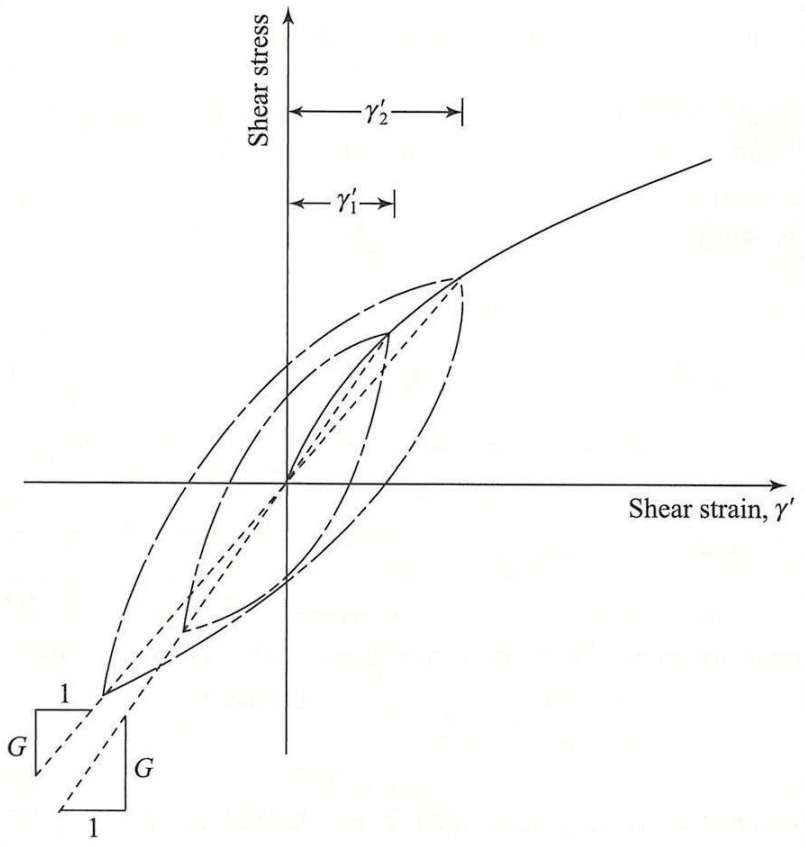

Figure 3.3 Shear stress-strain characteristics of soil (Das & Ramana 2009)

In earthquake related problems, the level of shear strain has a significant effect on the shear moduli and damping ratio of soils. As the magnitude of shear strain increases, the value of the shear modulus G, of a soil decreases (Figure 3.4), and the damping ratio increases. According to Figure 3.4, it can be inferred that the value of the maximum shear modulus G_{max}, is for a very small strain (i.e. measurement of field wave velocity).

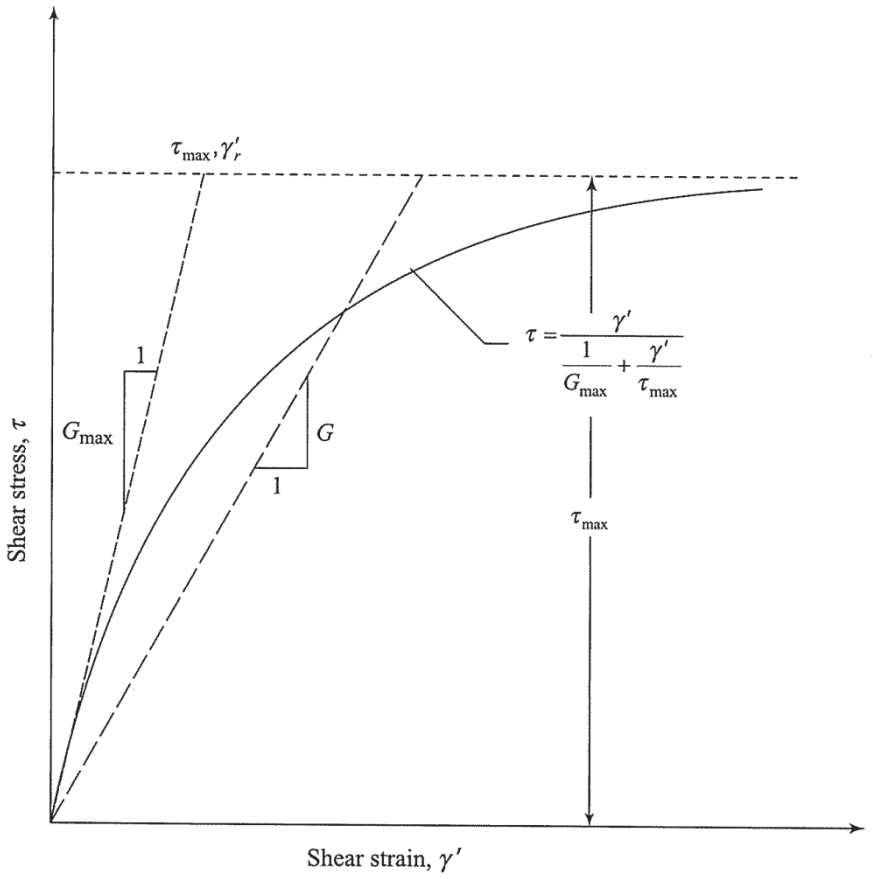

Figure 3.4 Nature of variation of shear modulus with strain (after Hardin & Drnevich 1972)

Estimation of Shear Modulus: Based on several experimental observations, Hardin and Drnevich (1972) proposed a generalised method where the variations of shear stress against strain of all soils can be approximated by a hyperbolic relationship (Figure 3.4).

$$\tau = \frac{\gamma'}{1/G_{max} + \gamma'/\tau_{max}} \tag{3.4}$$

where τ is the shear stress, γ' is the shear strain, initial tangent modulus $G_{max} = \frac{\tau_{max}}{\gamma'_r}$, γ'_r is the reference strain and τ_{max} is the maximum shear stress at failure.

Estimation of Damping Ratio: Hardin & Drnevich (1972) presented a relationship between the damping ratio and shear modulus as:

$$D = D_{max}\left(1 - \frac{G}{G_{max}}\right) \tag{3.5}$$

where, D_{max} is the maximum damping ratio.

After the inclusion of vertical reinforcement over conventional reinforcement, the value of the maximum shear stress τ_{max} rises as the apparent cohesion and the friction angle of the soil mass increases. This increased value of τ_{max} can boost the value of the shear stress τ, in dynamic loading, and the intactness of the soil mass by the connection of the reinforcing layers enlarges the damping ratio, according to Equation 3.5.

Wave Velocities: Das & Ramana (1995) presented the compression wave velocity, V_p, in a confined one-dimentional soil as a function of stiffness, E_{oed}, and the mass, ρ, as:

$$V_p = \sqrt{\frac{E_{oed}}{\rho}} \text{ where, } E_{oed} = \frac{(1-\nu)E}{(1+\nu)(1-2\nu)} \text{ and } \rho = \frac{\gamma}{g} \quad (3.6)$$

In which E= Young's modulus, ν = Poisson's ratio and g is the gravity acceleration (9.8 m/s^2).

A similar expression can be found for the shear wave velocity, V_s:

$$V_s = \sqrt{\frac{G}{\rho}} \text{ where, } G = \frac{E}{2(1+\nu)} \quad (3.7)$$

3.2.3 Internal stability calculations

Each layer of reinforcement holds part of the integrated earth pressure over a tributary area S_v, as illustrated in Figure 3.5, in pseudo-static/dynamic methods for walls that involve an assumed distribution of internal earth pressure. The magnitude of tensile force must be less than the allowable design load in the reinforcement based on tensile over stressing, strength of the facing connection and the pull out capacity of the layer. Figure 3.5 also shows that the inertial force due to the tributary portion of the facing column should be added to the reinforcement forces under seismic loading in the case of segmental walls. An important implication of the assumed distribution of earth pressure

using the pseudo-static M-O method explained earlier, is that the relative proportion of the load to be carried by the layers of reinforcement nearest to the crest of a wall with uniformly spaced reinforcement increases with increasing horizontal acceleration. Bathurst & Hatami (1998) suggested that a greater number of layers towards the top of the wall are required than is necessary for static load environments. A similar conclusion was made by Vrymoed (1989) using a tributary area approach which assumes that the inertial force carried by each layer of reinforcement increases linearly with height above the toe of the wall for equally spaced layers of reinforcement. Nevertheless, Bonaparte, Schmertmann & Williams (1986) concluded that higher strength reinforcement together with reduced factors of safety used for seismic loading cases would often result in no requirement to increase the layers of reinforcement used for static loading cases.

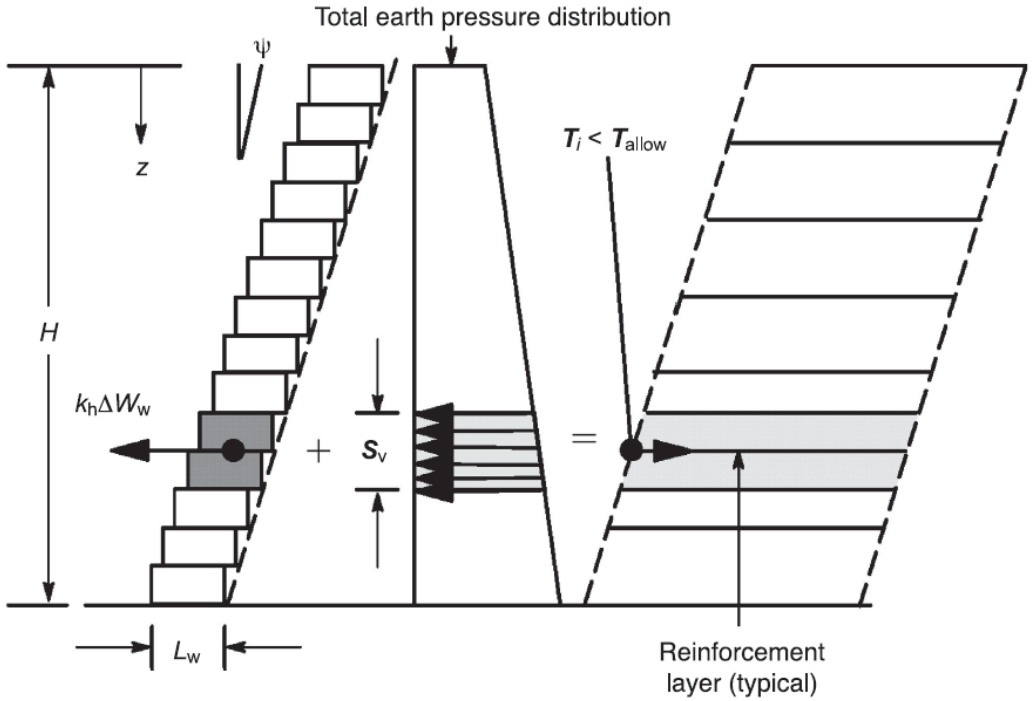

Figure 3.5 Calculation of tensile load, Ti, in a reinforcement layer due to dynamic earth pressure and wall inertia for segmental retaining walls (after Bathurst & Cai 1995)

The FHWA (1996) guidelines recommend the procedures shown in Figure 3.6 to assign reinforcement forces for over stressing and pull out calculations. The dynamic earth force is calculated as $\Delta P_{dyn} = k_h W_A$, where W_A is the weight of the static internal failure wedge. The distribution of the dynamic tensile reinforcement load increment ΔT_{dyn}, is weighted based on the length of total anchorage h in the resistance zone according to:

$$\Delta T_{dyn\,i} = \Delta P_{dyn} L_{ai} / \sum_{j=1}^{N} L_{aj} \tag{3.8}$$

where, N is the number of reinforcement layers and L_a is the length of the anchorage.

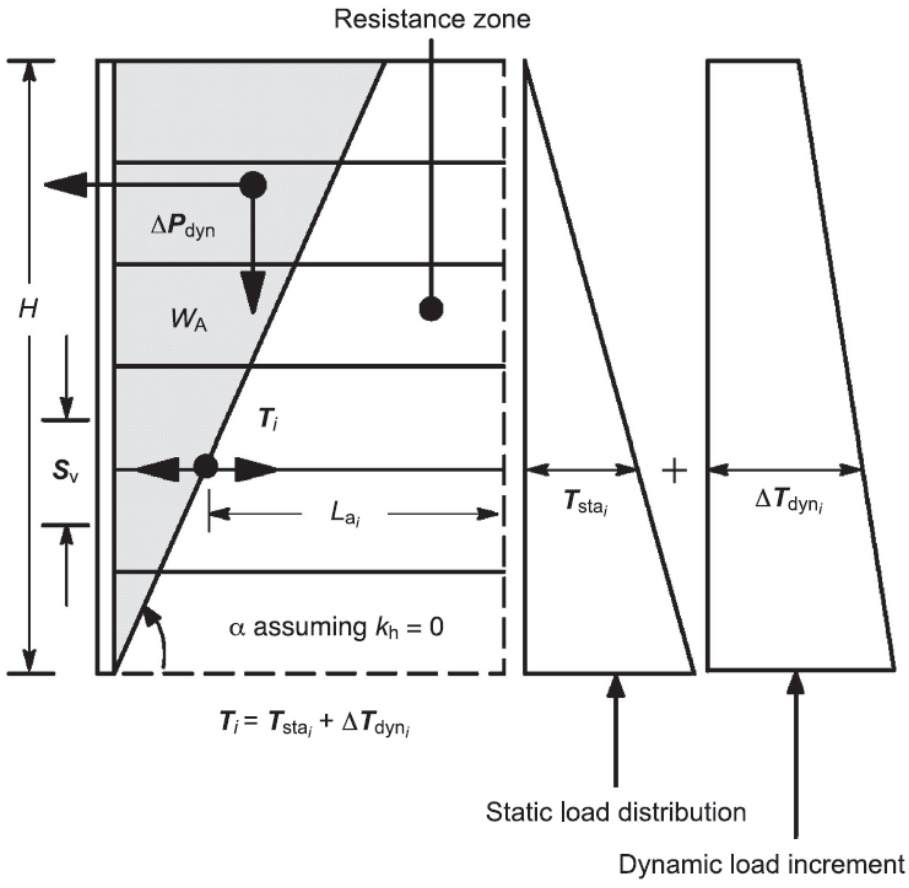

Figure 3.6 Calculation of tensile load, Ti, in a reinforcement layer for reinforced soil walls with extensible reinforcement (FHWA 1996)

3.2.4 Two-part wedge failure mechanism

The general solution for a trial, two part wedge failure mechanism in a slope subjected to horizontal and vertical acceleration is shown in Figure 3.7. The horizontal and vertical forces P_1 and V_1 acting on wedge 2 from wedge 1 are, respectively:

$$P_1 = \frac{(1 \pm k_v)W_1 + B_1 A_1 k_h W_1}{\lambda \tan\phi_f + B_1 A_1} \tag{3.9}$$

$$V_1 = \lambda P_1 \tan\phi_f \tag{3.10}$$

where,

$$A_1 = \frac{1}{\sin\theta_1 - \tan\phi_f \cos\theta_1} \tag{3.11}$$

$$B_1 = \tan\phi_f \sin\theta_1 - \cos\theta_1 \tag{3.12}$$

The quantity λ is the inter-wedge shear mobilisation ratio that varies over the range $0 \leq \lambda \leq 1$. Parameter ϕ_f is the factored soil friction angle expressed as:

$$\phi_f = \tan^{-1}(\tan\phi / FS) \tag{3.13}$$

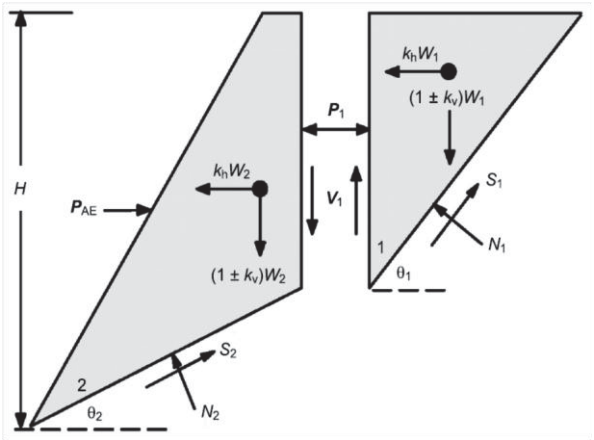

(a) Free-body diagram

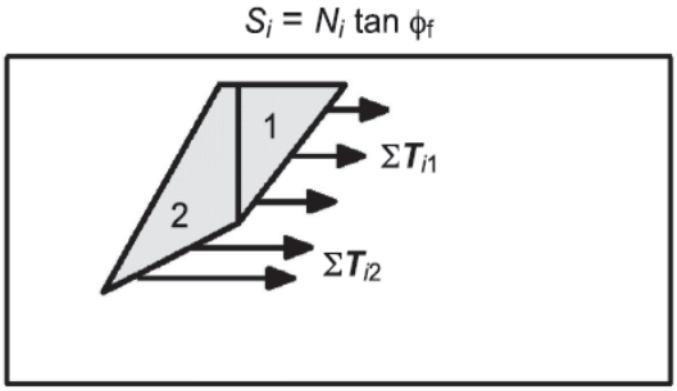

(b) With reinforcement forces

Figure 3.7 Two-part wedge analysis (after Bonaparte, Schmertmann & Williams 1986)

The horizontal out-of-balance force P_{AE}, is calculated as:

$$P_{AE} = P_1 + k_h W_2 - B_2 A_2 [(1 \pm k_v) W_2 + V_1] \quad (3.14)$$

where,

$$A_2 = \frac{1}{\sin\phi_f \sin\theta_2 - \cos\theta_2} \quad (3.15)$$

$$B_2 = \tan\phi_f \cos\theta_2 - \sin\theta_2 \quad (3.16)$$

By setting FS = 1 (i.e. $\phi = \phi_f$), an equivalent total active earth pressure coefficient for the most critical trial geometry (i.e. trial search that yields a maximum value for P_{AE} in the slope) can be calculated as:

$$K_{AE} = 2P_{AE}/\gamma H^2 \quad (3.17)$$

This approach has been used by Bonaparte, Schmertmann & Williams (1986) to generate seismic design charts for soil slopes reinforced by geosynthetics. The total design strength of the horizontal layers of reinforcement is taken as $\sum T_i = P_{AE}$. The two-part wedge approach with $\lambda = 0$ is used by the Geogrid Research Board (GRB 1990) to calculate K_{AE} according to Equations 3.14 and 3.17 for calculating internal stability.

The two-part wedge analysis degenerates to a single wedge analysis by restricting trial searches to $\theta_1 = \theta_2$ and setting $\lambda = 0$. All three solutions (M-O, single and two-part wedge) give the same solution for the horizontal component of total earth force when $\lambda = \Psi = 0$. In addition, direct sliding mechanisms, including those generated at the base of the reinforced soil mass or along the layers of reinforcement can be analysed using the two-part wedge approach.

An alternative strategy that extends the general approach used by Woods & Jewell (1990) for statically loaded slopes to the seismic case (Bathurst & Cai 1995) is to rewrite Equation 3.14 as:

$$P_{AE} = P_1 - \frac{B_1 A_1 \sum T_{i1}}{\lambda \tan\emptyset_f + B_1 A_1} + k_h W_2 - \sum T_{i2} - B_2 A_2 [(1 \pm k_v) W_2 + V_1] \quad (3.18)$$

The factor of safety (FS) for a given two-part wedge geometry corresponds to the value of FS that yields $P_{AE} = 0$. The factor of safety for a slope corresponds to the minimum value of FS from a search of all potential failure geometries. Equation 3.18 shows that the value of FS against collapse is independent of the location of the layers of reinforcement for $\lambda = 0$.

Ling, Leshchinsky & Perry (1996) developed design charts for calculating the strength and length of geosynthetic and reinforcement against direct sliding using a two-part wedge mechanism. Ling, Leshchinsky & Perry (1997) suggested that the direct sliding failure mode governs the length of reinforcement for lower layers as seismic acceleration increases. Tatsuoka et al. (1998) concluded that the two-part wedge geometry is a valid failure geometry for geosynthetic reinforced soil walls with a rigid full height facing and short lengths of reinforcement based on shake table tests. The pattern and location of the failure is controlled by the length of the reinforcement. Tatsuoka et al. (1998) proposed a modified two-part wedge method, and concluded that

the size of the failure wedge from the modified two-part wedge method was typically smaller than what would be predicted from conventional two-part wedge analysis, and more realistic according to experimental observations.

3.2.5 Log spiral failure mechanism

Log spiral failure mechanisms (Figure 3.8) have been applied to calculate the out-of-balance force to be carried by horizontal layers of reinforcement in slopes and walls under seismic loading (Leshchinsky, Ling & Hanks 1995). This method satisfies the moment equilibrium (i.e. the problem is statically determinate).

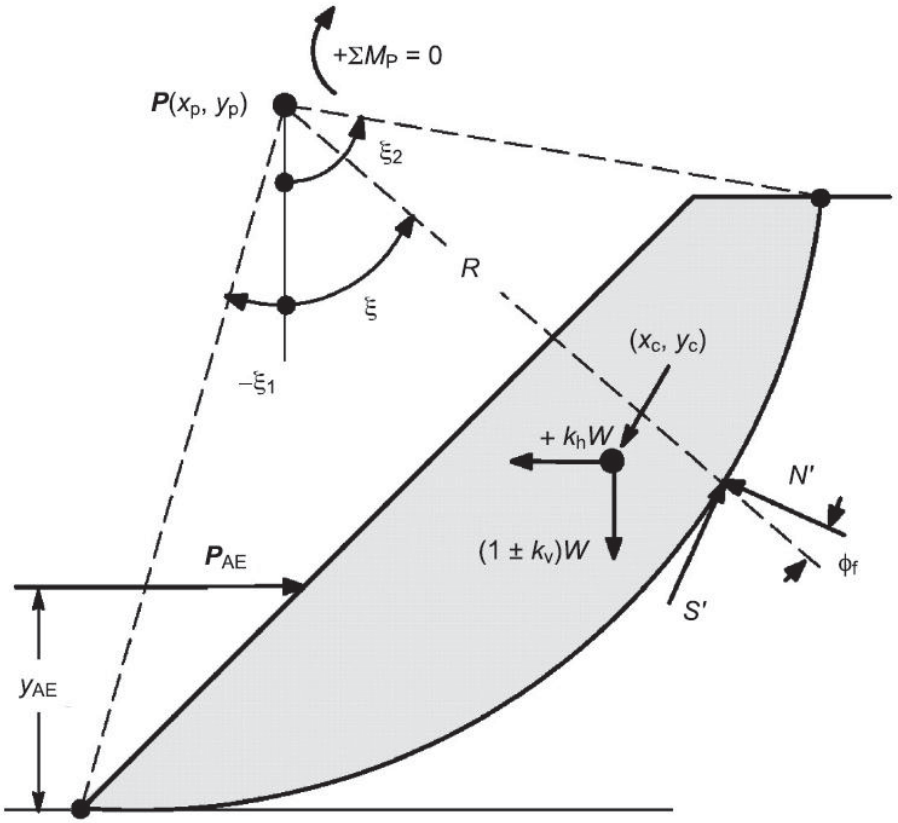

(a) Free-body diagram

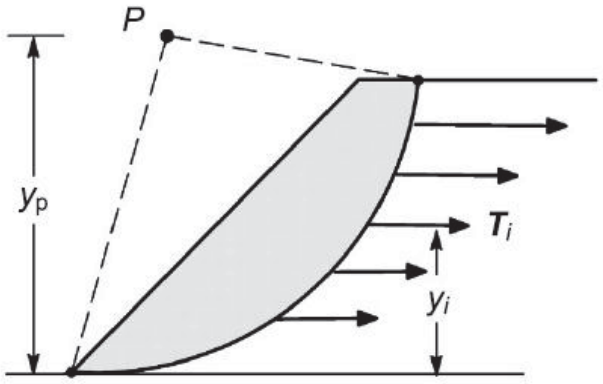

(b) With reinforcement forces

Figure 3.8 Log spiral analysis (after Leshchinsky, Ling & Hanks 1995)

The trace of a log spiral surface is given by:

$$R = Aexp^{\xi(-\tan\phi_f)} \tag{3.19}$$

where, ξ is an angle in radian as shown in Figure 3.8(a).

For an assumed surface (i.e. for any three independent parameters defining a log spiral, x_p, y_p and A), the moment equilibrium equation about the pole P can be explicitly written as:

$$\sum M_p = (1 \pm k_v)W(x_c - x_p) + k_h W(y_p - y_c) - P_{AE}(y_p - y_{AE}) = 0 \tag{3.20}$$

It should be noted that the moment about the log spiral pole is independent of the distribution of normal and shear stresses over the log spiral because their resultant must pass through the pole. The point of application for the components of seismic inertial forces is considered to be at the centre of the failure mass. The critical mechanism corresponds to a trace that produces the maximum value of P_{AE} required to satisfy Equation 3.20. Obviously the elevation y_{AE}, of the equivalent out-of-balance horizontal force P_{AE} affects the magnitude of P_{AE}. Here it is assumed a priori that $y_{AE} = H/3$. The

equivalent dynamic active earth pressure coefficient K_{AE} can be calculated using Equation 3.17 with FS = 1 (i.e.$\phi = \phi_f$).

In practice the factor of safety against the collapse of a reinforced slope can be determined by replacing $P_{AE}(y_p - y_{AE})$ with $\sum T_i(y_p - y_i)$ in Equation 3.20 and finding the minimum value for FS by searching all the potential failure geometries that yields $\sum M_p = 0$. This value corresponds to the minimum factor of safety for the reinforced soil slope (Leshchinsky, Ling & Hanks 1995). The formulation of Equation 3.20 illustrates that the FS against collapse is a function of the location of the layers of reinforcement.

Ling, Leshchinsky & Perry (1997) studied a log spiral failure pattern in tied back internal stability calculations, after which Ling & Leshchinsky (1998) then modified the method to calculate the stability and permanent displacement of geosynthetic reinforced soil walls under the combined effect of horizontal and vertical ground acceleration. They considered three different modes of failure, namely: (a) tie-back/compound failure, (b) direct sliding, (c) pull out, and also assumed a log spiral failure shape in their pseudo-static analyses of the tie-back/compound failure mechanism. As with all pseudo-static methods of analyses, it can result in a conservative design because a force momentarily induced by acceleration force is assumed to be acting permanently on the wall. However, they argue that an inherent conservatism in the method is required since possibility of amplified acceleration is disregarded.

3.2.6 Circular slip failure mechanism

Conventional methods of slices can be modified to account for the additional restoring moment due to the layers of reinforcement, and a general case can be referred to in

Figure 3.9. Moment equilibrium leads to the following equation to calculate the factor of safety against collapse:

$$FS = \frac{M_R + \Delta M_R}{M_D} \tag{3.21}$$

where, M_R is the moment resistance due to the shear strength of the soil, ΔM_R is the increase in moment resistance due to the reinforcement, and M_D is the driving moment. Introducing k_v into the derivations for Bishop's Simplified Method (e.g. Fredlund & Krahn 1976) results in the driving moment calculated as:

$$M_D = \sum W[(1 \pm k_v)R \sin \alpha + k_h y] \tag{3.22}$$

The moment resistance due to the cohesionless shear strength of soil is:

$$M_R = (1 \pm k_v)R \sum \left(\frac{W \tan \phi \sec \alpha}{1 + \tan \alpha \tan \phi_f} \right) \tag{3.23}$$

The additional resisting moment due to the tensile capacity of the reinforcement is calculated as:

$$\Delta M_R = R \sum T_i \cos(\varphi_i - \delta_i) \tag{3.24}$$

The summation term in Equation 3.24 considers the available force of tensile reinforcement in each layer (the lesser of tensile reinforcement strength based on over stressing or pull out) and the orientation δ_i of the force with respect to the horizontal.

For flexible geosynthetic reinforcement products, the restoring force T_i can be argued to act tangent to the slip surface at the incipient collapse of the slope, an assumption that leads to the summation term in Equation 3.24 becoming $\sum T_i R$. This approach is used in the FHWA (1996) guidelines together with $k_v = 0$. It is important to note that in the above formulation the influence of the reinforcement capacity T_i and the term for horizontal acceleration k_h on the sliding resistance of the base is not considered.

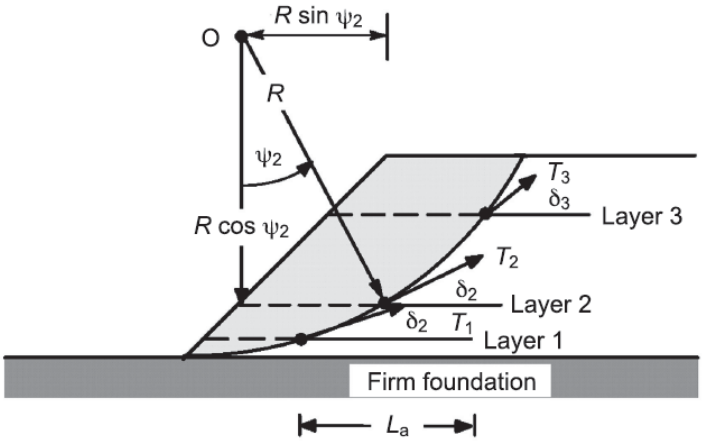

(a) Circular slip geometry

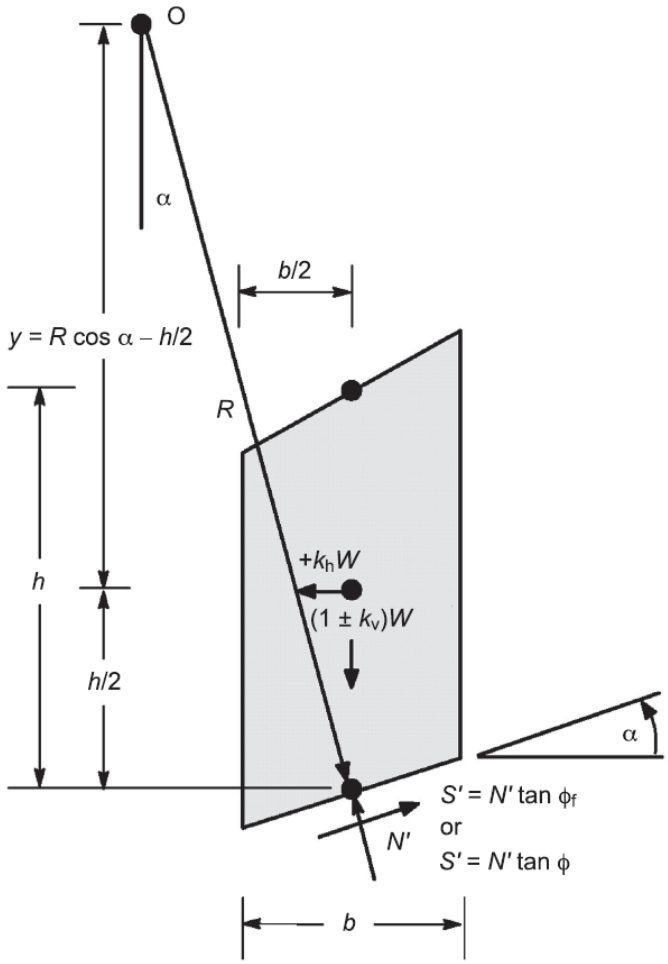

(b) Method of slices

Figure 3.9 Circular slip analysis (Fredlund & Krahn 1976)

An alternative strategy is to modify the `Ordinary Method' (e.g. Fredlund & Krahn 1976). In this approach the equations for vertical and horizontal equilibrium of slices include forces due to acceleration and reinforcement hence these parameters directly affect the base sliding resistance and the term for the resisting moment in Equation 3.21 becomes:

$$M_R = R\sum[(1 \pm k_v)W\cos\alpha - k_h W\sin\alpha]\tan\phi \quad (3.25)$$

And the incremental resisting moment due to the layers of reinforcement is:

$$\Delta M_R = R\sum T_i\,[\cos(\varphi_i - \delta_i) + \sin(\varphi_i - \delta_i)\tan\phi] \quad (3.26)$$

where, the summation term in Equation 3.26 is with respect to the layers of reinforcement. One advantage of the modified `Ordinary Method' is that the right hand side of Equation 3.21 is a linear function of FS. This approach is used by PWRI (1992) in Japan with $\delta_i = 0$ for retaining walls, and $\delta_i = \varphi_i$ for slopes. In the Japanese approach the distribution of the total reinforcement load is assumed to be uniform, with depth for slopes that are less than 45° from horizontal. For steeper slopes, including walls, the static portion of the reinforcement load required is assumed to increase linearly with depth below the crest, while the additional seismic portion is assumed to be distributed uniformly. FHWA (1996) guidelines allow the global factor of safety FS to be as low as 1.1 for the seismic design of slopes using pseudo-static methods.

3.3 Peak Ground Acceleration Coefficients

The pseudo-static M-O method depends entirely on the horizontal and vertical peak ground acceleration coefficients k_h and k_v, respectively. For engineering applications, k_v is often assumed to be two thirds of k_h (i.e., $k_v = {}^{2}/_{3}\,k_h$ Newmark and Hall 1982). However, in a typical seismic retaining wall design, state-of-practice is to assume that k_v equals zero and that k_h remains constant throughout the retaining structure (e.g. Day

2002). Furthermore, there is no consensus in determining the design value of k_h. Seed (1983) suggested that $k_h = 0.15$ be the maximum level ascribed to the limit equilibrium analyses, while Bonaparte, Schmertmann & Williams (1986) suggested that $k_h = 0.85A$, where A is the peak horizontal ground acceleration coefficient found in Section 3 of AASTHO Division I-A. Whitman (1990) recommended that k_h be ranged from 0.05 to 0.15, and Segrestin & Bastick (1998) suggested that k_h be found as:

$$k_h = (1.45 - A)A \quad \text{for } 0.05 \leq A \leq 0.5 \tag{3.27}$$

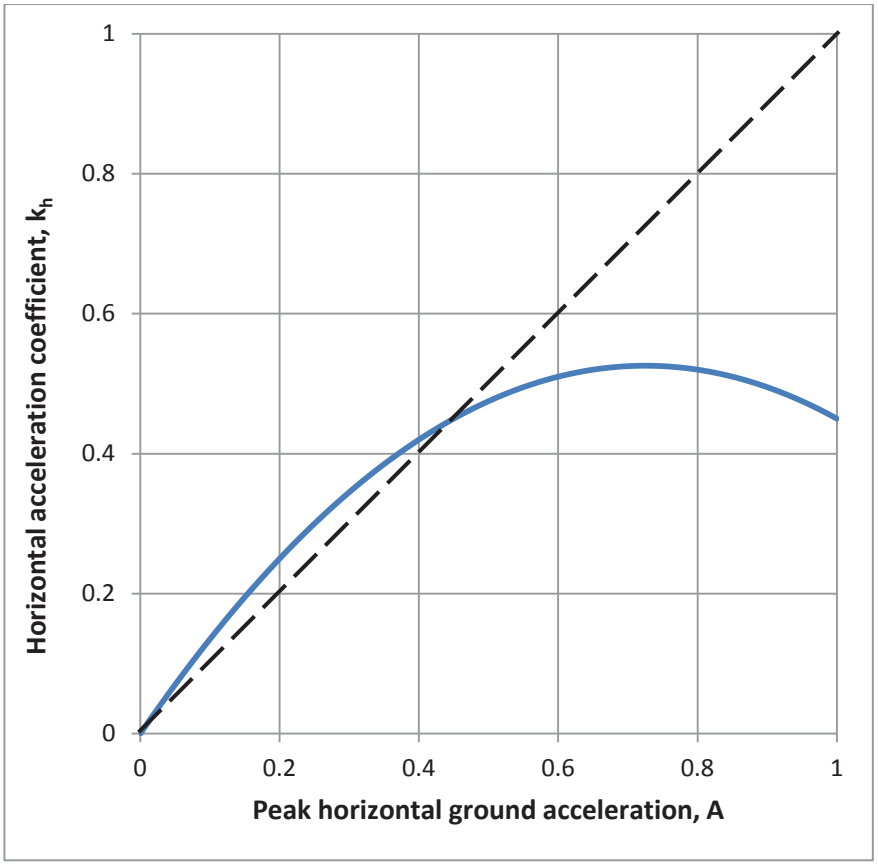

Figure 3.10 Relationship between A and k_h

Note that the above equation was incorporated in both the FHWA and NCMA manuals. Figure 3.10 shows the relationship between k_h and A as determined from Equation 3.27. As depicted in Figure 3.10, amplification of the peak horizontal ground acceleration is

observed for A<0.45. For A> 0.45, k_h is greater than A, and the maximum of the curve occurs at A = 0.725.

3.4 Conceptual Design of Vertical Reinforcement

In this study the conventional horizontal layers of reinforcement are connected using additional reinforcement that is set up either vertically, or inclined. The procedures for compacting the soil are similar to those used for conventional reinforcement where the selected granular material is compacted over the horizontal reinforcement up to a given height, and then another layer of horizontal reinforcement is laid down. Afterwards, the vertical reinforcements are inserted perpendicularly or at an angle, as per the design requirements. The cross sectional configurations of the vertical reinforcing elements are shown in Figure 3.11.

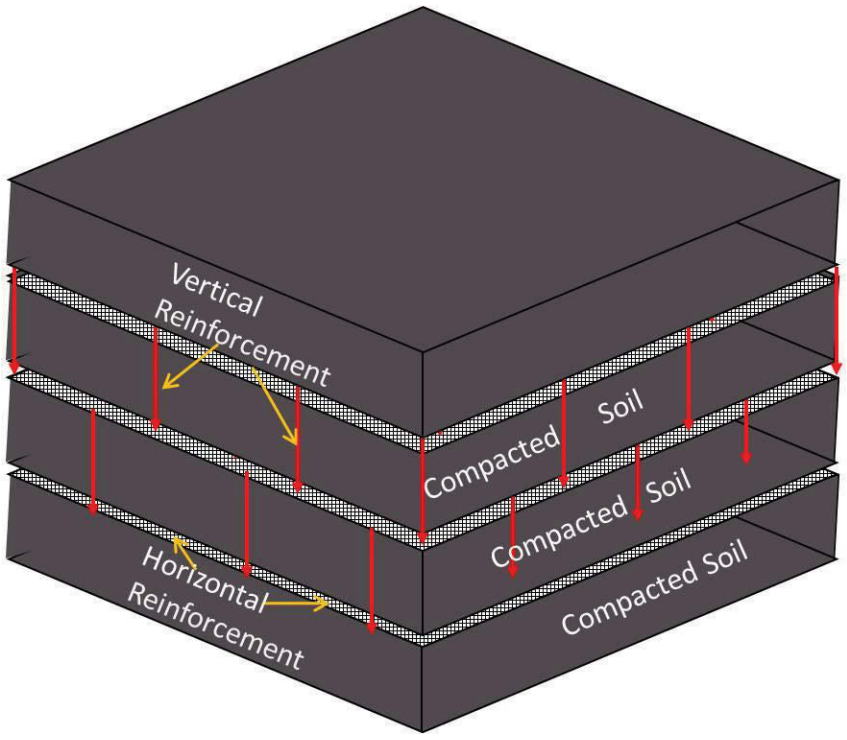

Figure 3.11 A typical reinforced soil wall using vertical reinforcement

The cross sectional configurations of vertical reinforcing elements are shown in Figure 3.12.

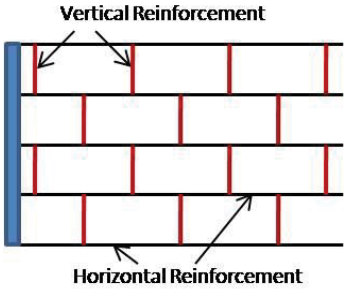

(a) Horizontal layers combined with vertical reinforcement

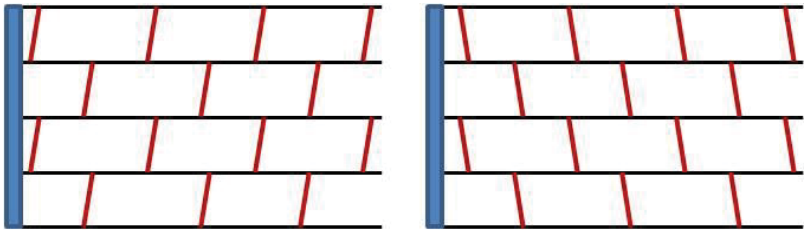

(b) Horizontal layers combined with inclined reinforcement

Figure 3.12 Cross-section of typical vertical reinforcement

3.5 Improving the Behaviour of Reinforced Soil

The reinforcement function is a mechanical method of improving the performance of the soil by supporting the tensile forces in two ways: (a) to reduce the shear force that must be carried by the soil, and (b) to enhance the shearing resistance in the soil by increasing the normal stress acting on the potential shear surfaces.

The resistance of soil to shearing stems from frictional contact between the particles subjected to effective compressive stress. Deformation in the soil causes tensile or compressive stresses to develop in the reinforcement. The magnitude of these stresses depends on the inclination of the reinforcement in the direction of tensile or compressive stresses in the soil. As reported by Jewell (1996), the reinforced force that can be mobilised is ultimately limited by the available bond and acts to alter the force equilibrium in the soil mass.

Shear deformation in the soil will cause tensile force T_r to be mobilised in the reinforcement and provide two additional components of resistance in the slope (Figure 3.13a). The tangential component of the reinforcement force $T_r \sin\theta$ directly resists the disturbing shear force in the soil, while the normal component of the force $T_r \cos\theta$, mobilises additional frictional shearing resistance $T_r \cos\theta \tan\phi$.

Vertical reinforcement adds two more components: $T_{vr} \cos\theta$ resists the disturbing shear force, and $T_{vr} \sin\theta$, the normal component of the force, provides extra frictional shearing resistance $T_{vr} \sin\theta \tan\phi$ as shown in Figure 3.13b. In addition to this, it will cage the soils in different units alongside the layers by horizontal reinforcement to produce an intact effect in the soil mass.

For granular materials, the shear resistance of the soil is given by $\tau = \sigma_1 \tan\phi$, where σ_1 denotes the vertical stress, τ is the shear stress, and A_h is the area of the shear surface.

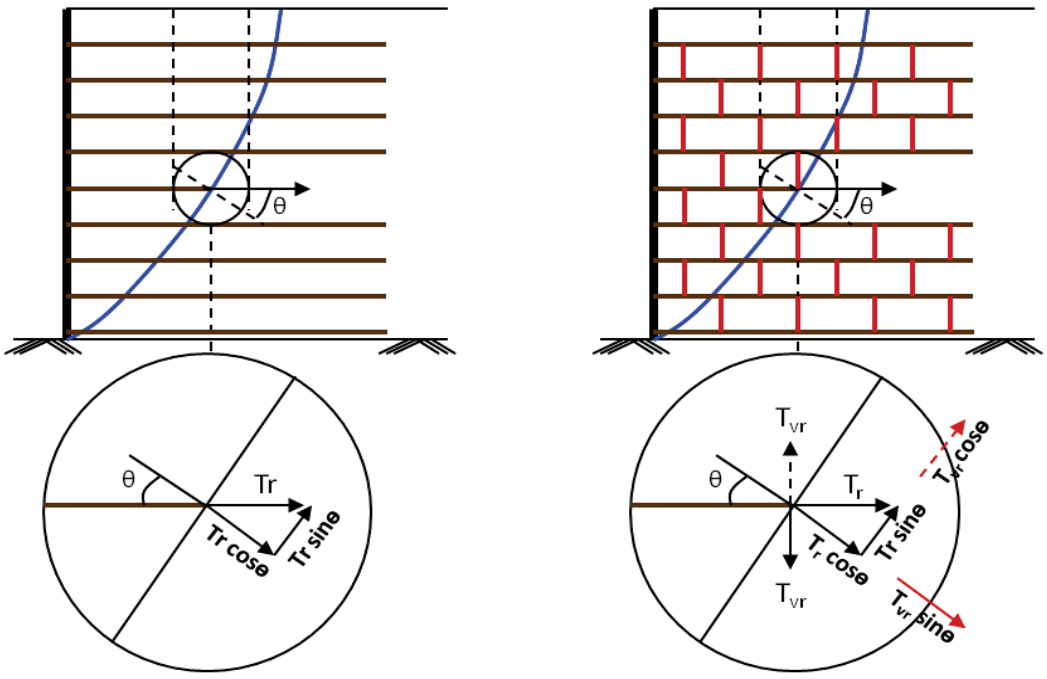

(a) Horizontal reinforcement (b) Horizontal and vertical reinforcement

Figure 3.13 Effect of reinforcement on equilibrium

The shearing force that increases due to horizontal reinforcement is given as:

$$\tau = \sigma_1 \tan\phi + (T_r/A_h)(\sin\theta + \cos\theta \tan\phi) \quad (3.28)$$

Equation 3.28 is further modified to increase the shear force due to vertical reinforcement as:

$$\tau = \sigma_1 \tan\phi + (T_r/A_h)(\sin\theta + \cos\theta \tan\phi) + (T_{vr}/A_{vr})(\cos\theta + \sin\theta \tan\phi) \quad (3.29)$$

In addition, for an inclined reinforcement from the vertical, as shown in Figure 3.14, the additional shear strength provided by inclined reinforcement can be estimated by the following equation:

$$\tau = \sigma_1 \tan\phi + (T_r/A_h)(\sin\theta + \cos\theta \tan\phi) + (T_{vr}/A_{vr})(\cos(90-\varphi) + \sin(90-\varphi)\tan\phi) \quad (3.30)$$

Where A_{vr} is the area of the shear surface of vertical reinforcement, ϕ is the angle of shear distortion expressed as $\tan^{-1}[1/(m + (\tan i)^{-1})]$, and where i is the initial angle of inclination with respect to shear surface, m is the shear distortion ratio ($m = x/z$). Gray & Lieser (1982) studied root-reinforcement models using the similar concept for root-soil interactions and recommends that the optimal orientation for roots to provide the additional shear strength in an inclination between 40° and 70° rather than in a vertical orientation.

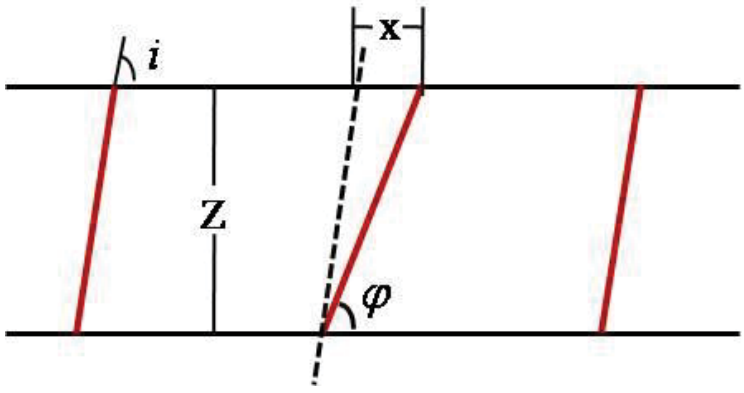

Figure 3.14 Inclined-Horizontal Reinforcement Model

Furthermore, the vertical component of inclined reinforcement provides a tensile force, while its horizontal component along with horizontal reinforcement provides a horizontal tensile force during seismic loading.

3.6 Enhancement on Current Analytical Methods

As discussed in the section 3.2, the influence of seismic induced forces on the stability of retaining walls has been addressed by various analytical approaches. Those analytical methods and their consecutive equations may be modified to intercept the constructive effect of the vertical reinforcement inclusion as below:

In internal stability calculation, the distribution of the dynamic tensile reinforcement increment $\Delta T_{dyn\,i}$ is weighted based on the length of the total anchorage in the resistance zone. Vertical reinforcement increases the anchorage length. Hence, the equation to distribute the dynamic tensile reinforcement increment (Equation 3.8) may be modified as:

$$\Delta T_{dyn\,i} = \Delta P_{dyn} L_{ai} / (\sum_{j=1}^{N} L_{aj} + \sum L_{vr}) \tag{3.31}$$

where, L_{vr} is the length of vertical reinforcement in anchorage zone.

In two-part wedge failure mechanism, the approach used by Bonaparte, Schmertmann & Williams (1986) for the total design strength of the horizontal layers of the reinforcement will be changed from as $\sum T_i = P_{AE}$ to $\sum T_i + \sum T_{vi} = P_{AE}$. The Equation 3.18, extended general approach for seismic case by Bathurst & Cai (1995), may be changed as:

$$P_{AE} = P_1 - \frac{B_1 A_1 \sum T_{i1} + \sum T_{vr,i1}}{\lambda \tan\emptyset_f + B_1 A_1} + k_h W_2 - \sum T_{i2} + \sum T_{vr,i1} - B_2 A_2 [(1 \pm k_v) W_2 + V_1] \tag{3.32}$$

where, T_{vr} is the tensile strength of the vertical reinforcement.

In Log-spiral failure mechanism, the moment equilibrium equation about the pole P will include the effect of the vertical reinforcement by changing the Equation 3.20 as:

$$\sum M_p = (1 \pm k_v)W(x_c - x_p) + k_h W(y_p - y_c) - (\sum T_i + \sum T_{vr})(y_p - y_i) = 0 \quad (3.33)$$

Similarly, the circular slip failure mechanism can take account for the additional restoring moment due to the vertical reinforcement. For this, the equation of the additional resisting moment due to tensile capacity of the reinforcement (Equation 3.24) may be extended as:

$$\Delta M_R = R(\sum T_i + \sum T_{vr,i})\,[\cos(\varphi_i - \delta_i) + \sin(\varphi_i - \delta_i)\tan\phi] \quad (3.34)$$

Moreover, the magnitude of the dynamic force increment due to shaking evaluated entirely depending on the horizontal and vertical peak ground acceleration coefficients k_h and k_v, respectively because the ground shakes both horizontal and vertical direction in earthquake loading. The proposed vertical reinforcement may intercept the vertical component of the earthquake loading.

3.7 Improvement against Modes of Failure

The advantage of proposed reinforcement mechanisms against failures such as, bearing capacity, tensile over stress and pull out are analysed in this section.

3.7.1 Bearing capacity of the foundation

Many experimental and analytical studies have been performed to investigate the behaviour of reinforced soil foundation (RSF) for different types of soil. The method of superposition can be used to include the contribution of reinforcement and the bearing capacity including increased bearing capacity due to reinforcement (Sharma et al. 2009) and can be given as:

$$q_{u(R)} = q_{u(UR)} + \sum_{i=1}^{N} \frac{4T_i[u+(i-1)h]}{B^2} \quad (3.35)$$

where, $q_{u(R)}$ is the total bearing capacity after the reinforcement, T_i is the tensile force in the i^{th} layer of reinforcement, u is the depth of reinforcement location, $q_{u(UR)}$ is the bearing capacity of the unreinforced soil foundation depending on the friction angle of the soil.

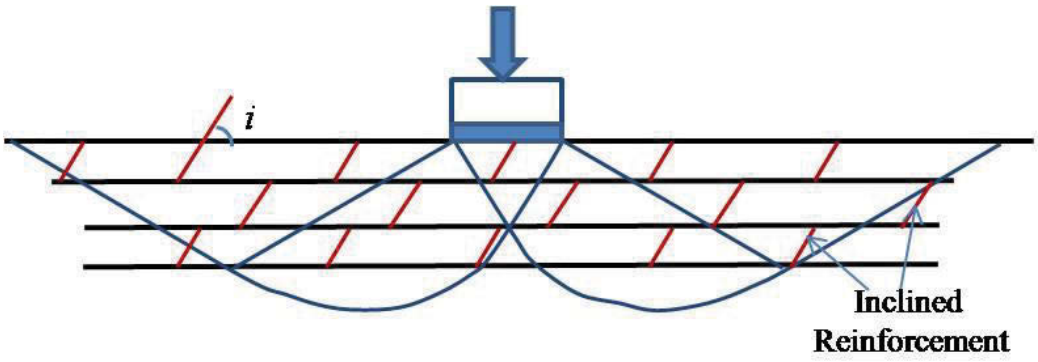

Figure 3.15 Failure mode within reinforced zone of soil foundation

The possible failure mode due to bearing capacity is shown in Figure 3.15. Vertical reinforcement enhances the tensile strength and provides bending effects which ultimately increases the bearing capacity, with some modification in Equation 3.35, as follows:

$$q_{u(R)} = q_{u(UR)} + \sum_{i=1}^{N} \frac{4(T_i+\Delta T_{vi})[u+(i-1)h]}{B^2} \quad (3.36)$$

where, ΔT_{vi} is the increased tensile force due to the vertical reinforcement.

3.7.2 Tensile failure of reinforcement

Failure by rupture occurs in reinforcement after the internal tensile force exceeds its strength. In current design, rupture failure is being checked and the vertical spacing between the layers of reinforcement should be decreased if the strength of the reinforcement is less than the tensile force, or reinforcement with a higher allowable tensile strength should be selected.

The failure envelop of unreinforced c-ϕ soil is given by:

$$\sigma_1 = \sigma_3 N_\phi + 2c\sqrt{N_\phi} \tag{3.37}$$

where, c is cohesion and N_ϕ can be defined as, $N_\phi = \tan^2(45 + \phi/2)$ this envelope can be modified if we used horizontal reinforcement, which is given by:

$$\sigma_1 = (\sigma_3 + R_T/S_Z)N_\phi \tag{3.38}$$

where, R_T is the tensile strength of the reinforcing materials per unit length and S_Z is the spacing of reinforcements, a comparison of Equations 3.37 and 3.38 gives:

$$c = R_T/2S_Z\sqrt{N_\phi} \tag{3.39}$$

Therefore, the failure envelope of reinforced and unreinforced soils is parallel and exhibits the same angle of internal friction. Any additional strength develops in the form of anisotropic apparent cohesion.

3.7.3 Pull out failure

Pull out failure occurs when the tensile force in the reinforcement exceeds the friction between the reinforcement and the soil. A number of numerical and experimental tests have been carried out to identify the behaviour of the pull out strength for different types of reinforcement (Saran 2005).

For slippage failure, the failure envelope is given by:

$$\sigma_1 = \sigma_3 N'_\phi \tag{3.40}$$

where,

$$N'_\phi = N_\phi/1 - (2b_r.f^*/S_Z)N_\phi \tag{3.41}$$

As $N'_{\phi} > N_{\phi}$, then $\phi_R > \phi$.The parameter N_{ϕ} can be expressed as: $N_{\phi} = \tan^2(45 + \phi_R/2)$ and f* represents the coefficient of internal friction between the reinforcing material and soil.

As a result, with the failure of reinforcement due to slippage, the failure envelope of reinforced sand will also pass through the origin, which indicates an increase in the angle of internal friction. The application of vertical reinforcement increases the total area of reinforcement, which enlarges the internal friction angle and ultimately enhances the strength of the soil.

3.7.4 Overturning mode under dynamic loading

In an overturning mode, the reinforced zone moves outwards in a simple shear manner, like a rigid block with internal deformation. As Sabermahani, Ghalandarzadeh & Fakher (2009) reported, surfaces with multi-line failures were formed in the unreinforced backfill because there was no failure in the reinforced zone. A settlement profile shaped like steps formed on the surface of the ground due to maximum settlement behind the reinforced zone.

Vertical/inclined reinforcement ties each layer to another which overcomes multi-line failure. This extra reinforcement reduces internal sliding by mobilising its tensile strength before one layer slips over another. Moreover, the vertical component of inclined reinforcement can reduce the wall settlement.

3.7.5 Bulging mode under dynamic loading

According to Sabermahani, Ghalandarzadeh & Fakher (2009), walls in a bulging mode are more flexible and form a single failure surface at the reinforced zone. The convex deformation of the facing causes a concave settlement to form on the surface of the ground with a maximum value at the middle of the reinforced zone.

A caging effect will be obtained by using vertical and horizontal reinforcement where each layer is tied to another so they act as one, which reduces the total force at the back of the facing panel. Therefore, the chance of bulging is reduced with vertical reinforcement.

3.7.6 Expected failure mode after the inclusion of vertical reinforcement

As discussed in the sections 3.7.1 to 3.7.5, the influence of seismic induced forces on the stability of retaining walls will be reduced after the inclusion of vertical reinforcement. Vertical reinforcement adds the reinforced length which enhances against pullout failure. This extra reinforcement binds each layer to another, which produces a caging effect and enhances against multi-line failure and bulging failure. In addition, it reduces internal sliding by mobilising its tensile strength before one layer slips over another. Despite the improvements on various failure modes, toppling failure may be expected after the inclusion of vertical reinforcement as the reinforced soil zone behaves as a block.

3.8 Field Construction Techniques

The primary reason for using vertical reinforcement is to stitch each horizontal layer of reinforcement to another, and since this proposed technique is a new concept, the detailed process of construction can be another major challenge.

To address this challenge a 10-20 mm diameter long tensile rod or pipe with a conical tip can be used, which is similar to a cone penetration test. As the spacing of reinforcement is generally not more than 500mm, the maximum depth of insertion for this equipment can be around one metre, so a large force to insert and pull the rod out is not needed. The details of this equipment can be designed after consulting with the manufacturers, but for this purpose, different techniques are presented below.

3.8.1 Push-pull method

Firstly, horizontal reinforcement is laid down and covered by a compacted layer of soil, and then a fibre cord with a V-shaped flexible tip which will open like an umbrella under the first layer, is inserted just below the lower reinforcement with a metal hose, as shown in Figure 3.16. When the fibre cord is pulled out the V-shape tip will open up then the cord can be tied to the upper layer of horizontal reinforcement.

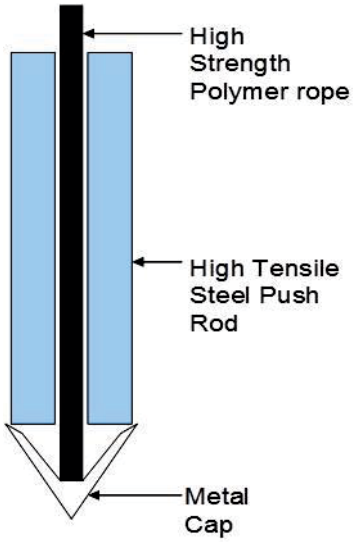

(a) Schematic of vertical reinforcement insertion mechanism

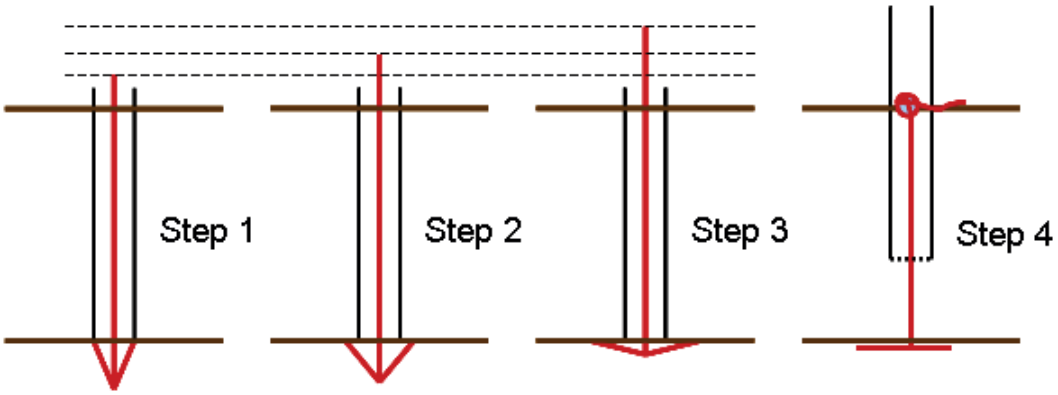

(b) Opening of umbrella under the first layer with a metal hose

Figure 3.16 Construction steps for push-pull method

3.8.2 Sewing method

A truck with the sewing mechanism mounted as shown in Figure 3.17a, can be very useful for large scale work because here two inserting rods stitch two layers of reinforcements. The inserter rod is inserted into the vertical reinforcement and the puller rod is pulled out, as shown in Figure 3.17b.

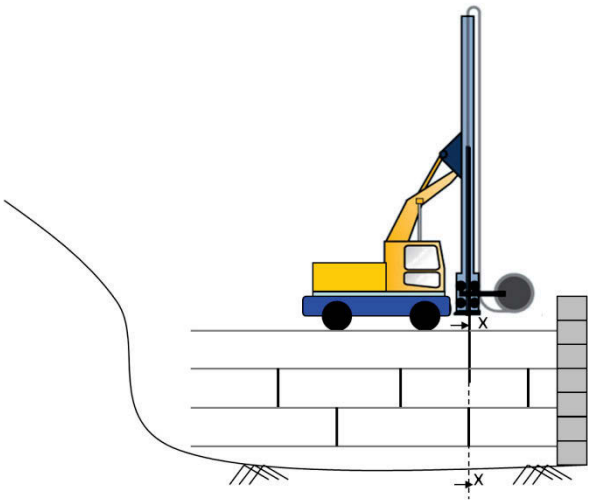

(a) Sewing mechanism mounted on truck

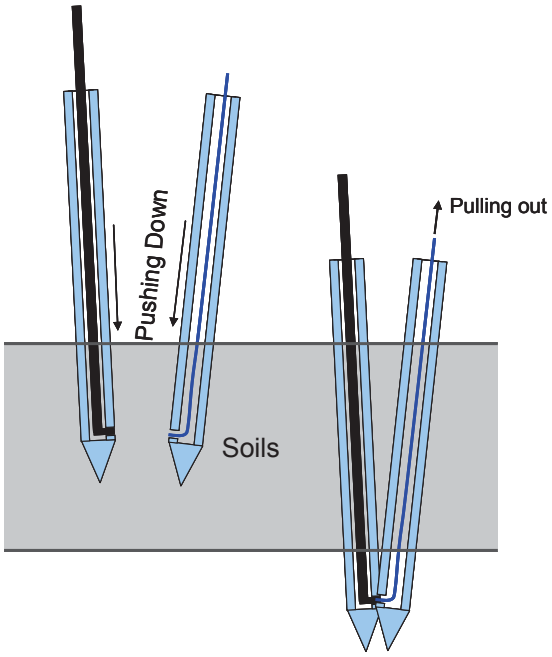

(b) Insertion process

Figure 3.17 Sewing mechanism

The two rods are inserted with a V-angle downwards depending on the spacing of the reinforcement, and after penetrating the lower horizontal reinforcement, they come in contact with each other so that the puller rod comes out bringing the vertical reinforcement upwards. This phenomenon will fasten the horizontal reinforcement. As with the previous method, vertical reinforcement is inserted to tie up two horizontal layers of reinforcement.

3.8 Summary

The proposed vertical reinforcement is a connection of consequent conventional horizontal layers with an additional reinforcing element to unite the soil vertically and horizontally. Pseudo-static seismic analysis and design of GRS walls only estimate the factors of safety against various modes of failure or collapse of the wall. Deformation of the wall could not be estimated directly from pseudo-static analysis because analytical considerations only show the enhanced performance of the GRS walls with the inclusion of vertical reinforcement, and probable improvement against modes of failures.

The inclusion of vertical and horizontal reinforcement into the soil improves its properties by preventing various failure modes. This additional reinforcement enlarges the apparent anisotropic cohesion and the friction angle, which gives the soil an additional tensile strength, which reduces the chance of rupture in the reinforcement. The construction technique presented here shows its potential for implementation in the field while the details of this equipment can be designed after consultation with manufacturers.

Chapter 4

4. Verifying the Concept Using Numerical Modelling

4.1 Introduction

Numerical investigations of the seismic response of GRS walls are more economical than those conducted by physical model tests. Although numerical investigations suffer from the idealism compared to physical model tests, they are generally more rigorous than the conventional limit equilibrium approaches because they satisfy the force-equilibrium conditions, strain-compatibility conditions, and the constitutive material laws. Indeed both qualitative and quantitative performances can be obtained from numerical investigations. For instance, the effect of the design parameters on the natural frequency of a GRS wall was investigated by Hatami & Bathurst (2000), and numerical modelling by Rowe & Ho (1998) suggested that the tensile stiffness at the reinforcing elements has a significant effect on the deformation of GRS walls.

Several researchers have presented analytical models for estimating the ultimate bearing capacity of strip footing (Binquet & Lee 1975a, 1975b; Michalowski 2004) and rectangular footing (Kumar & Saran 2003; Wayne, Han & Akins 1998) on reinforced soil. The performance of a reinforced soil foundation depends not only on the properties of the soil and reinforcements; it also depends on the interaction between them. For this reason, the finite element procedure becomes complex compared to the simulation of a regular soil foundation. Most of the analytical solutions available in literature assume that all the reinforced layers either fail by rupturing under tension or having the reinforcement pulled out. This assumption implies that the tensile force developed in

reinforcement increases with the increasing depth of reinforcement (since normal load increases with depth), which contradicts the tensile forces measured along the reinforcement in the model footing tests conducted by Chen et al. (2007) and Abu-Farsakh, Chen & Yoon (2008).

In this study the vertical reinforcing components (connecting each layer of horizontal reinforcement) are employed using numerical modelling, and then the performance of combined vertical and horizontally reinforced soil versus conventional horizontal reinforcement under earthquake loads is compared. The response of two inclined reinforcement models and one vertical reinforcement model stabilised with layers of horizontal reinforcement are evaluated under seismic loading. The main goal of this chapter is to justify the suitability of the inclusion of vertical reinforcement in GRS wall for seismic stability. For this, numerical investigations are carried out to analyse the stability of reinforced soil structures with inclined reinforcements, and then compare those results with conventional horizontal reinforcement. Furthermore, the changes of stresses on the foundation of the wall after the insertion of vertical reinforcement as well as conventional reinforcement are also discussed. It can be noted that this numerical study is a pre-verification of the concept of vertical reinforcement before proceeding to extensive laboratory experiments to evaluate the performance of a soil wall with vertical reinforcement.

4.2 Finite Element Model

The finite element program PLAXIS 2D Version 9.0, was used for a two-dimensional analysis of deformation and stability in geotechnical engineering to conduct the numerical analysis reported herein. This PLAXIS 2D program, including the 2D Dynamics, is a robust, user friendly finite element package intended for a two dimensional analysis of deformation and stability in geotechnical engineering. The 2D

Dynamics module is an extension to PLAXIS 2D. Geotechnical applications require advanced constitutive models capable of simulating the non-linear, time dependent and anisotropic behaviour of soils and/or rock. This 2D Dynamics module has the tools to analyse the propagation of waves through soil and their influence on structures. This allows for an analysis of seismic loading as well as vibrations due to construction activities. 2D Dynamics offers the possibility of performing dynamic calculations in individual calculation phases. In this study, 15 node triangular elements were used, as shown in Figure 4.1.

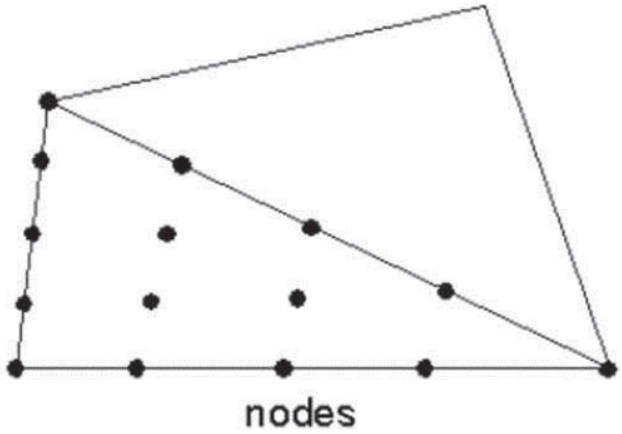

Figure 4.1 Triangular elements with 15 nodes

The geometry of a reinforced soil wall was chosen based on data taken from literature (Carrubba & Colonna 2000) and several geotechnical reports known for the reliability of their results. The wall was 10 m high, with an inclined facing of 1(H) in 20(V), and had 7m long reinforcement. This reinforced soil wall was modelled for a total height of 10 m to ensure an adequate distance from the assumed rough/rigid bottom boundary condition to the zone of influence due to the construction of the wall. To increase the accuracy in the outputs, the effect of stiffness on the boundary 30 m below the surface was considered, so the soil on the front side and back side were fixed at 30 m and 20 m, respectively. Because compaction close to the facing elements is usually poor, 0.5 m of

soil in this vicinity (facing soils) was considered to be weaker than the rest of the reinforced soil.

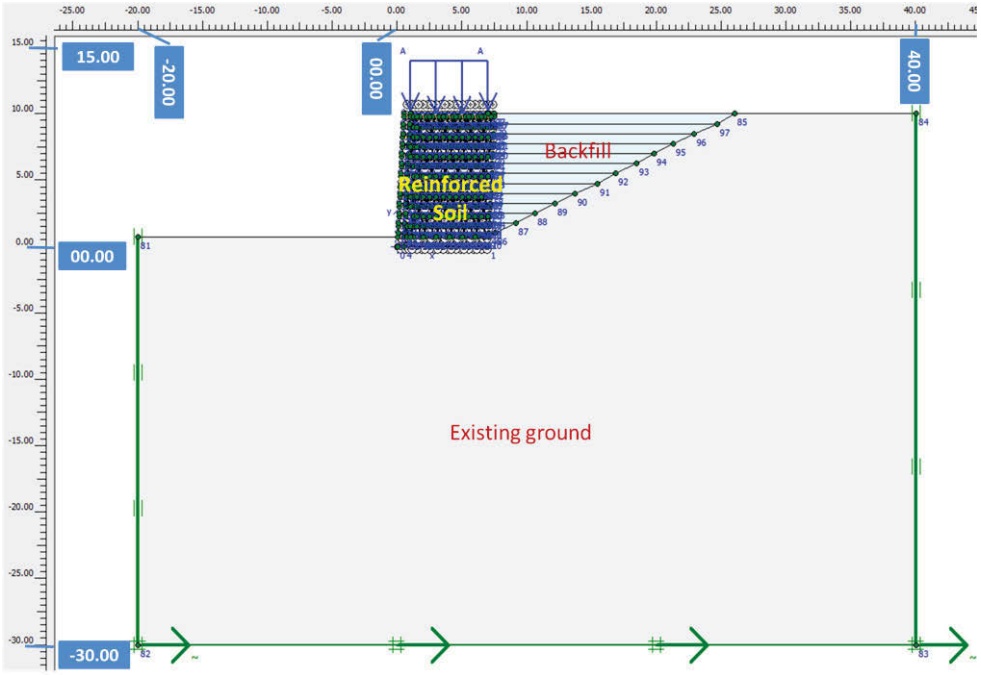

(a) Geometric model created in PLAXIS

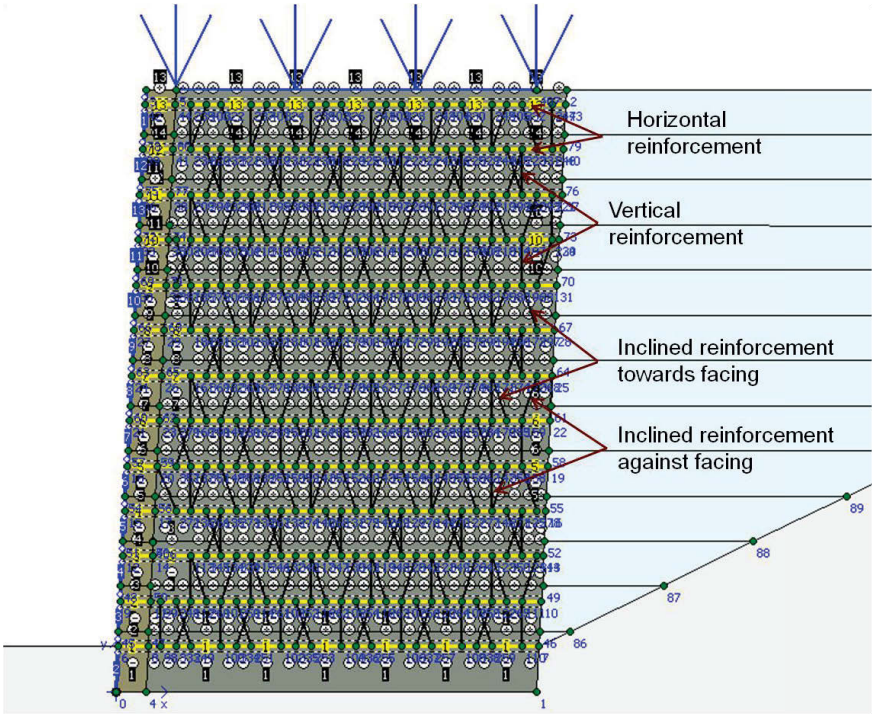

(b) Enlarged size of the reinforced soil

Figure 4.2 General model of the reinforced soil wall used in the numerical analysis

An analysis of the construction of the wall simulated field practices considering layer by layer placement. The wall consists of thirteen layers of conventional horizontal reinforcement underlain by medium dense soil. Compaction stresses induced during construction were not considered in this analysis because this study is an attempt to verify the concept before moving ahead for the experiments. So a simple but reliable method of calculation was chosen. For simplicity, the level of the water table was assumed to be well below the foundation of the wall. A surcharge load of 30 kN/m was placed on top of the middle section of the horizontally reinforced layers for a length of 6 metres. The creation of a geometric model was carried out as shown in Figure 4.2.

4.3 Model Parameters

The sand and interface properties of the model are given in Table 4.1. The initial geo-static stress in the foundation of the soil was based on its unit weight and the effective coefficient of lateral earth pressure at rest (K_0') for each layer. There were four types of soil in the model, namely: backfill soil, reinforced soil, facing soil, and natural ground. The reinforced soil is the material to be compacted between the layers of geogrid, the fill material is used as backfill between the reinforced soil wall and the natural ground, and the facing soil represents the relatively less compacted soil close to the facing elements. Interface reduction factors in the range of 0.67-0.85, were assumed for the interface between the soils and reinforcement, and the soils and facing elements.

The interface reduction factor (R_{inter}) is taken into account for the strength and stiffness decrease of the interface element in the corresponding soil layer. R_{inter} serves to model the soil-structure interface by reducing the cohesion (c), the friction angle (ϕ) and shear modulus (G) at the interface using the following relationships:

$$C_{inter} = R_{inter} \times C_{soil} \tag{4.1}$$

$$\tan[\emptyset_{inter}] = R_{inter} \times \tan[\emptyset_{soil}] \leq \tan[\emptyset_{soil}] \quad (4.2)$$

where, R_{inter} is the interface reduction factor (<1), C_{inter} is the cohesion of the interface, C_{soil} is the cohesion of the surrounding soil, ϕ_{inter} is the friction angle of the interface, ϕ_{soil} is the friction angle of the surrounding soil.

Table 4.1 Sand and interface properties

Parameter	Name	Reinforced soil	Ground	Backfill	Facing	Unit
Material model	Model	Mohr-Coulomb				-
Type of material	Type	Drained				-
Soil unit weight	γ_{unsat}	19	18	17	17	kN/m^3
Young's modulus	E_{ref}	60000	50000	40000	30000	kN/m^2
Poisson's ratio	ν	0.3	0.2	0.3	0.3	-
Cohesion	c	0.5	0.5	5	5	kN/m^2
Friction angle	Φ	38	33	30	32	degree
Dilatancy angle	Ψ	4	3	2	4	degree
Interface	R_{inter}	0.85	0.75	0.67	0.7	-

For inclined reinforcement modelling, the use of geogrid elements for the inclined reinforcement cannot represent the proposed vertical reinforcement because it represents a planner form of reinforcement. The proposed reinforcement is similar to an anchor connecting two consecutive horizontal layers which only works in tension, just like other types of reinforcement. Therefore, node to node anchor was chosen. An anchor element designed in PLAXIS 2D version 9.0 has both tensile and compression strengths, but the additional reinforcement being proposed can only be activated in the case of tensile forces. Therefore, the compressive strength chosen is close to zero because the system will not run for the nil value in the anchor.

The vertical reinforcement, horizontal geogrids, and facing wall parameters are given in Table 4.2. The facing wall is constructed with concrete slabs 750 mm high by 180 mm thick.

Table 4.2: Properties of the vertical reinforcement and geogrids

Elements	Parameter	Symbol	Value	Unit
Vertical reinforcement	Normal stiffness	EA	1500	kN
	Spacing out of plane	Ls	1	m
	Strength	$F_{max,\ compression}$	0	kN
		$F_{max,\ tension}$	2.5	kN
Horizontal Geogrids	Normal stiffness	EA	5000	kN/m
	Tensile strength	Np	100	kN/m
Facing (diaphragm wall)	Normal stiffness	EA	7.00E+07	kN/m
	Flexural rigidity	EI	1.45E+07	kNm^2/m
	Equivalent thickness	d	0.18	m
	Weight	w	10	kN/m/m
	Poisson's ratio	ν	0.4	-

The values of all the interface reduction factors were chosen so they were weaker than the two materials in contact with each other. They were reduced from 70% to 85% to reflect a reasonable reduction in the strength of the interface. The results of this analysis are discussed in detail in the next section.

The generation of plane strain mesh by PLAXIS version 9.0 used here follows a robust triangulation procedure to form ‘unstructured meshes’. These meshes are considered to be numerically efficient compared to regular ‘structural meshes’. The powerful 15-node element provides an accurate calculation of stresses and failure loads. The earthquake

was modelled by imposing a prescribed displacement at the bottom boundary, and the default absorbant boundary conditions were applied at the furthest vertical boundaries to absorb outgoing waves. The generation of refined mesh was as shown in Figure 4.3.

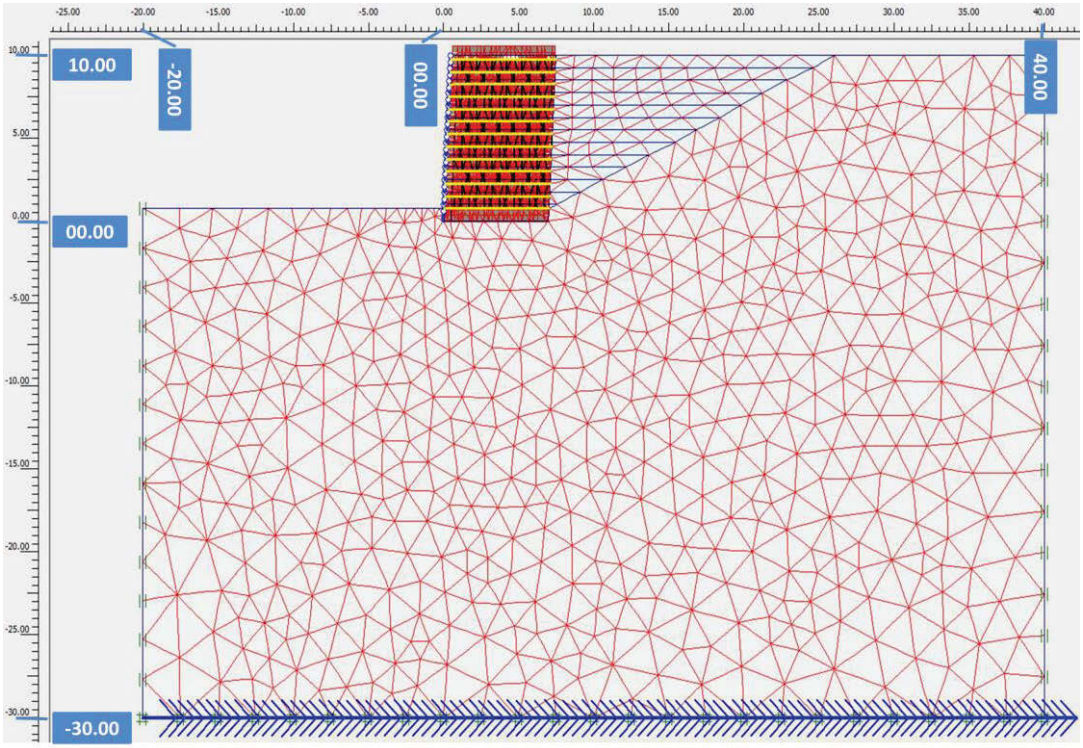

Figure 4.3 Plane strain finite element mesh

After the mesh was generated a respective pattern was chosen for the output results which will be used for an exact comparison of the results of different cases.

This calculation involves two stages; stage one is a normal plastic calculation where the reinforced walls constructed, and stage two is associated with a dynamic analysis where an earthquake is simulated. To maintain uniformity of the model in all four cases, the three inclined reinforcement patterns are built in the input stage followed by the generation of mesh, and a respective pattern is chosen for the output as an exact comparison of the results in different cases. The spacing between two consecutive inclined reinforcements was 1.5 m. The geometry of the numerical models and selection of a particular form of vertical reinforcement are shown in Figure 4.4. Figure 4.4a

represents the conventional reinforced soil model, Figure 4.4b demonstrates horizontal reinforcement with vertical reinforcement, Figure 4.4c shows the connection of horizontal layers with inclined reinforcement towards the facing, and Figure 4.4d illustrates the inclusion of inclined reinforcement towards the wall to the horizontal reinforcement. Both of the last two cases are inclined in a ratio of 1(H):1.5(V).

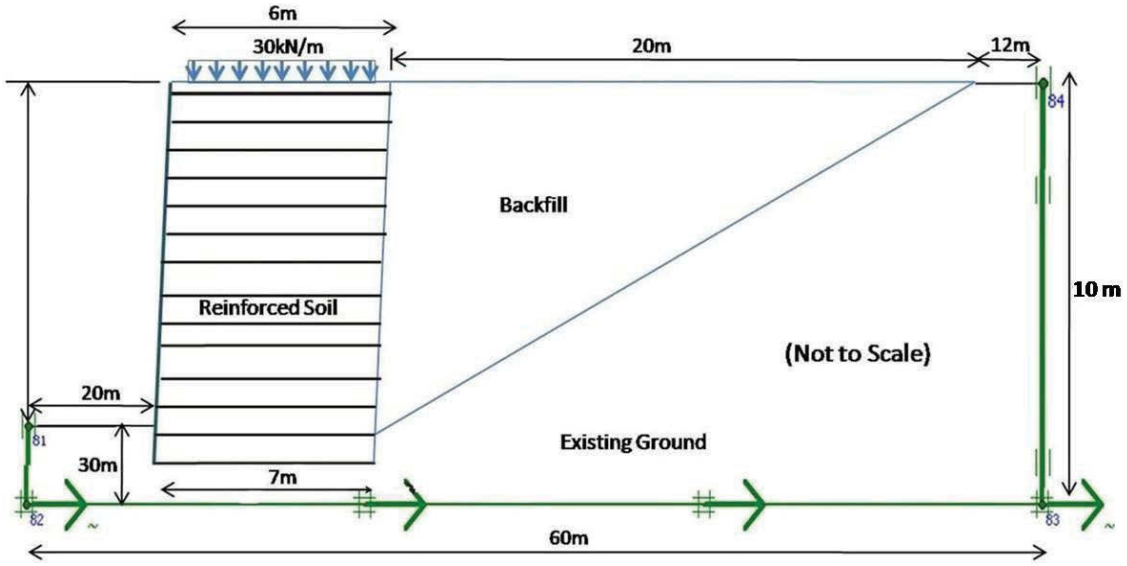

(a) Conventional horizontal reinforcement

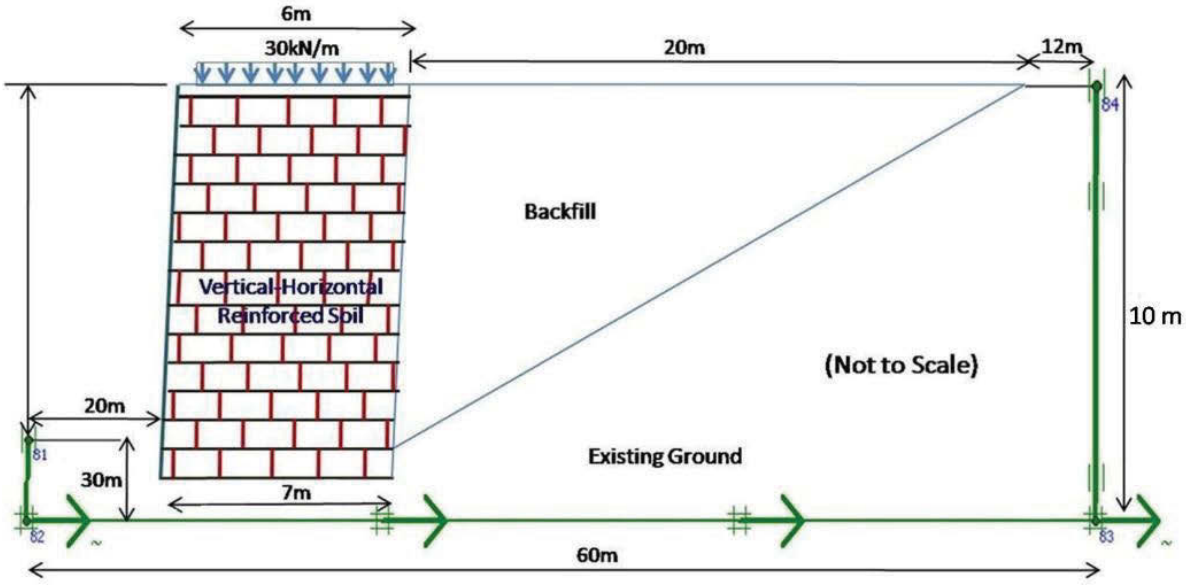

(b) Vertical-horizontal reinforcement

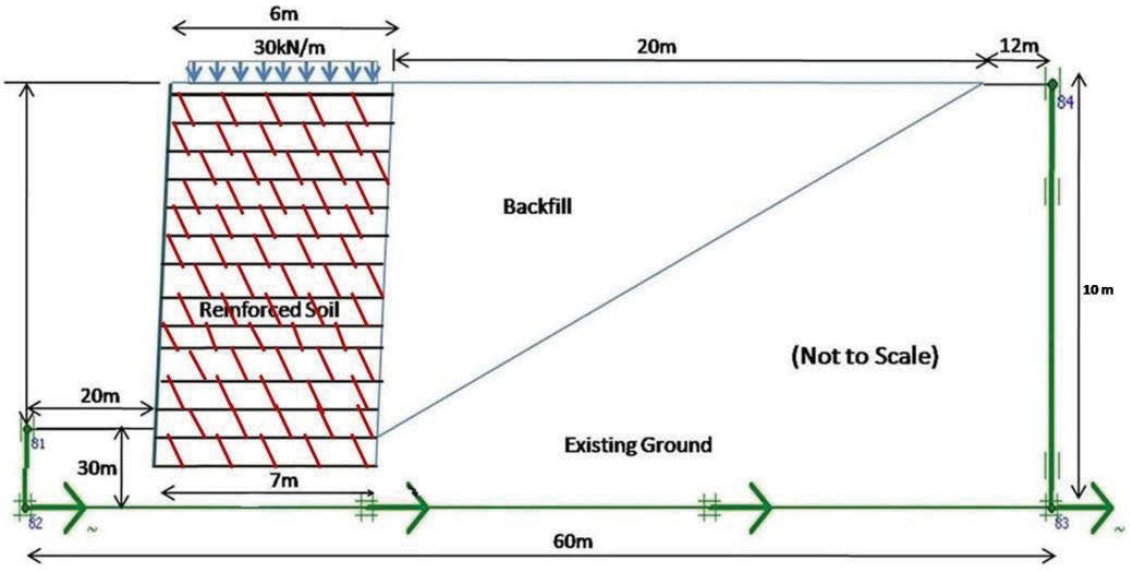

(c) Inclined towards the facing

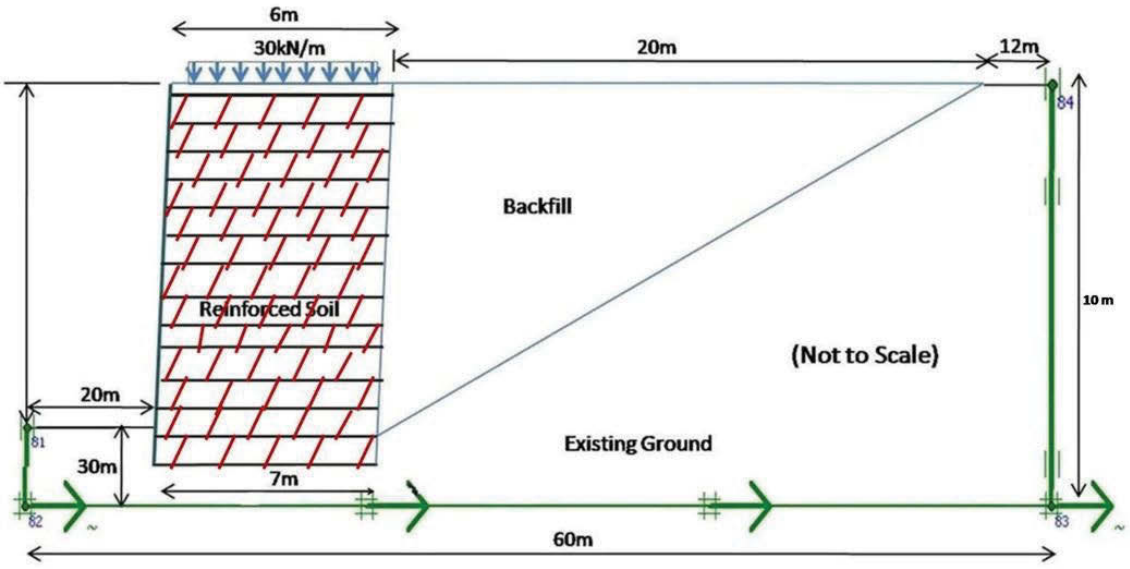

(d) Inclined towards the wall

Figure 4.4 General models of the reinforced soil wall

For a seismic analysis of the models, an earthquake load of 1995 Kobe earthquake using a 50 seconds accelerogram was used, as shown in Figure 4.5. This earthquake had a local magnitude of 7.2 on the Richter scale and a peak acceleration of 0.833g, where g is the Earth's gravitational acceleration.

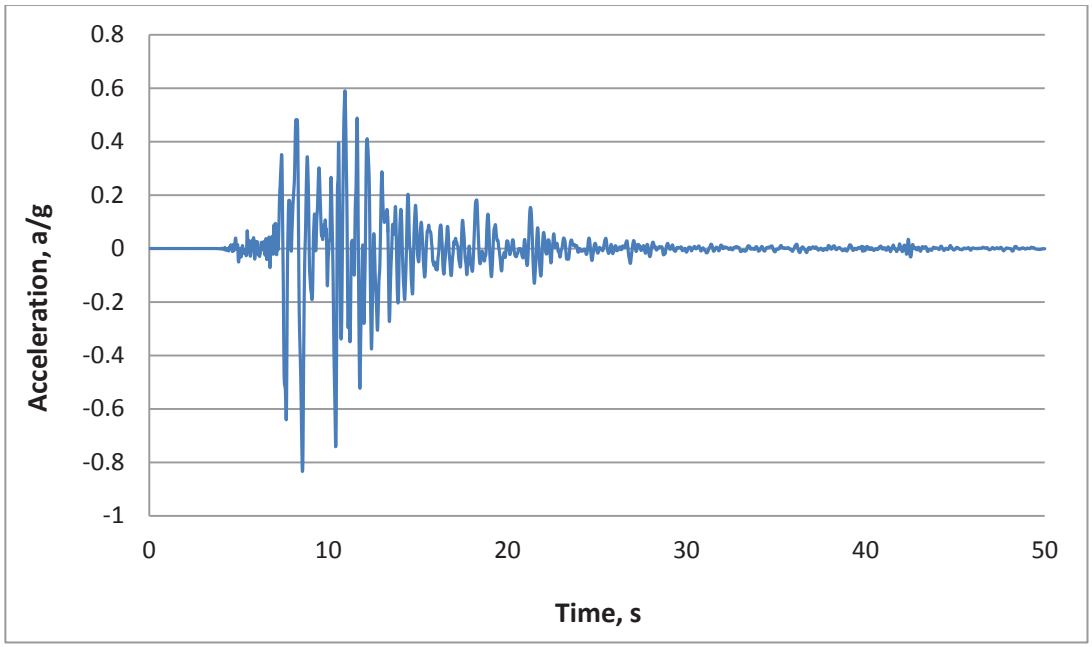

Figure 4.5 Accelerogram of Kobe earthquake

4.4 Analysis of Results

The results of the finite element analyses, using the above mentioned parameters, are discussed in different cases of reinforced walls, and with, and without inclusion of the inclined reinforcement under seismic loading. Deformation of the facing along the base of the wall, the stresses along the base of the wall and the facing blocks, and strains in various layers of reinforcement were all calculated and compared. The results are reported after the application of seismic loads.

4.4.1 Horizontal deformation

For a visualisation, the shaded horizontal displacements with and without horizontal reinforcement is presented in Figures 4.6 and 4.7, respectively. For a clear view, the retaining partn of the wall is focused in both cases.

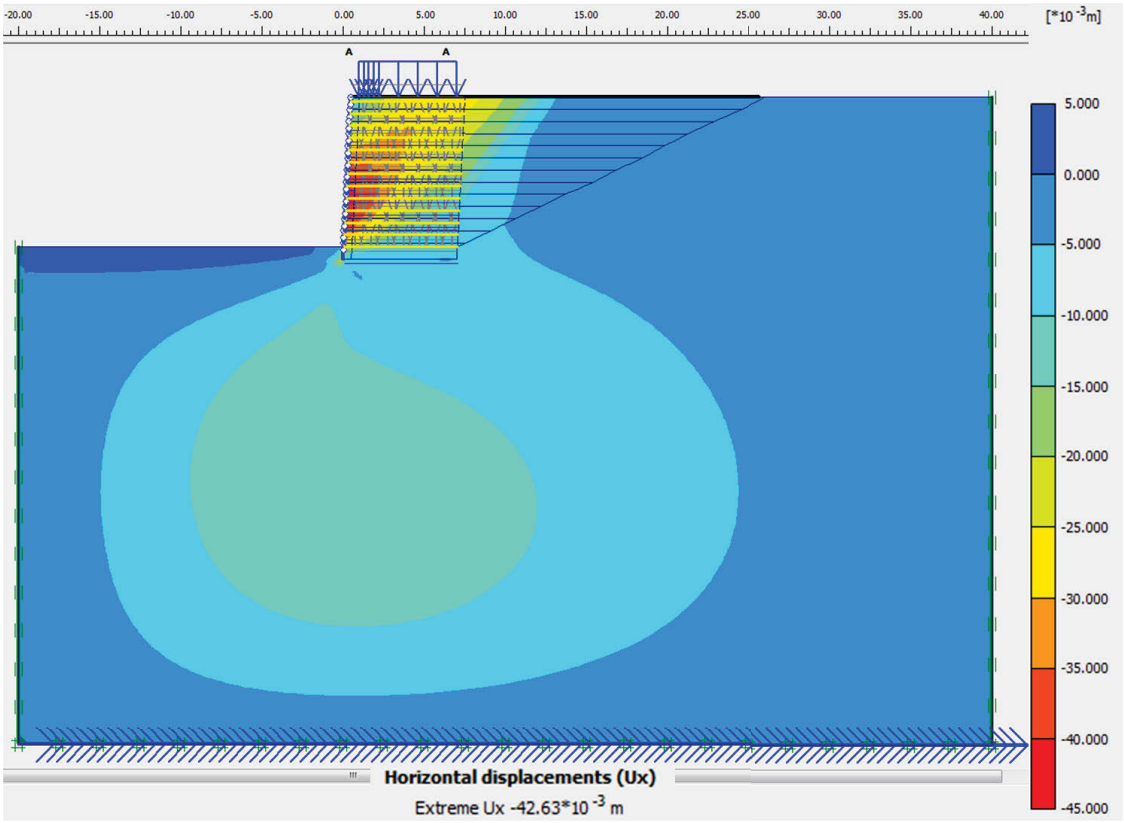

Figure 4.6 Horizontal displacements without vertical reinforcement

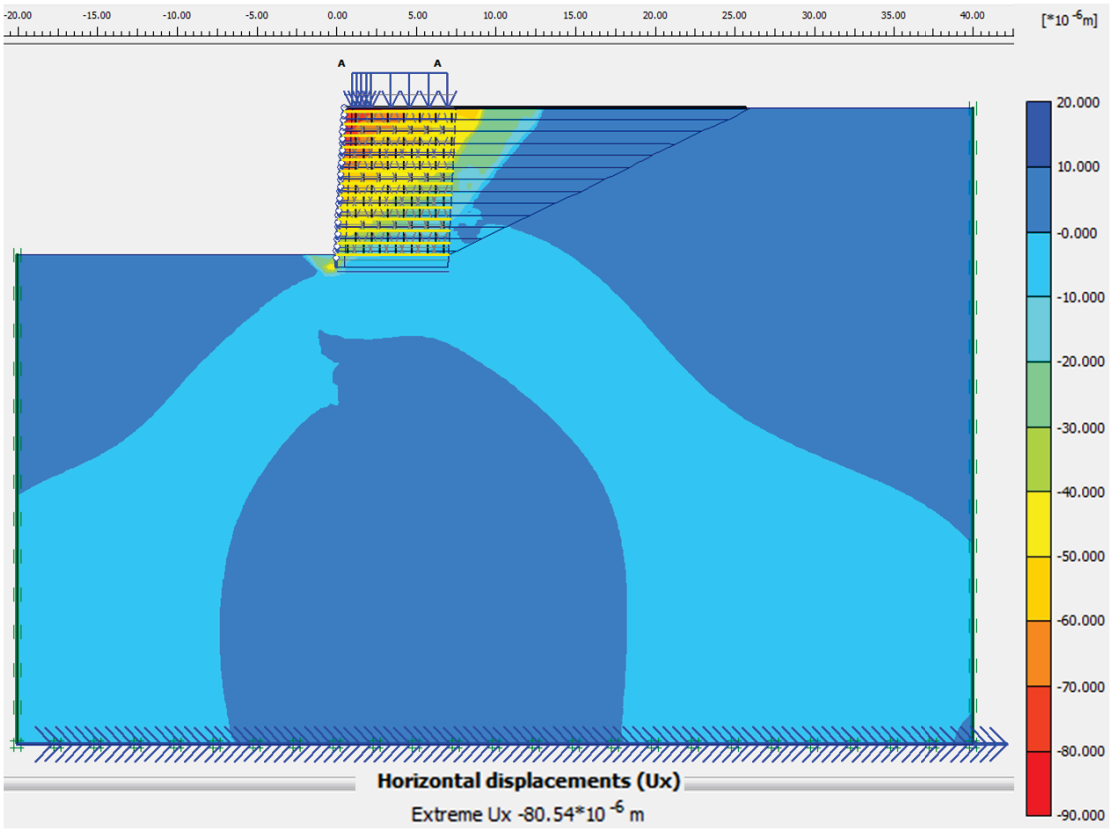

Figure 4.7 Horizontal displacements with vertical reinforcement

The horizontal deformation of walls towards the facing in all four cases were analysed and are presented in Figure 4.8. The results indicate that using additional inclined elements over conventional soil reinforcement to reduce horizontal deformations is promising. The final horizontal displacement in every layer of the wall, from 0 to 10 m high, is shown in Figures 4.8a and 4.8b, depict the height of the retaining wall versus horizontal deformation. As shown in Figure 4.8a, without vertical reinforcement, the wall deforms in a parabolic shape with a significant displacement. A comparison of all four cases shows that in the three events, apart from the case, not using vertical reinforcement falls in the same region, as shown in the graph. For that reason, in those three cases: with vertical reinforcement, with reinforcement inclined towards the facing, and with reinforcement inclined towards the wall, are presented in Figure 4.8b. This figure shows that reinforcement with the case inclined towards the facing had the most deformation, whereas the case with vertical reinforcement had the least. However, those values of deformation do not offer a significant difference for practical applications compared to a wall without vertical reinforcement.

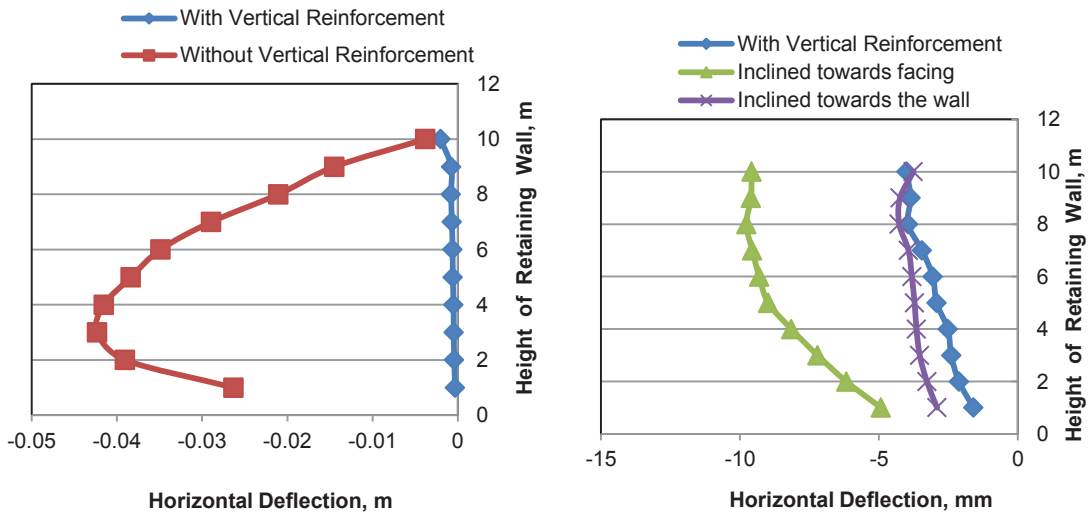

(a) With and without vertical reinforcement (b) Vertical and inclined reinforcements

Figure 4.8 Horizontal deformation of the wall

4.4.2 Vertical deformation

The outputs of the analysis in the shaded form of vertical deformations, with and without the inclusion of vertical reinforcement, are shown in Figures 4.9 and Figure 4.10, respectively.

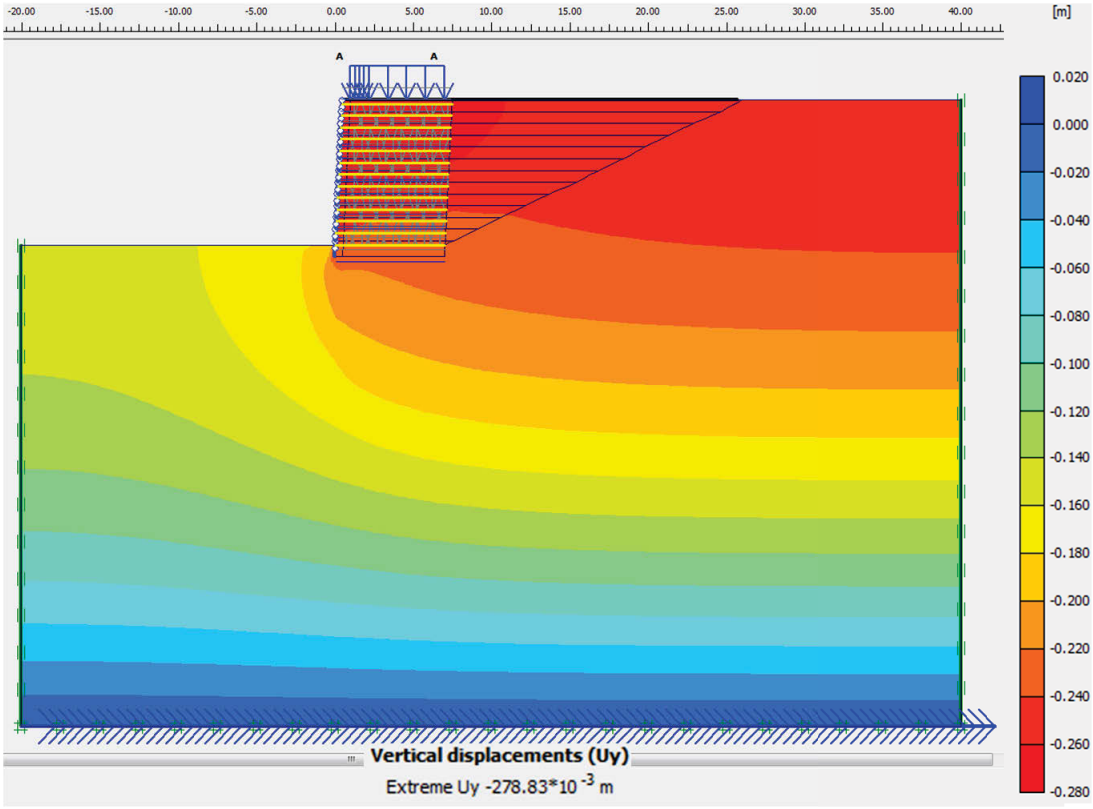

Figure 4.9 Vertical displacement without vertical reinforcement

The vertical deformation at the face of wall in every layer of reinforcement were calculated, compared, and presented in Figure 4.11. Deflection in the retaining wall with vertical reinforcement was dramatically less than a conventionally reinforced wall. As with horizontal deformation the wall "without vertical reinforcement," deformed in a convex curve with a significant amount of displacement, as shown in Figure 4.11(a). Once again, deformation in every event, except for the "without vertical reinforcement" case, followed the same pattern with very close data so it cannot be seen properly in the same graph of reinforced soil without vertical reinforcement. Thus in these three cases:

with vertical reinforcement, with reinforcement inclined towards the facing, and with reinforcement inclined towards the wall, are presented in Figure 4.11(b). By and large, this figure followed the same pattern where the reinforcement with the case inclined towards the facing has the most deformation, whereas the case with vertical reinforcement had the least. Then again, those values of deformation are close to each other and in practice there is no significant difference.

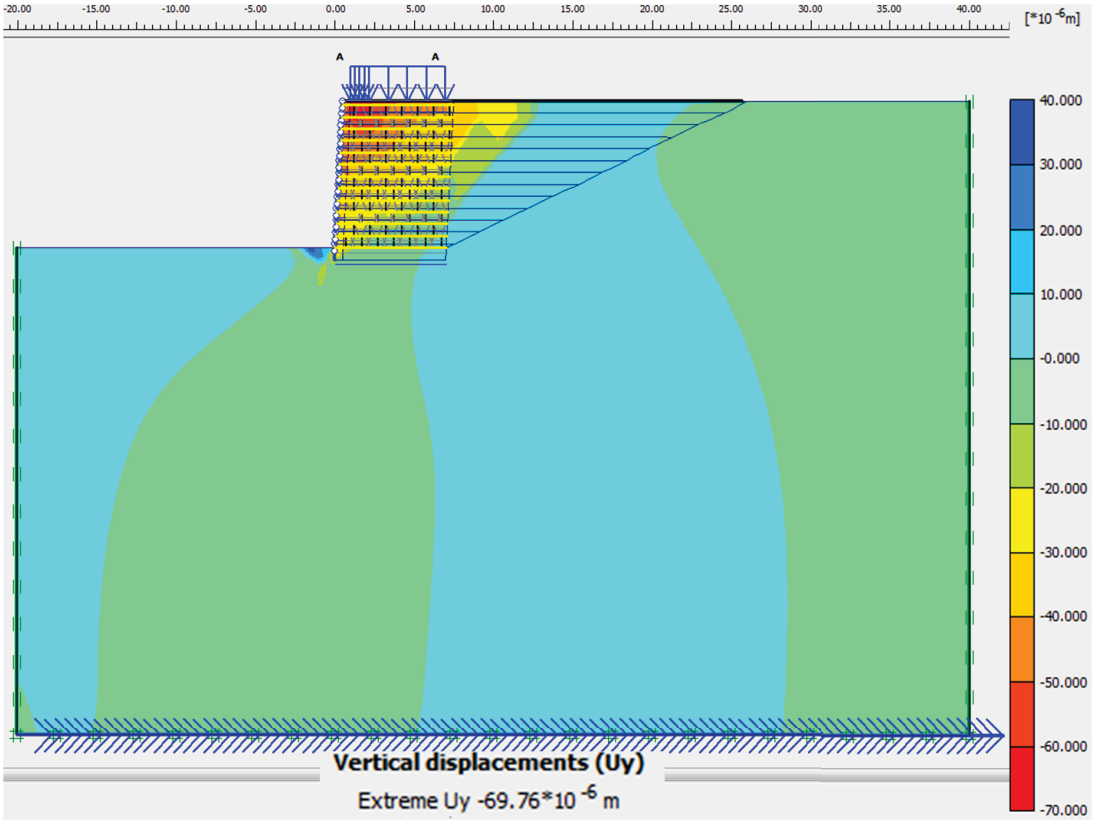

Figure 4.10 Vertical displacements with vertical reinforcement

To investigate why there was an improvement after vertical elements were applied, axial stresses in the horizontal reinforcement were observed and found to have almost similar values in both cases. Latha & Krishna (2008a) also observed similar results with different types of reinforcing materials and concluded that this is due to very low levels of strain in the layers of reinforcement.

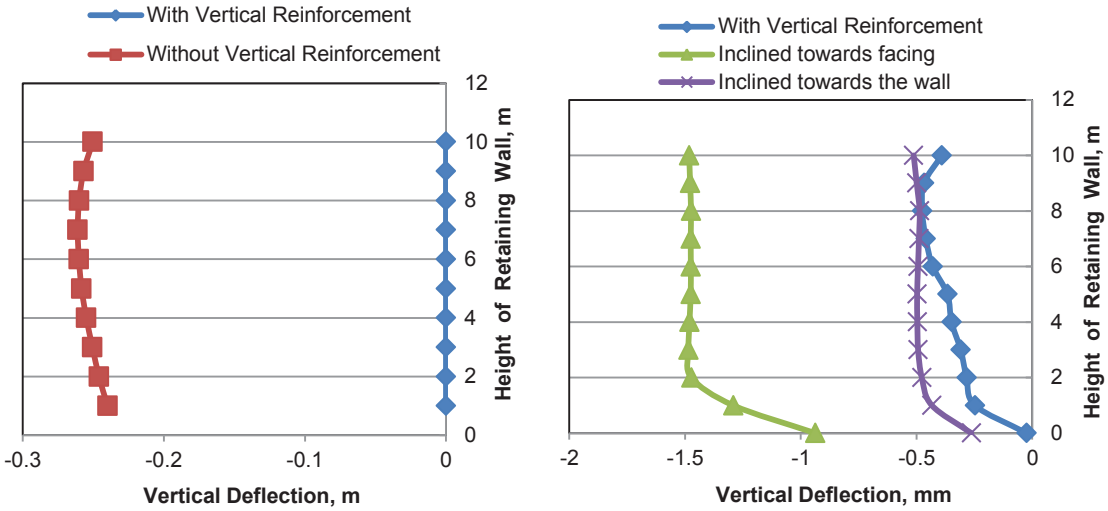

(a) With and without vertical reinforcement (b) Vertical and inclined reinforcements

Figure 4.11 Vertical deformation of wall

The forces in the vertical reinforcement were varied with higher values concentrated towards the opposite side of the toe. This might be due to the reinforced wall having a rocking effect. Those outputs demonstrate that vertical elements can hold the layers of horizontal reinforcement in place during a seismic load.

4.4.3 Stresses on the foundation of the wall

Figure 4.12 compares the vertical stresses on the reinforced soil foundation (RSF) with and without the application of vertical reinforcement and shows minor differences. Although the discrepancy is small, the results generally indicate that the constructive effects of vertical reinforcement can reduce stress on the foundation. Variations in the displacement calculated along the base of the wall can be attributed to different values of stiffness inherent in the various materials along the base. The stresses are highest near the front toe of the wall because a portion of the self-weight pressure from the backfill is transferred from the reinforcing and the soil to the facing wall, while the wall also rotates slightly which increases the pressure at the toe relative to the heel of the wall.

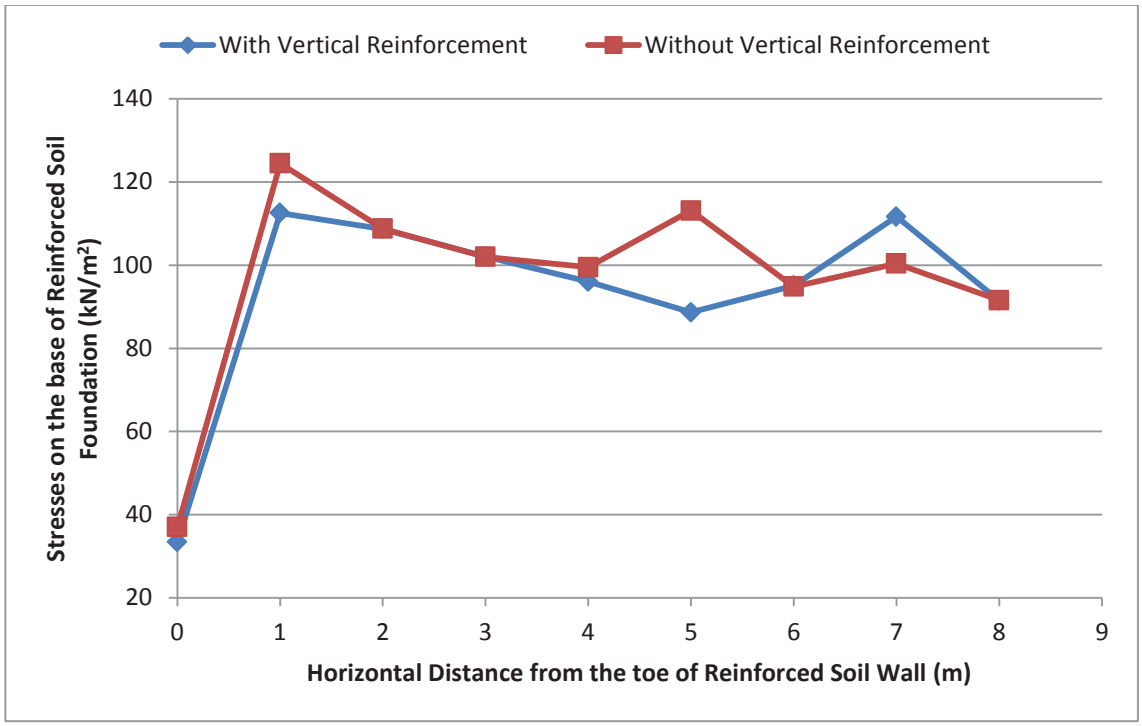

Figure 4.12 Comparison of vertical stresses on the RSF with and without inclusion of vertical reinforcement

An examination of the vertical shear stress between each layer revealed a promising outcome because they are much lower in the case of vertical reinforcement. The values of equivalent forces from the shear stress diagram between each layer are presented in Figure 4.13. The values of equivalent vertical forces were automatically calculated in PLAXIS outputs after the multiplication of the shear stress by the area of applied force. The Kinking of some points could be due to the wall deforming when seismic forces were applied. It can be inferred from these results that connecting the horizontal layers can increase integrity of the system due to confinement, while the wall acts as a block during seismic load events.

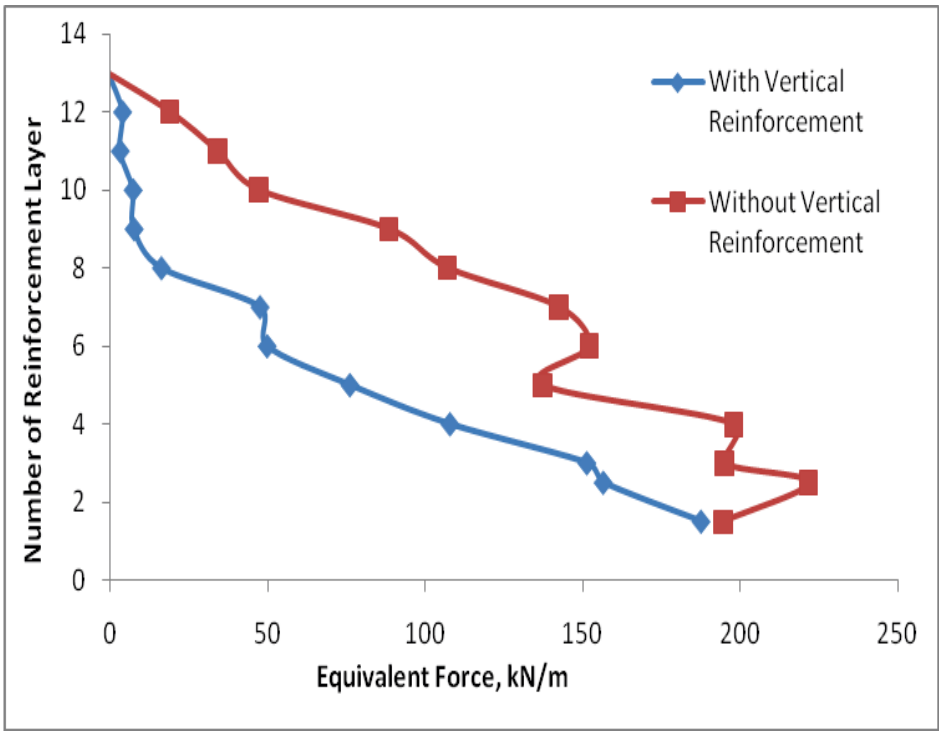

Figure 4.13 Comparison of equivalent vertical force between horizontal layers

4.5 Summary

Reinforced soil retaining walls have proven to be an appropriate solution for preventing walls from failure caused by earthquakes. A numerical study of reinforced soil retaining walls under seismic loads was conducted by varying the extent of the slopes of the angled reinforcements: a) 1H:1.5V inclined towards the facing, b) exactly vertical, c) 1H:1.5V inclined towards the wall, and d) without any additional reinforcement, by developing proper numerical models using PLAXIS software. Connecting each subsequent layer resulted in a remarkable reduction in the deformation of facing panels and vertical settlement. It was observed that an inclination of additional reinforcement does not have a significant effect on the performance of the wall, that is, the deformation values were very close to each other and cannot make any significant difference in practice. The results only differ markedly between with and without vertical reinforcement inclusion, whereas vertical reinforcement induced integrity into

the wall and reduced lateral deflection. The findings of this numerical study indicate that the proposed inclusion of vertical components into reinforced soil walls provides better stability compared to conventional reinforced soil systems under earthquake loading. Each conventional layer of reinforcement connected by vertical reinforcement is enhanced by additional components of tensile forces, and increased the frictional resistance.

The findings of this chapter clearly indicate that the application of vertical reinforcement in a reinforced soil system enhances its performance not only under static loads but also in seismic loading conditions. This vertical insertion increases the integrity of a reinforced wall, creates block actions, and reduces deformation at both the facing elements and foundation of the wall.

It should be noted that this proposed technique is innovative, and therefore the findings acquired from these numerical analyses need further validation. Further investigations have been carried out based on large scale laboratory testing with an advanced shake table to validate the results of the numerical analysis. Chapters 5 and 6 give details of these procedures and the results of this experimental program.

Chapter 5

5. Experimental Program

5.1 Introduction

This chapter focuses on the design of the model container, the tests associated with the shake table experiments, and it also includes the procedures for constructing the model and a description of the instrumentation used to conduct the tests. The laboratory test procedures and results, properties of selected fill materials, the materials used for constructing the container and its assembly are presented in detail. The specific scaling factors and similitude rules between the model, and the prototype for the material selection and input parameters, are also discussed in this chapter.

5.2 Shake Table

5.2.1 Previous shake table tests

Several studies have been conducted on the effect of reinforcement design parameters, including length, stiffness, and number of layers (i.e. vertical spacing between layers) in a systematic reinforcement scheme, on the response of reinforced soil retaining walls under static gravity and earthquakes.

Richardson & Lee (1975) pioneered shake table tests on a small scale model of a reinforced soil wall 380 mm high, reinforced with metallic strips and then subjected to horizontal sinusoidal seismic loadings of various base accelerations and frequencies. The laboratory tests showed that the walls responded like a nonlinear damped elastic system to the input vibrations. It was recommended that much more work was required

to understand the various aspects of reinforced walls under seismic loading conditions. Sakaguchi (1996) carried out reduced scale shake table tests on 1.5 m high reinforced soil models with a wrapped face and light weight modular block configurations. It was reported that the maximum lateral wall displacement of the wall reduced significantly by increasing the layers of reinforcement. Similar results have also been reported by Bathurst & Hatami (1998) using a numerical model of a 3 m high wall with a hinged toe. Koseki et al. (1998) carried out shake table tests on conventional and reinforced soil retaining walls of 0.5 m high and observed that the critical acceleration increased by about 20% when the top layer of reinforcement was lengthened by a factor of four and the fourth layer by a factor of 2.25. However, the shake table test results reported by Sakaguchi (1996), and the results of numerical modelling of walls subjected to simulated seismic shake by Bathurst & Hatami (1998), showed there may be a diminishing benefit from uniform length reinforcement beyond L/H = 1. Matsuo et al. (1998) carried out shake table tests on six reduced scale model reinforced soil walls reinforced with polypropylene geogrids, in two different heights where H = 1 and 1.4 m, and different ratios of length reinforcement to wall height (i.e. L/H = 0.4 & 0.7). The input base acceleration was sinusoidal with a frequency of 5 Hz and a stepwise increase in amplitude.

Nova-Roessig & Sitar (2006) used centrifuge tests to study the dynamic behaviour of soil slopes reinforced with geosynthetics and metal grids using centrifuge tests, and observed that the magnitude of deformation was related to the density of the backfill, the stiffness and spacing of the reinforcement, and inclination of the slope. They varied the relative density of the backfill sand by 55% and 75% and emphasised the use of relative density in the design, along with other parameters. El-Emam & Bathurst (2007) examined the influence of reinforcement properties on the response of reinforced soil

retaining walls to simulated seismic loading, using the results of a series of reduced scale reinforced soil retaining wall models built on a shake table. All the model walls were loaded to failure using a stepped amplitude harmonic excitation record applied to the base of the model. The results of this experiment showed that the magnitude of the accumulated facing lateral displacement subjected to base excitation decreased by increasing the length of the reinforcement, more layers of reinforcement, and stiffer reinforcement elements.

A background to the experimental design, equipment, and instrumentation of the models in that test program can be found in El-Emam & Bathurst (2004) . They investigated the influence of facing geometry, facing mass, and facing toe boundary condition on the response of the wall. Bathurst, Hatami & Alfaro (2002) summarised many studies related to the seismic aspects of soil walls reinforced with geosynthetics and reviewed the work associated with the properties of cohesionless soil, geosynthetic reinforcement, and facing components under cyclic loading. Ling et al. (2005) presented an experimental study of three 2.8 m high modular block soil walls reinforced with geosynthetic and subjected to shake that simulated the Kobe earthquake. Latha & Krishna (2008b) studied the influence of the relative density of the backfill soil on the seismic response of reinforced soil wall models. Sabermahani, Ghalandarzadeh & Fakher (2009) performed twenty 1 g shake table tests on soil walls reinforced with geosynthetics and observed different failure modes such as overturning and bulging of the facing, together with an additional base sliding mode that occurred simultaneously with the bulging and overturning modes. A summary of previous shake table tests of height less than a metre is listed in Table 5.1.

Despite the number of shake table tests performed on reinforced soil walls, there is no information in the literature on the physical modelling of vertical reinforcement

connecting horizontal layers under dynamic loading. In this study the response of the reinforced soil walls with the inclusion of vertical or angled reinforcements, as well as horizontal reinforcement layers, are analysed and compared with conventional cases based on the experimental results obtained from a large scale shake table. The performance of a combined vertical or inclined-horizontal reinforced soil wall versus conventional horizontal reinforcement under earthquake loads has been carefully investigated. In the present experimental study the parameters of the model such as its length, the spacing and stiffness of the reinforcements, density of the soil, and the amplitude, frequency, and duration of input motion were kept constant so the effects of vertical reinforcement on the seismic response of the wall could be compared, with an emphasis being placed on the modes of deformation and failure mechanisms at the wall. The goal is not only to compare the performance of a reinforced soil wall with and without the inclusion of vertical reinforcement, but also to evaluate its performance under dynamic loads, due to the angle of vertical reinforcement.

Table 5.1 Summary of different shake table tests of ≤ 1 m wall height from previous studies

Reference	Wall height, mm	Facing type	Reinforcement type	Input motion	Deformation mode
Koseki et al. (1998)	500	Full-height rigid facing	Grid strip	Sinusoidal	Overturning
Watanabe et al. (2003)	500	Full-height rigid facing	Phosphor-bronze strips	Scaled Kobe earthquake	Overturning
Richardson and Lee (1975)	28–410	Curved aluminium	Aluminium foil	Sinusoidal	Overturning
El-Emam and Bathurst (2007, 2004, 2005)	1000	Full-height rigid facing	Geogrid	Stepped sinusoidal	Overturning
Krishna and Latha (2007)	600	Wrap around	Woven geotextile	Sinusoidal	Overturning
Sabermahani et al. (2008)	1m	Wrap around	Weft knitters textile	Sinusoidal	Overturning-Bulging

5.2.2 UTS shake table facility

The dynamic behaviour of models of reinforced soil walls was undertaken on the current MTS Systems Corporation's uni-axial shake table located at the University of Technology, Sydney (UTS). The table is capable of high fidelity seismic reproductions across a range of key parameters. The specifications of the UTS shake table are shown in Table 5.2.

Table 5.2 UTS shake table specifications

Descriptions	Quantity
Size of table	3 m × 3 m
Maximum payload	10 tonnes
Overturning moment	100 kN-m
Maximum displacement	+/- 100 mm
Maximum velocity	+/- 550 mm/sec
Maximum acceleration	+/-2.5g or 0.9g (full load)
Testing frequency	0.1 – 50 Hz

5.3 Similitude Rules

Model tests were performed on scaled versions of prototype structures. It is important for this type of testing to correctly scale down the soil and the reinforcement properties, including the stress dependent behaviour of the soil and boundary conditions, and to conform to similitude requirements in order to accurately predict the behaviour of the prototype structure.

It should be noted that since soil behaviour is stress dependent, the seismic response of GRS walls in 1 g shake table tests cannot be completely compared with a prototype due to the low confining stress. Moreover, as noted by El-Emam & Bathurst (2007), the interaction between the reinforcement and granular soil under very low confining pressures (the topmost layer of reinforcement in these tests) can be expected to be less than the corresponding layer of reinforcement located at a greater depth at prototype scale. Since physical models are shorter versions of prototype walls, the frequency of induced input motions should be scaled to produce effects that are similar to those of earthquakes on prototype walls.

In this study, the shake table models are based on the prototype of a 6.5 m high GRS wall. Considering the above mentioned aspects of similitude between model and prototype, the scaling factors for various parameters were obtained based on the scaling relationships proposed by Iai (1989b) and discussed and developed by Wood (2004). The scaling factors for this study are presented in Table 5.3.

Table 5.3 Scaling factors for shake table tests

Description	Parameter	Scale factor	Scale factor M/P	Scale factor P/M
Acceleration	a	1	1	1
Length	L	1/N	0.1	10
Displacement	d	$1/N^{1.5}$	0.032	31.623
Frequency	f	$N^{0.75}$	5.62	0.177
Shear wave	Vs	$1/N^{0.25}$	0.56	1.77
Time	t	$N^{0.75}$	0.177	5.62

Note: N = 10, M= Model, P= Prototype

5.4 Design and Assembly of Model Container

After reviewing past experiments and the facility available in the UTS laboratory, the following configurations of the container and the model were prepared for the shake table tests proposed for this study (Table 5.4). Figure 5.1 shows a side view of the proposed model with 6 layers of reinforcements 100 mm high.

Table 5.4 Proposed shake table configuration

Wall height	Facing type	Reinforcement type	Input motion
0.65 m	Wrap around	Geonet	Stepped sinusoidal

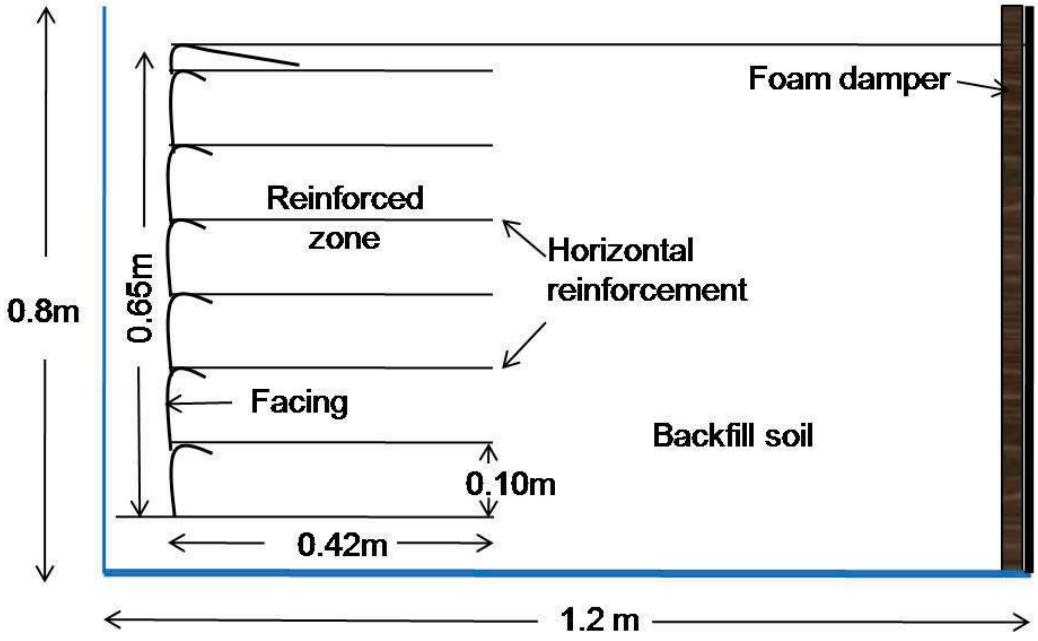

Figure 5.1 Model general configurations

5.4.1 Model geometry

The physical models were constructed into a 0.75 m wide by 1.80 m long by 0.8 m high container, which were fabricated from plywood at the base and backside, and rigid transparent Plexiglas sheets on two sides. The main purpose of using acrylic sheet was

to be able to observe the failure mechanisms more closely and accurately. All the model parameters were identical in all experiments except for the inclusion of vertical or inclined reinforcement, and with the horizontal reinforcement. The geometry of materials used to prepare the box is illustrated in Figure 5.2.

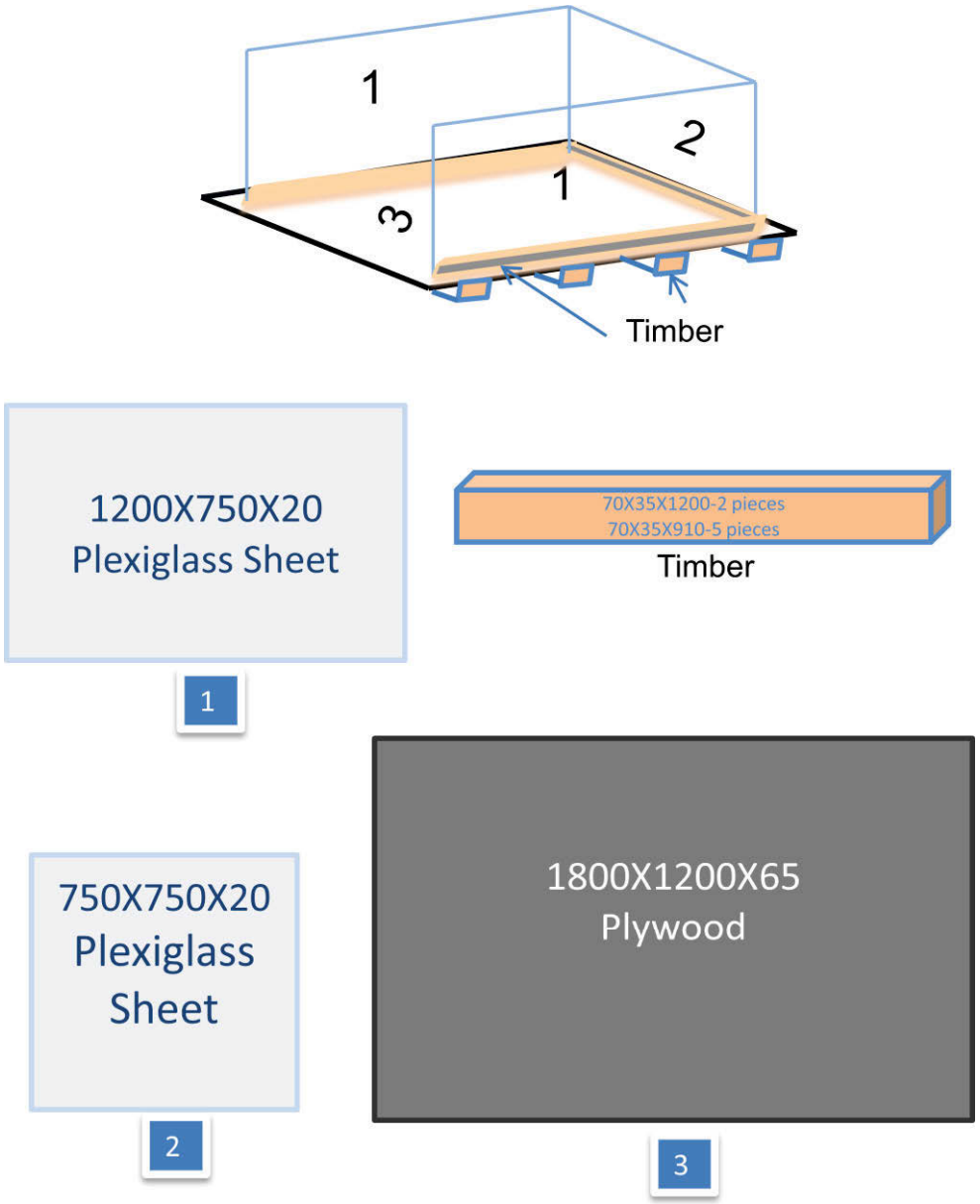

Figure 5.2 Required materials for container (all dimensions are in mm)

The important feature governing the scaling effects and response of the model compared to the prototype is the height of the wall. Obviously, more realistic results can be

obtained with models with higher walls. In this study, 0.65 m high wall was adopted similar to some models previously published in literature.

5.4.2 Container assembly

The type of materials and its dimensions are illustrated in Figure 5.3 in details.

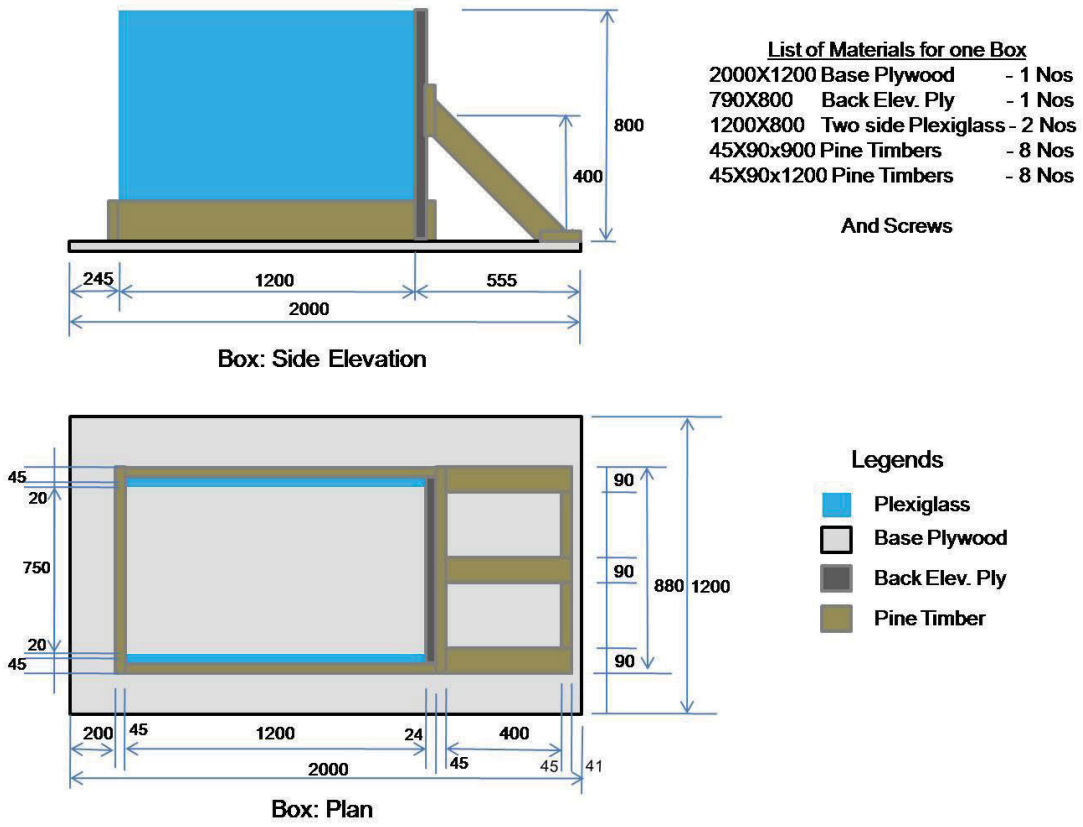

Figure 5.3 Details of the model box elements (all dimensions are in mm)

Figure 5.4 is the photograph of the container before the lamination was peeled from both sides of acrylic sheet. Likewise, the backside of the container is shown in Figure 5.5, which was made from plywood and fitted with three braces to resist the high lateral forces induced during shaking.

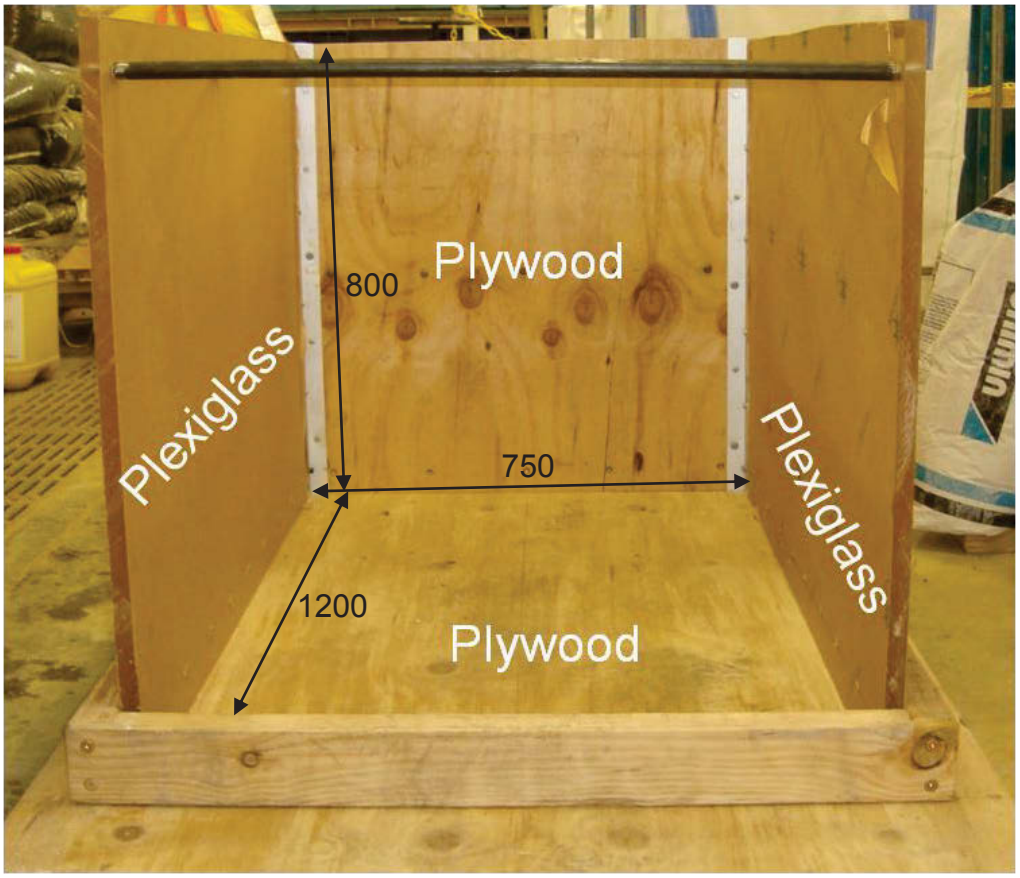

Figure 5.4 Front view of container

Figure 5.5 Rear view of container

5.4.3 Facing elements

Transparent plastic sheets were used as a wrap around type of facing, although it can deform into different curved or linear shapes. Sabermahani, Ghalandarzadeh & Fakher (2009) used similar facing elements because these flexible facings did not interact with the rigid planar elements (compared to the modular block or rigid, full height facings). The fabrication of the facing element with horizontal reinforcement for the first layer back fill is shown in Figure 5.6. Bathurst, Hatami & Alfaro (2002) measured the displacements of the wall for several models with different types of facing. They found that vertical walls with rigid, full height facings had better resistance and less deformation than segmented block facing walls with no shear connections. Walls with wrap around facings were expected to show more displacement than other types because they have no structural stiffness against lateral displacement.

Figure 5.6 Fabrication of facing with reinforcement

5.4.4 Back boundary

A high damping rubber sheet was attached to the back of the plywood wall, as shown in Figure 5.7. The rigid back wall of the strong box may influence the dynamic response of the model walls, as noted by El-Emam & Bathurst (2005). As reported by Bathurst & Hatami (1998) in a numerical study, far field boundary conditions have a significant effect on the response of reinforced soil walls, although comparatively the wave reflection and boundary effects will decrease when a compressible 16 mm thick ductile rubber boundary is used in the models rather than rigid wooden walls.

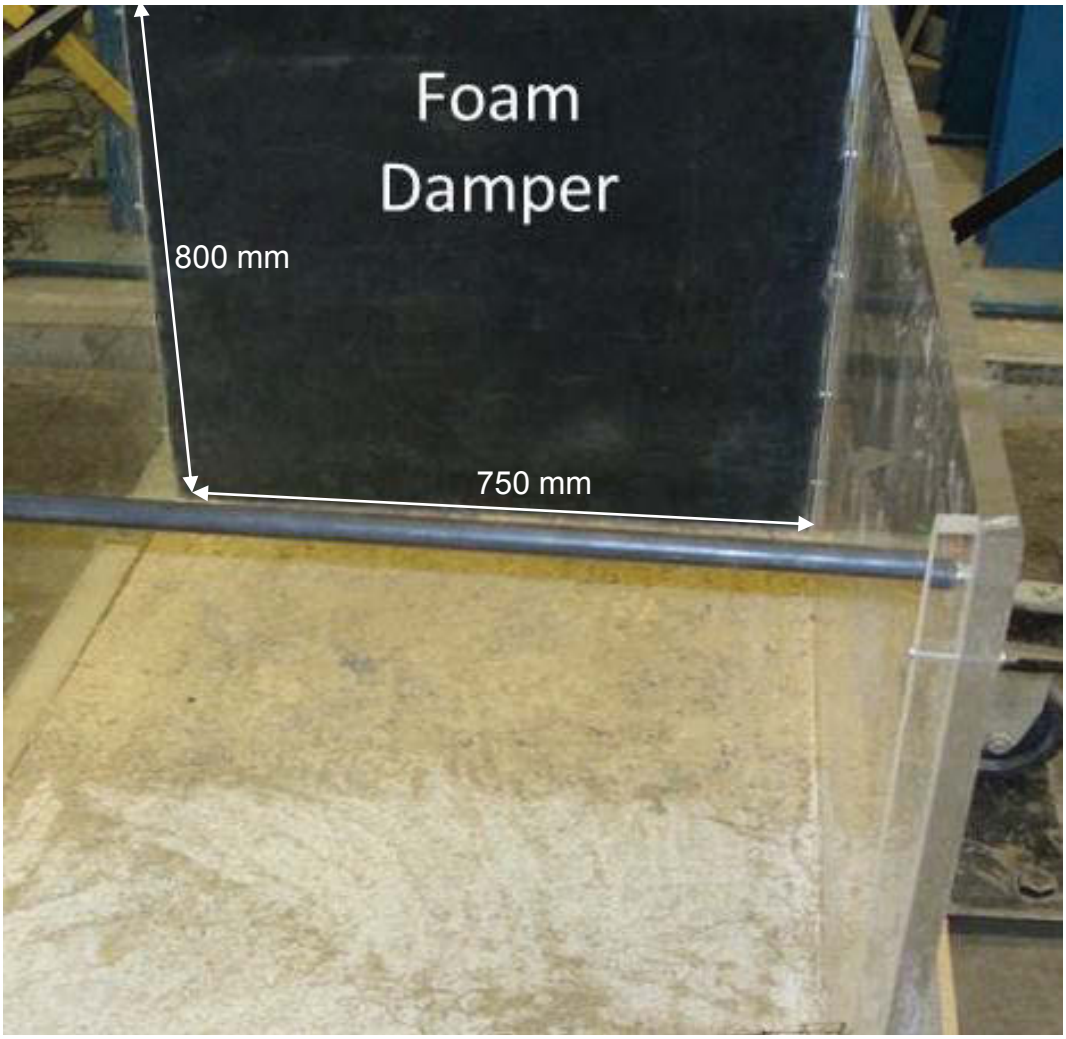

Figure 5.7 Foam damper at the back of model box

5.4.5 Foundation and toe boundaries

The foundation was 150 mm thick due to limitations in the height of the container and total weight of the model. The foundation layers were compacted after construction using enough vibration to make a firm rigid layer for all the model walls and also to reach its maximum dry density. It is important to note that thickness and stiffness of the foundation can influence the seismic response of superstructures. El-Emam & Bathurst (2005) showed that the base boundary type (hinged or free sliding toe) is an important factor influencing the quantitative and qualitative responses of reduced scale shake table tests. Construction of the wall began on the surface of the foundation so none of the reinforced layers of soil were buried in the foundation layer. Consequently, the toe boundary of the wall could be expected to slide freely horizontally. The surface of the foundation prepared for the model is shown in Figure 5.8.

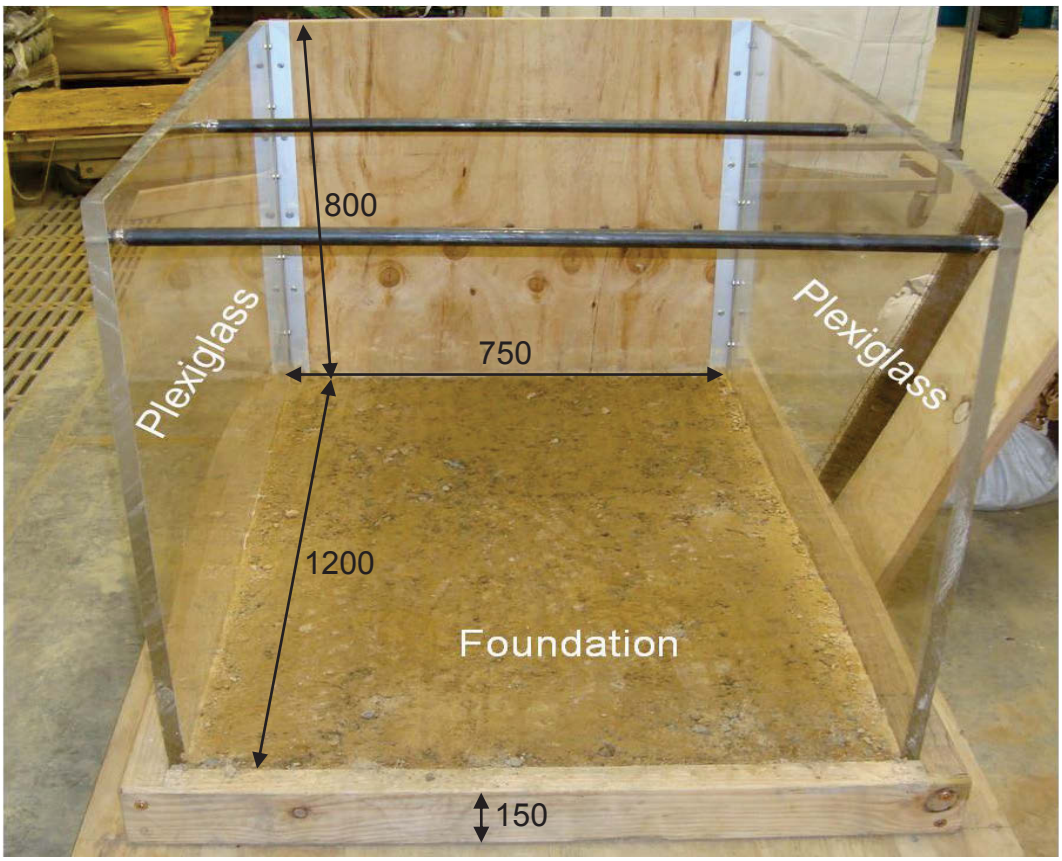

Figure 5.8 Foundation layer after compaction (all dimensions are in mm)

5.4.6 Materials required to prepare the shake table model

The most important material here is the soil and its reinforcement. The materials used to prepare the model for shake table tests are presented in Table 5.5.

Table 5.5 List of materials

SN	Particulars	Quantity
1	Sand for backfill soil	3 m^2
2	Geogrid net	20 m^2
3	Vertical reinforcement (0.2mm diameter wire)	150 m
4	Foam damper	2 m^2
5	Acrylic plastic sheet	10 m^2
6	Wooden strips for the installation of VR	5 pieces
7	Knot-bolts, pins, glues, etc.	Sufficient quantities

5.5 Physical Properties of Sand

5.5.1 Sieve analysis

River sand from Queensland was used as backfill sand. A sieve analysis was carried out according to Australian Standard 1289.5.5.1-1998 *Soil compaction and density tests-Determination of the minimum and maximum dry density of a cohesionless material – Standard method*. The grain size distribution of sand used in all shake table tests is shown in Figure 5.9.

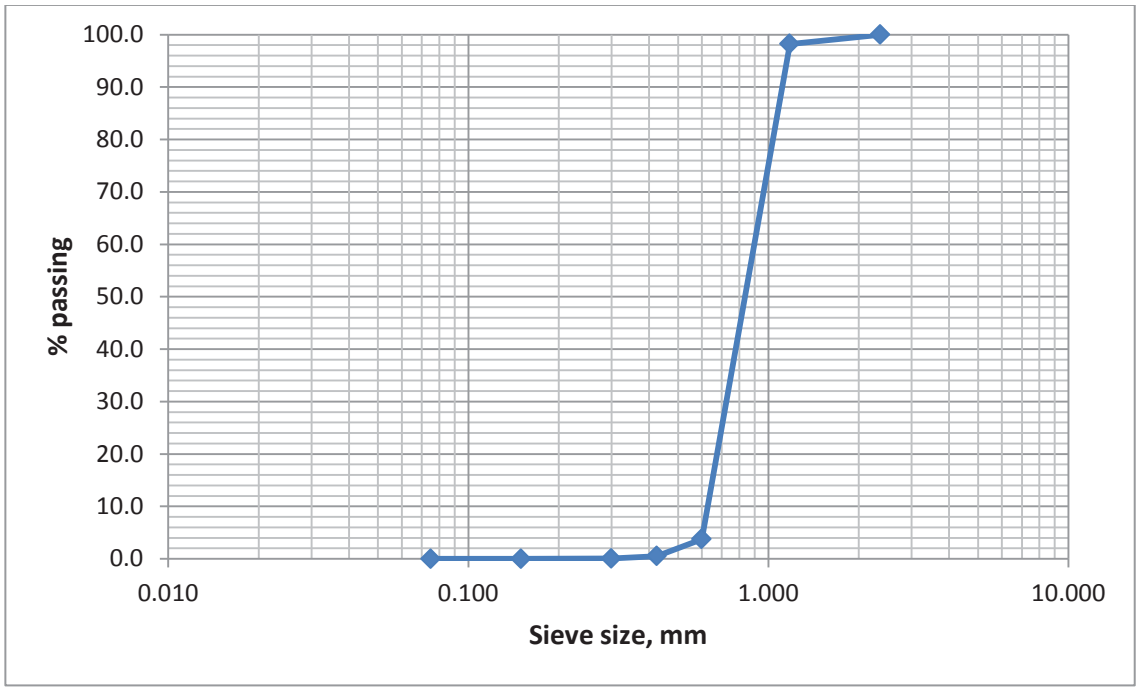

Figure 5.9 Grain size distribution of sand used in all shake table tests

The sand used was gap graded with a maximum particle size of 1.5 mm, the coefficient of curvature of C_c = 0.96, the coefficient of uniformity of C_u = 1.5 and with a negligible fines content (Table 5.6).

Table 5.6 Backfill soil properties

Specific gravity	Maximum void ration	Minimum void ratio	Mean diameter	Uniformity coefficient	Coefficient of curvature
G_s	e_{max}	e_{min}	D_{50} (mm)	C_u	C_c
2.65	0.65	0.43	0.85	1.5	0.96

5.5.2 Minimum and maximum density tests

The following methods cover the laboratory procedures used to determine the minimum and maximum dry densities of a cohesionless material according to Australian Standard

1289.5.5.1 – 1998, using loose pouring to obtain the minimum dry density and vibratory compaction to obtain the maximum dry density.

Minimum dry density: A mould with a volume of 1×10^3 cm^3 and an internal diameter of 105 mm and a 13-mm funnel were selected. The funnel was used to fill the mould to overflowing by pouring the soil in as loosely as possible. The funnel allows the soil to flow not more than 20mm in a steady stream, while simultaneously moving the funnel in a spiral motion from outside towards the centre of the mould to form a layer of uniform thickness and with the minimum of segregation, as shown in Figure 5.10. A steel straightedge was then used to level the sand in the mould.

Figure 5.10 Sand placing by pouring funnel to find out minimum dry density

The densities of two tests obtained by dividing the mass of sand by its volume were 15.96 kN/m^3 and 16.06 kN/m^3, so the lowest value of 15.96 kN/m^3 was used as the minimum dry density.

Maximum dry density: The same mould was used for this test, but in time it was placed on a vibratory table which had a uni-directional vibrator with a nominal operating frequency of 50 Hz. The saturated sand was mixed to obtain an even distribution of particle size, transferred to the mould and fitted with a collar assembly. The mould assembly with a surcharge of 5 kg was attached to the vibratory table as shown in Figure 5.11.

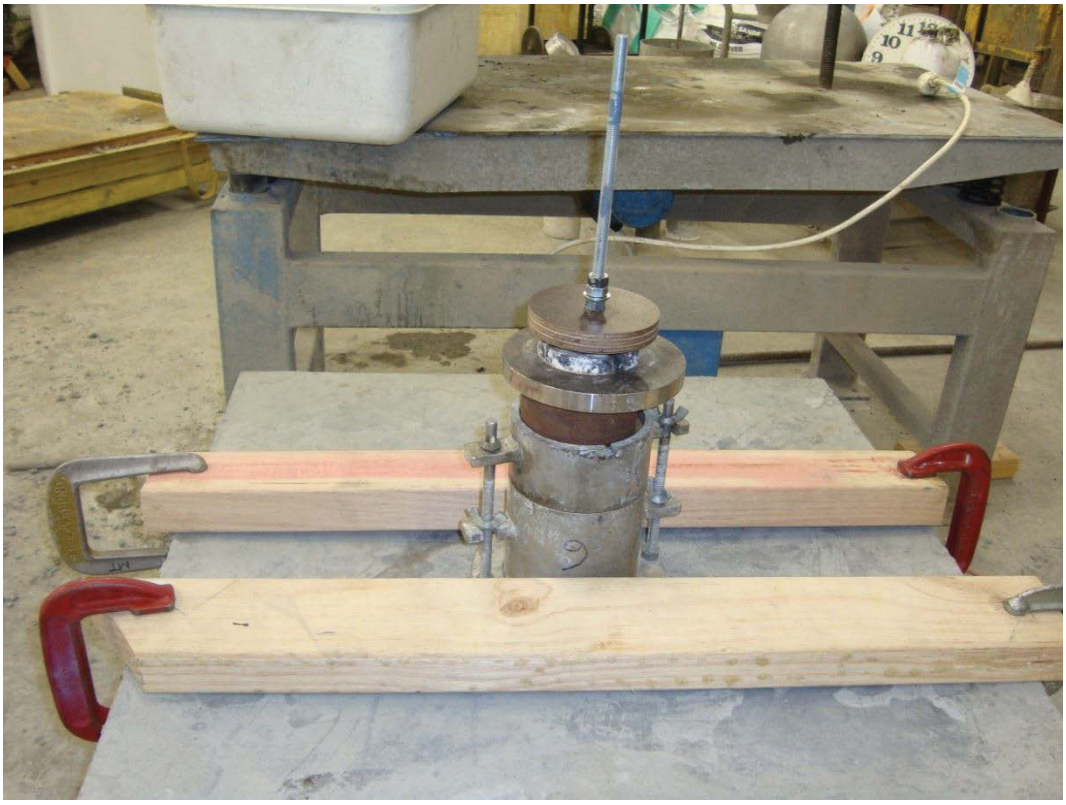

Figure 5.11 Mould assembly and the vibratory table

The mould assembly was vibrated for 5 minutes to dissipate any water that appeared above the surface of the test material, and then it was vibrated again for a further 10 minutes. The surcharge was removed and sand was levelled with a straightedge. The calculated dry densities for the three samples were 18.12 kN/m^3, 18.16 kN/m^3, and 18.16 kN/m^3 respectively, so the maximum dry density of 18.15 kN/m^3 was adopted as an average of those three tests.

5.5.3 Direct shear tests

A direct shear test is a quick and inexpensive method estimating the shearing strength of soils. The test equipment consists of a split metal box with internal dimensions of 60mm × 60mm, in which the soil specimen is placed. The two halves of the box can be moved relative to each other to create a failure plane. A normal vertical force is applied to the failure plane by a hanger while a shear force is applied by moving one half of the box relative to the other half at a constant rate of 1 mm/minutes, causing failure in the soil specimen. The shear force transmitted by the soil to the upper half of the box can be measured at different stages of loading. In this study, normal forces of 156 N, 245 N, and 334 N were used for three runs. The weight of hanger was 66.7 N, and therefore the normal stresses applied in three different tests were 43.33, 68.05, and 92.78 kN/m^2, respectively.

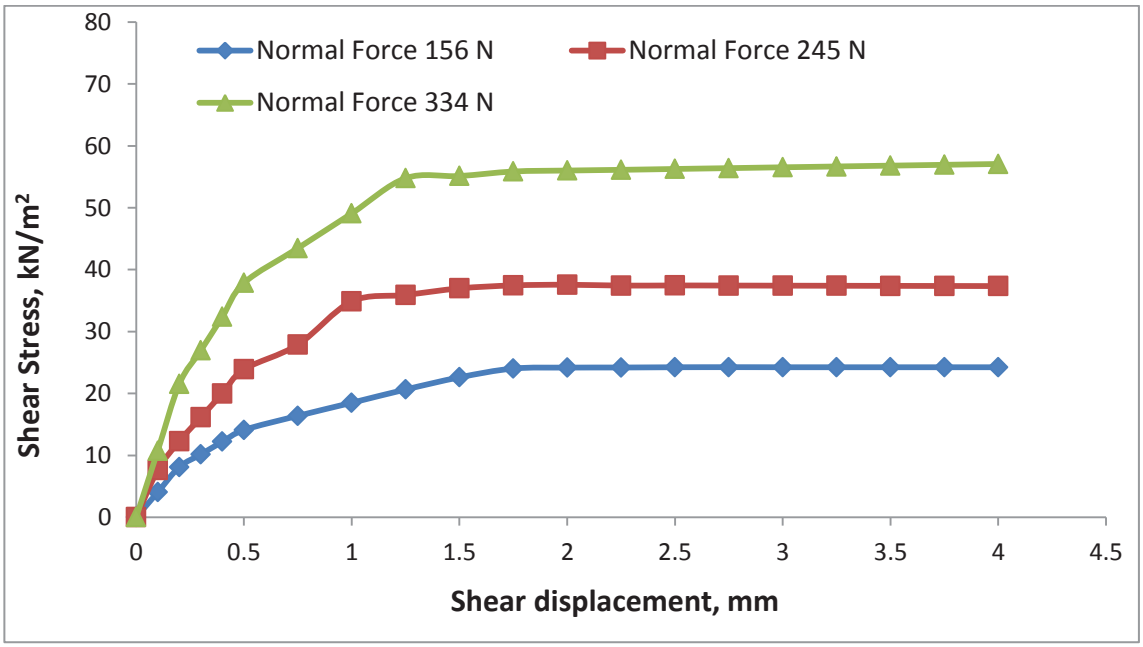

Figure 5.12 Shear stress versus shear displacement

From Figure 5.12, the variation of shear strength of sand with normal shear stress was obtained as shown in Table 5.7.

Table 5.7 Deviation of shear stress with normal stress in sand

Normal stress, σ kN/m^2	Shear stress at failure, τ kN/m^2
43.33	24.2
68.05	37.5
92.78	56

The shear strength parameters of sand used in this study was identified by plotting the above data, as shown in Figure 5.13.

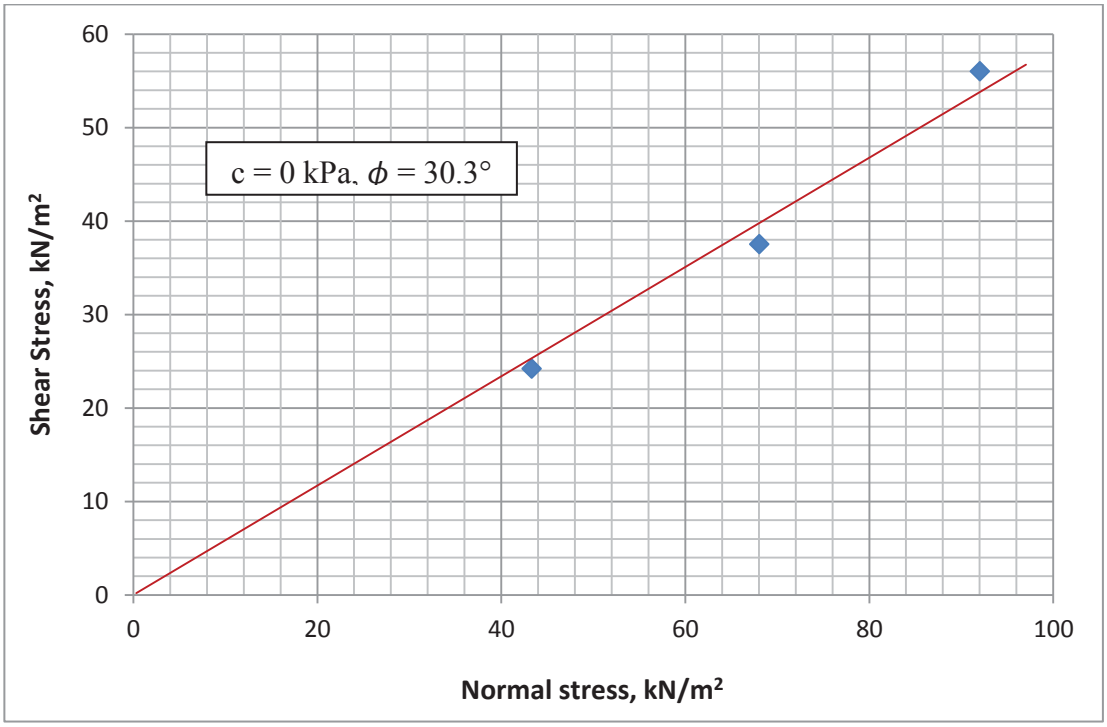

Figure 5.13 Shear stress versus normal stress

The graph shows that the sand had a peak friction angle of 30.3° at the target compaction level.

5.5.4 Summary of test results

A moving mechanical elevation system was designed to place the sand layer by layer as a backfill material moving across the container longitudinally and vertically. During construction the dry unit weight was controlled at approximately 15.1 kN/m^3 which resulted in a relative density of 32%. The sandy soil was gap graded with a maximum particle size 1.5 mm, a coefficient of curvature C_c = 0.96, a coefficient of uniformity C_u = 1.5, and with negligible fines content (Table 5.8). Direct shear box tests, 60 mm by 60 mm in plan, were carried out on the soil with the above mentioned level of compaction. Accurate measurements indicated that the peak friction angle was 33°. To achieve the relative density required for all the layers, soil pluviation was carried out from a constant height. This was accomplished by raising the level of the trapdoor for each level so that a constant height was maintained between each layer. The opening size suggested by Latha & Krishna (2008b) was adopted for this purpose.

5.6 Material Testing of Reinforcements and Damping System

Viswanadham & Mahajan (2007) reported that the selection, modelling, and instrumentation of idealised materials were major factors in the research involving physical models using geosynthetic materials. The creation of models with similitude does not allow for the use of identical geosynthetic materials in the model or the prototype studies. A lightweight, scaled down and commercially available geonets were used as horizontal reinforcement to provide similitude and observe failure mechanisms in the physical models. Commercially available binding wires were used as a vertical reinforcement after their tensile strengths were measured.

5.6.1 Tensile tests for geonets

Special commercially available geonets were examined based on several tensile tests and then used as horizontal reinforcement. The ultimate tensile strength of the horizontal reinforcement was determined by the strip method as per AS 2001.2.3.1 2001: *Methods of test for textiles*, using a Universal Testing Machine (Figure 5.14). The machine operates via a stationary clamp and a moving clamp that operates at a constant speed throughout the test. The rigidity of this testing system means that it operates virtually free from any deflection.

Figure 5.14 The Universal Testing Machine and the associated data acquisition system used for conducting tensile tests

Each test specimen was 50 mm wide and was long enough to allow a gauge length of 250 mm. The samples were glued with plywood to ensure that clamping was perfect. A number of tested samples are shown in Figure 5.15.

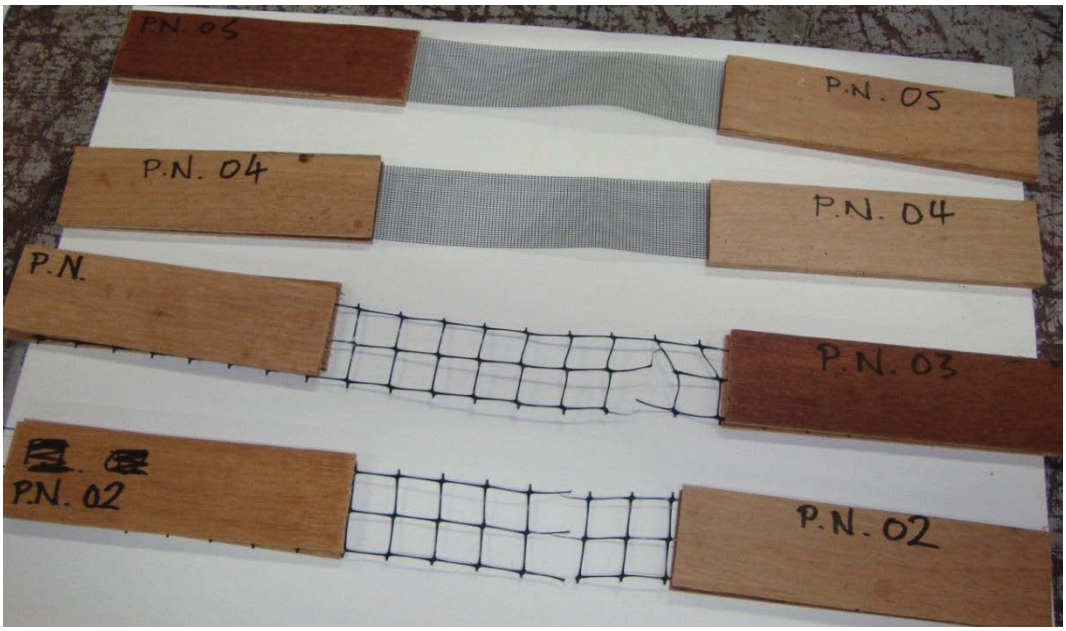

Figure 5.15 Test specimens for tensile tests

The test setup before the commencement of test is demonstrated in Figure 5.16.

Figure 5.16 A clamped specimen during a tensile test

The results and analyses of the tests of fine and coarse geonets are shown in Table 5.8.

Table 5.8 Results and analyses of tensile tests

SN	Type of geonets	Sample name	P_{max} (kN)	Tensile stiffness (kN/m)
1		PN-01	0.162	205
2	Fine nets	PN-02	0.216	270
3		PN-03	0.235	240
4		PN-04	0.531	535
5	Coarse nets	PN-05	0.401	475
6		PN-06	0.461	495

The sample load verses elongation for the used geonets (PN-05) is shown in Figure 5.17.

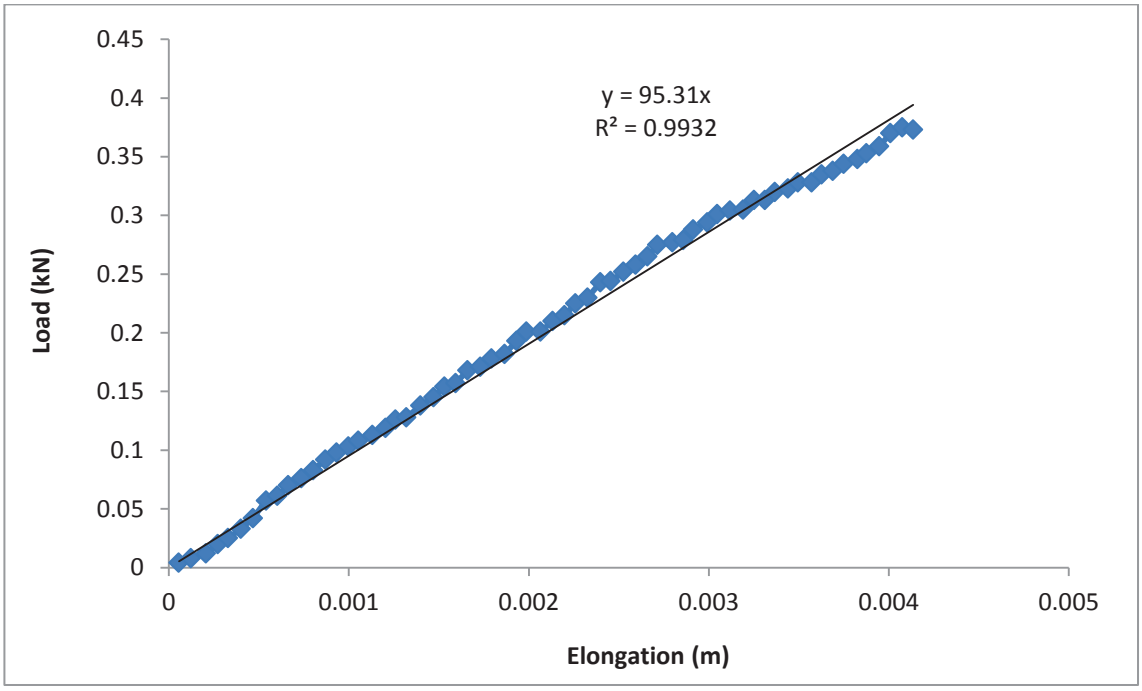

Figure 5.17 Load verses elongation graph of the adopted geonet polymer (PN-05)

For instance, Figure 5.17 shows the slope is equal to EA/L, where EA is the stiffness and L is the length of the specimen. The tensile stiffness per metre is calculated (475 kN/m) from the slope (95 kN/m) multiplying by the length of the specimen (0.25 m) and divided by the width of the strip (0.05 m). The calculated tensile stiffnesses of the different samples are presented in Table 5.9. A coarse net was used as horizontal reinforcement in the model because of its appropriate tensile stiffness, which is adopted as 500kN/m for further analyses.

5.6.2 Tensile tests for binding wires

A commercially available plastic coated binding wire 0.2mm in diameter was used for vertical reinforcement. The wire was tested beforehand according to Australian Standard AS 1391-2007: *Metallic materials – Tensile testing at ambient temperature, to measure its ultimate tensile strength*. Because the wire was less than 4 mm in diameter the testing procedure was according to Appendix B of this standard. The original gauge length was taken as 200 mm. The testing machine and a close view of the clamps are shown in Figures 5.18 and 5.19, respectively.

Tensile test of three samples were carried out to determine the ultimate tensile strength and the stiffness of the wire. The results of the tests and analysis are presented in Table 5.9.

Tensile stiffness is the multiplication of Young's Modulus (E) and cross sectional area of the wire (A), where E is the secant modulus taken at the mid stress level calculated from the stress-strain curve (Figure 5.20).

Table 5.9 Results of tensile test of wires

Sample no.	Test	P_{max} (N)	Tensile stiffness (kN)
1	Tensile Test 1	85	4.42
2	Tensile Test 2	88	4.87
3	Tensile Test 3	84.5	4.99
	Adopted	85	4.5

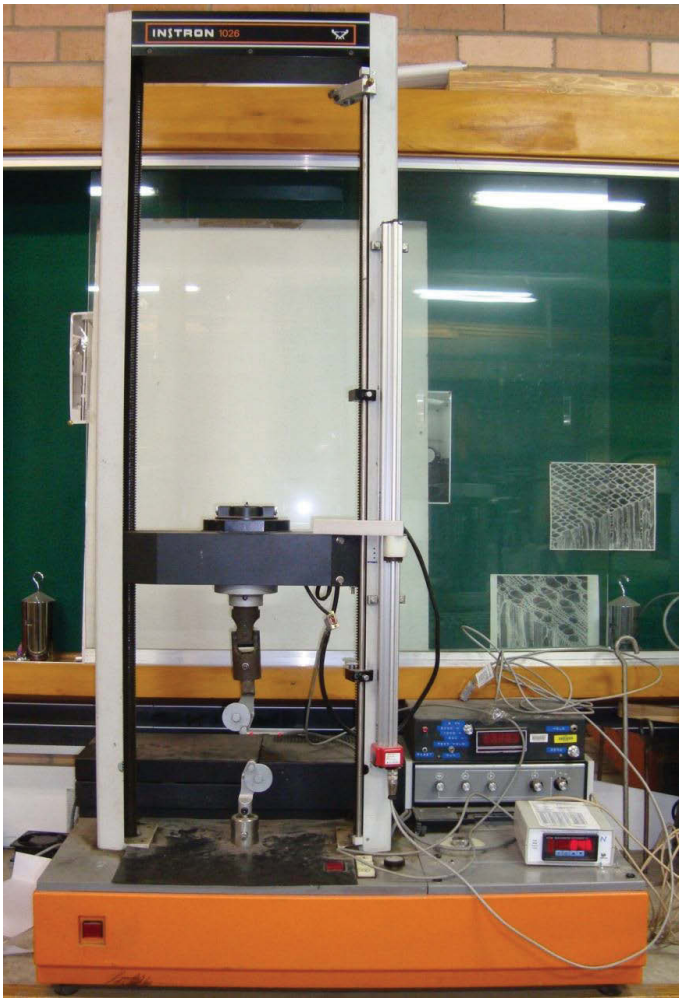

Figure 5.18 Tensile test on wires used as vertical reinforcement

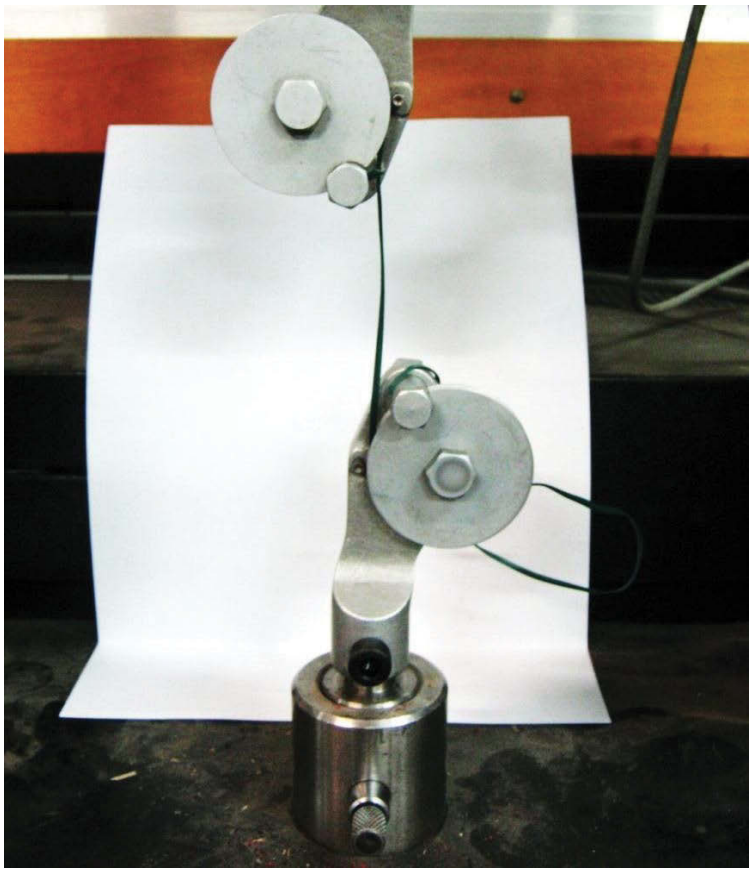

Figure 5.19 A clamped specimen during a tensile test of the wire

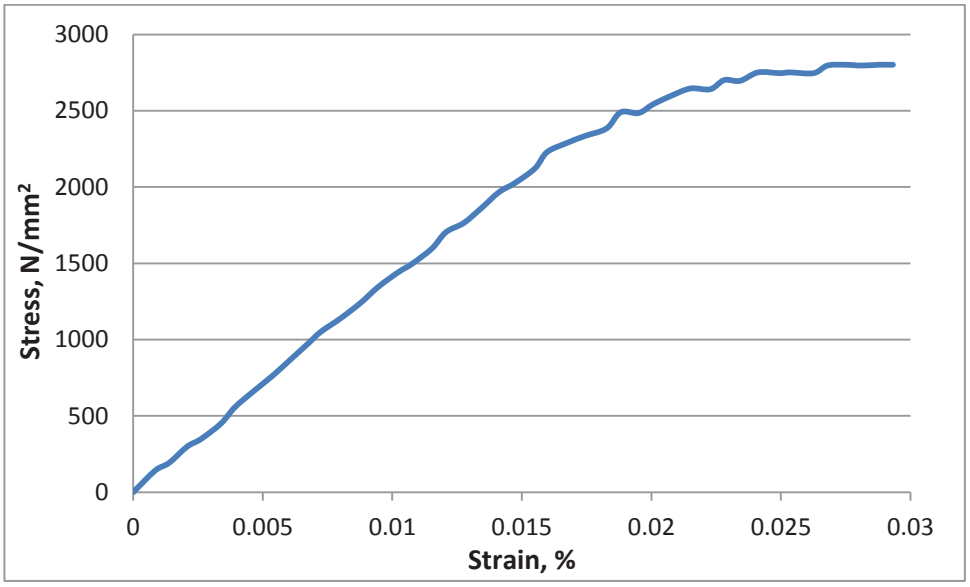

Figure 5.20 Stress verses strain curve of Tensile Test 2 of the wire.

5.6.3 Damping test

A 16 mm thick rubber sheet with a high damping effect was used at the back of the rigid wall to reduce the boundary effects under dynamic loads. The damping ratio was quantified using free vibration tests, as shown in Figure 5.21.

Figure 5.21 Free vibration test to measure the damping ratio

A 16 mm × 16 mm × 50 mm sample of the rubber was glued to a metal strip, as shown in Figure 5.21, and then hit with a special hammer whose impact and acceleration were recorded in the data acquisition system. The effect of damping free vibration is shown in Figure 5.22.

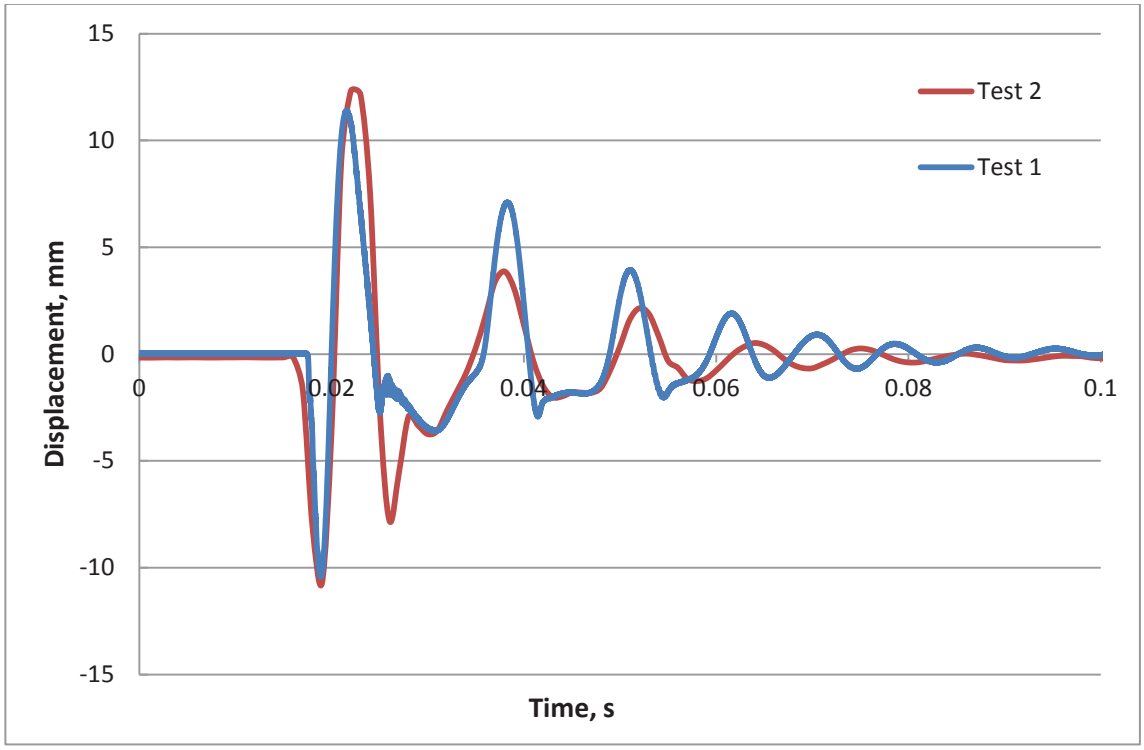

Figure 5.22 Effect of damping the vibration

To evaluate the vibration in underdamped systems, the damping ratio, D was calculated in a very simplified way, based on the following equation:

$$D = \frac{u_n - u_{n+m}}{2m\pi u_{n+m}} \quad (5.1)$$

Where u_n is the first term and u_{n+m} is the second term of the series. Using Equation 5.1, the damping ratio was estimated to be around 20%.

When observing damped vibrations experimentally, a convenient method for estimating the damping ratio is to count the number of cycles required to reduce the amplitude by 50%. As a rule of thumb, it is convenient to remember that for 10% critical damping, the amplitude is reduced by 50% in one cycle. Based on this rule, the damping ratio was also found to be close to 20%.

5.6.4 Summary of test results

The properties of the horizontal and vertical reinforcement used in the shake table investigations are summarised in Table 5.10.

Table 5.10 Properties of reinforcements

Reinforcement type	Description	Value
Horizontal reinforcement (geonet)	Mass/unit area (g/m^2)	56.5
	Thickness (mm)	1
	Ultimate tensile strength (kN/m)	0.52
	Tensile strength (kN/m) at 2% strain	0.43
	Tensile stiffness (kN/m) at 2% strain	500
Vertical reinforcement (binding wires)	Diameter (mm)	0.2
	Ultimate tensile strength (kN)	0.085
	Tensile stiffness (kN) at 2% strain	4.5

5.7 Model Preparation and Instrumentation

Four different models were prepared in this study. They were categorised as GRS walls without vertical reinforcement (Model 1), with the inclusion of vertical reinforcement (Model 2), with reinforcement inclined towards the wall face (Model 3), and with reinforcement inclined away from the wall face (Model 4). The foundation was 150mm thick, which reflected the limitations due to the height of the container and total weight of the physical model. The foundation layers were heavily compacted to make a firm rigid layer for all the model walls. It is important to note that the thickness and stiffness of the foundation can influence the seismic response of superstructures. El-Emam & Bathurst (2005) showed that the type of base boundary (hinged or free sliding toe) is an

important factor influencing the quantitative and qualitative response of the reduced scale shake table tests. Construction of the wall began on the surface of the foundation, so none of the layers of reinforced soil were buried in the foundation layer.

One side of the model box was open towards the wall face. A scaffolding system was erected so that the wall face could be built. Six pieces of Plexiglass (plank) 100 mm × 750 mm were used to support the facing. Each layer of geogrid was wrapped at the facing for a length of 100 mm. To achieve a uniform density the sand was pluviated into the model box through a device which moved the sand to and fro so that it spread evenly. This device was constructed by inserting a 300 mm diameter funnel into a bucket so that the sand passes through a 15 mm internal diameter hole in the neck. The height from which the sand fell to achieve the desired density required was determined by trial and error until it was found that a height of 750mm (Figure 5.23) corresponded to the target density.

Figure 5.23 Determination of falling height for sand backfilling

Figure 5.24 Sand backfilling in the model

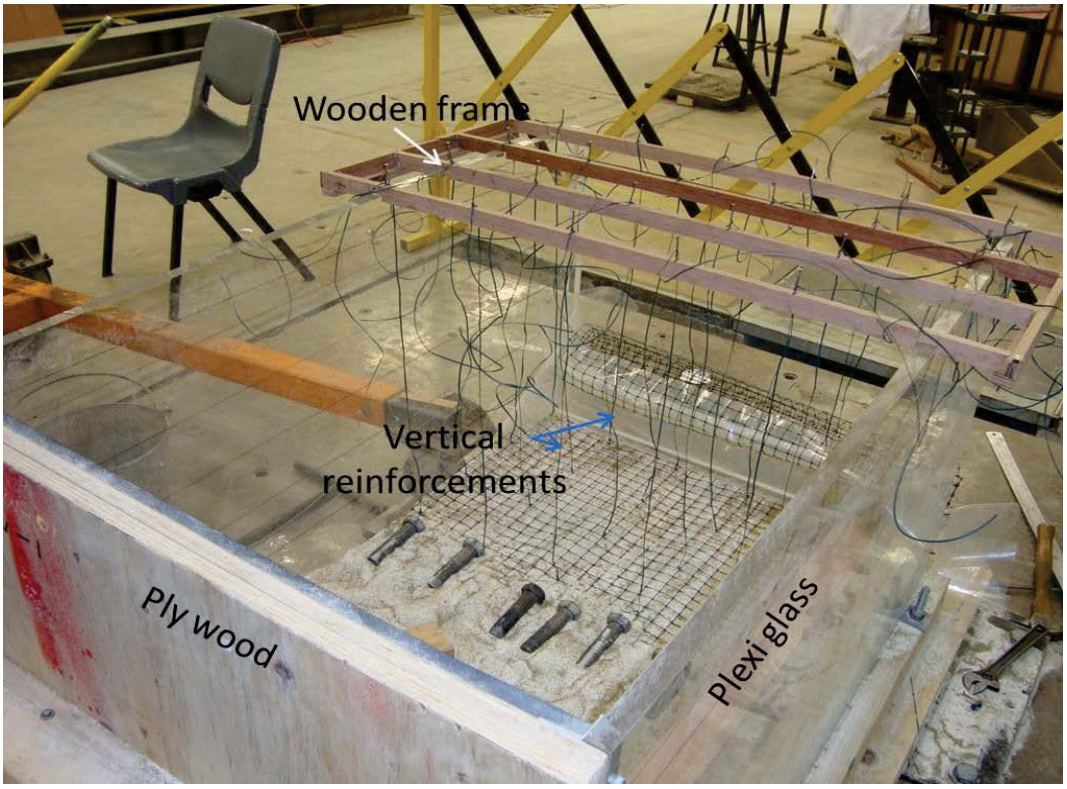

Figure 5.25 Installation of vertical reinforcements

The actual relative densities achieved in each test were monitored by collecting samples in a mould of a known volume that was placed at different locations and levels while the model retaining wall was being prepared. The relative densities measured from these moulds varied by 2% for each test, which was almost uniform, unlike the gross relative density that was computed based on the dimensions of the model and the quantity of backfill soil consumed. The back filling process for the sand is shown in Figure 5.24.

The configurations of the reinforced soil wall were similar in all the models, apart from the insertion of vertical reinforcement (Model 2), and angled reinforcement (Models 3 and 4). To install the vertical reinforcement, a wooden frame was made and placed on the top of the box, as shown in Figure 5.25, and then the wires to be used as vertical reinforcement were supported by the frame and also tied to the bottom layer. Then, as with Model 1 (conventional reinforcement), the selected granular material was compacted over the horizontal reinforcement to a height of 100 mm and then another layer of horizontal reinforcement was laid down. Afterwards, the vertical reinforcements were tied to the corresponding nodes of geonets (horizontal reinforcement). There is a possibility that the relative density of the sand may be altered due the disturbance produced by tying vertical reinforcement. However, those disturbances were overcome by consequent over lay. The reinforcements angled towards the wall and away from the wall face (2V in 1H, i.e. 26.6° to the vertical) were fabricated in Model 3 and Model 4 in a similar way. The installation and arrangement of the vertical reinforcement is shown in Figure 5.25.

Figure 5.26 shows the completed reinforced wall. The support formwork was carefully withdrawn after the backfill layers were in place. The 420 mm length (L) of geotextile reinforcement at the interface between the layers of sand was kept the same in all tests

of the reinforced soil walls. This length corresponds to the L/H ratio of 0.7, which is the minimum required for reinforced earth structures (FHWA 2001).

Figure 5.26 Wall with temporary support in facing

This experimental program has been devised to observe the influence of vertical/angled reinforcement on the dynamic response of reinforced soil retaining wall models with the same configurations and facing systems, and under identical shake conditions. The accelerations and deformations were measured using accelerometers and displacement transducers (LVDT sensors), respectively. The acceleration sensors were positioned inside the soils, but on the top of each alternate layer, and 50 mm away from the facing, as shown in Figure 5.27.

Figure 5.27 Installation of the accelerometer

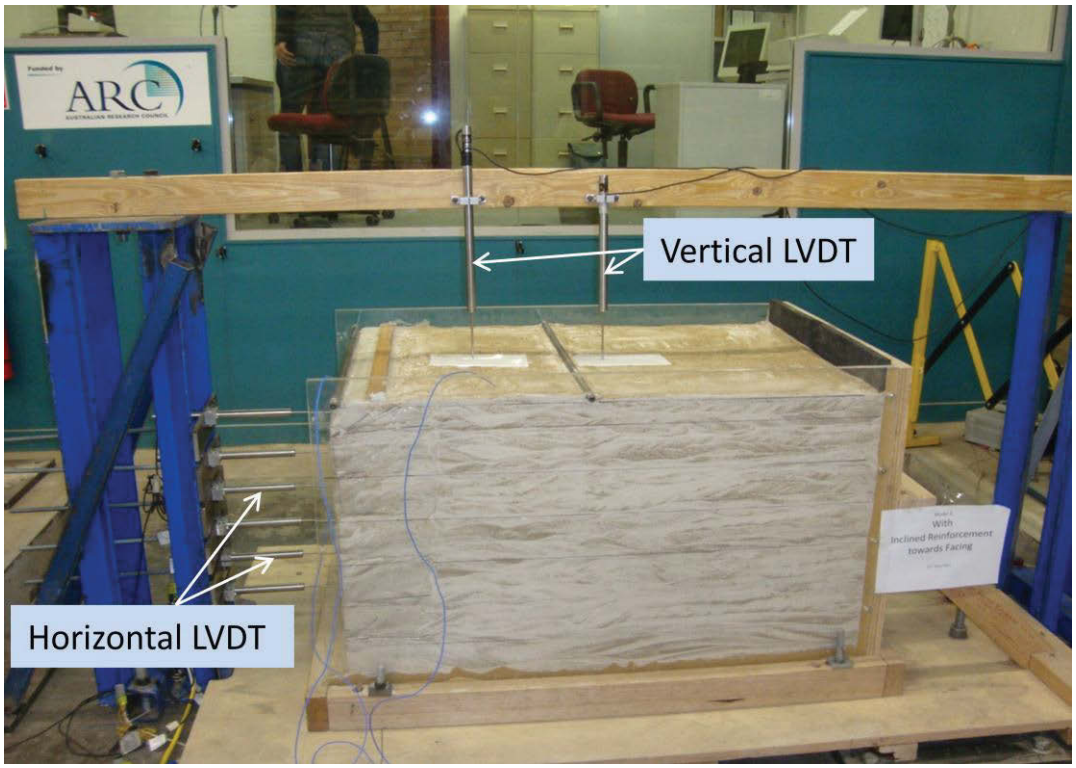

Figure 5.28 Installation of LVDTs prior to the test

Facing deformations were measured using LVDTs attached to a rigid column, which was fastened to the body of the chamber with a stiff beam. As shown in Figure 5.28, the

horizontal and vertical deformations of the facing were measured by six horizontal LVDTs installed in the mid-level of each layer and two vertical LVDTs set up 200 mm and 400 mm away from the facing. The positioning details of the instrumentation are illustrated in Figure 5.29.

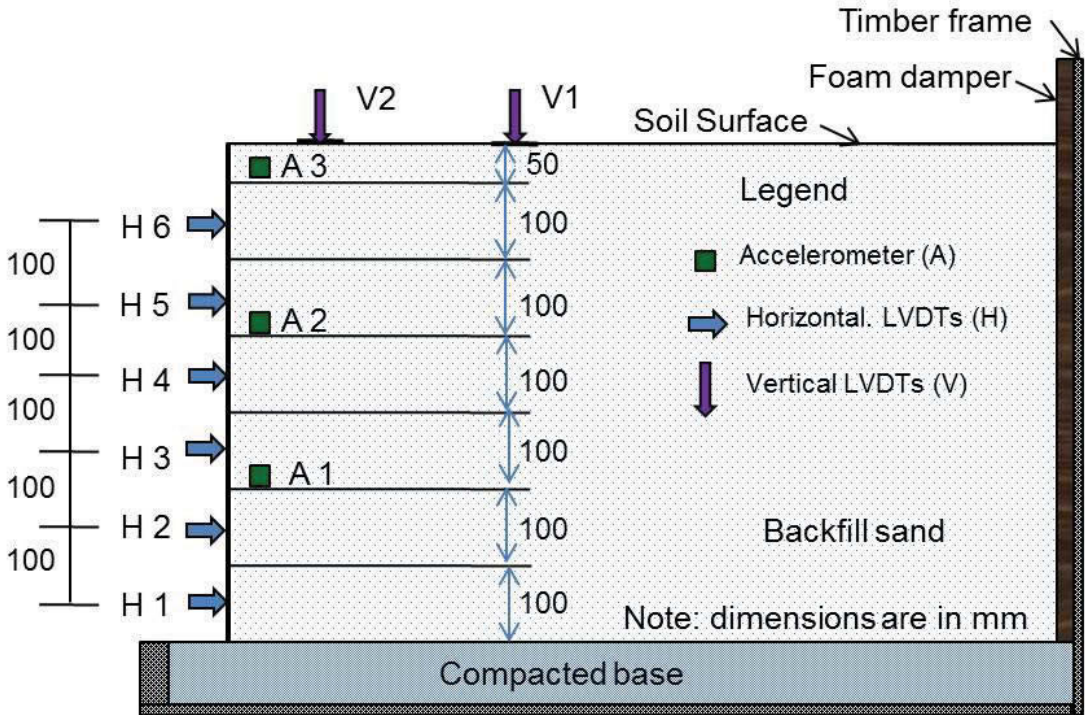

Figure 5.29 Schematic diagram for instrumentation details

5.8 Fundamental Frequency and Input Motion

In this study the fundamental frequency of the reinforced wall was calculated based on the impact test. The acceleration was recorded by hitting a mechanised hammer onto the top of the backside of the wood framed wall, in the middle. The acceleration was recorded at a height of 0.61 m (refer to accelerometer A3 in Figure 5.29) and its variation with time is illustrated in Figure 5.30a.

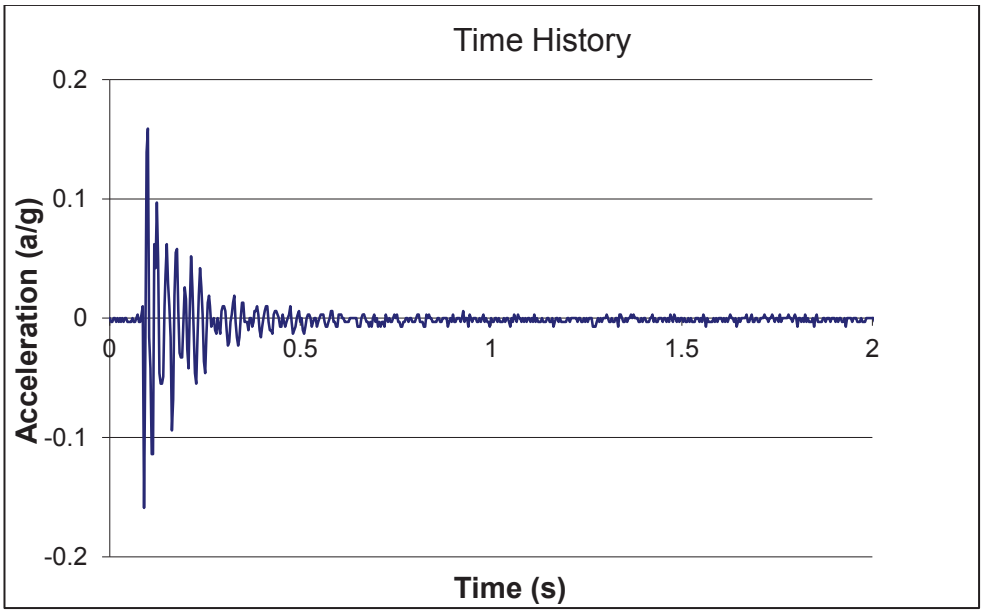

(a)) Impact pulse test

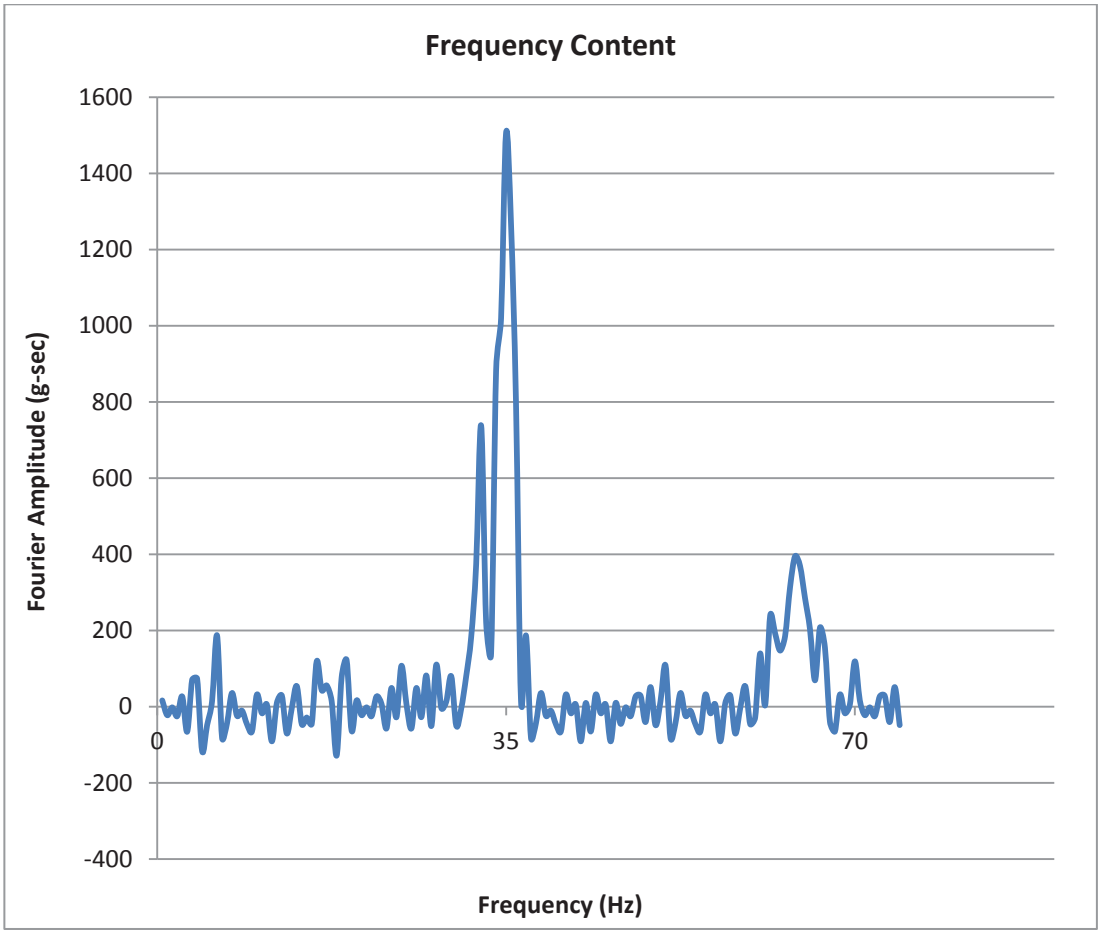

(b) Free vibration Fourier spectrum

Figure 5.30 Impact pulse test for fundamental frequency

The fundamental frequency of the model walls was approximately 35 Hz, considering the frequency of the vibration after the impact pulse. The free vibration Fourier spectrum is illustrated in Figure 8.30b. According to the scaling laws proposed by Iai (1989b), the scale factor for frequency in shake table tests is

$$f_{model} = f_{prototype} N^{0.75} \quad (5.1)$$

where, N is the scale reduction factor. The 15 Hz frequency at 1/10 model scale corresponds to 2.67 Hz at prototype scale. It should be noted that as explained by Bathurst & Hatami (1998), frequencies of 2-3 Hz are representative of typical predominant frequencies of average to rather severe earthquakes. The applied horizontal base acceleration was a stepped-amplitude sinusoidal function with a predominant frequency of 15 Hz and a frequency that is well below the fundamental frequency of the models (35 Hz). As shown in Figure 5.31a, the amplitude of acceleration increased by increments of 0.05g in every 5 seconds until the model became excessively deformed.

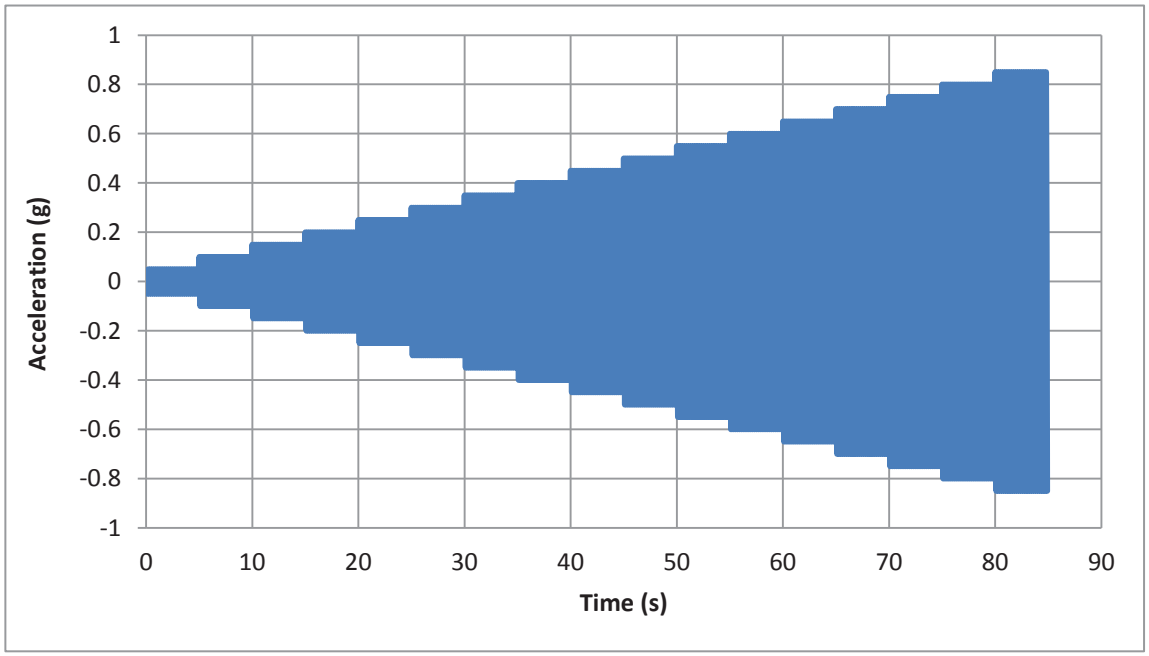

(a) Base input accelerogram

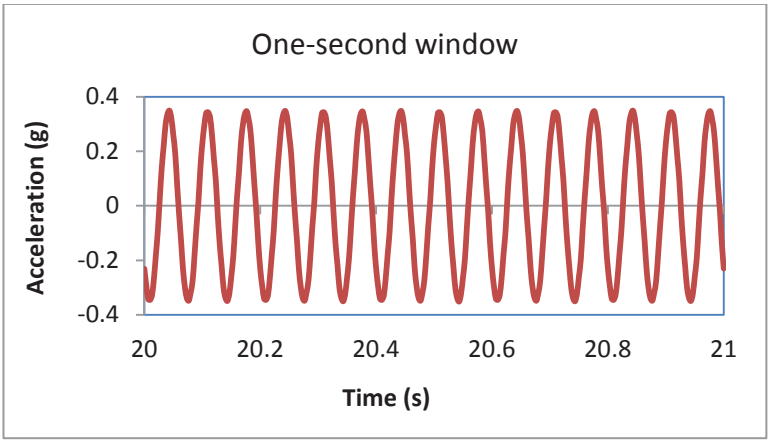

(b) One-second window

Figure 5.31 Input base acceleration characteristics

This simple base excitation record is more aggressive than a typical earthquake record with the same predominant frequency and amplitude (Bathurst & Hatami 1998; Matsuo et al. 1998). However, this simple base acceleration-time history was used to ensure that all the models were excited in the same controlled manner, and to facilitate the quantitative comparisons between different test configurations. A one second window of the acceleration is shown in Figure 5.31b.

Chapter 6

6.0 Results and Discussion of Experimental Investigations

6.1 Introduction

The experimental aspect of this study consisted of conducting four reduced scale reinforced wall shake table tests, the results of which are presented in this chapter. The container was fabricated to accommodate the wall and then constructed inside an existing container on the shake table facility, designed and installed at the University of Technology, Sydney. The locations of the instruments, which were identical for each test, are given in Table 6.1. The horizontal displacement and backfill settlement for each test are presented, followed by the plots for the accelerometers. In the last section of the chapter, the test results are compared and discussed.

6.2 Test Model 1: without Vertical Reinforcement

This model is associated with a conventional reinforced soil wall with horizontal layers of geogrids. The horizontal displacement due to step-up sinusoidal excitations is shown in Figure 6.1, where the graph illustrates the horizontal deformation of the wall. Note that the maximum deflection occurs at the top of the wall and then the displacement decreases towards the bottom. The base excitation continued for 80 seconds, after which time the wall failed completely. Figure 6.1 shows that maximum displacement at the

top layer (layer 6) was reached after 45 s, while maximum deflection of the bottom layer (layer 1) was reached after 79 s.

Table 6.1 Location of instruments for all tests

Transducers	Symbol	Coordinates (mm)	
		X	Y
Linear Variable Transducer (Lateral Displacement)	H1	0	50
	H2	0	150
	H3	0	250
	H4	0	350
	H5	0	450
	H6	0	550
Linear Variable Transducer (Settlement)	V1	200	650
	V2	450	650
Accelerometers	A1	50	210
	A2	50	410
	A3	50	610

Note: The intersection of facing plane and foundation is the origin (i.e. X = 0, Y = 0)

The measured settlement of the backfill during the test period is shown in Figure 6.2. As the input motion was sinusoidal, the middle part of the backfill settled faster than the front side.

Figure 6.3 shows the acceleration recorded at locations A1, A2, and A3 (see Figure 6.3), in test wall Model 1. The results indicate that the response within the wall was fairly uniform, although amplification in the top portion of the wall was larger than the foundation, as shown in the plots presented in Figure 6.3. The mid-level accelerometer did not record any data because the connections during shaking were poor. The figure

shows that the acceleration is slightly high for a fraction of seconds in each shift of the stepped-up input acceleration.

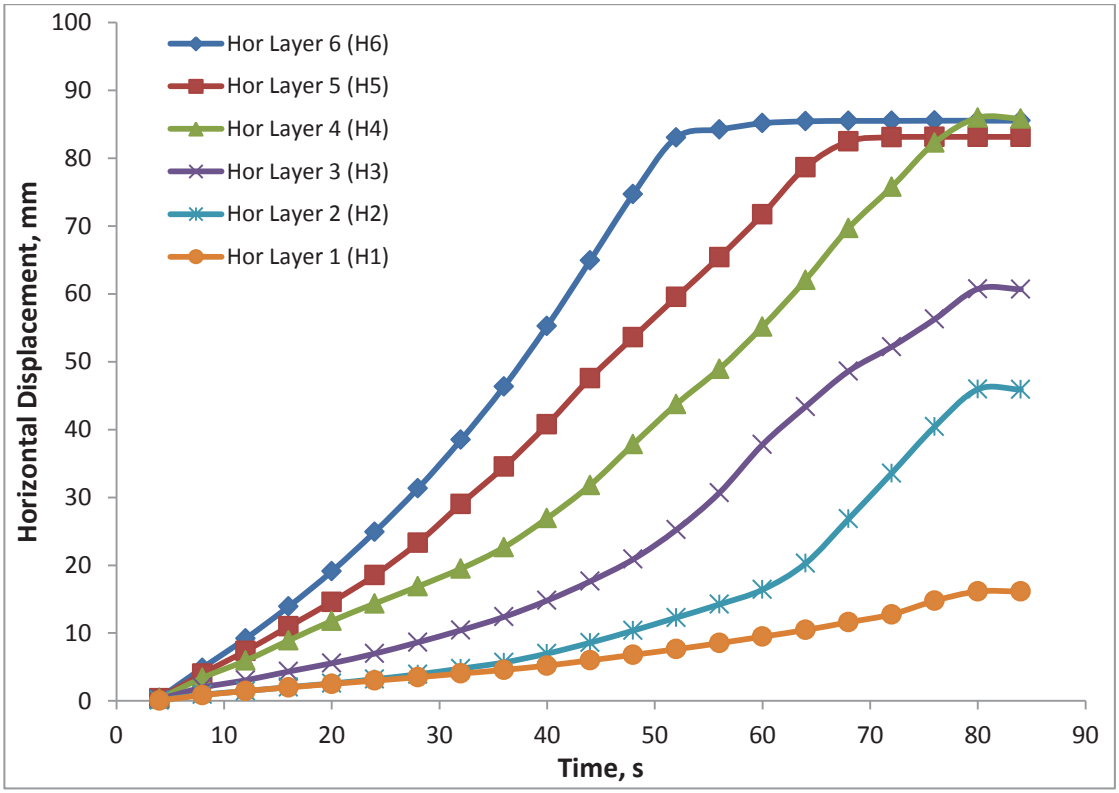

Figure 6.1 Horizontal deformation of the wall (no vertical reinforcement)

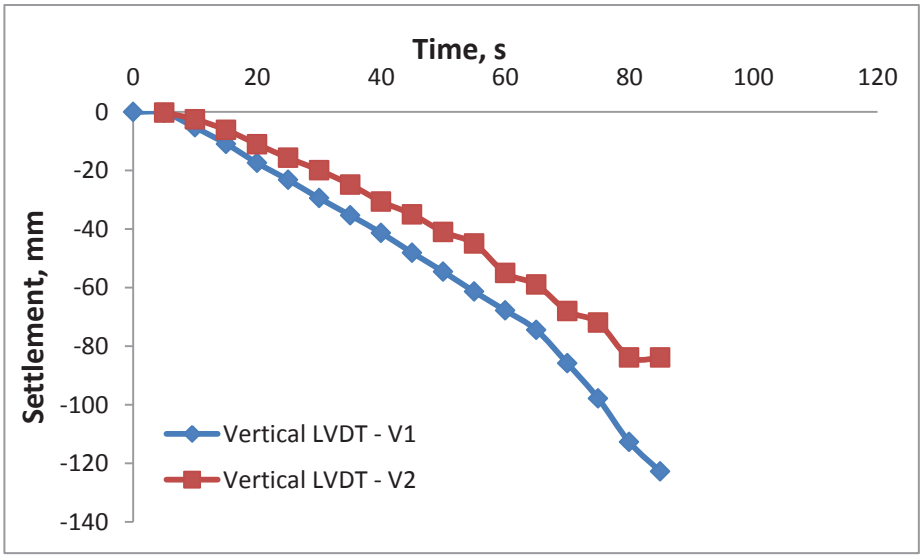

Figure 6.2 Vertical deformations of the backfill

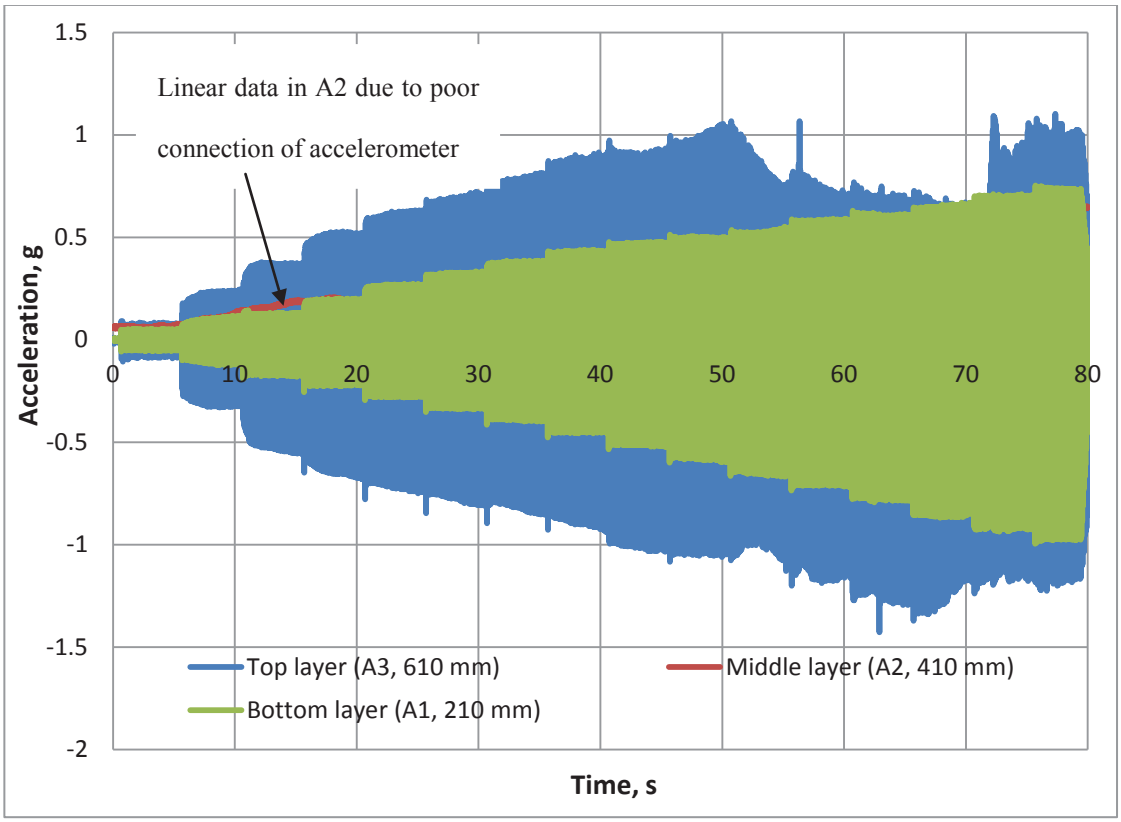

Figure 6.3 Recorded shaking accelerations

Figure 6.4 Prior to the test: Model 1 and its instrumentation

Figure 6.5 Impact of shaking: Model 1 topping failure and its undulated surface

The photographs taken before and after the shake table test, without vertical reinforcement, are shown in Figures 6.4 and 6.5, respectively. The first photo shows the final shape of the model with instrumentation installed prior to the test, while the second photo shows the wall after a load has been applied, tilted towards the facing and with a wavy surface.

6.3 Test Model 2: with Vertical Reinforcement

Figure 6.6 illustrates the pattern of deflection in the wall with vertical reinforcement included. The same stepping up sinusoidal load was used for this test. The base was excited for 135 seconds, after which the top layer failed at a peak acceleration of approximately 1.0g. The curves in this model have similar trends, except for the second layer of Model 2 which malfunctioned due to slip in connection with the facing that

occurred 55 seconds after the test commenced. However, the rates of horizontal deformation were higher in the wall without vertical reinforcement than the walls with vertical reinforcement.

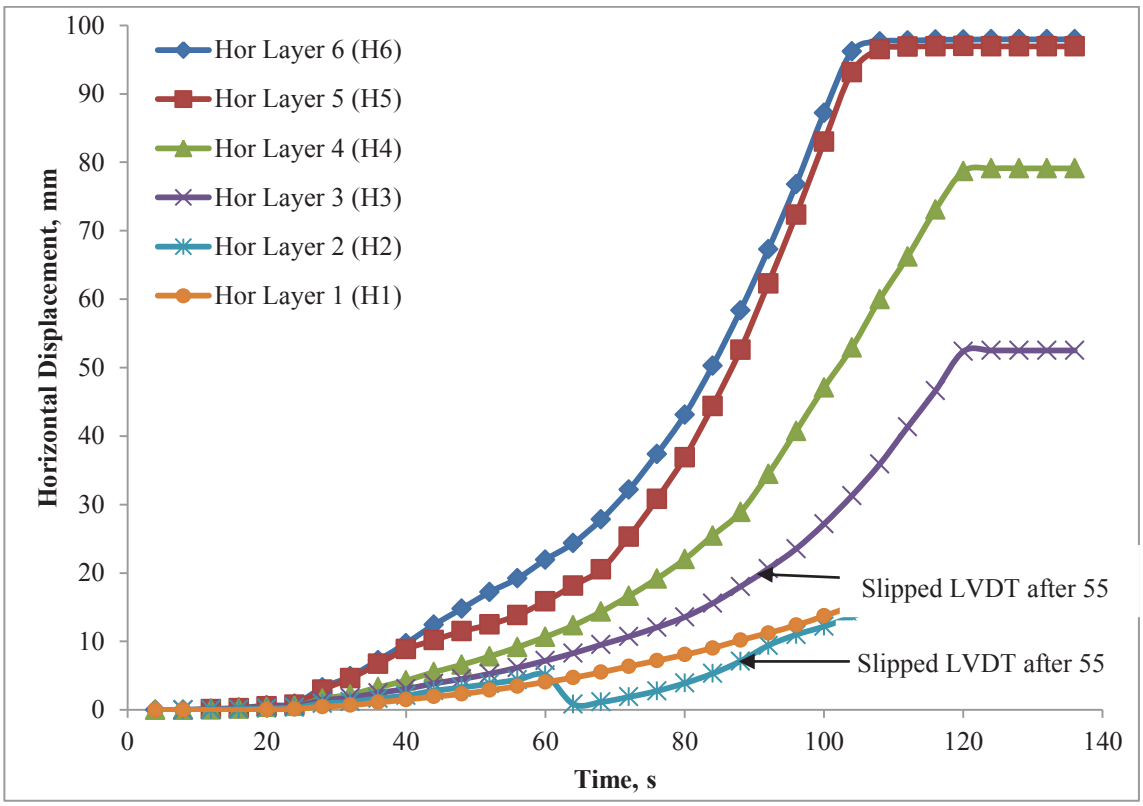

Figure 6.6 Horizontal deformation of wall (with vertical reinforcement)

The settlement of backfill measured during this test period is shown in Figure 6.7, showing that the middle part of the backfill settled faster than the front side. Permanent settlement recorded in the shaking increased to about 45 mm at the end of the test.

Acceleration recorded at locations A1, A2, and A3 in test wall 2 are shown in Figure 6.8. The results indicated that the response within the wall was rather uniform, although amplification in the top portion of the wall was larger than the foundation, as is evident from the plots presented in Figure 6.8. Acceleration was amplified on the top

accelerometer after 80 seconds and 60 seconds on the bottom accelerometer, after which they gradually decreased, and then increased again.

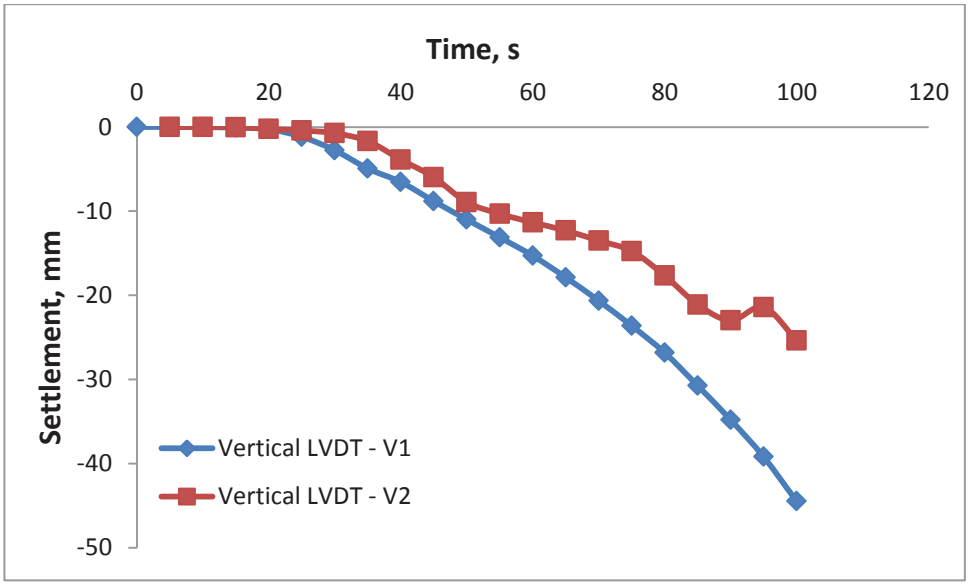

Figure 6.7 Vertical deformations of backfills

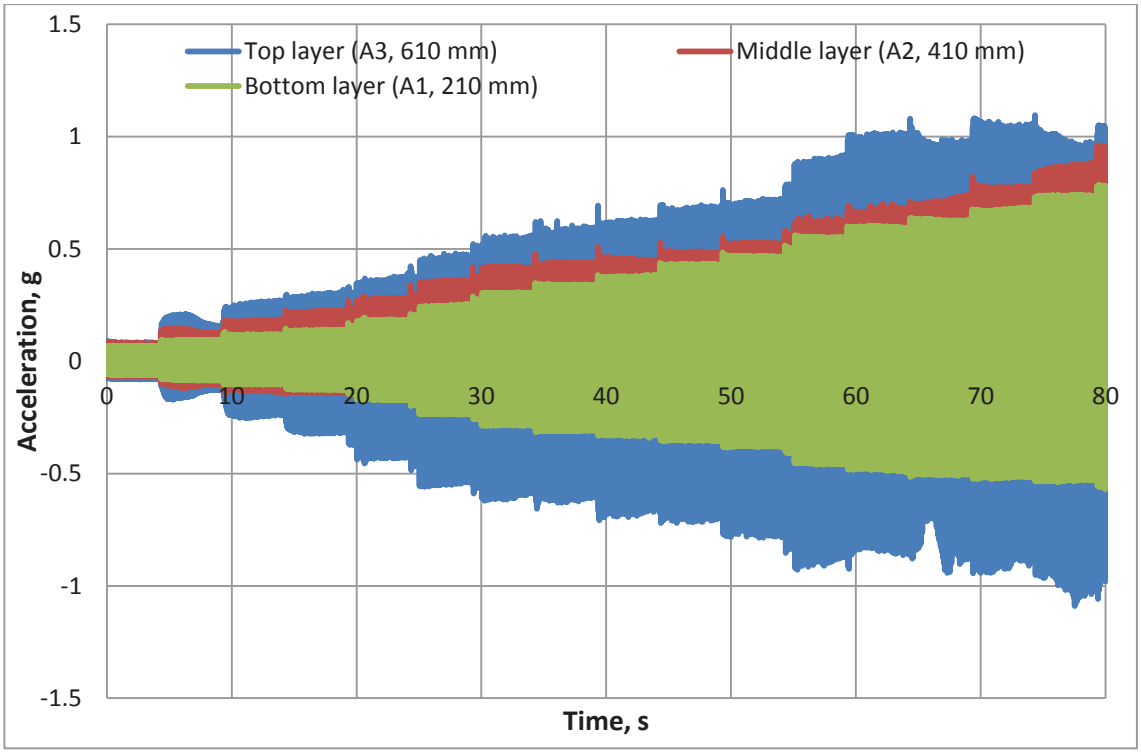

Figure 6.8 Recorded shaking accelerations

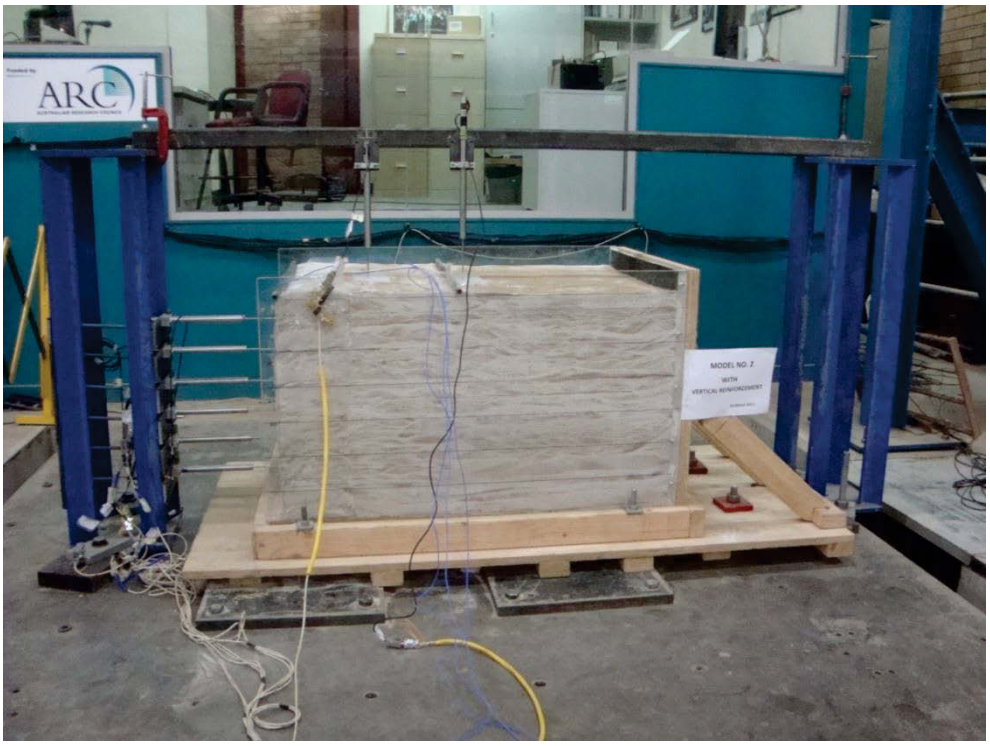

Figure 6.9 Prior to the test: Model 2 and its instrumentation

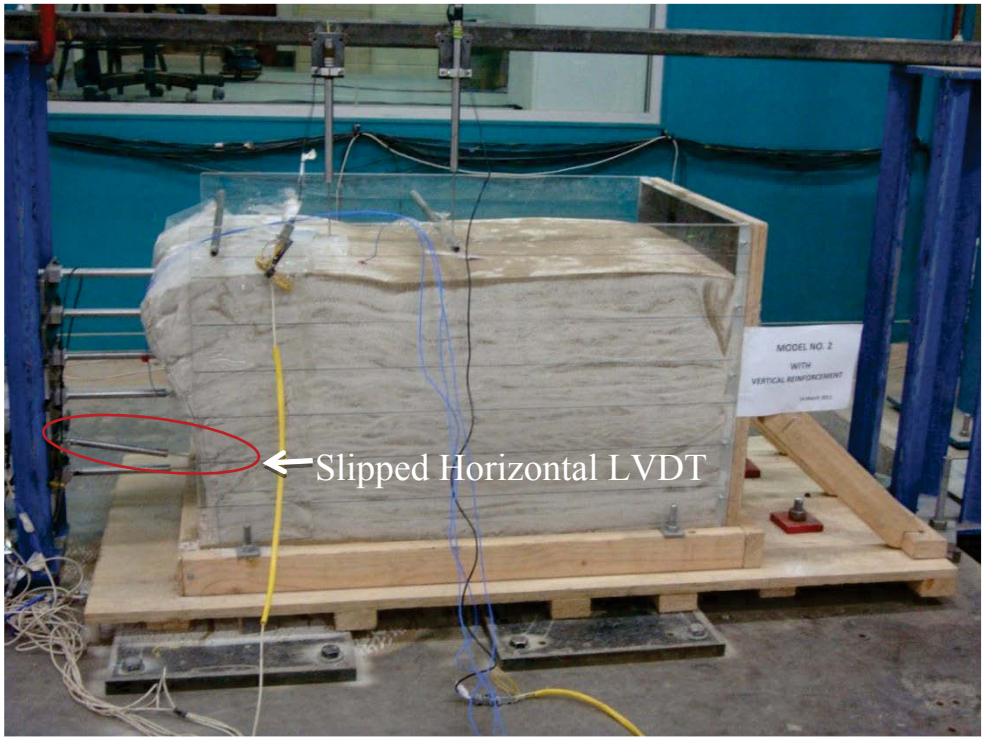

Figure 6.10 Impact of shaking: Model 2 topping failure and its deformed top surface

The photographs of test Model 2 (using horizontal and vertical reinforcements) taken before and after the dynamic load was applied to the shake table are illustrated in Figures 6.9 and 6.10, respectively. The first photo shows the final shape of the model and instrumentation installed prior to the test, while the second photo shows the wall with an undulating surface and tilted towards the facing.

6.4 Test Model 3: with Reinforcement Inclined away from the Facing

Two more models were prepared with the reinforcement inclined towards the wall and away from the wall facing, instead of a fully vertical inclusion (Model 2). These models were then tested to investigate the effect of the gradient of reinforcements that connected the horizontal layers together. In this section the model with 63.4° (2V: 1H) of reinforcement inclined away from the facing wall (towards the back of wall) is discussed, and the test model with reinforcement inclined towards the facing wall is explained in Section 6.5.

Test Model 3 was interrupted after 30 seconds because the metal stand supporting the horizontal LVDTs began to vibrate at a high resonance, in fact it began after the bolts on the base of the stand were unscrewed. After facing that mechanical problem, the test was conducted for a further 60 seconds, with the pattern of the failure mechanism being similar to previous tests. However, the test data was only recorded for 20 seconds in both steps because the system had not been reset after the free-vibration tests. Free-vibration tests were conducted with an auto-stop after 20 seconds to determine the natural frequency. Therefore, the results of Test Model 3 are not presented in this dissertation despite the recorded results were similar to those from previous tests.

6.5 Test Model 4: with Reinforcement Inclined towards the Facing

In this section the behaviour of a model with reinforcement inclined 63.4° (2V: 1H) towards the wall facing is discussed. The same step-up and sinusoidal excitation as in Model 3 were also used in this test. Figure 6.15 illustrates the pattern of displacement of the reinforced wall on the shake table with the inclusion of near vertical reinforcement. This figure shows the deflection of the wall and indicates that maximum deflection occurred at the top and less displacement occurred towards the bottom of the wall. Base excitation was continued for 135 seconds, when the wall failed completely. Figure 6.11 shows that maximum displacement at the top layer (layer 6) reached 100 mm after 110s, whereas maximum deflection of the bottom layer (layer 1) was about 65 mm for the same time.

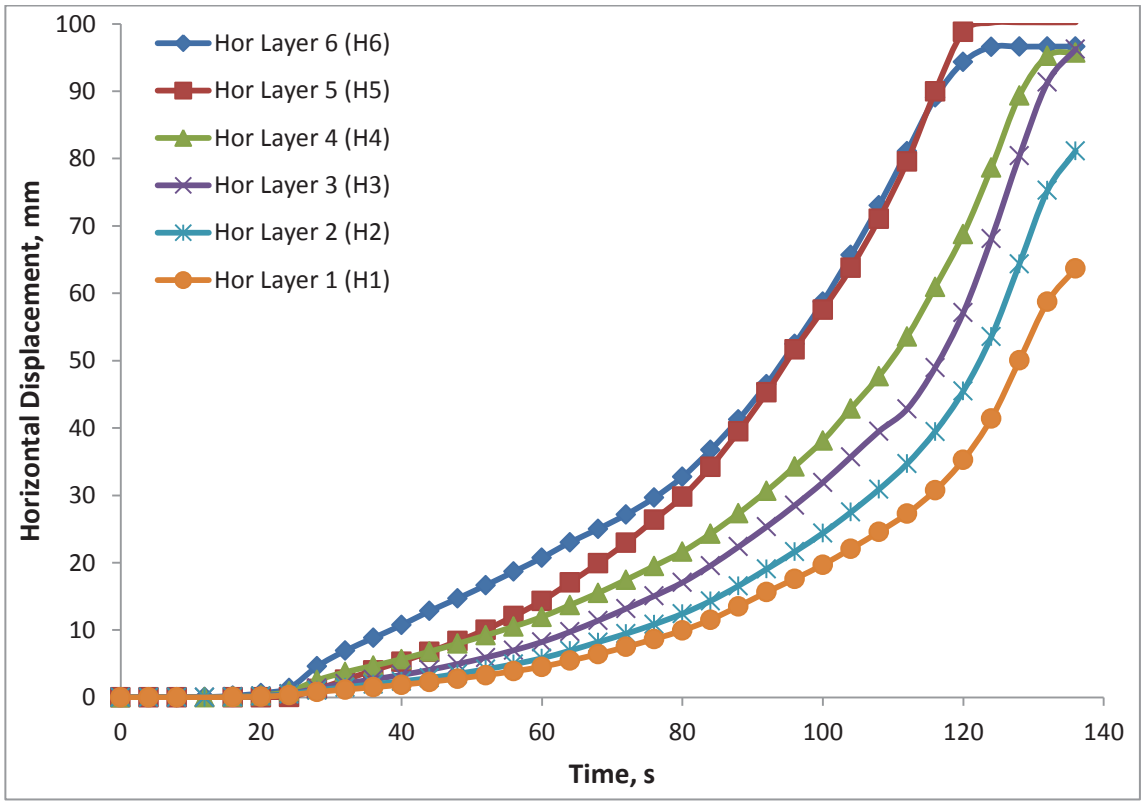

Figure 6.11 Horizontal deformation of wall (with an angled reinforcement towards the back of the wall)

The settlement of the backfill measured during this test period is shown in Figure 6.12 where the middle part of the backfill settled faster than the front side. The graph shows that the settlement measured at LVDT (V1) is less than V2 after 65 seconds, which is due to dragging of LVDT at V2 by the horizontal net. The permanent settlement recorded during shaking increased to about 45 mm at the end of the test.

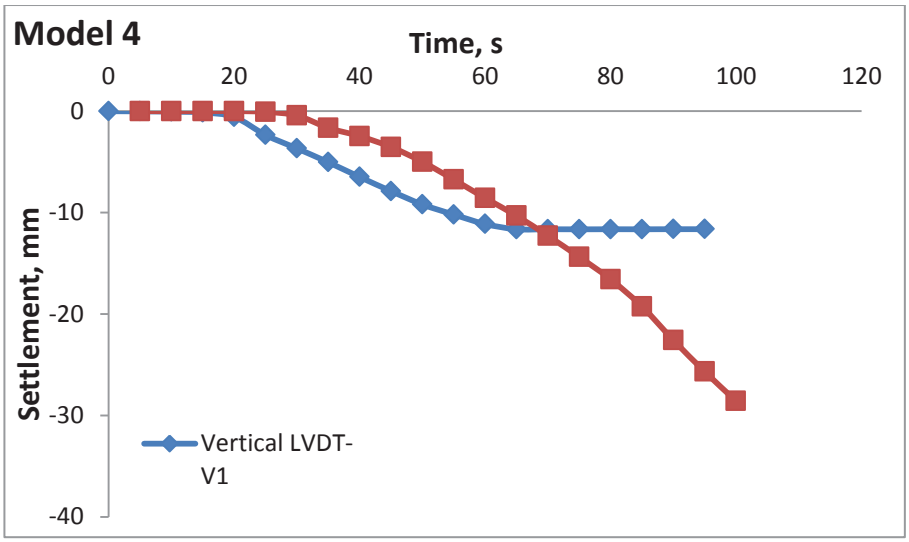

Figure 6.12 Vertical deformations of the backfill

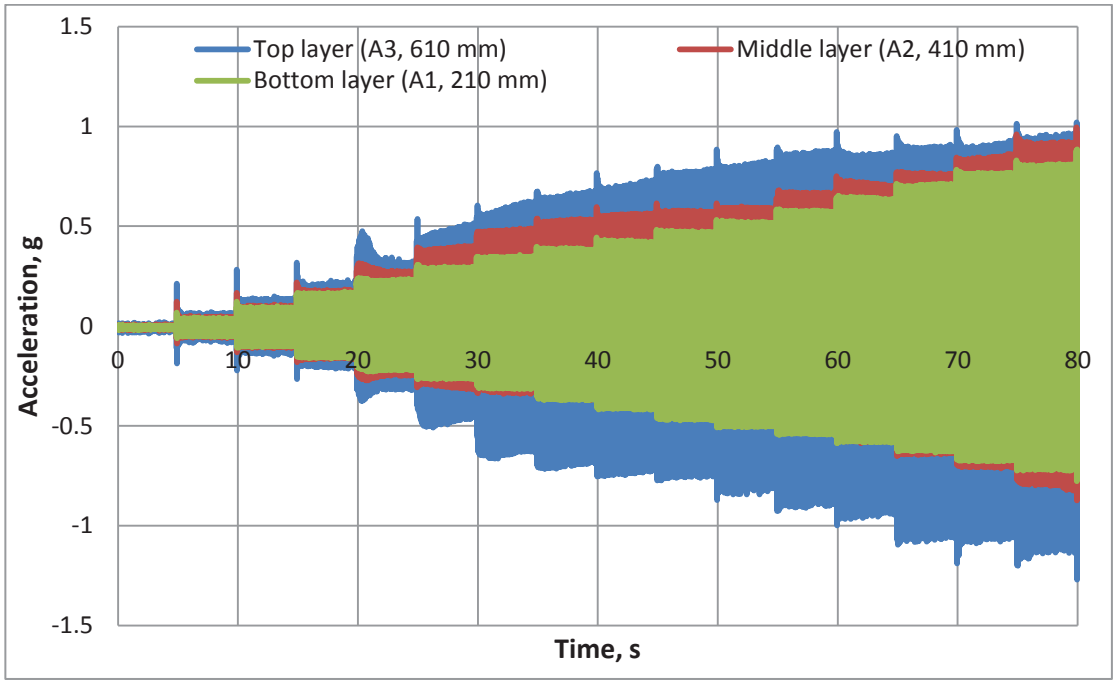

Figure 6.13 Recorded shaking accelerations

The acceleration recorded at all three locations of the test wall 4 are shown in Figure 6.13, with the results showing that response within the wall was almost uniform. However, the top portion of the wall was highly sensitive, having ups and downs, while the base and mid accelerometers remained steady from the beginning to the end of the test.

The photographs of Model 4 taken before and after the dynamic load was applied to the shake table are shown in Figures 6.14 and 6.15, respectively. The first photo shows the final configuration of the model with its instrumentation installed prior to the test, while the second photo shows the wall tilted towards the facing wall with an undulating top surface as a consequence of shaking.

Figure 6.14 Prior to the test: Model 4 and its instrumentation

Figure 6.15 Impact of shaking: Model 4 topping failure and its deformed top surface

6.6 Discussion of the Results

The results of various test models are analysed, compared, and interpreted in this section. It can be noted that the outcomes of test Model 3 are not included in this discussion even though the results were within the expected ranges, as the test was interrupted due to an error related to the time set up.

6.6.1 Horizontal deformation

As the results of the horizontal displacement show, displacement was larger at the top of the wall than the bottom, as expected, although the magnitude of displacement during construction was insignificant. A comparison of the lateral displacement of three models (Models 1, 2 and 4) are shown in Figure 6.16. For the sake of comparison, only the lateral deflection of the first layer (layer 6) is considered. Around 60 mm of horizontal displacement was induced at 0.4g peak acceleration in the reinforced soil model without

vertical reinforcement (Model 1). Meanwhile, an almost identical amount of horizontal deformation in Model 2 and Model 4 was achieved when the peak amplitude crossed 0.8g after 80 seconds. These values clearly indicate that the inclusion of vertical or near vertical reinforcements in the reinforced soil wall reduced its lateral deformation to less than half.

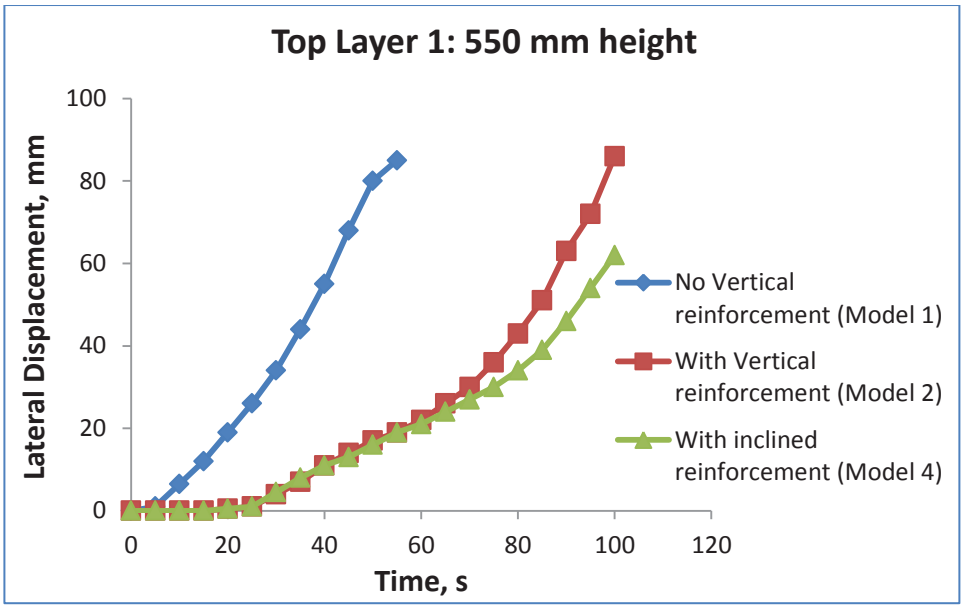

(a) Layer 1

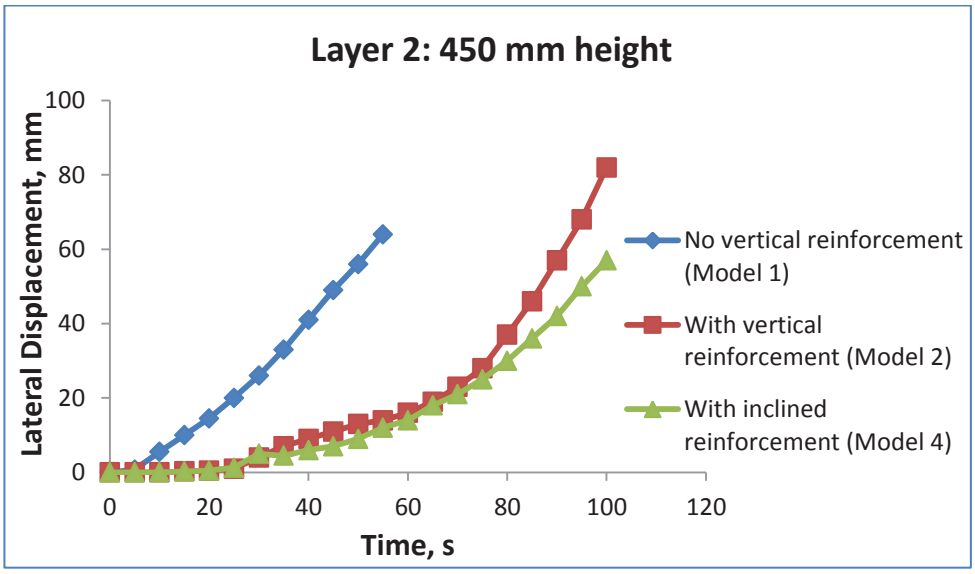

(b) Layer 2

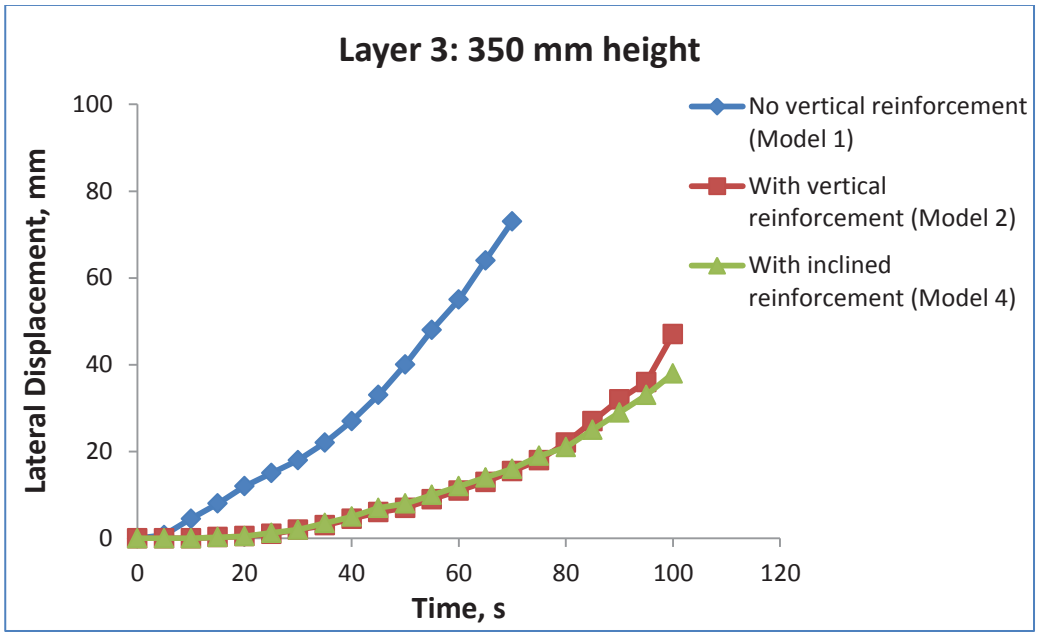

(c) Layer 3

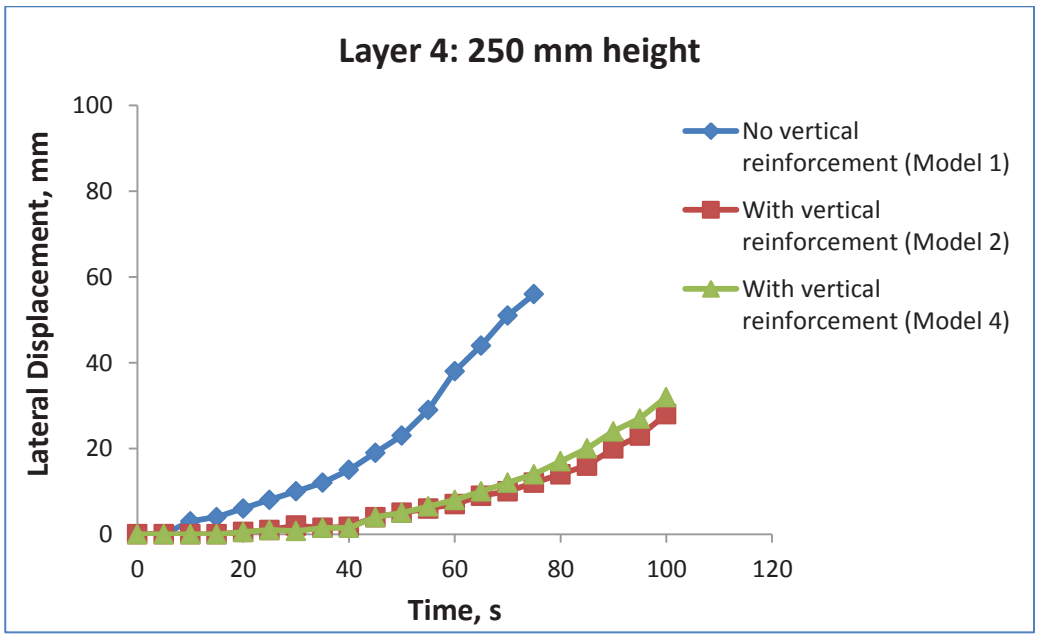

(d) Layer 4

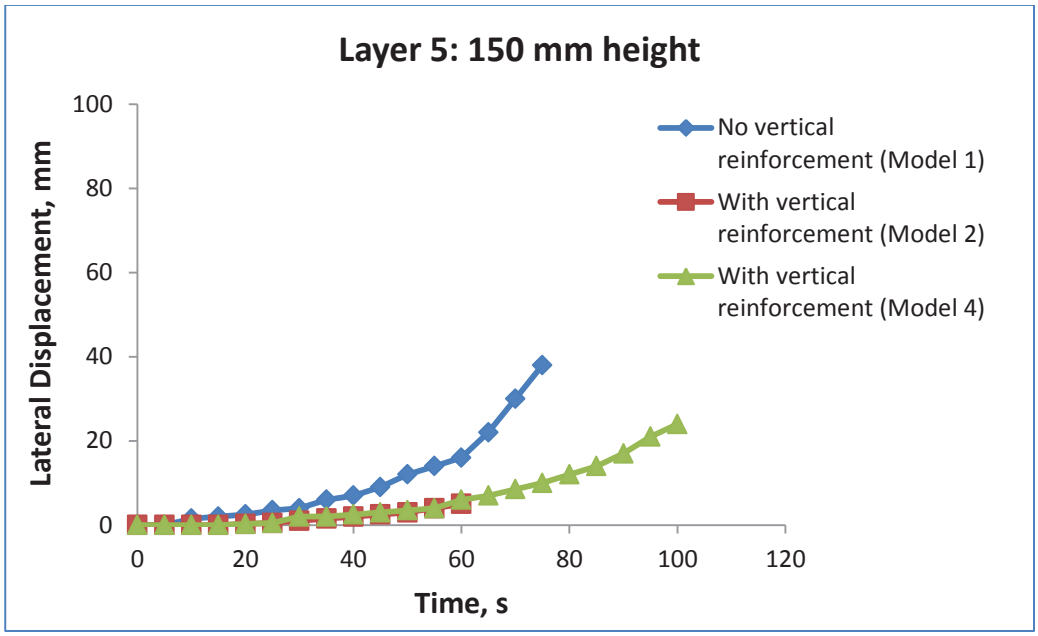

(e) Layer 5

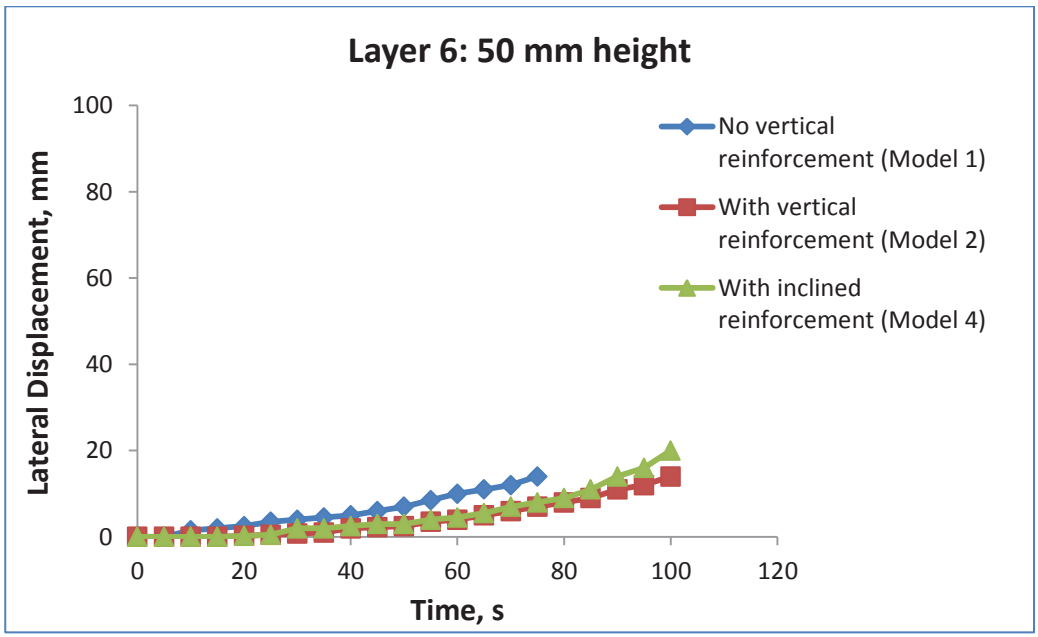

(f) Layer 6

Figure 6.16 Comparison of horizontal deformations of different models

A comparison of horizontal deformation within the same peak amplitude also reveals that the highest rate of deformation is associated with the model without any vertical/angled reinforcements. For example, between 45-50 seconds from the

commencement of the tests, the peak amplitude was 0.5g, and the facing deformation increased from 68 to 80mm (12 mm increase), from 14 to 17mm (3 mm increase), and from 13 to 16 (3 mm increase) in Model 1, Model 2, and Model 4, respectively.

Iai (1989a) proposed a scale factor of the prototype to model for time and displacement as $t = 1/N^{0.75}$ and $d = N^{1.5}$, respectively. Using these formulae and a scaling factor of 10, 5 seconds would be equivalent to 28.2 seconds, and 12 mm and 3 mm displacement would be equivalent to 380 mm and 95 mm for the prototype, respectively. It can be concluded that the horizontal deformation reduced four times by introducing vertical/horizontal reinforcement. These results clearly prove the potential benefits of adding vertical elements to conventional soil reinforcement to reduce horizontal deformation.

If we compare the deflection of walls with perfect vertical reinforcement and angled reinforcement, deformation was slightly higher in the first case in the top three layers. The lower three layers have different results because those walls with inclined reinforcement were somewhat weaker than the other case. Hence, the result reveals there is no significant difference with a slight change in the angle. This is an important finding because it makes field construction more convenient, and the results will only vary marginally if a minor change in the angle occurs during difficult constructions.

6.6.2 Vertical deformation

Vertical deformations recorded using two LVDTs, were evaluated and compared in Figure 6.17. The vertical deformation in Model 1, without vertical reinforcement, was very rapid compared to the other models, and settlement behind the reinforced soil zone was the largest due to horizontal movement of the entire reinforced soil zone. It is obvious that when the horizontal deflection is greater, so too is settlement, while the

variations in settlement were very similar. It is noted that LVDT V1 (placed 400 mm away from the facing wall) recorded higher vertical deformations compared to the LVDT V2 (used 200 mm away from the facing wall). This is due to the formation of a sinusoidal soil surface while the wall was being shaken. The general trend of vertical deformations was similar to the horizontal deflections.

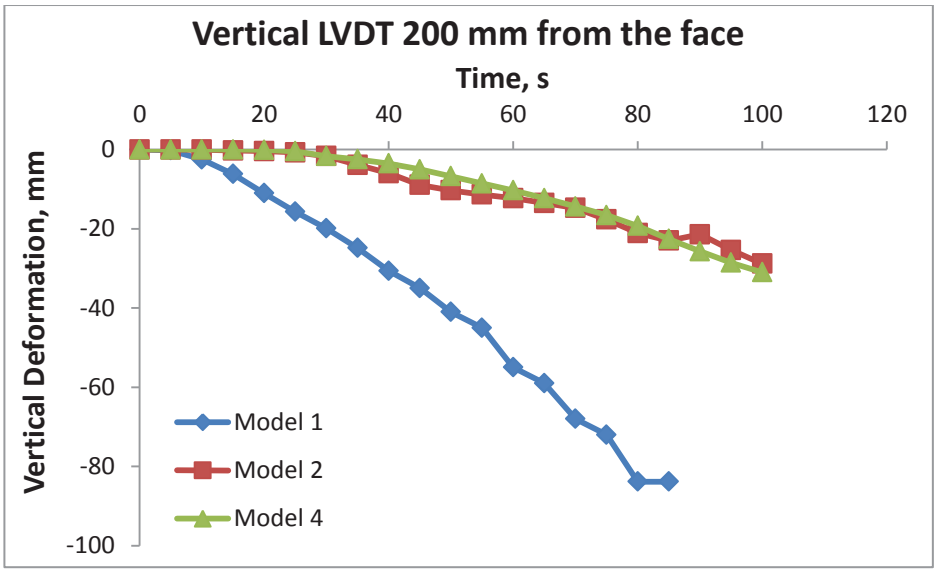

(a) Front LVDT (V2)

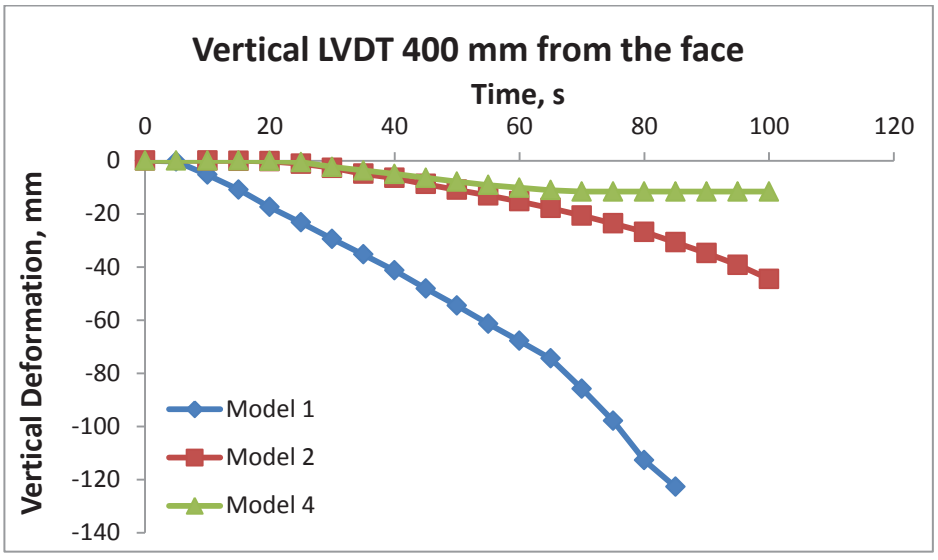

(b) Rear LVDT (V1)

Figure 6.17 Comparison of vertical deformations of three models

It should be mentioned that a similar pattern of results was observed for both horizontal and vertical directions by Shrestha, Khabbaz & Fatahi (2011) in their numerical studies of reinforced soil retaining walls under seismic loading, with and without the inclusion of vertical reinforcements in addition to conventional horizontal reinforcements. Vertical reinforcements not only tie horizontal layers to each other, they also encounter some components of tensile forces which increase the frictional resistance, raises the anisotropic cohesion, and increase the frictional angle. The major component of seismic force can be resisted by the combined effect of both reinforcements, while each component can resist by corresponding reinforcement. The attempt by vertical reinforcement to create a blocking action against seismic forces is a very important measure that is used to protect structures from lateral forces induced by earthquakes or other dynamic loads.

6.6.3 Response of the accelerometers

The results of the accelerometers recorded at different heights shows that acceleration was amplified at the top more than the bottom. These variations in the rate of acceleration with the sinusoidal step up input motion were compared in Models 1, 2, and 4, and recorded at heights of 210 mm, 410 mm, and 610 mm. Those results recorded at A1, A2, and A3 are presented in Figures 6.22, 6.23, and 6.24, respectively. The lengths of each accelerogram were different for different tests, which were conducted until the models failed completely. In Figure 6.18, all the models show almost similar responses at the height of 210 mm (position of A1).

Figure 6.19 shows the comparison between the accelerograms of the model with vertical and without vertical reinforcement, as the mid-accelerometer of Model 1 failed and did not record any data. This display of data shows that the accelerations were almost

similar for the first 20 seconds, after which Model 4 became amplified higher than Model 2.

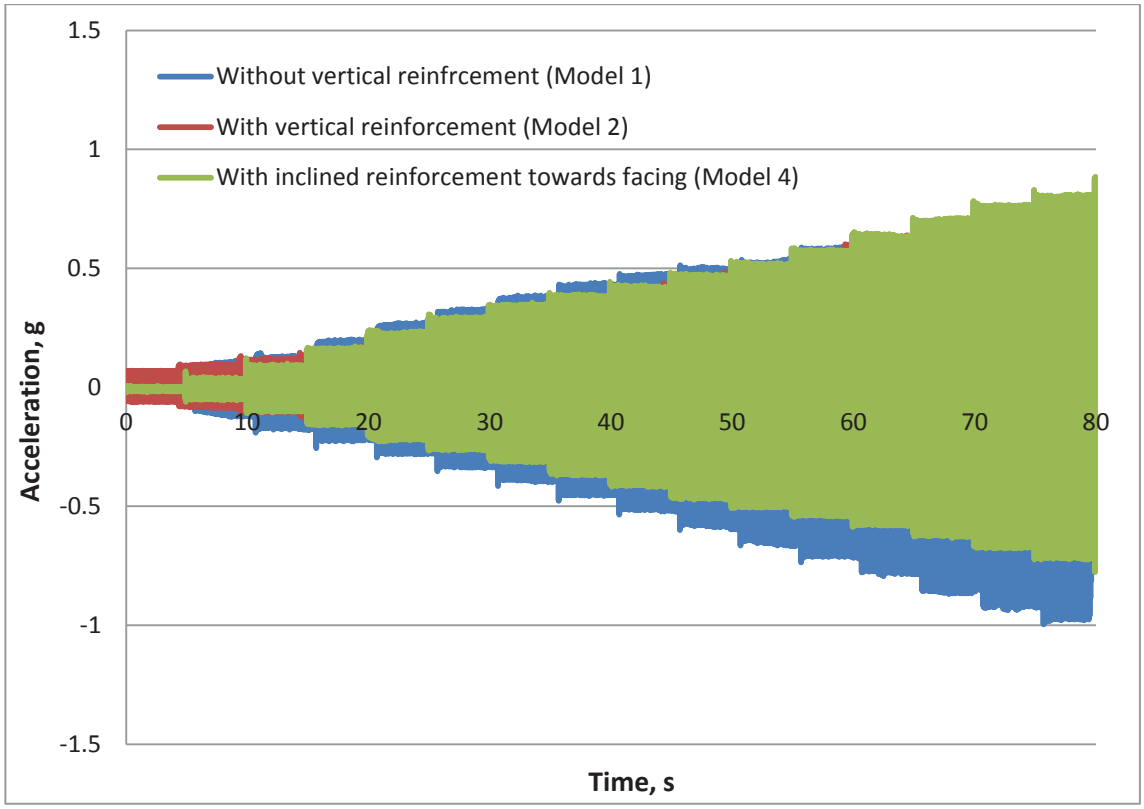

Figure 6.18 Comparison of accelerations (A1) responses at the level of 200 mm

Figure 6.20 illustrates that the accelerations were amplified higher in Model 1 than the models with vertical or inclined reinforcement, and the acceleration in Model 4 was higher towards end of the test (after 80 seconds).

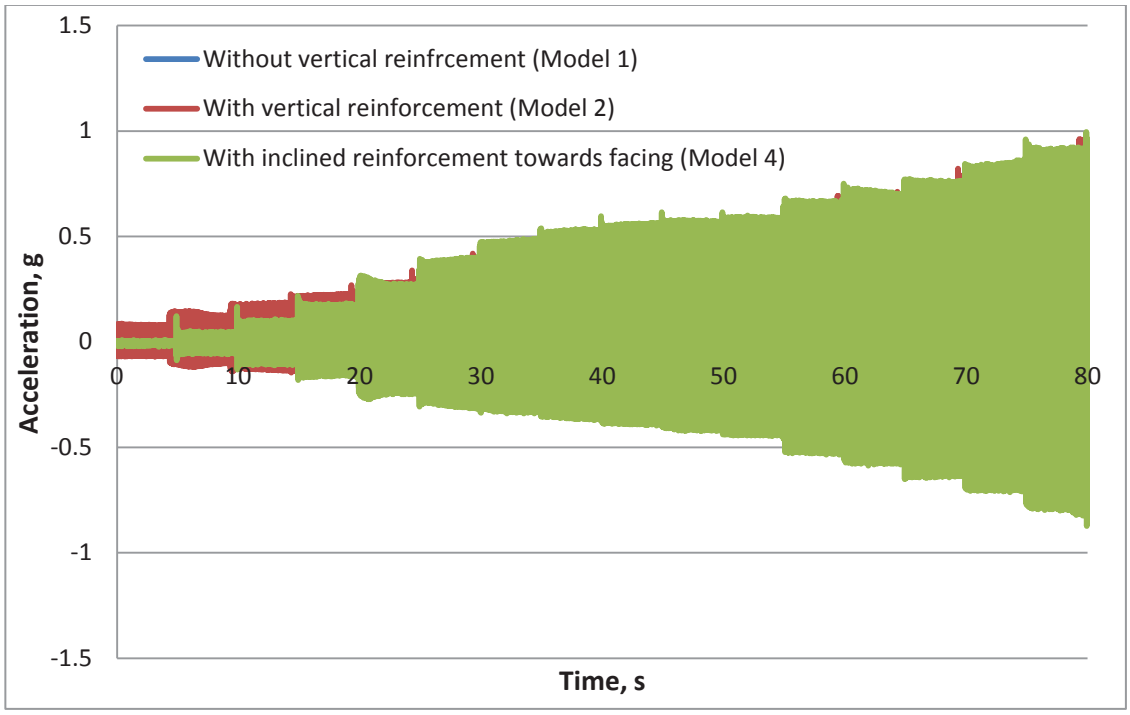

Figure 6.19 Comparison of accelerations (A2) responses at the level of 410 mm

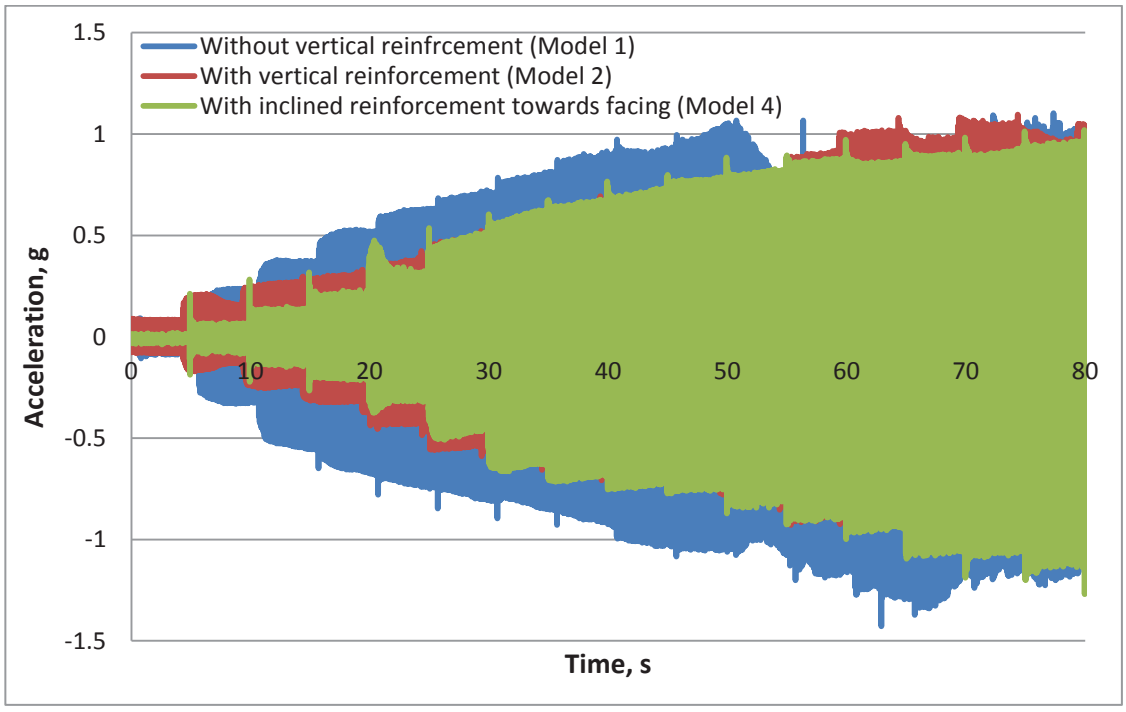

Figure 6.20 Comparison of accelerations (A3) responses at the level of 610 mm

6.7 Summary

The tests that were conducted gave consistent results in evaluating the seismic performance of the walls. The results of the shake table tests clearly indicate that the inclusion of vertical/angled reinforcements in reinforced soil walls reduces lateral deformation compared to the wall without any vertical reinforcement. When these values were converted to the prototype according to similitude rule at the particular amplitude of base excitation, horizontal deformations were reduced by a factor of four when vertical/horizontal reinforcement was used. These outcomes highlight the potential benefits of the inclusion of vertical elements in conventional soil reinforcement for reducing horizontal deformation under dynamic loads.

The deformation of walls with vertical reinforcement and slightly angled reinforcement were almost similar, although vertical reinforcement resulted in more deformation in the top three layers and less deflection in lower three layers compared to the wall with angled reinforcement. Vertical settlement in the wall with vertical and angled reinforcements was almost identical during the tests. Obviously, when horizontal deflection is greater, the backfill settles more. This finding is beneficial for the field implementation of vertical reinforcement because the performance of wall will not vary much with a minor change in the angle of installation.

The results also show that the amplification of acceleration increases with the height of model, while the model wall where vertical or inclined reinforcement was inserted produced less amplification of acceleration compared to the wall without any vertical reinforcement.

To summarise, the results of the dynamic model tests, using the reduced scale shake table facility, clearly demonstrated that reinforced soil walls are more stable under

earthquake loads, when vertical or inclined reinforcement is inserted in addition to the conventional horizontal reinforcement.

Chapter 7

7. Numerical Verification and Parametric Studies

7.1 Introduction

Laboratory model tests are very useful in increasing our understanding of the dynamic behaviour of reinforced soil walls under controlled conditions. Some studies can be conducted based on full scale dynamic tests using a large scale shake table, which would be more accurate but more expensive than reduced scale models, which is why reduced scale shake table tests were carried out in this study. The test results were presented in the previous chapter while in this chapter the behaviour of the walls has been analysed using the finite element method that incorporates validating the numerical procedures. In addition, parametric studies were also conducted and predictions have been made using a finite element computer program.

7.2 Finite Element Model

The shake table results have been analysed using the commercial finite element code PLAXIS 2D Version 9.0 equipped with the Dynamic Module. For the dynamic load, the following basic equation is considered for the time-dependent movement of a volume:

$$M\ddot{u} + C\dot{u} + Ku = F \qquad (7.1)$$

Here, M is the mass matrix, u is the displacement vector, C is the damping matrix, K is the stiffness matrix and F is the load vector. The displacement, u, the velocity, $\dot{u}$, and the acceleration, $\ddot{u}$, can vary with time. The last two terms in the equation ($Ku = F$) correspond to the static deformation.

This theory is described on the basis of linear elasticity. However, in principle, various models in PLAXIS can be used for dynamic analysis. In the matrixM, the mass of the materials (soil + water + any constructions) is taken into account. In PLAXIS, the mass matrix is implemented as a lumped matrix.

The matrix C represents the damping of the materials, which plays an important role in dynamic analysis of structures and foundations. In reality, material damping is caused by friction or by irreversible deformations (plasticity or viscosity). With more viscosity or more plasticity, more vibration energy can be dissipated. If elasticity is assumed, damping can still be taken into account using the matrix C. To determine the damping matrix, extra parameters are required, which are difficult to determine from tests. In finite element formulations, C is often formulated as a function of the mass and stiffness matrices (Rayleigh damping) (Gughes 1987; Zeienkiewicz & Taylor 1991) as:

$$C = \alpha M + \beta K \tag{7.2}$$

where, C = damping matrix of the physical system, M = mass matrix of the physical system, K = stiffness matrix of the system, α and β are pre-defined constants.

Aversa, Maiorano & Tamagnini (2007) reported the analysis of the seismic response of a cantilevered RC diaphragm wall in a dry granular soil using elastic-perfectly plastic Mohr-Coulomb model. Jesmani & Kamalzare (2010) carried out the comparison between numerical and analytical solution of dynamic response of circular shallow footing and concluded that in loose sands with a module of elasticity less than 35000 kPa which are prone to become plastic, elasto-plastic behaviour of Mohr-Coulomb model become more suitable than others. Celebi, Goktepe & Karahan (2012)mentioned that the computational simulation of the wave propagation problem with soil-structure interaction effects was directly achieved by employing a 2-D finite element model under

plane-strain conditions including plastic deformations of the underlying soil medium under Mohr-Coulomb failure criterion.

The elastic-perfectly plastic Mohr-Coulomb model involves five input parameters, i.e. E and ν for soil elasticity; ϕ and c for soil plasticity and ψ an angle of dilatancy. In general, stress states at failure in drained conditions are quite well captured by using the Mohr-Coloumb failure criterion with effective strength parameters ϕ' and c'.

In contrast to the Mohr-Coulomb model, the Hardening Soil model also accounts for stress-dependency of stiffness moduli. However, hardening model does not account for softening due to soil dilatency and debonding effects. In fact, it is an isotropic hardening model so that it models neither hysterestic and cyclic loading nor cyclic mobility or anisotropic behaviour. In order to model cyclic loading with good accuracy one would need a more complex model. Moreover, the use of the Hardening Soil model generally results in longer calculation times, since the material stiffness matrix is formed in each calculation step. Hence, as loose sands were used in shake table test, Mohr-Coulomb elastic-perfectly plastic model has been adopted for the analysis.

7.3 Numerical Modelling

The seismic response of a GRS wall is preferred to be investigated using a detailed numerical modelling approach as conducting a series of full scale physical tests with different types of soils and reinforcements under various seismic loads is generally very costly and often impractical. Although, numerical modelling study would be a more economical and practical approach, the numerical predictions should be validated using proper physical model tests under controlled conditions. A review of numerical simulation on the seismic performances of GRS structures is provided in Lee, Chang & Ko (2010).

Four models having the same dimensions and physical properties of materials were developed for this experimental program; the materials used were backfill sand, foundation soil, geogrids, vertical reinforcements, interfaces (soil and vertical reinforcement, soil and geogrids), facing units and a foam damper. The properties of the sand and interface are summarised in Table 7.1.

Table 7.1 Sand and interface properties

Parameter	Symbol	Backfill sand	Foam damper (soil)	Foundation soil	Unit
Soil unit weight	γ_{unsat}	16.5	11	18	kN/m^3
Young's modulus	E	6000	1000	40000	kN/m^2
Poisson's ratio	ν	0.3	0.35	0.3	-
Cohesion	c	0	0	0.5	kN/m^2
Friction angle	ϕ	30	-	36	°
Dilatancy angle	Ψ	0	-	6	°
Interface reduction factor	R_{int}	0.75	0.75	0.8	-
Shear wave velocity	V_s	47.80	18.16	91.52	m/s
Compression wave velocity	V_p	89.40	37.81	171.2	m/s
Damping	D	0.15	0.20	-	-

The unit weight of backfill sand was calculated and monitored in each test by collecting samples in a mould of a known volume that was placed at different locations and levels as described in the Section 5.7. As the consistency of the sand is loose, the Young's modulus and Poission's ratio values were adopted based on Das (1999) suggested values. The friction angle and cohesion was determined from the direct shear test as described in Section 5.5.3.

The dilatency of sand depends on both the density and the friction angle. For quartz sands the order of magnitude is $\psi = \phi$ - 30°. In most cases, however, the angle of

dilatency is zero for ϕ values of less than 30° (Bolton 1986). Hence, the friction angle of sand was 30°; the dilation angle of the sand was adopted as 0° for the backfill soil. The compression wave velocity and shear wave velocity were derived from Equations 3.5 and 3.6. The damping value was calculated based on the approach, described in Section 5.6.3 for the foam damper.

A high damping rubber sheet was placed behind the backfill inside the box. To model the rubber, a very loose sand layer was defined as there is no such a rubber element in PLAXIS. The foundation soil was modelled based on clayey sand properties. The selected parameters are summarised in Table 7.1.

Table 7.2: Properties of the vertical reinforcement and geogrids

Elements	Parameter	Symbol	Value	Unit
Vertical reinforcement	Normal stiffness	EA	4.5	kN
	Spacing out of plane	Ls	0.15	m
	Strength	F_{max}, tension	0.085	kN
		F_{max}, comp	0	kN
	Material type	Elastoplastic		
Geonets	Normal stiffness	EA	500	kN/m
	Material type	Elastic		
Facing (Plate)	Normal stiffness	EA	345	kN/m
	Flexural rigidity	EI	1.15×10^{-6}	kNm^2/m
	Equivalent thickness	d	2×10^{-4}	m
	Poisson's ratio	ν	0.495	-
	Material type	Elastoplastic		

The parameters of vertical reinforcement, horizontal geogrids and wall facing are given in Table 7.2. The facing was constructed from plate elements of PLAXIS which had properties suitable for matching the behaviour of the facing close to the laboratory model in which plastic facing was used.

The parameters of the vertical reinforcement and geonet determined in the Section 5.6 are used in this modelling. Plastic films of 0.2mm in thickness were used as facing elements. The stiffness and flexural rigidity parameters were derived based on the Young's modulus of plastic, $E = 2.3 \times 10^6$ kN/m^2 adopted from Engineering Toolbox (2012).

As explained earlier in Chapter 4, the 15-node element mesh generated by PLAXIS version 9.0 was used for numerically efficient structural meshes. The earthquake was modelled by imposing a prescribed displacement at the bottom boundary of the wall. At the far end of vertical boundaries, absorbent boundary conditions were applied to absorb any outgoing waves. The first phase calculation was a normal plastic calculation in which the reinforced wall was constructed, while the second step consisted of conducting a dynamic analysis using the same stepped up amplitude of acceleration that was increased by an increment of 0.05 g every 5 seconds, up to 0.7 g (Figure 5.27a).

To produce identical base models in all cases, one vertical and two inclined reinforcement patterns were built in the input stage, followed by generating the mesh, while the respective pattern was chosen for the output in order to readily compare the results of different cases. The spacing between two consecutive inclined reinforcements was 0.1 m.

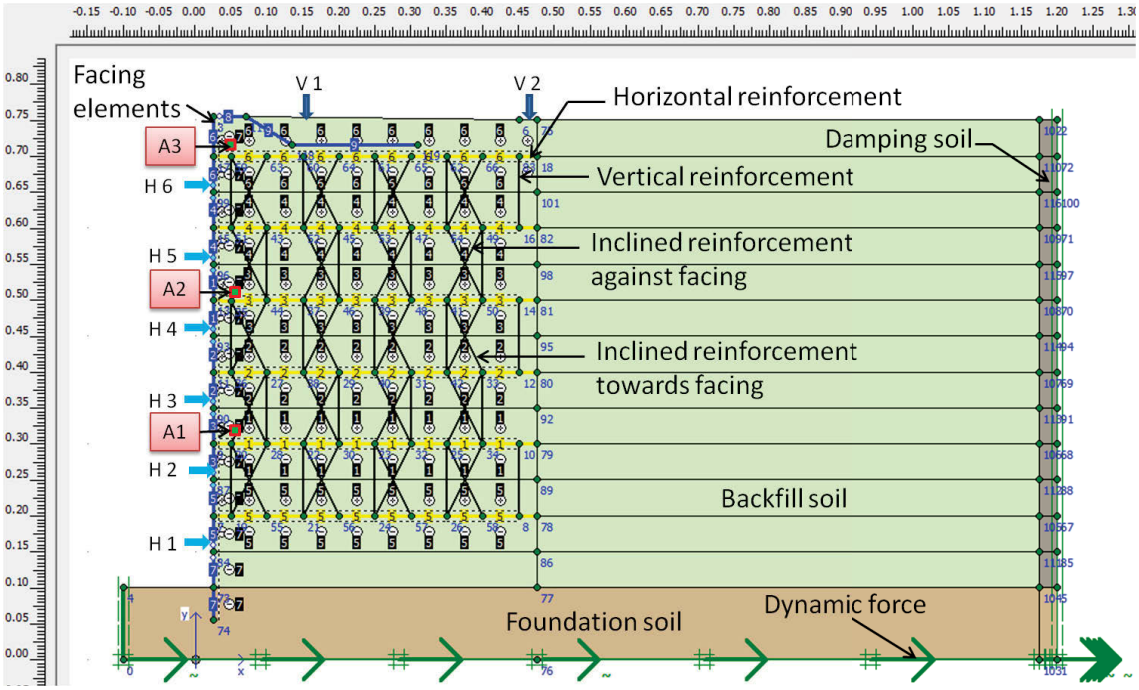

Figure 7.1 Details of finite element models

The ideal numerical model developed for the numerical analysis is shown schematically in Figure 7.1. Six points from H1 to H6 and two points V1 and V2 were chosen to measure the horizontal and vertical deformation in the model, respectively. Similarly, the acceleration response points A1 to A3 were chosen, as shown in Figure 7.1. The corresponding vertical elements of reinforcement were selected for different cases of the numerical analysis.

7.3.1 Model 1: Reinforced wall without vertical reinforcement

This model represents a conventional horizontally reinforced soil wall without any vertical reinforcements. No vertical elements were selected for this analysis, as shown in Figure 7.2.

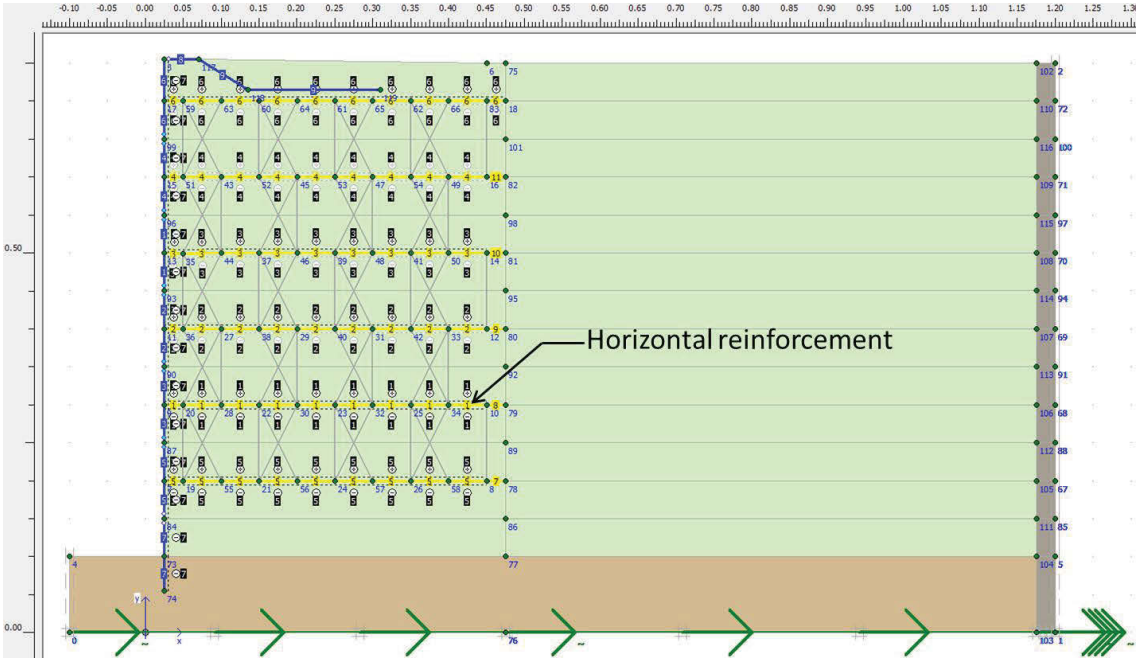

Figure 7.2 Conventional horizontal reinforcement model

The stepped up sinusoidal base excitation was continued for 60 seconds. The results for the employed step-up sinusoidal excitations for horizontal displacements are shown in Figure 7.3. This figure shows how the wall deflected and indicates that the maximum deflection occurred at the top following a smaller displacement towards the bottom of the wall. This pattern of deformation was similar to that obtained from the shake table test where the rate of deformation gradually increased with elapsed time and the amplitude of acceleration that was applied.

The calculated settlement at points V1 and V2 from numerical modelling is shown in Figure 7.4. It is obvious here that the middle part of the backfill will settle faster than the front side due to the sinusoidal input loading.

Figure 7.5 shows the acceleration, calculated at the second (A1), fourth (A2), and sixth (A3) layer in the model, which followed the input of stepped-up sinusoidal acceleration every 5 seconds, from 0.05g for 60 seconds. As expected, these results indicate that

acceleration increases with respect to the height of the wall, and are the same as the pattern that was observed in the results of the shake table based laboratory tests.

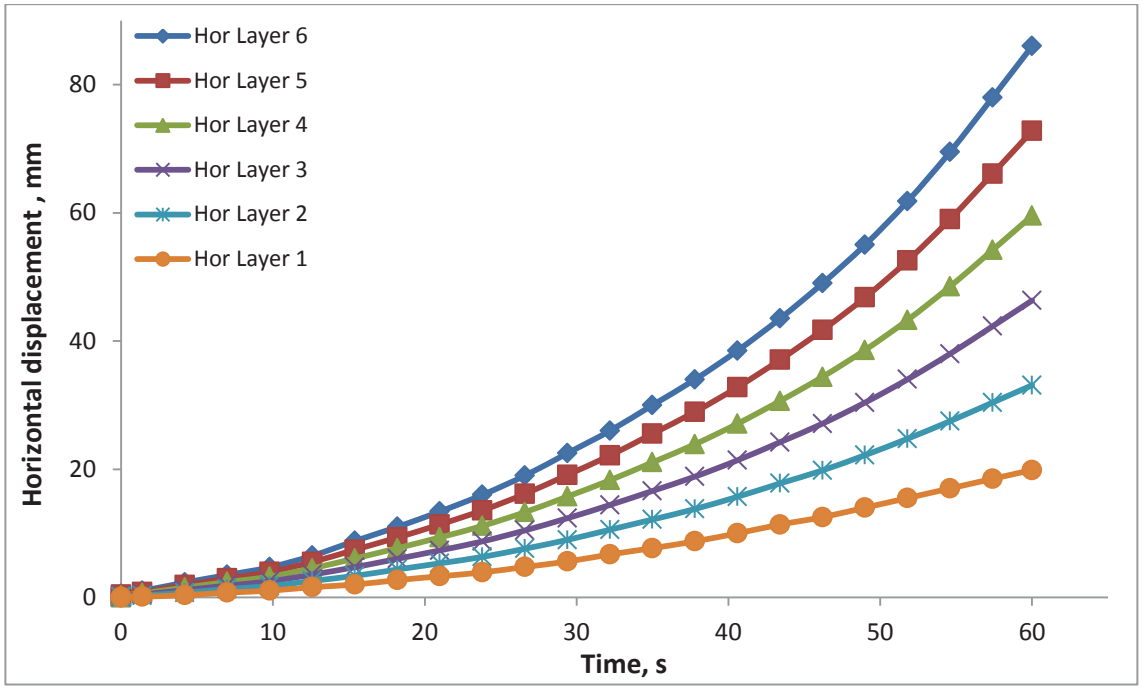

Figure 7.3 Horizontal deformation of the reinforced wall (no vertical reinforcement)

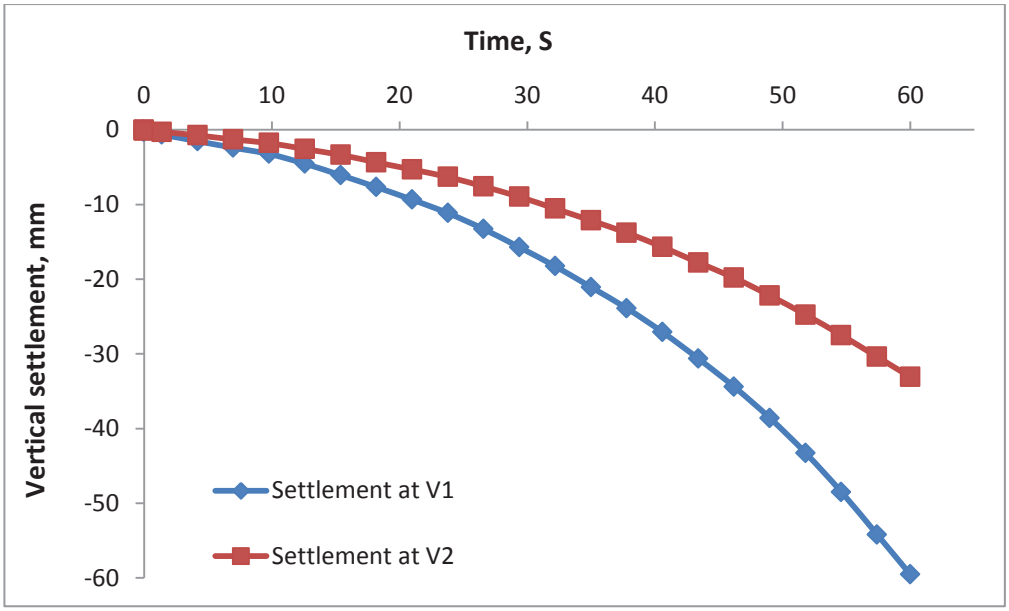

Figure 7.4 Vertical deformations of the reinforced wall (no vertical reinforcement)

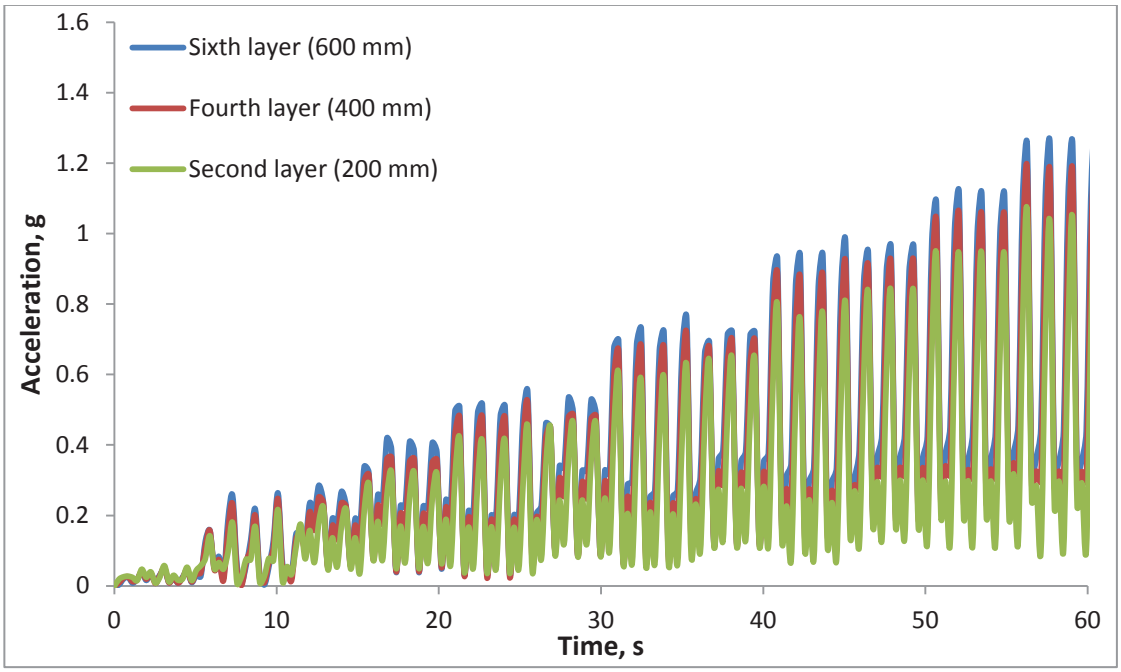

Figure 7.5 Analysed accelerations in Model 1

7.3.2 Model 2: Reinforced wall with vertical reinforcement

The vertical reinforcement activated in this model and the layers of horizontal reinforcement as is shown in Figure 7.6, where the same sinusoidal force was used for 60 seconds, which is similar to Model 1.

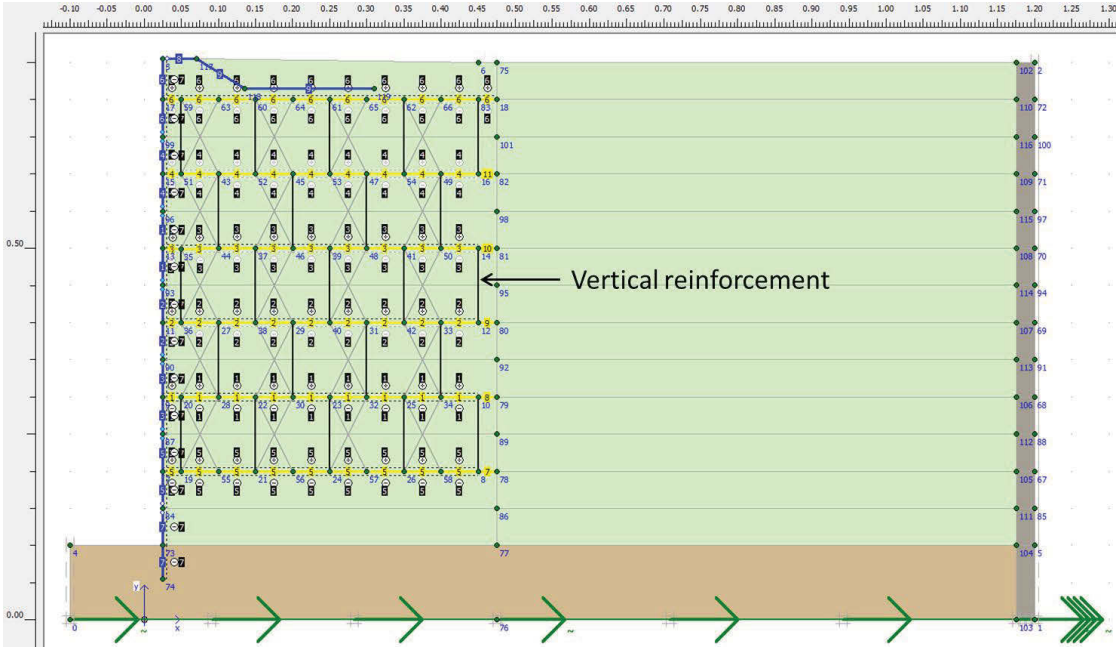

Figure 7.6 Vertical – horizontal reinforcement model

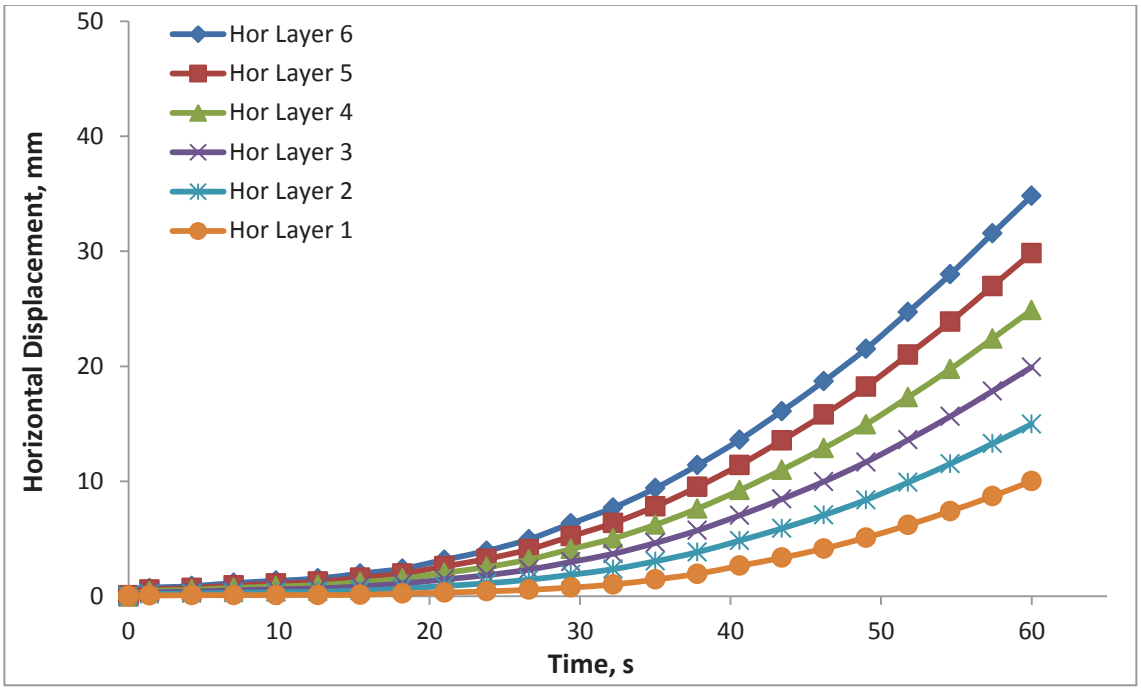

Figure 7.7 Horizontal deformation of the reinforced wall (with vertical reinforcement)

Figure 7.7 illustrates the pattern of deflection of the reinforced wall with the inclusion of the vertical reinforcement. The curves in this model are almost similar to the previous case, although the rates of horizontal deformation are lower in the reinforced wall with vertical reinforcement than is the case without vertical reinforcement.

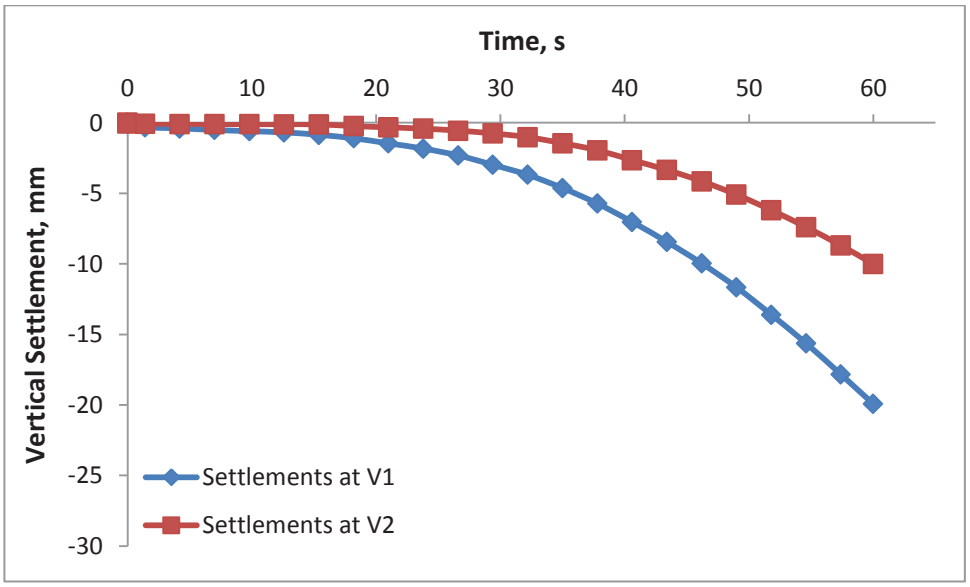

Figure 7.8 Vertical deformations of the reinforced wall (with vertical reinforcement)

The calculated settlements at V1 and V2 on the backfilled soil are shown in Figure 7.8. The middle part of the backfill will settle faster than the front side.

The acceleration traced at locations A1, A2, and A3 with the inclusion of vertical reinforcement, are shown in Figure 7.9. These results indicate that the response within the wall versus the input acceleration was fairly uniform, although the top part of the wall had a larger amplification than the foundation.

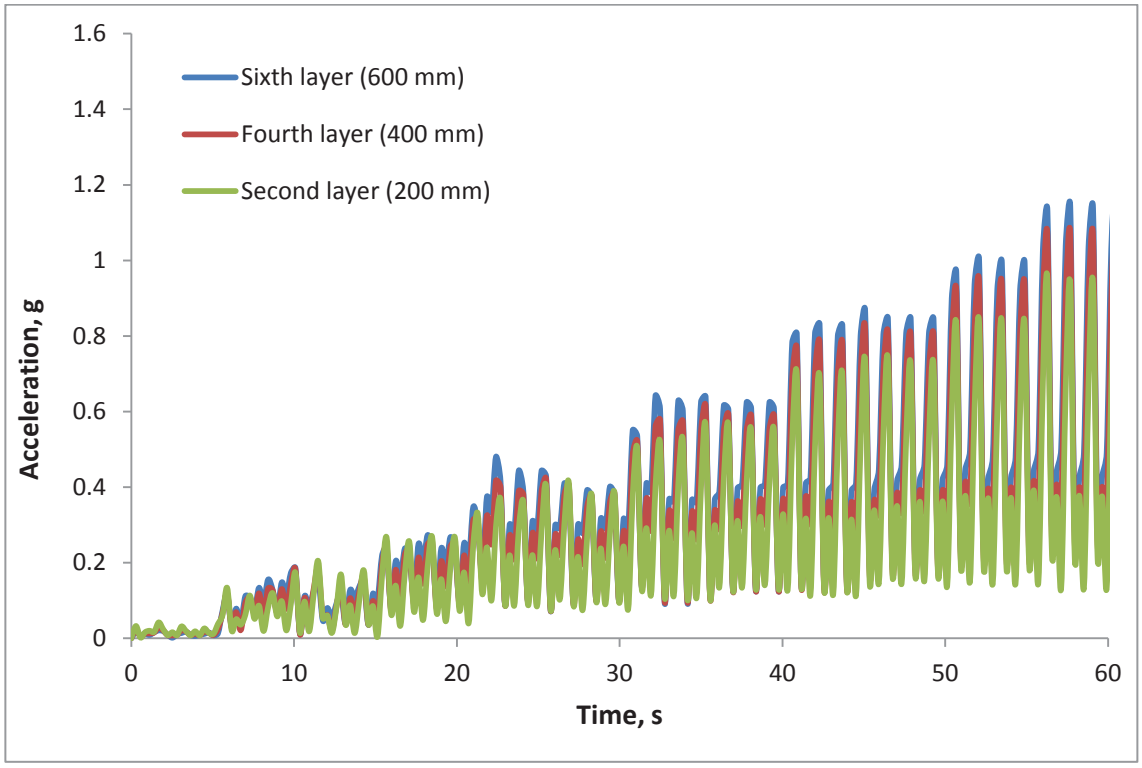

Figure 7.9 Acceleration responses in Model 2

7.3.3 Model 3: Reinforced wall with reinforcement inclined towards the facing

The elements for the inclined reinforcement were selected for analysis as in this model is shown in Figure 7.10, and the same stepped up sinusoidal force was applied for the same duration. The results followed a similar pattern to previous models and the values are close to the model with vertical reinforcement, as shown in Figure 7.11. This figure

also shows the deflection on the reinforced wall so that maximum deflection occurred at the top following smaller displacements towards the bottom.

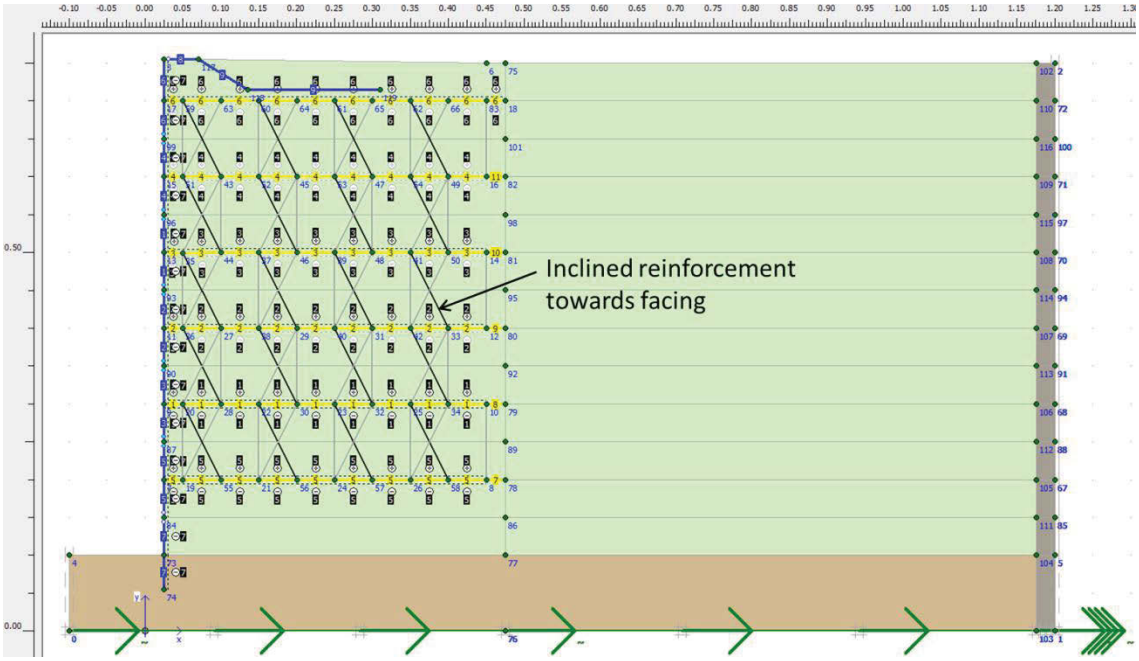

Figure 7.10 Model details with reinforcement inclined towards the wall facing

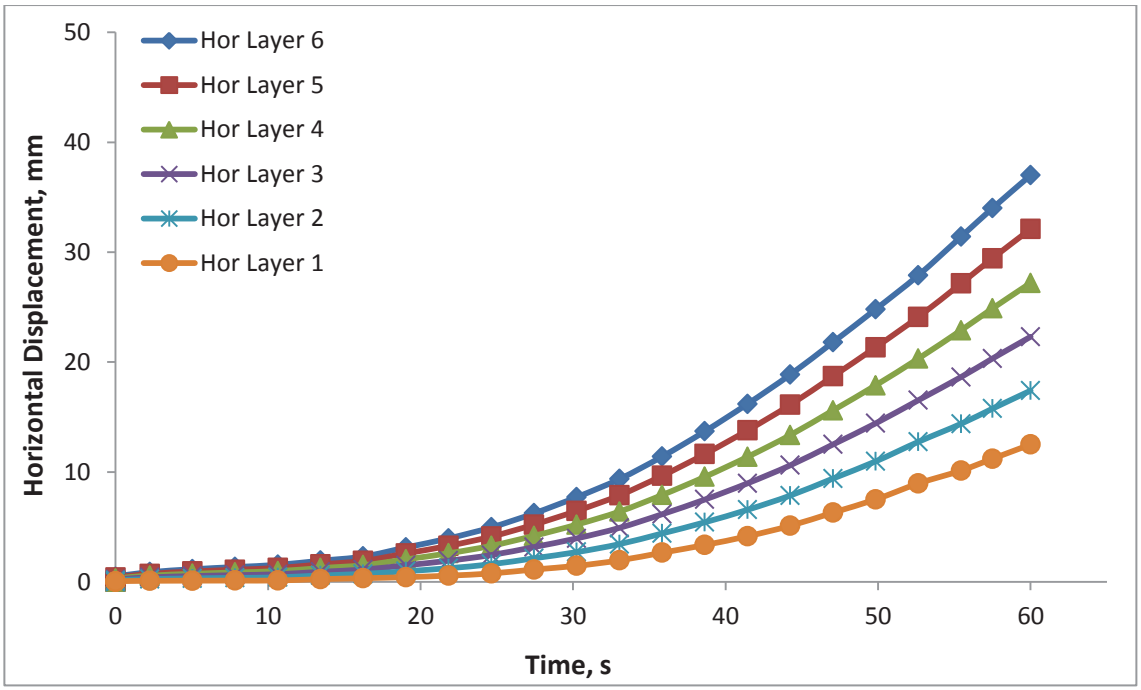

Figure 7.11 Horizontal deformation of the reinforced wall (with reinforcement inclined towards the facing)

The calculated settlement of the backfill using sinusoidal shaking is shown in Figure 7.12.

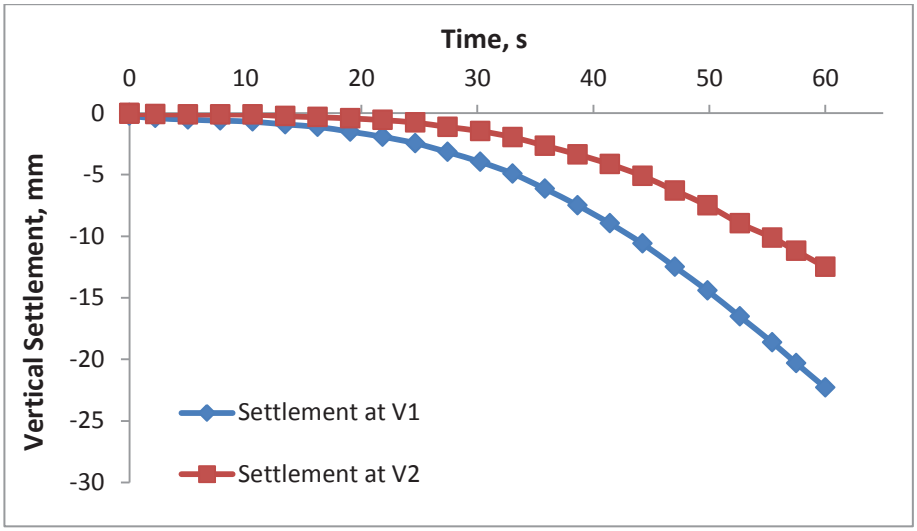

Figure 7.12 Vertical deformation of the reinforced wall (with reinforcement inclined towards the facing)

The pattern of acceleration calculated at A1, A2, and A3 is similar to Model 1, as shown in Figure 7.13, where the response increased proportionately as the amplitude of input acceleration increased every five seconds.

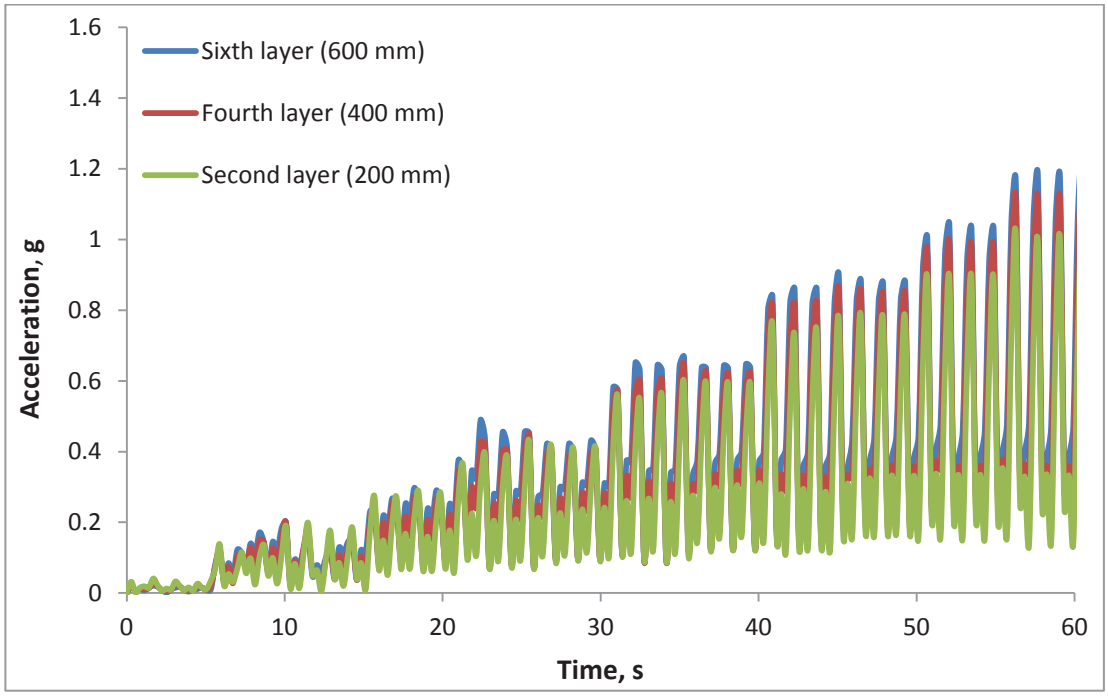

Figure 7.13 Response of Acceleration in Model 3

7.3.4 Model 4: Reinforced wall with reinforcement inclined against the facing

Figure 7.14 illustrates the model with reinforcement inclined away from the facing.

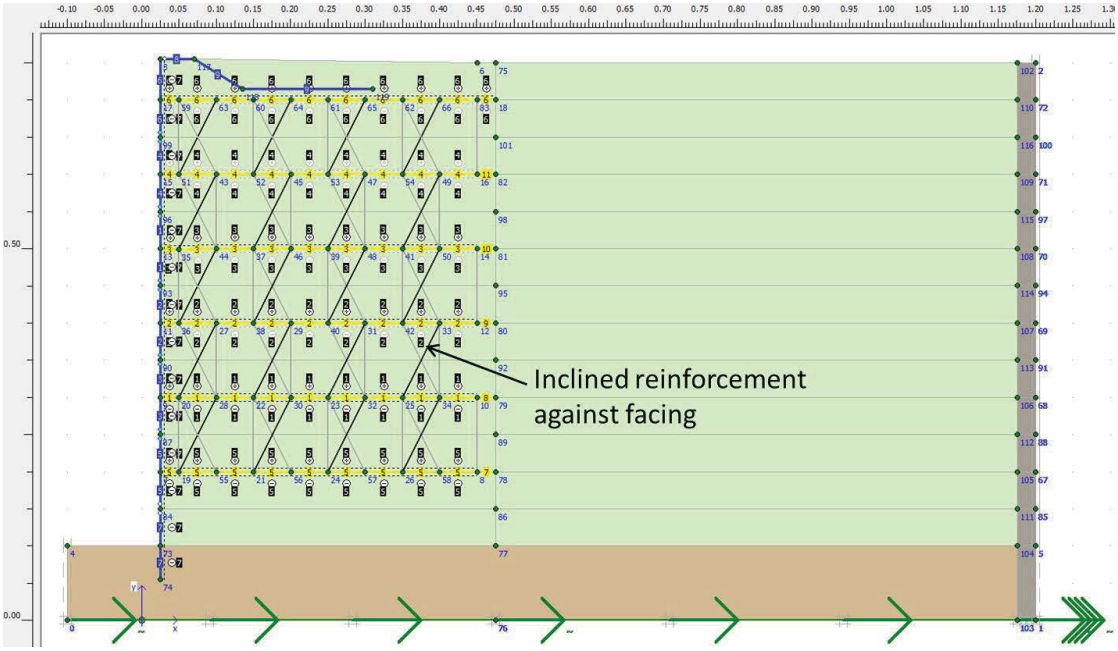

Figure 7.14 Model details with reinforcement inclined away from the facing

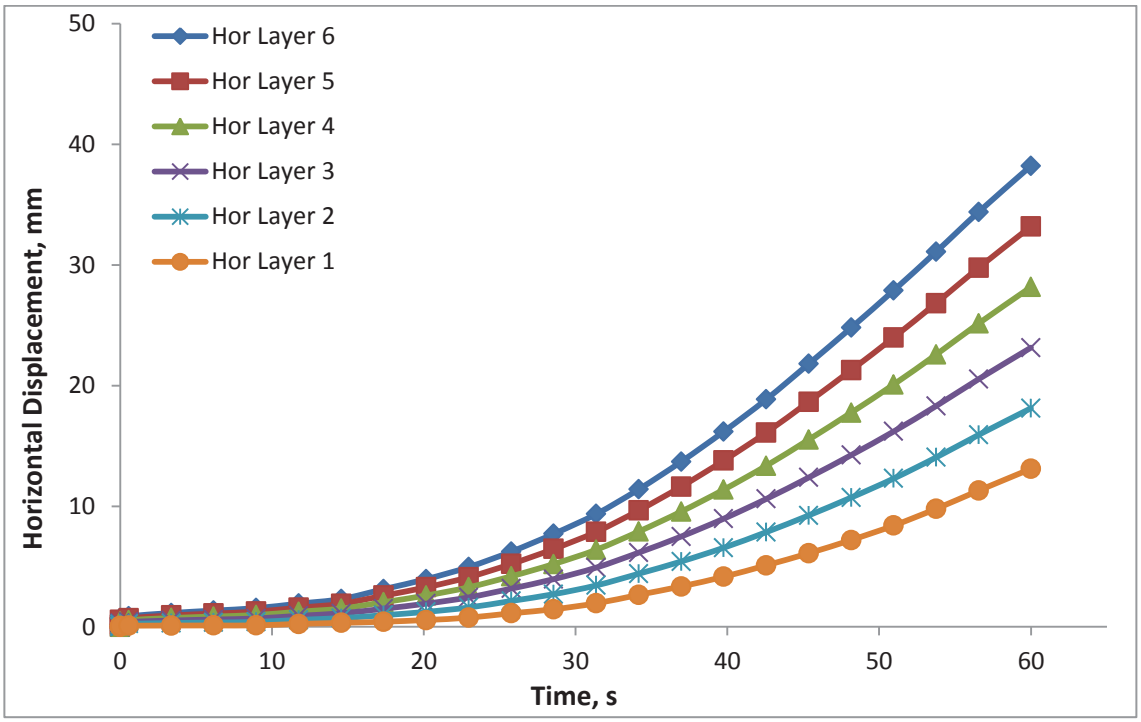

Figure 7.15 Horizontal deformation of the reinforced wall (with reinforcement inclined away from the facing)

Figure 7.15 shows the deflection on the wall, with the same pattern of maximum deflection at the top and less at the bottom of the reinforced wall.

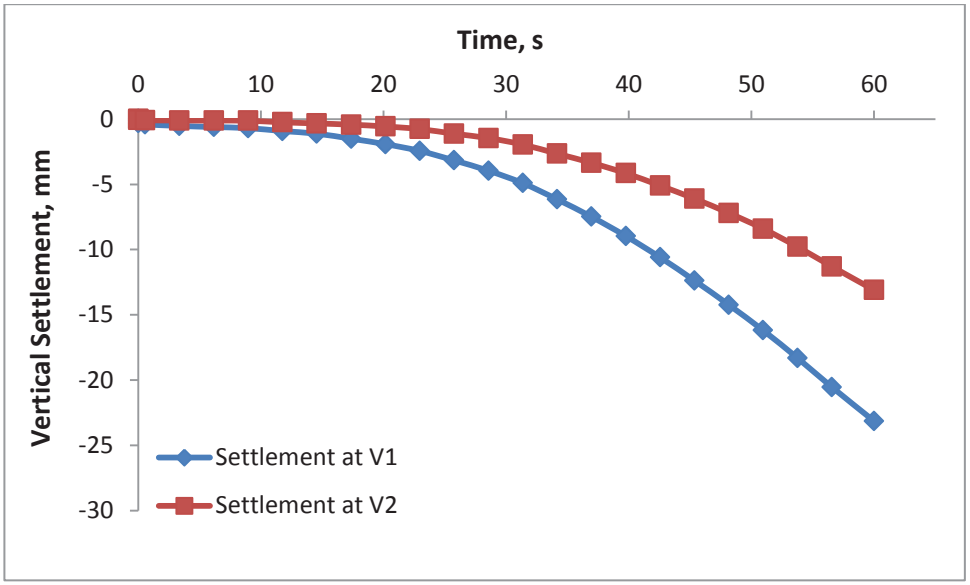

Figure 7.16 Vertical deformation of the reinforced wall (with reinforcement inclined against the facing)

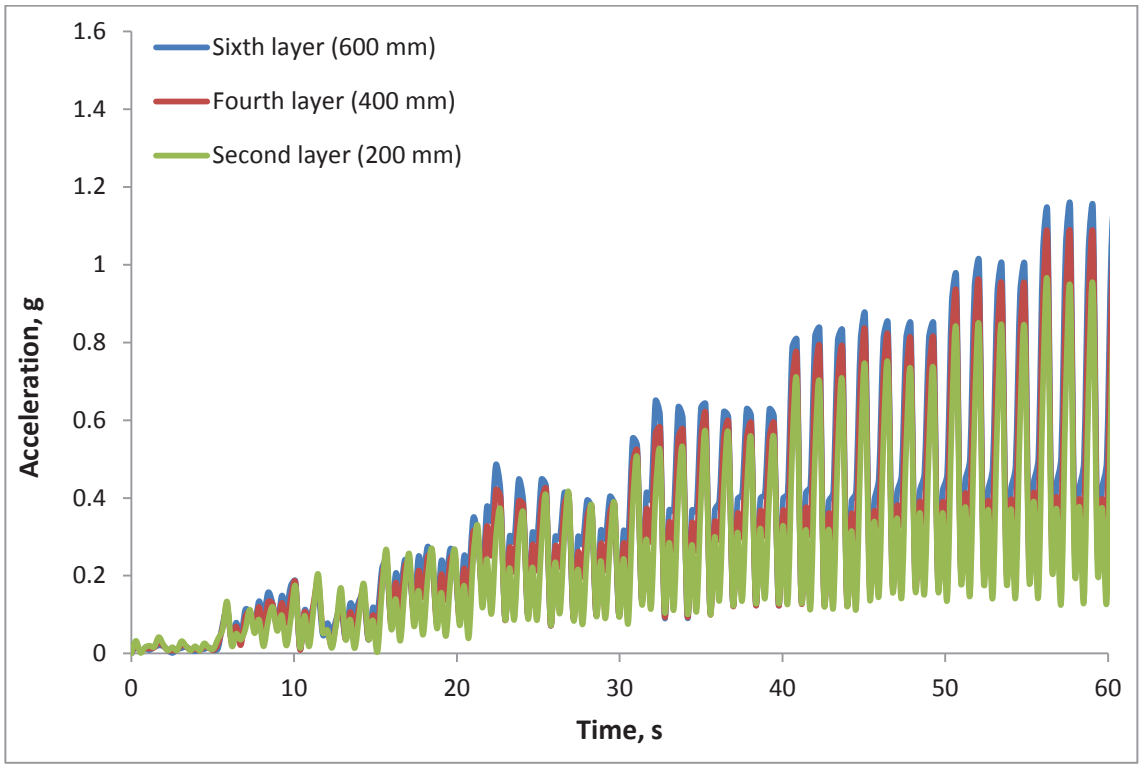

Figure 7.17 Response to acceleration in Model 4

The acceleration recorded in all three locations of test Model 4 are shown in Figure 7.17, where the top part of the wall is very sensitive compared to the levels near the base and the middle.

7.3.5 Comparing the results of different models

In this section the results of all the numerical models are analysed and compared. The patterns of horizontal deformation and acceleration in different locations are very close to each other. Therefore, only the horizontal deformation of top layer (Layer 6) of all four reinforced wall models: (1) without any vertical reinforcement, (2) with vertical reinforcement, (3) with reinforcement angled against the facing, and (4) with reinforcement angled towards the facing, were compared. In the former models the reinforcements was inclined by 26.5 degrees to the vertical axis. The response to acceleration of the four models at A3 (Layer 6) were compared to evaluate the effect of different types of reinforcement.

It is obvious that horizontal displacement is larger at the top of the wall than the bottom. The comparison of lateral displacement at the top layer of four Models at layer 6 (H6) are shown in Figure 7.18.

Figure 7.18 illustrates the results of lateral deflection in the top layer of the model of all four walls. The curve of results clearly shows that the deformation without vertical reinforcement is very high compared to when vertical reinforcement has been inserted. For instance, after 40 seconds of shaking (base acceleration was 0.4g), the horizontal displacement in the curve without vertical reinforcement was 38 mm and the others are only about 14 mm, which is almost half. This is similar to the results of the shake table experiments.

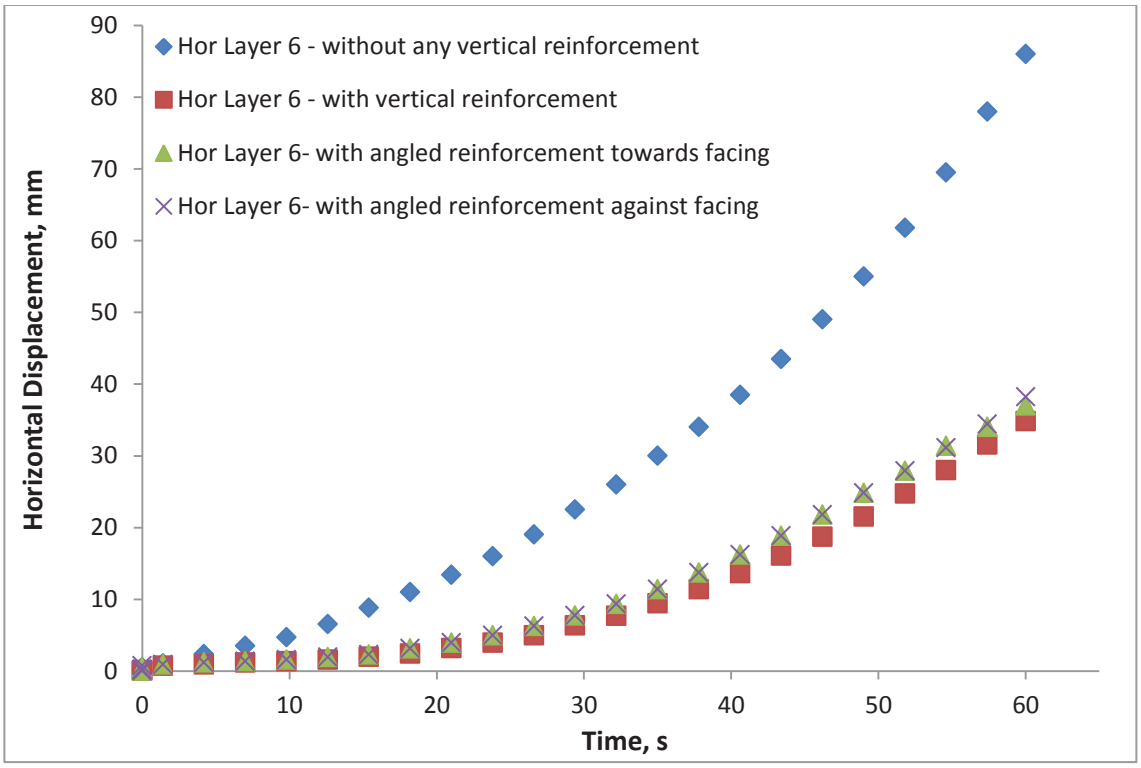

Figure 7.18 Comparison of horizontal deformation at the top layer from numerical analysis

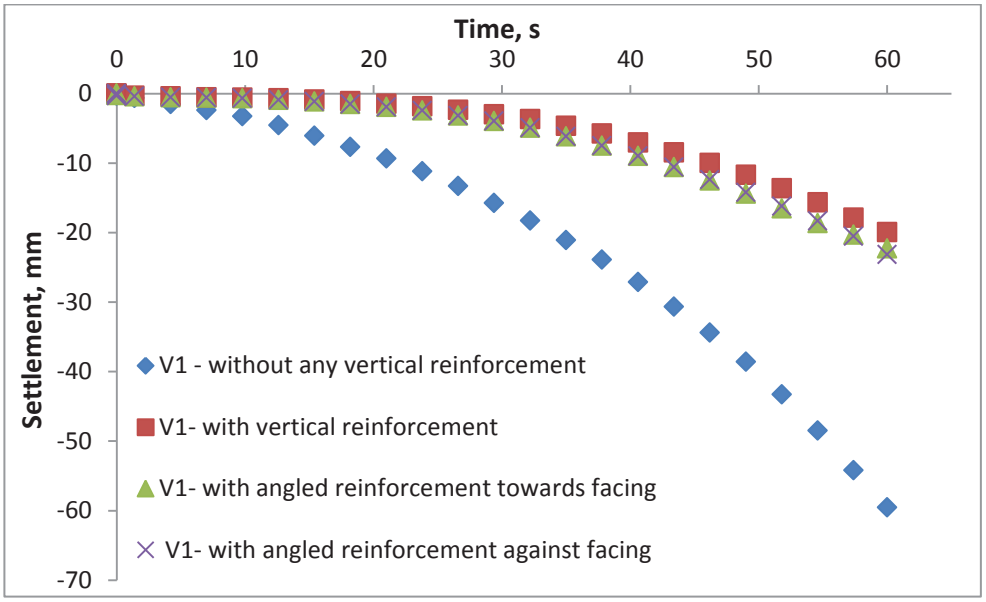

Figure 7.19 Comparison of settlements at V1

Vertical deformation calculated at locations V1 and V2 in different models were compared in Figure 7.19 and 7.20. With Model 1 (without vertical reinforcement), settlement occurred faster than the other two models, and settlement behind the

reinforced soil zone (V1) is more advanced than that close to the facing (V2). It is obvious that when there is more horizontal, there is more settlement, although the settlement values and variations are very similar.

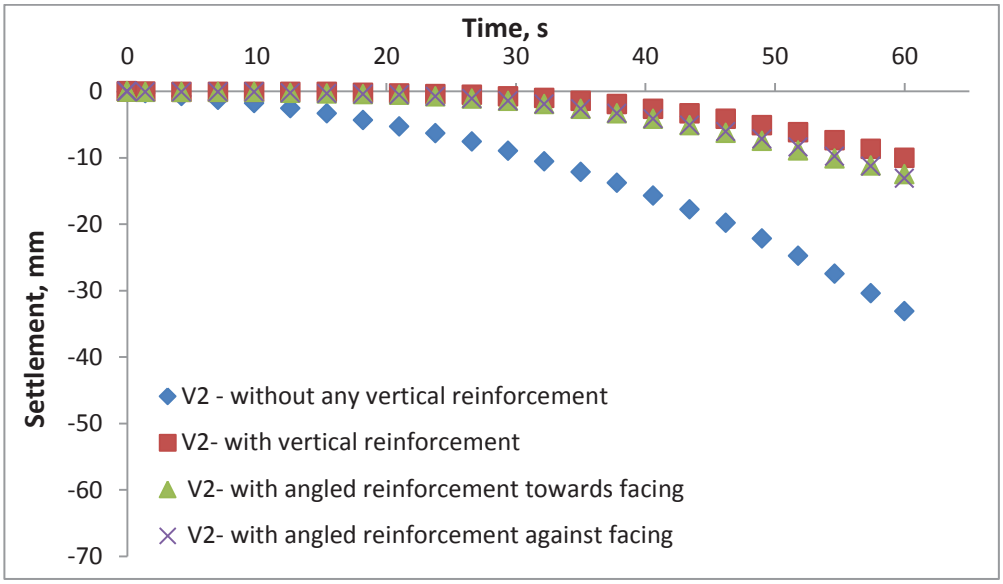

Figure 7.20 Comparison of settlements at V2

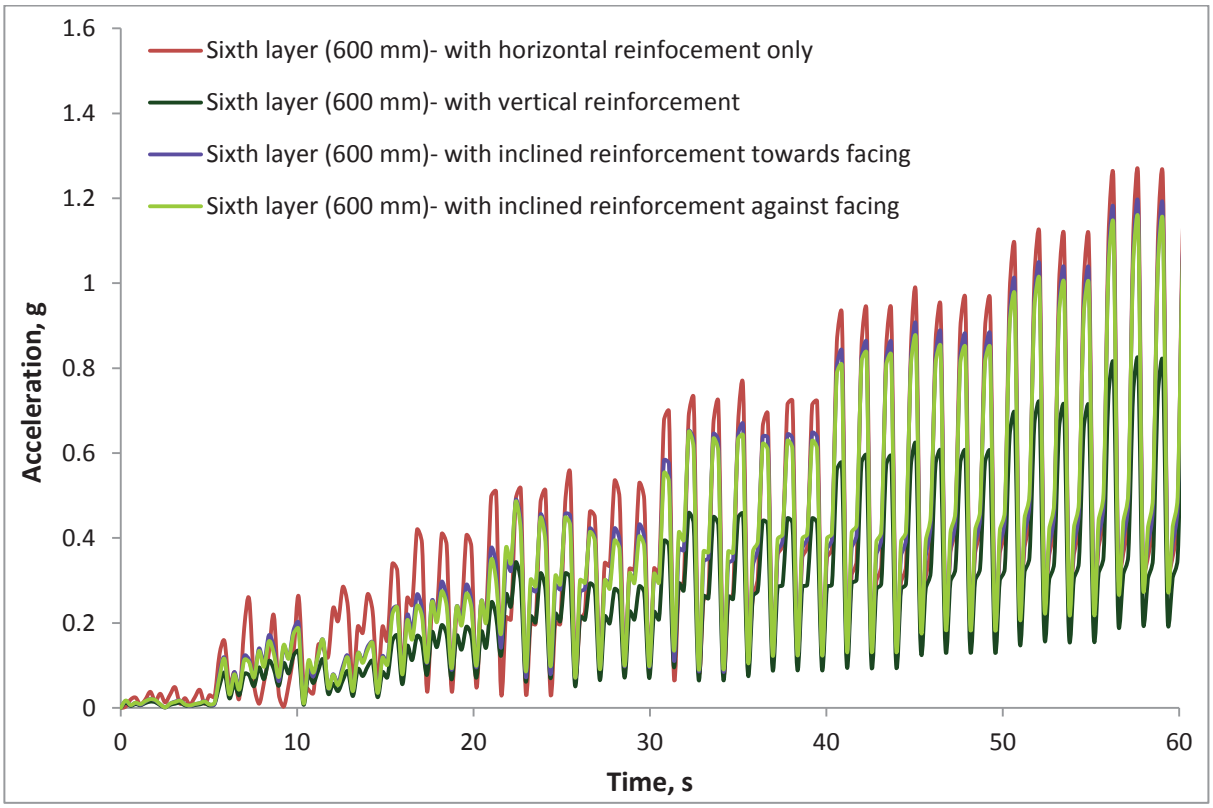

Figure 7.21 Response of different models at the top layer to acceleration

Acceleration at different heights clearly shows they were amplified at the top of the wall. Figure 7.21 presents the variation in the acceleration of the models with the stepped up sinusoidal input and recorded at a height of 610 mm (the top layer).

Figure 7.21 shows that the acceleration amplified considerably in Model 1 compared to other models, and the other three models (i.e. Models 2, 3, and 4) responded in a similar way. This output obviously shows that the amplification of acceleration is reduced with the inclusion of vertical reinforcement, which as a consequence, causes less deformation.

The curves with vertical reinforcement and with reinforcement inclined towards the facing and against the facing, are very close to each other. This similarity shows that a small change in the angle of vertical reinforcements has no significant effect. These results are similar to the laboratory experiments using the shake table.

7.4 Experimental verses Numerical Analysis

The results of the numerical simulation of soil walls reinforced by geosynthetics using shake table tests were compared with the performances reported by Ling et al. (2005), Burke (2004) and Lee, Chang & Ko (2010) where all the models were constructed with horizontal reinforcement. In this section the results obtained from the shake table experiments and numerical modelling using similar parameters were compared to each other to verify the inclusion of vertical reinforcement in conventional reinforced walls. As mentioned in Chapter 6, the results taken from the shake table test associated with Model 3 were incomplete and therefore the output of reinforced walls, Model 1 (with horizontal reinforcement), Model 2 (with vertical reinforcement towards the facing), and Model 4 (with reinforcement inclined towards the facing), were are matched and discussed.

7.4.1 Horizontal displacement

A comparison of the three test walls, between the calculated and measured wall facing with horizontal displacement at the top and the middle layers was discussed. As expected, displacement in the wall facing increased with an increase in the dynamic loads. It was observed that the numerical simulation over estimated the displacement in the wall. Note that the profile of horizontal displacement between the calculated and measured response where displacement at the top of the wall is the largest and is least at the base of the wall, is the same.

Figure 7.22 presents the numerical and experimental results for the bottom to top layers of the wall facing the displacement for the case with horizontal reinforcement only. The figure shows that at H1 to H6, the calculated and measured displacements are close to each other, and although the trend of displacement is similar, the calculated analyses are more conservative than the experimental values in the middle layer, whereas it is the other way round for the top layer.

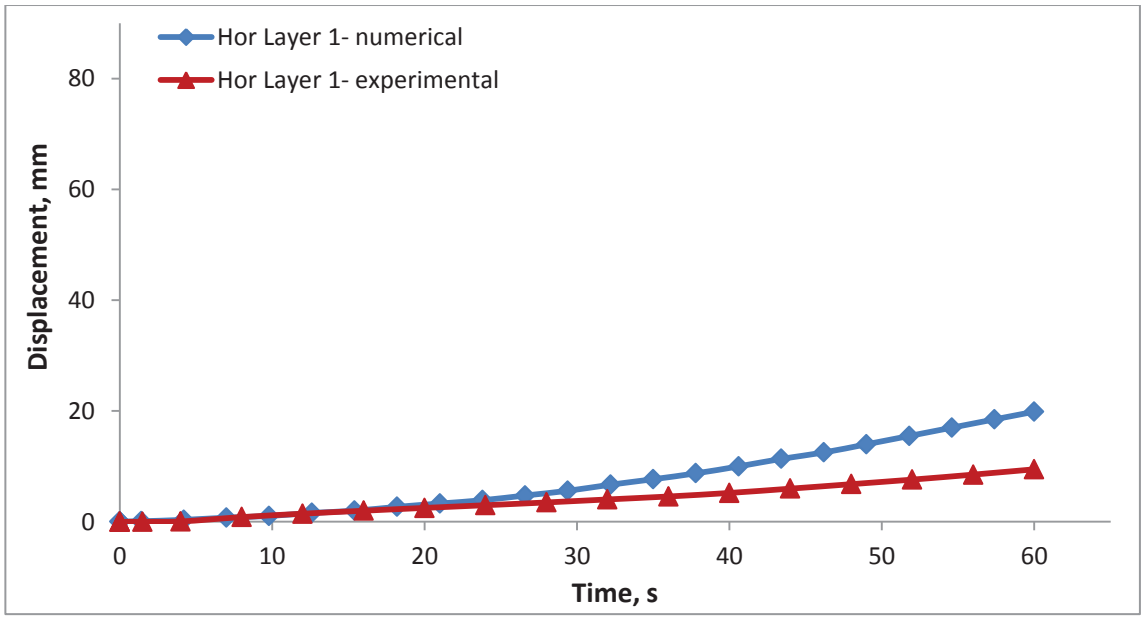

(a) Horizontal layer 1 (H1)

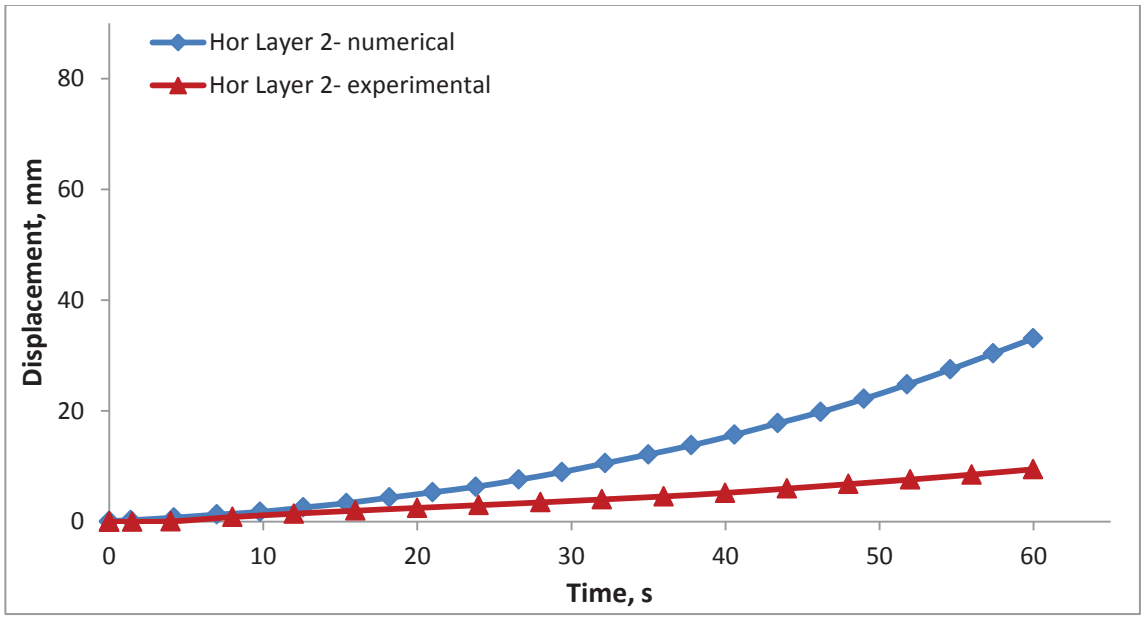

(b) Horizontal layer 2 (H2)

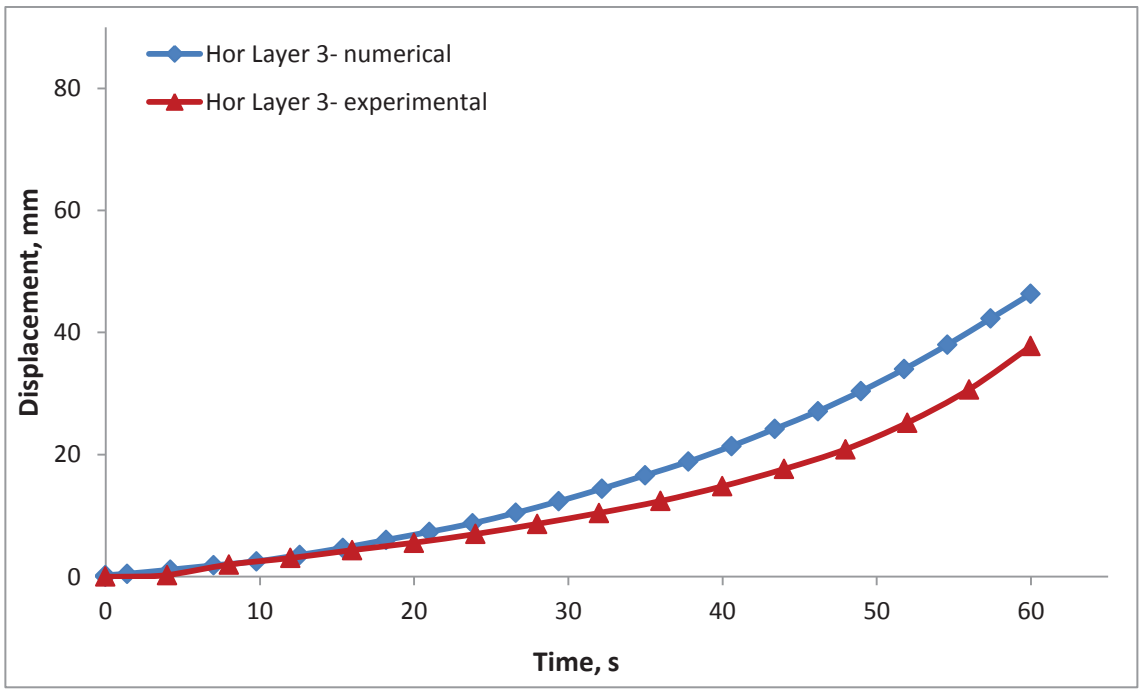

(c) Horizontal layer 3 (H3)

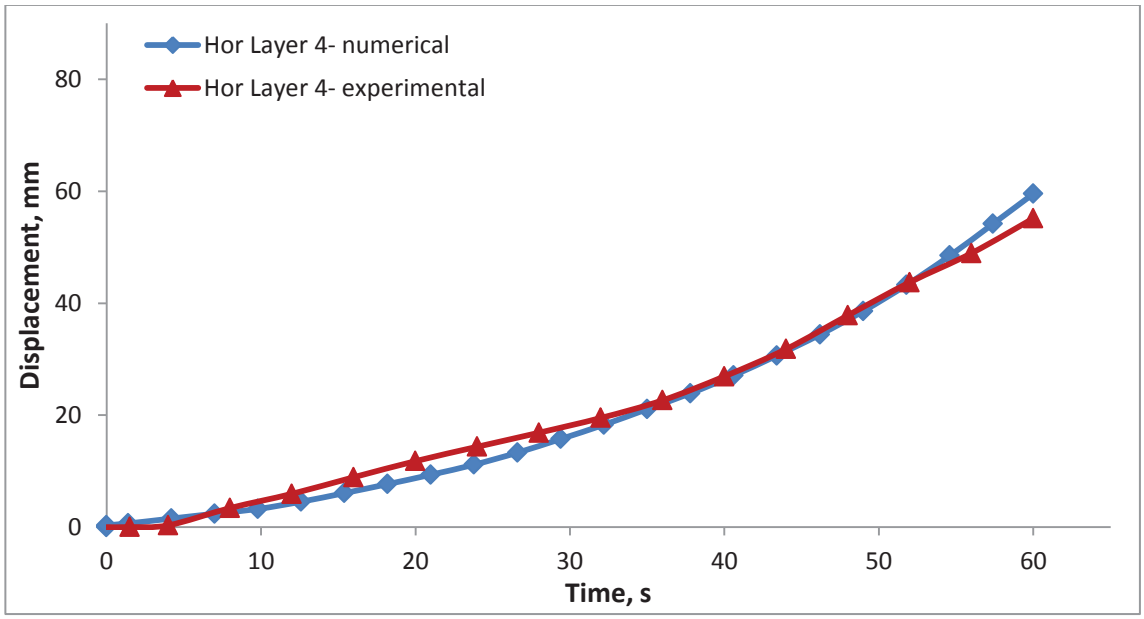

(d) Horizontal layer 4 (H4)

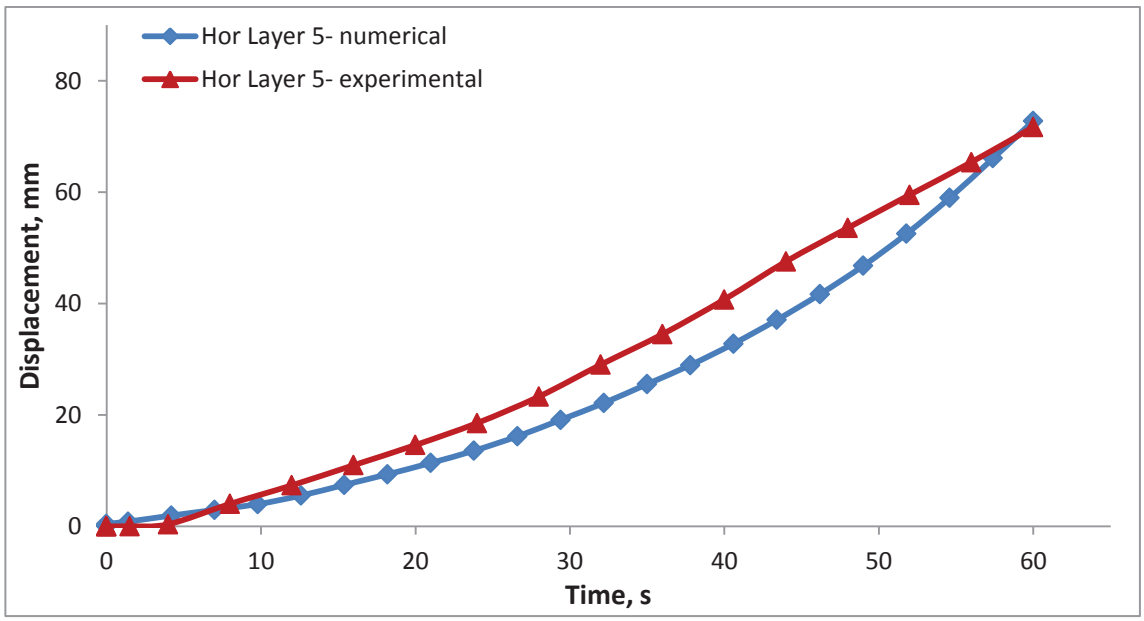

(e) Horizontal layer 5 (H5)

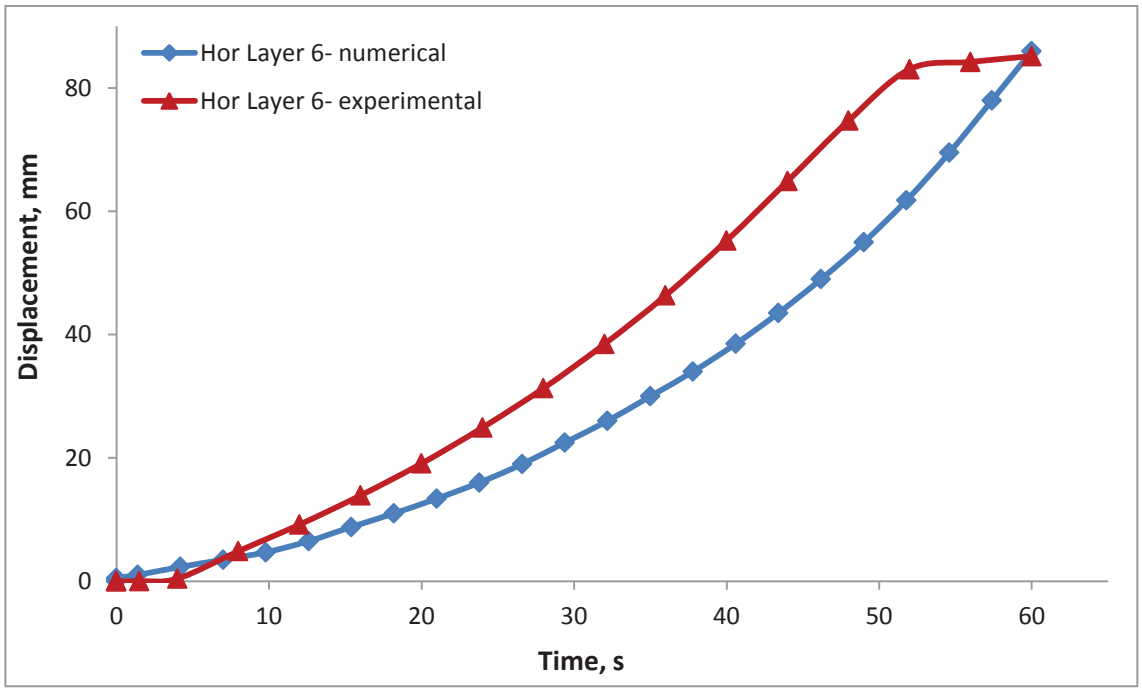

(f) Horizontal layer 6 (H6)

Figure 7.22 Comparison between displacement at the top and middle layers of the wall facing, without vertical reinforcement

Figure 7.23 shows the comparison displacement between the experimental and numerical values of the wall facing, with vertical reinforcement. The numerical analysis shows there was significant displacement compared to the experimental output, although the curves follow a somewhat similar trend. The rate of change of displacement with respect to time follows the same pattern in both layers.

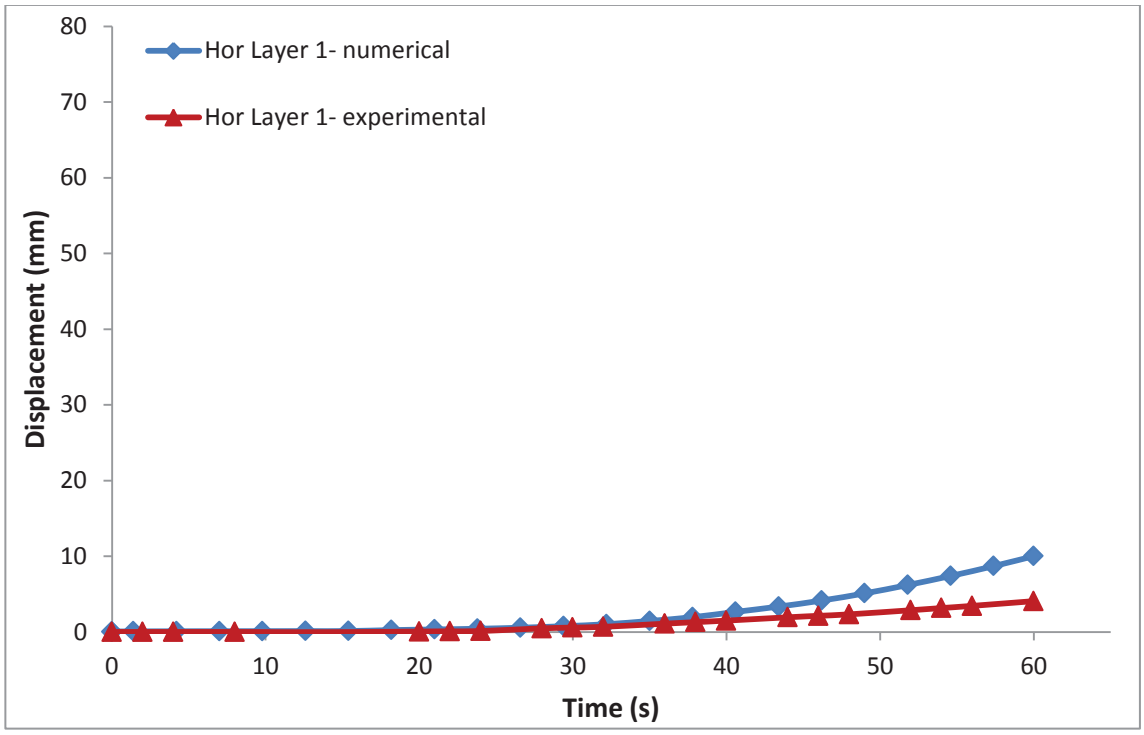

(a) Horizontal layer 1 (H1)

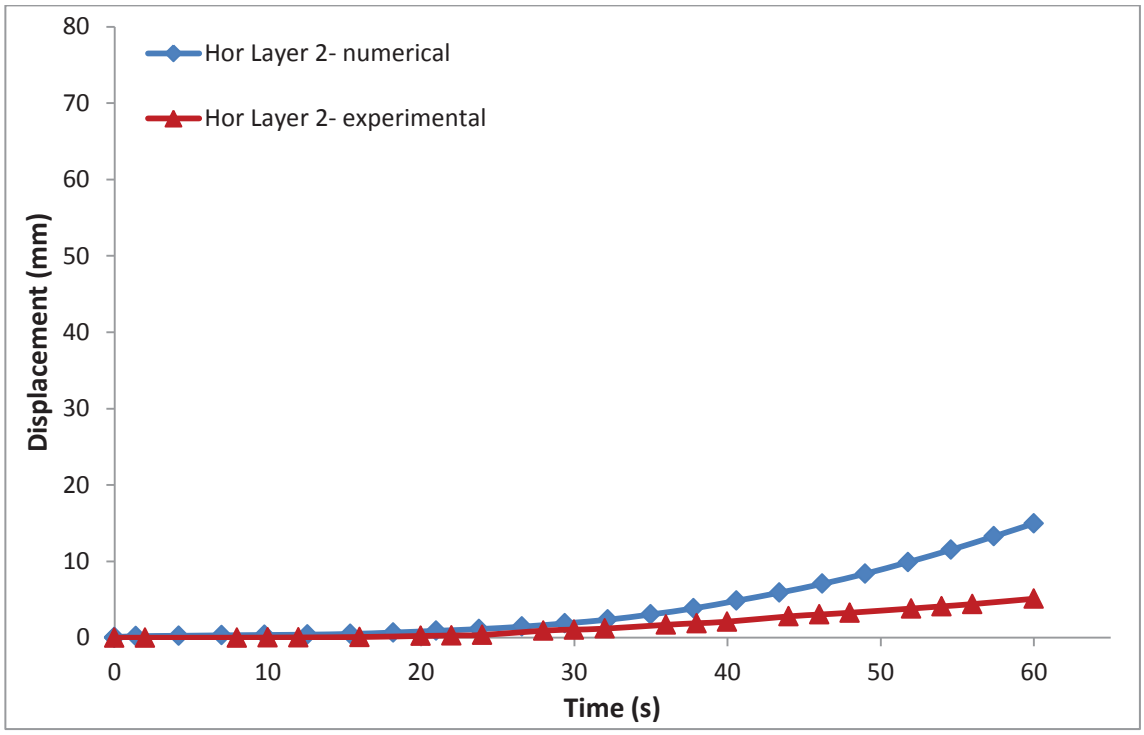

(b) Horizontal layer 2 (H2)

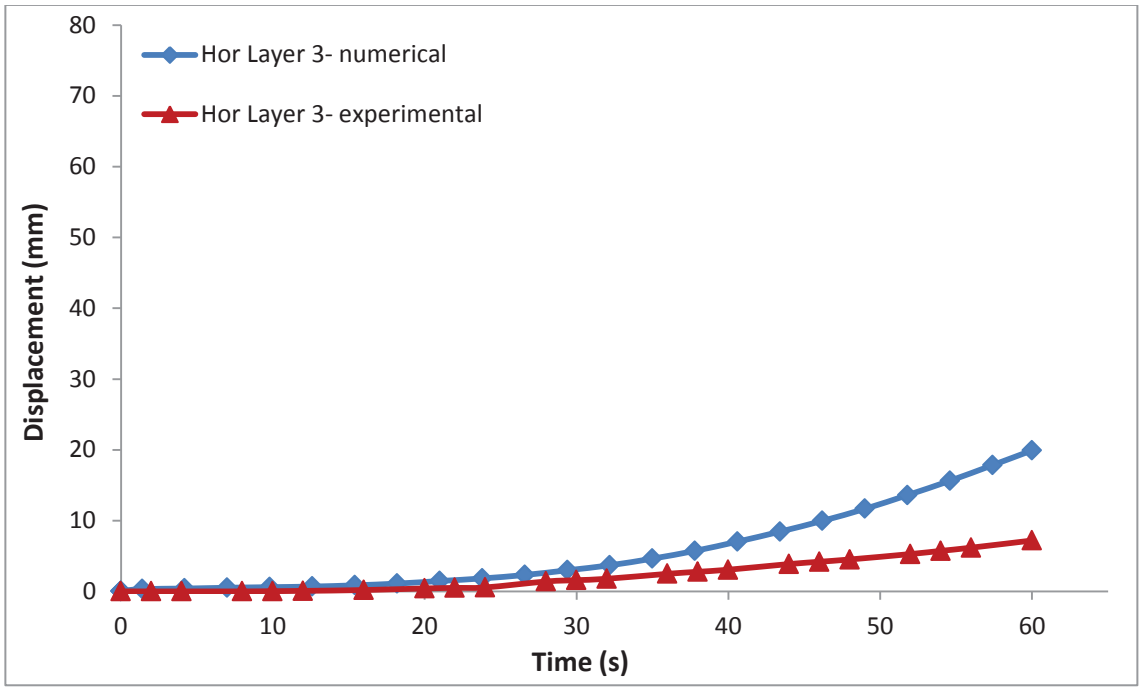

(c) Horizontal layer 3 (H3)

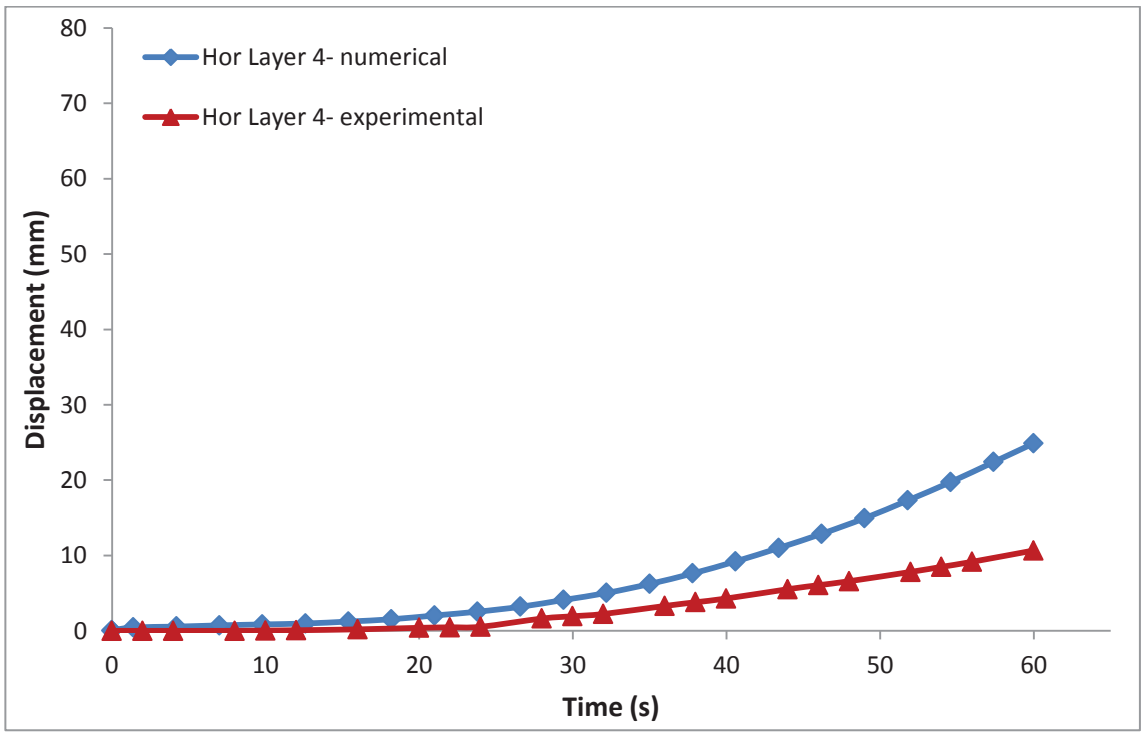

(d) Horizontal layer 4 (H4)

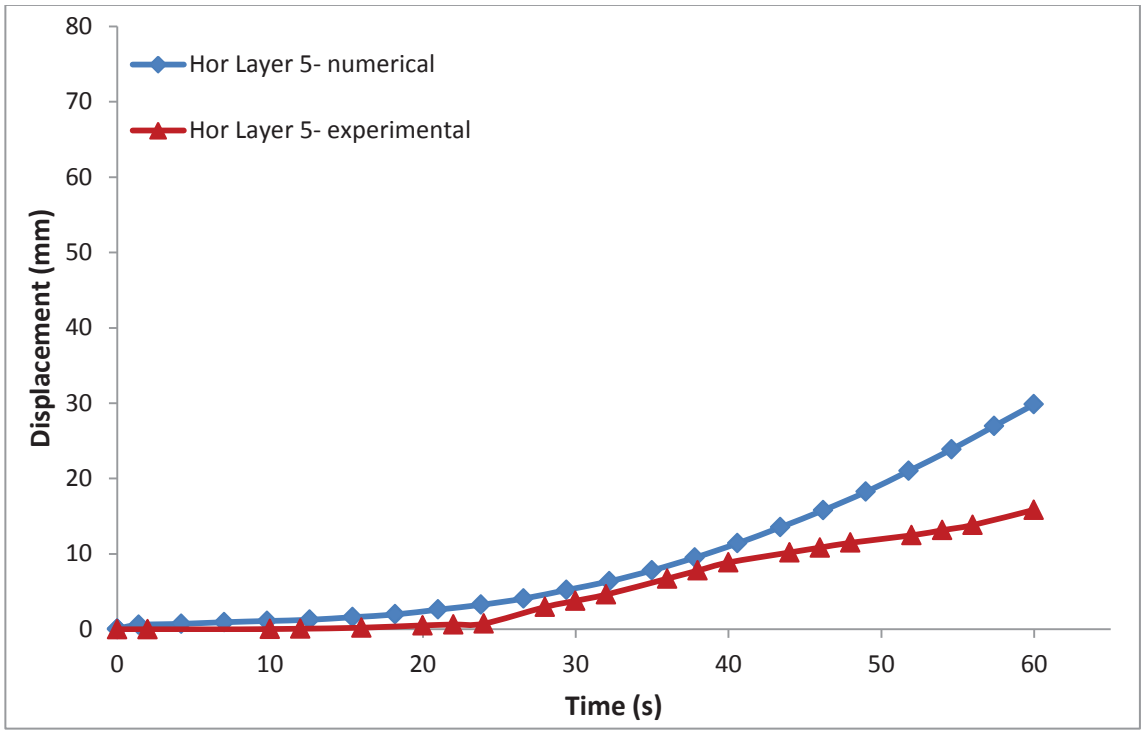

(e) Horizontal layer 5 (H5)

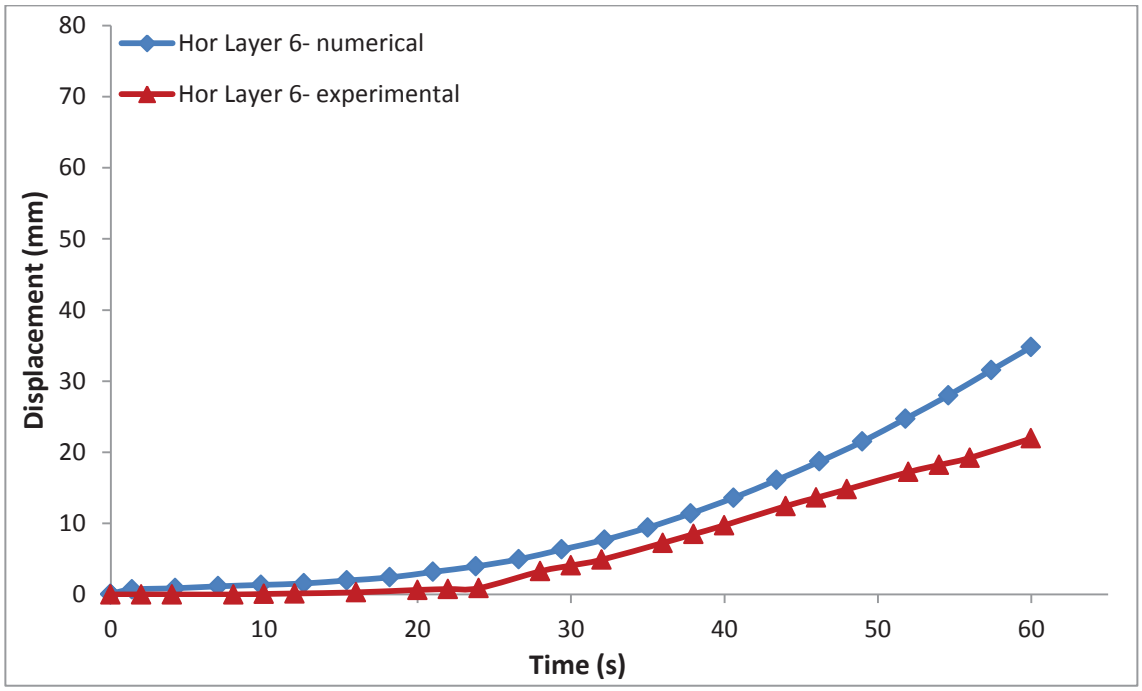

(f) Horizontal layer 6 (H6)

Figure 7.23 Comparison of displacement in the top and middle layers of the wall facing, with vertical reinforcement

Similarly, Figure 7.24 shows the comparison between horizontal deflections at the top to bottom layer with reinforcement inclined towards the facing. The displacement curves follow the same pattern and the change of displacement with time follows the same pattern in all layers.

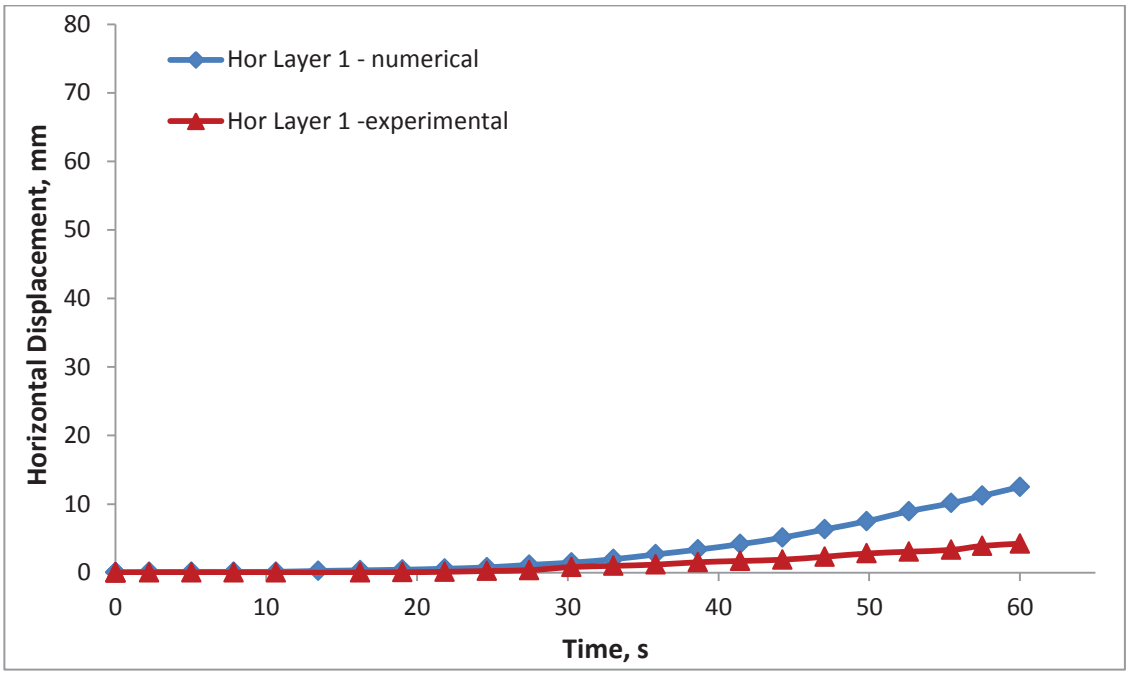

(a) Horizontal layer 1 (H1)

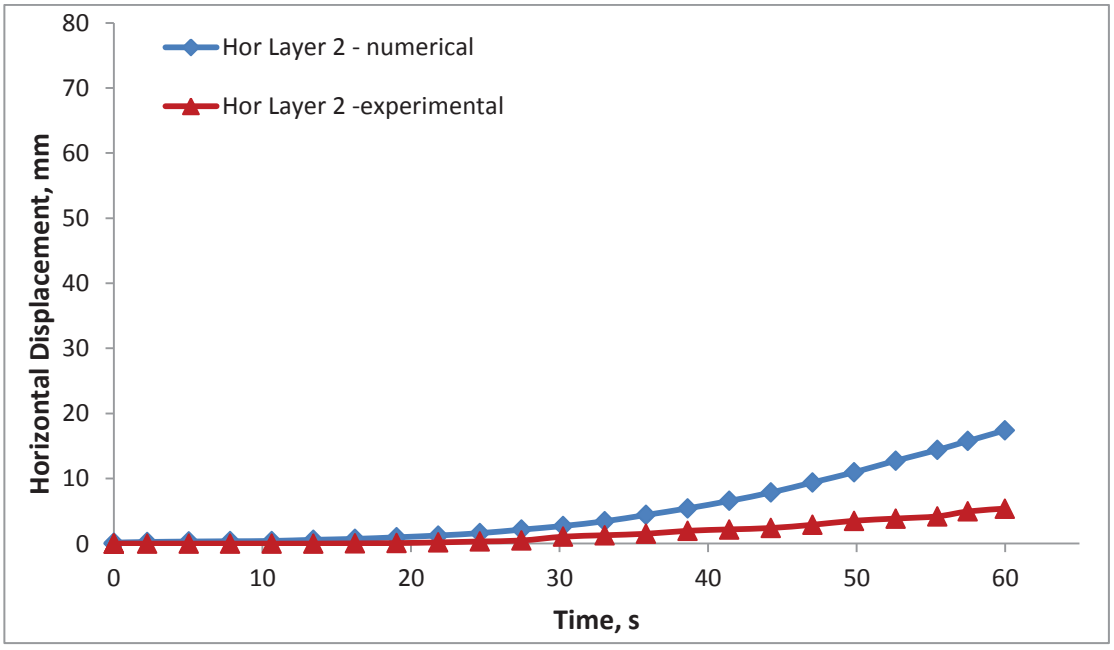

(b) Horizontal layer 2 (H2)

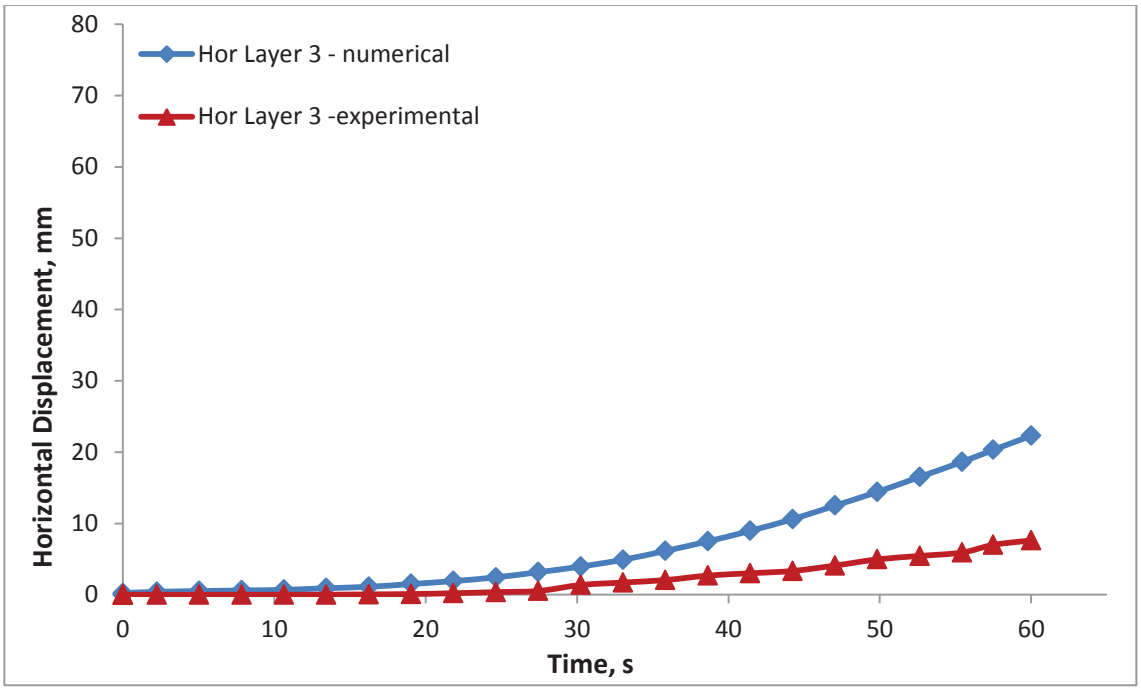

(c) Horizontal layer 3 (H3)

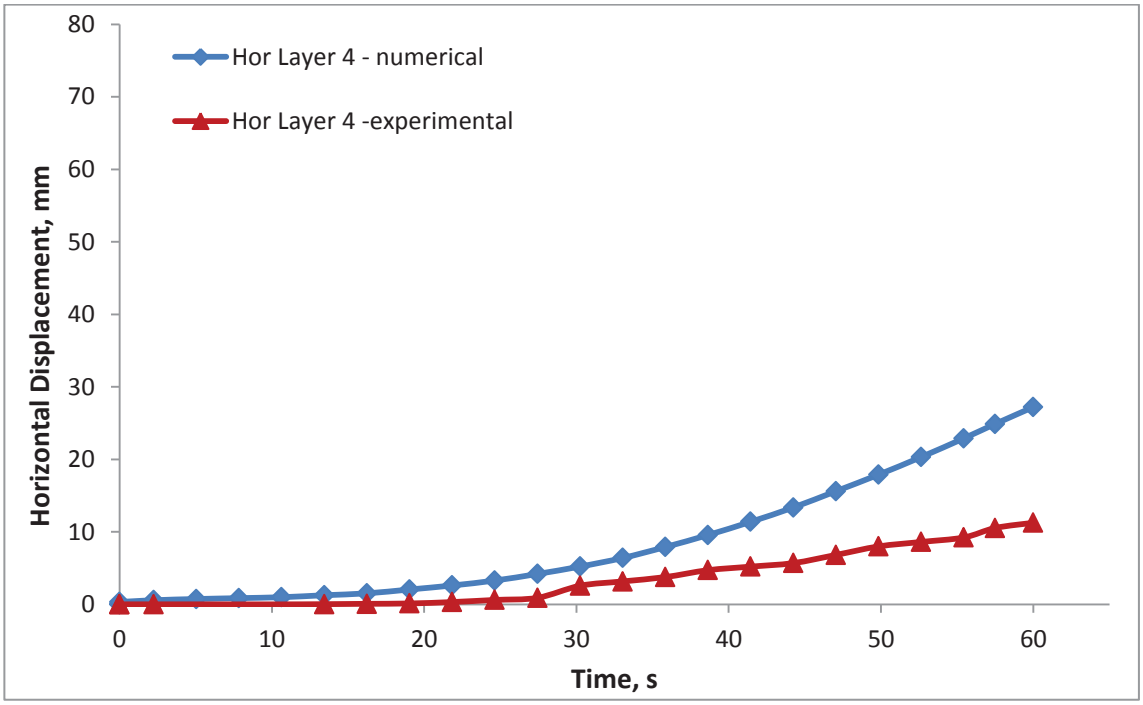

(d) Horizontal layer 4 (H4)

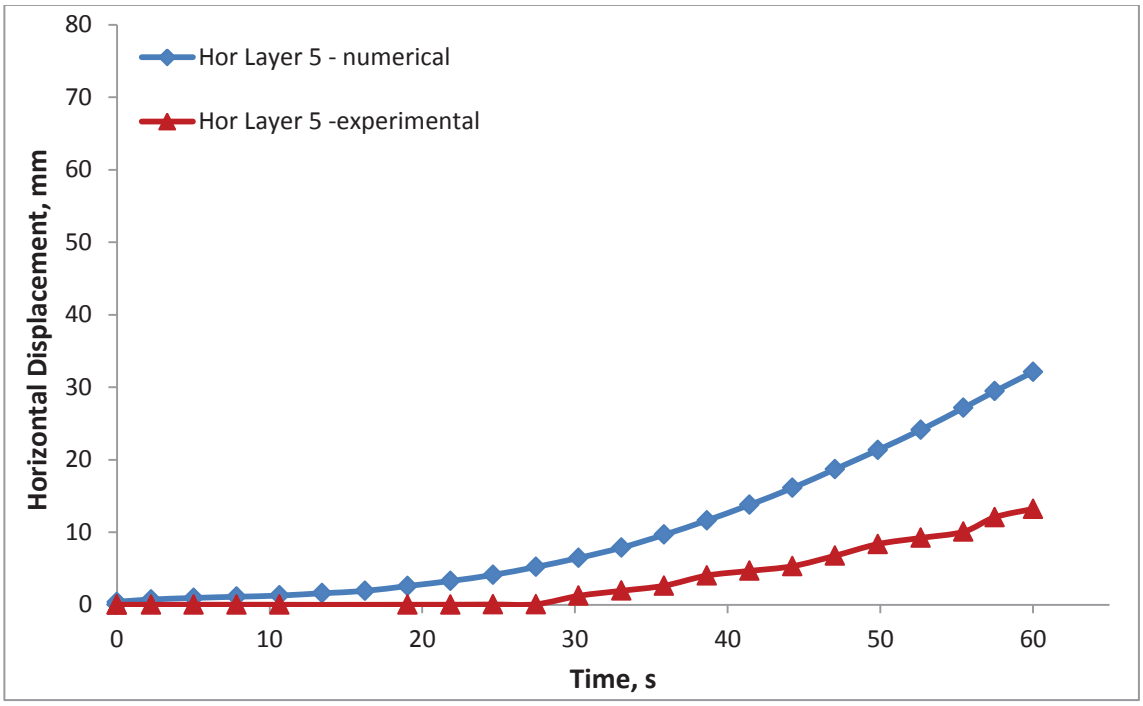

(e) Horizontal layer 5 (H5)

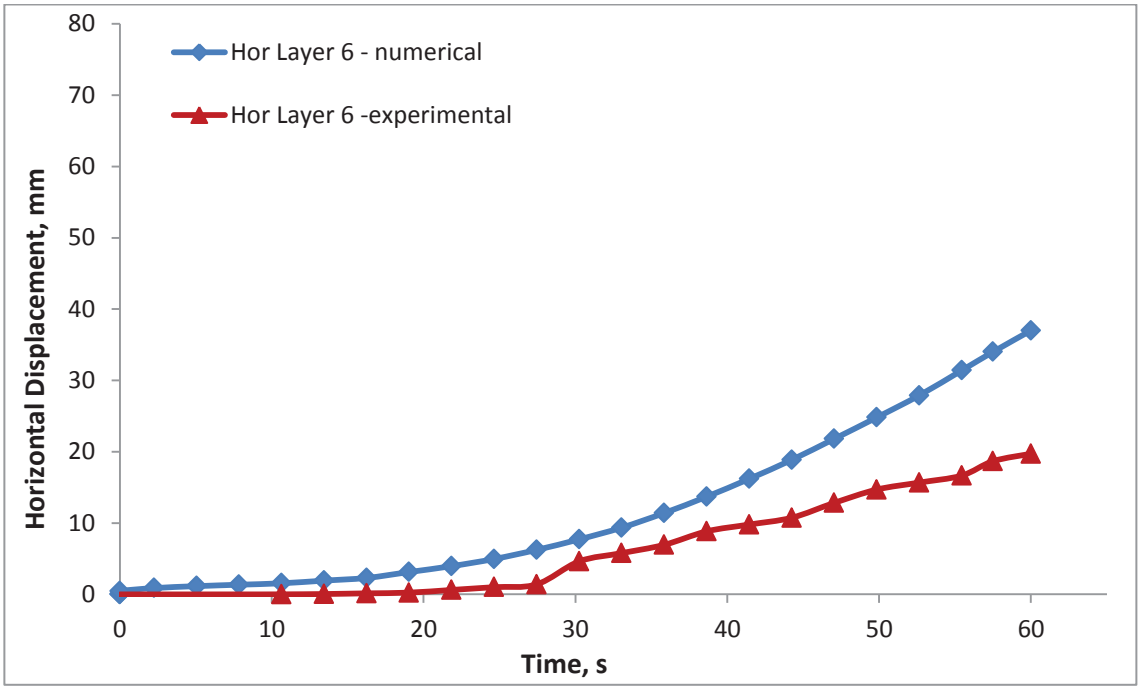

(f) Horizontal layer 6 (H6)

Figure 7.24 Comparison of displacement in the top and middle layers of wall facing, with reinforcement inclined towards the facing

The reason there were more displacements in the numerical modelling was due to a higher amplification of acceleration, that is, the shake table models may have a higher damping factor than the values considered in the numerical calculations.

7.4.2 Settlement of the backfill surface

An evaluation of the calculated and measured settlement of the backfill surface for the three wall models is discussed in this section, with Figure 7.25 illustrating the pattern of settlement in Model 1. In Figure 25a and 25b, the values at V1 and V2 show that the rate of settlement is higher in the experimental curve than the numerical curve.

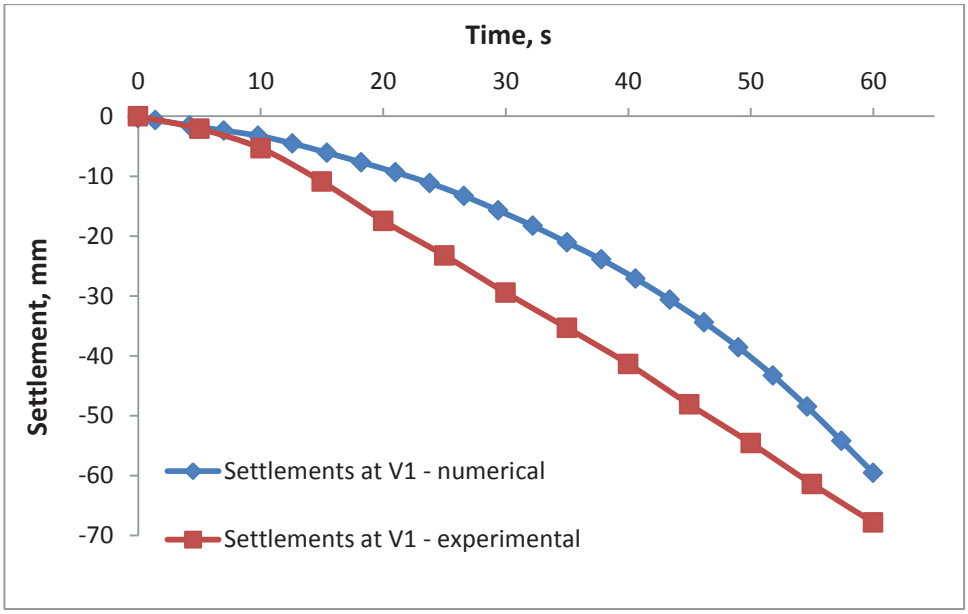

(a)

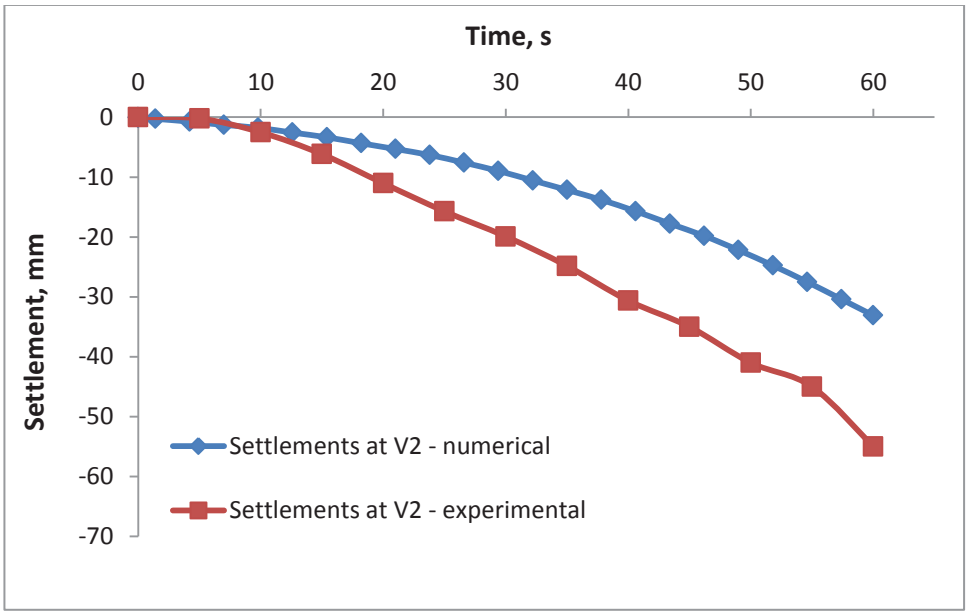

(b)

Figure 7.25 Comparison of settlement without any vertical reinforcement.

A comparison between settlement at V1 and V2 of the model with vertical reinforcement is illustrated in Figure 7.26 and shows that rate of settlement is less than the model without vertical reinforcement. The calculated settlements are high at location V1 and low at V2.

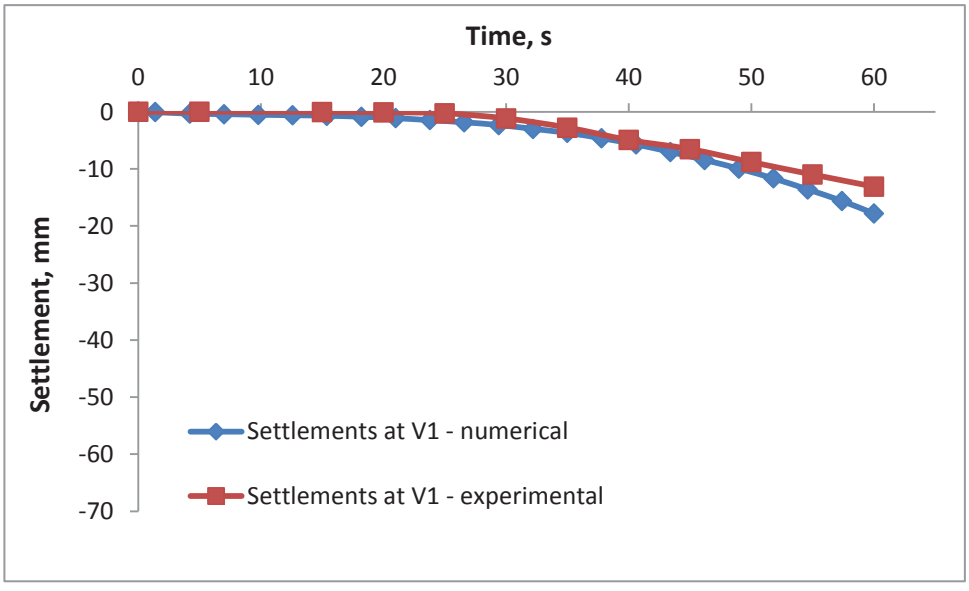

(a)

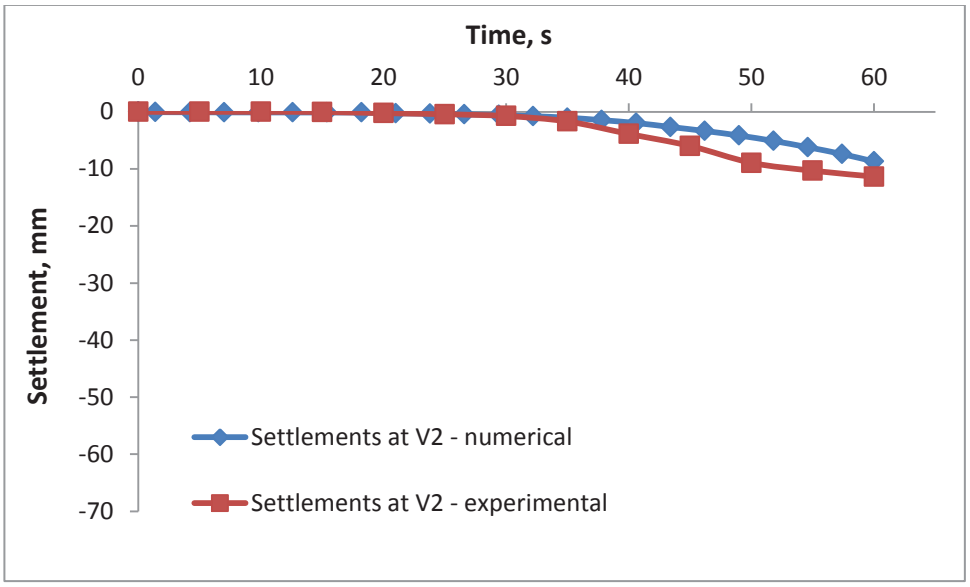

(b)

Figure 7.26 Comparison of settlement with vertical reinforcement

Similarly, Figure 7.27 presents a comparison of the settlement at V1 and V2 of model with reinforcement inclined towards facing. The rate of settlement from numerical analyses was higher in both cases.

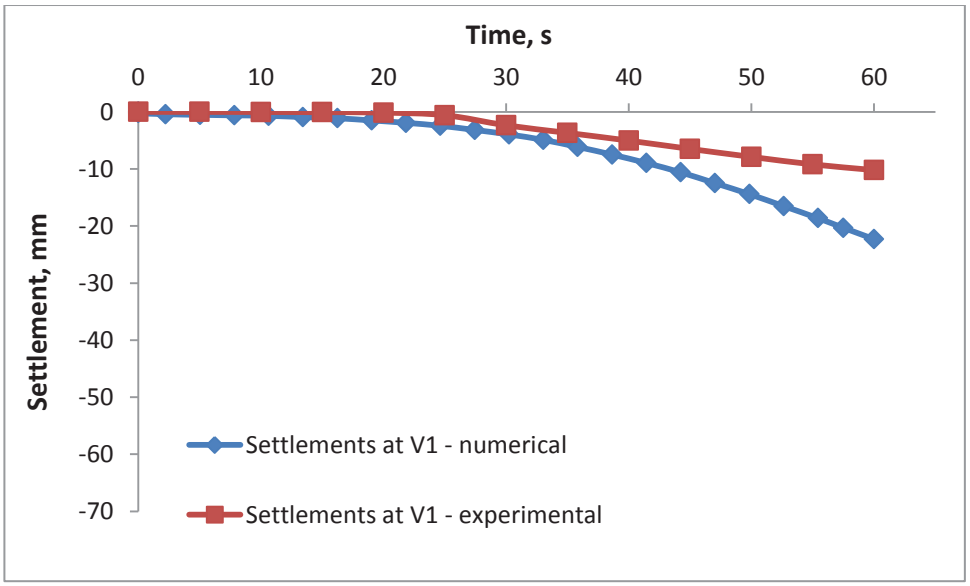

(a)

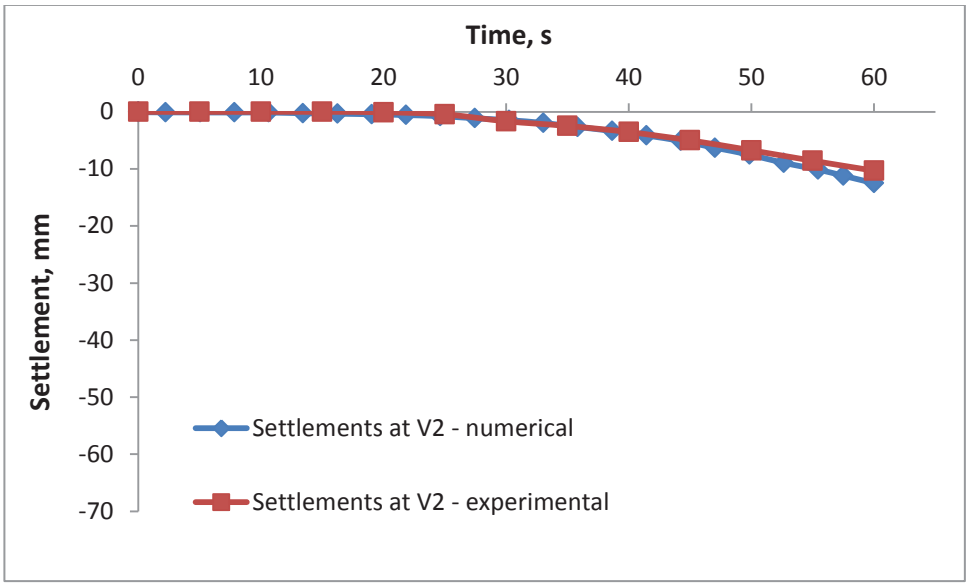

(b)

Figure 7.27 Comparison of settlements with reinforcement inclined towards the facing

In summary, the numerical simulation over estimated the permanent settlement, which was similar to the prediction of displacement in the wall face. Both the calculated and measured results show a similar settlement profile where more settlement took place between the reinforced and the retained soil zones and less took place towards the front and back of the wall. Note that the results obtained from the shake table tests varied greatly. It can be concluded that various degrees of stiffness exist between the reinforced and retained soil zones. Despite the measured results varying greatly, the simulation of the stepped-up sinusoidal loading in numerical modelling could estimate surface settlement of the wall in all three target models closely.

Although the settlement was more than that obtained in the experimental tests, the results are deemed acceptable because the differences are rather small.

7.4.3 Acceleration

The comparison of absolute peak horizontal acceleration (PHA) between the calculated and measured results in the facing of the reinforced soil wall is presented in Figures 7.28-7.30. An amplified acceleration occurred in both the calculated and measured results, although amplification in the measured results was less pronounced, especially at the higher amplitude of input acceleration.

Figure 7.28 shows the calculated and experimental PHA results for Model 1. This figure shows that in the initial phase, the experimental measurements were slightly higher than the numerical.

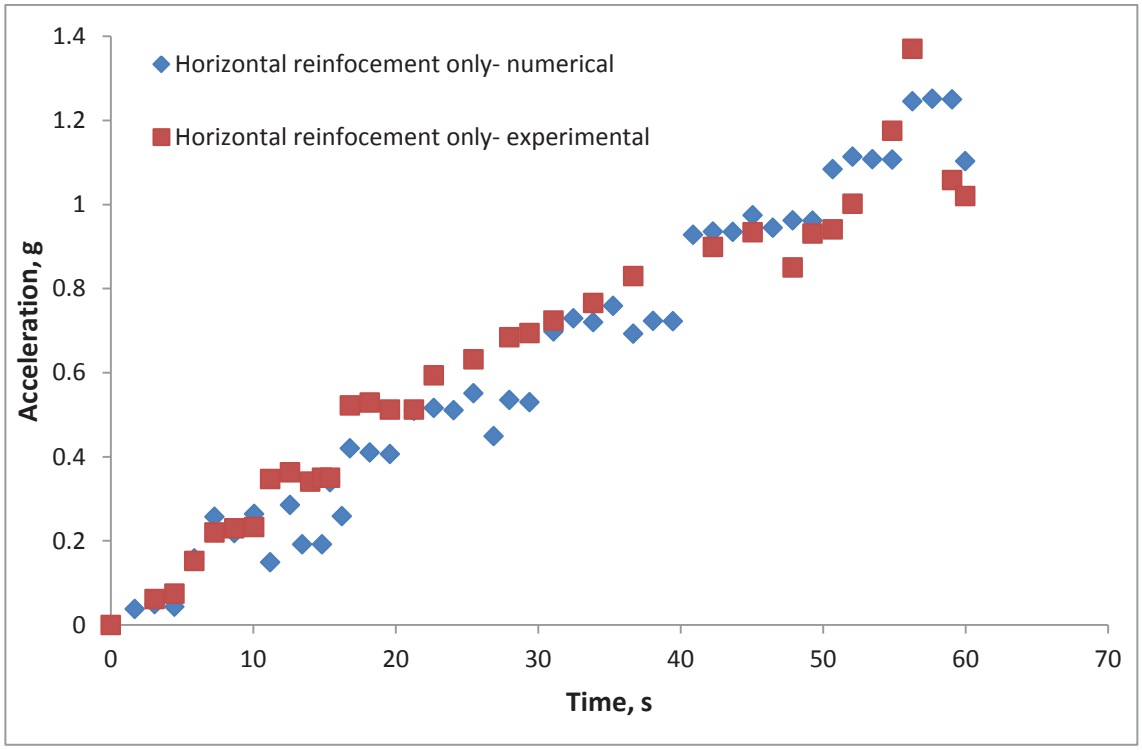

Figure 7.28 Comparison of PHA of the reinforced wall (with horizontal reinforcement only)

A comparison of PHA results in the model with vertical reinforcement is illustrated in Figure 7.29, with the results showing that the numerically calculated accelerations were slightly more than those obtained from the shake table test. Similar results were

obtained when PHA in the model was assessed with the reinforcement inclined towards facing, as shown in Figure 7.30.

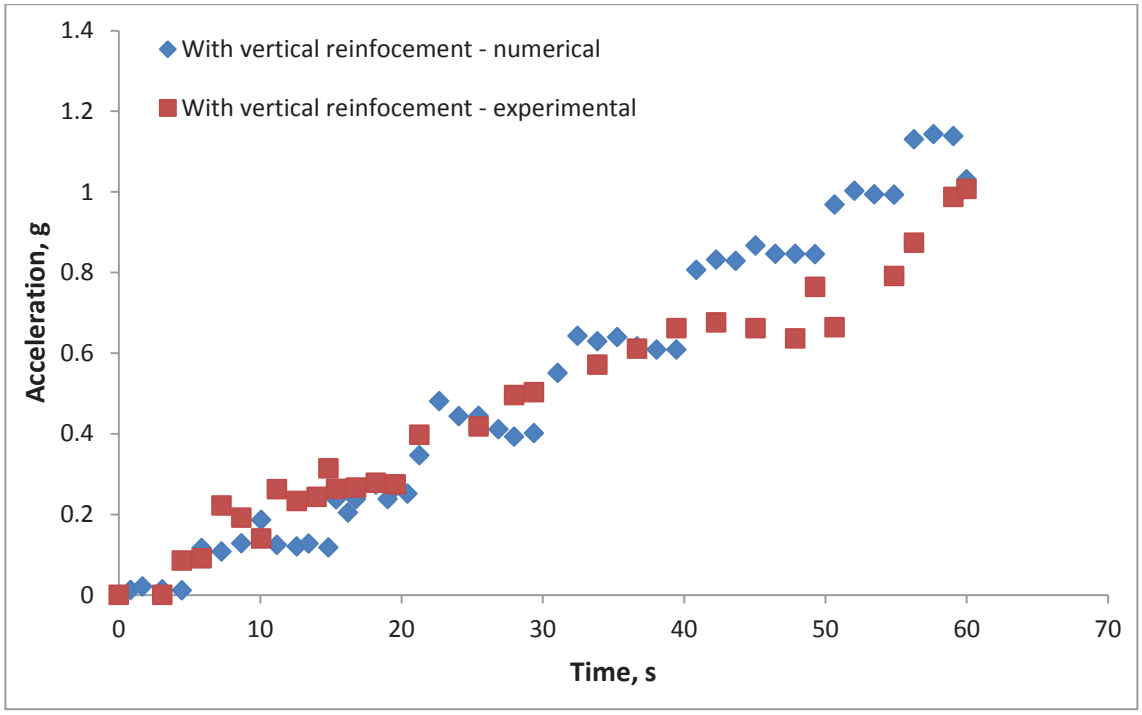

Figure 7.29 Comparison of PHA with vertical reinforcement

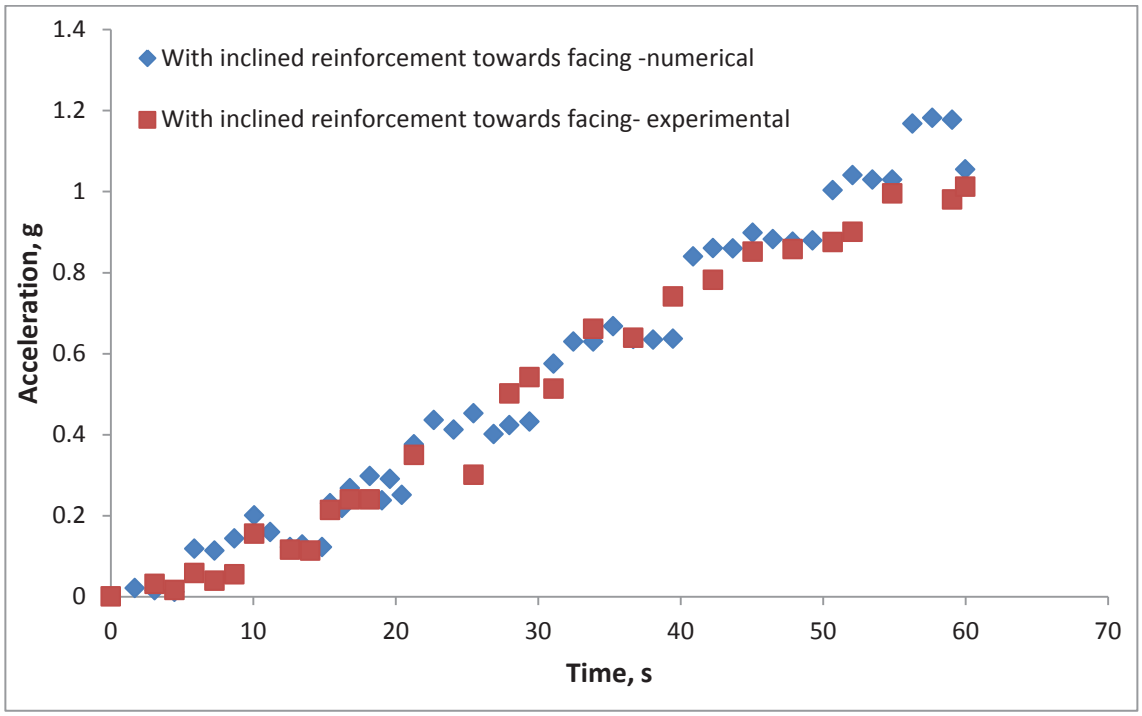

Figure 7.30 Comparison of PHA with reinforcement inclined towards the facing

The numerical simulations indeed showed that displacement in the wall facing is proportional to the amplified acceleration amplification, although it is more apparent in the calculated results that upper layers experience more acceleration than layers lower down. The effect of vertical reinforcement is also noticeable in the numerically calculated results.

This result shows a reasonable agreement between the measured and calculated displacements, settlements and acceleration of the backfill surface, even though there were some differences in terms of magnitude. These differences would be due to the practical behaviour of structures and theoretical assumptions and models. For instance a number of parameters used in the numerical analysis may not resemble those used in the experiments. Variability within the measured data is thought to have contributed to some discrepancies in the comparison. Thus, although some differences existed due to variations in the assumed parameters, there was sufficient evidence to conclude that the seismic modelling of models to compare the effect of vertical reinforcement achieved the desired result. Similar comparative results and discrepancies in experimental and numerical evaluations were observed by Burke (2004).

Lee & Chang (2012) discussed the relationship between validation and prediction pertaining to geotechnical problems and noted that the prediction could not indicate the accuracy of a complex system that has not been validated; rather, the accuracy could only be inferred based on the previous quantitative comparison.

7.5 Parametric Studies

7.5.1 Introduction

A few parametric studies of reinforced soil walls subject to dynamic behaviour (e.g. Cai & Bathurst 1995a; Helwany, Budhu & McCallen 2001; Segrestin & Bastick 1998; Yogendrakumar, Bathurst & Finn 1992) have been reported. For instance, Hatami & Bathurst (2000) studied the fundamental frequency of reinforced soil walls and showed that it is not affected by different structural components under moderate earthquakes of 0.2 m/s^2. Bathurst & Hatami (2001) provided a detailed review of the numerical modelling of reinforced soil walls. Bathurst & Hatami (1999) presented numerical studies using a finite difference approach for propped soil walls reinforced with panels, and where the effects of their height and the stiffness and spacing of the reinforcement were investigated. A series of seismic studies by the same research group are also documented in several publications, including Bathurst & Hatami (1999), (Bathurst & Hatami 1998, 2001), and Bathurst, Hatami & Alfaro (2002). Ling et al. (2004) analysed the construction of a full scale (6 m) reinforced soil retaining wall and the dynamic analysis of five centrifugal models with prototype heights of 7.5 m. The results indicated that the layout of the reinforcement (its length and spacing) played an important role in determining how well the wall performed. Lee, Chang & Ko (2010) reported an LS-DYNA validation assessment and quality of simulation where the shake table tests performed by Ling, Liu & Mohri (2005) were selected as the validation experiments.

This study was carried out to examine the seismic performance of soil walls with vertical reinforcement by numerical simulation. The validated numerical model was used to perform a parametric study by selecting a baseline case which is then compared with other cases where the parameters investigated were changed. These parameters

included the reinforced soil friction angle, spacing of the vertical reinforcement, and stiffness of the soil under the same basic stepped-up sinusoidal acceleration. The effect of each parameter was studied by changing its value from the baseline case and keeping all the other parameters the same. The parametric study showed trends of how each parameter studied affected the failure modes that were considered.

7.5.2 Parameter value ranges and the baseline case

The dimensions and parameters used for the baseline case are shown in Tables 7.1 and 7.2. A reinforced wall 650 mm high and with vertical reinforcement spaced every 10mm was used as the baseline case. All the soils (reinforced soil, backfill/retained soil, and foundation soil) were considered to be without cohesion. The unit weight and friction angle of all the soils was assumed to be 18 kN/m^3 and 35°, respectively. Table 7.3 shows the properties and values used in the baseline case, and the ranges used in the parametric study.

Table7.3 Variation of key parameters and typical results

SN	Varying parameter	Soil modulus E, MPa	Friction angle ϕ°	V-Spacing, mm
1	Soil stiffness	5	30	0.10
2		10	30	0.10
3		15	30	0.10
4		20	30	0.10
5	Soil friction angle	5	28	0.10
6		5	30	0.10
7		5	32	0.10
8		5	34	0.10
9	Vertical reinforcement spacing	5	30	0.05
10		5	30	0.10
11		5	30	0.15
12		5	30	0.20

7.5.3 Results of parametric studies

7.5.3.1 Effect of the soil friction angle

Five soil friction angles: 26°, 30°, 32°, 34° and 36° were evaluated in the parametric study. The dynamic response of the maximum horizontal displacement with vertical reinforcement for those soil friction angles are compared in Figure 7.19. The results indicate that the magnitude of dynamic response increased when the friction angle decreased. The calculated displacements are in agreement with the notion that a reinforced soil wall built using backfill with higher friction angles would be more stable than backfill with a lower friction angle. Similar results were reported by Lee & Chang (2012) in a parametric study of reinforced soil walls with horizontal reinforcement under real multi-directional ground shaking.

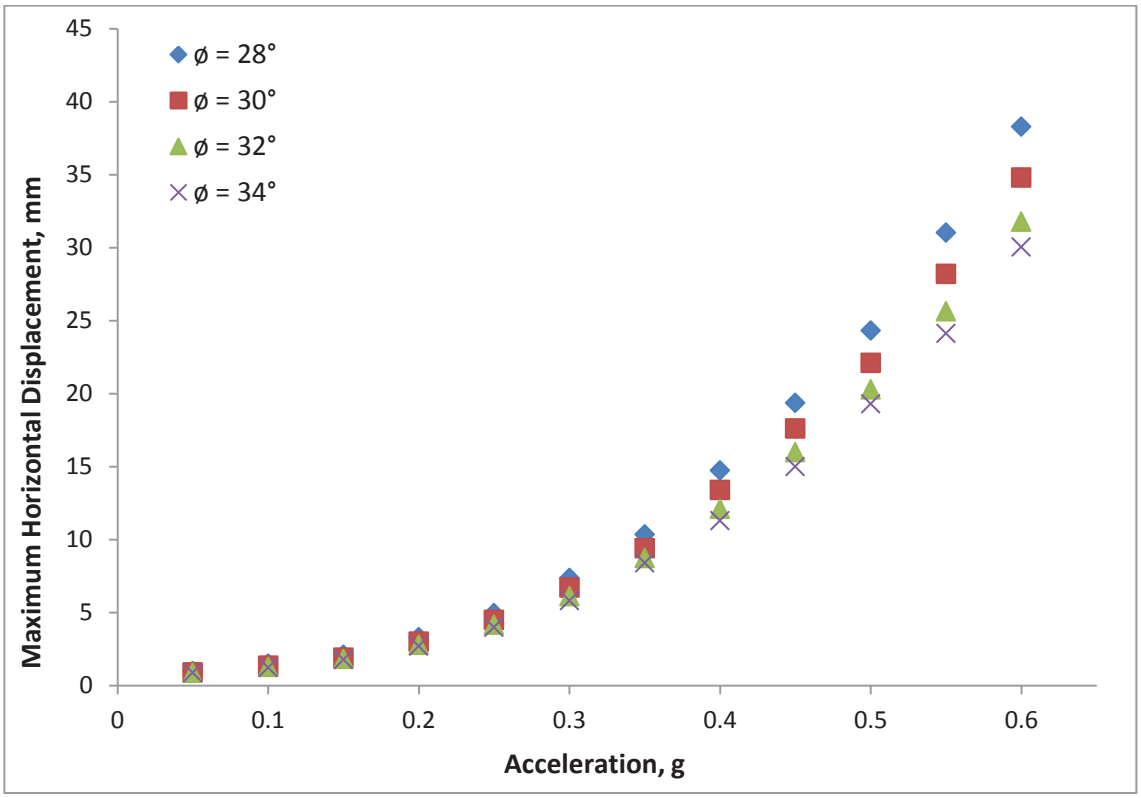

Figure 7.31 Effect of the soil friction angle on maximum horizontal displacement

It can be noted that the maximum displacements were not noticeably reduced when the friction angle increased from 34° to 36°, a finding that indicates that after a certain value the friction angle has a marginal effect on maximum displacement of a wall under dynamic loads.

7.5.3.2 Effect of the spacing of vertical reinforcement

Four vertical reinforcements with 5 mm, 10 mm, 15 mm, and 20 mm spacings were examined in the parametric study. The dynamic response of maximum horizontal displacement for these four reinforcement spacing are plotted in Figure 7.20.

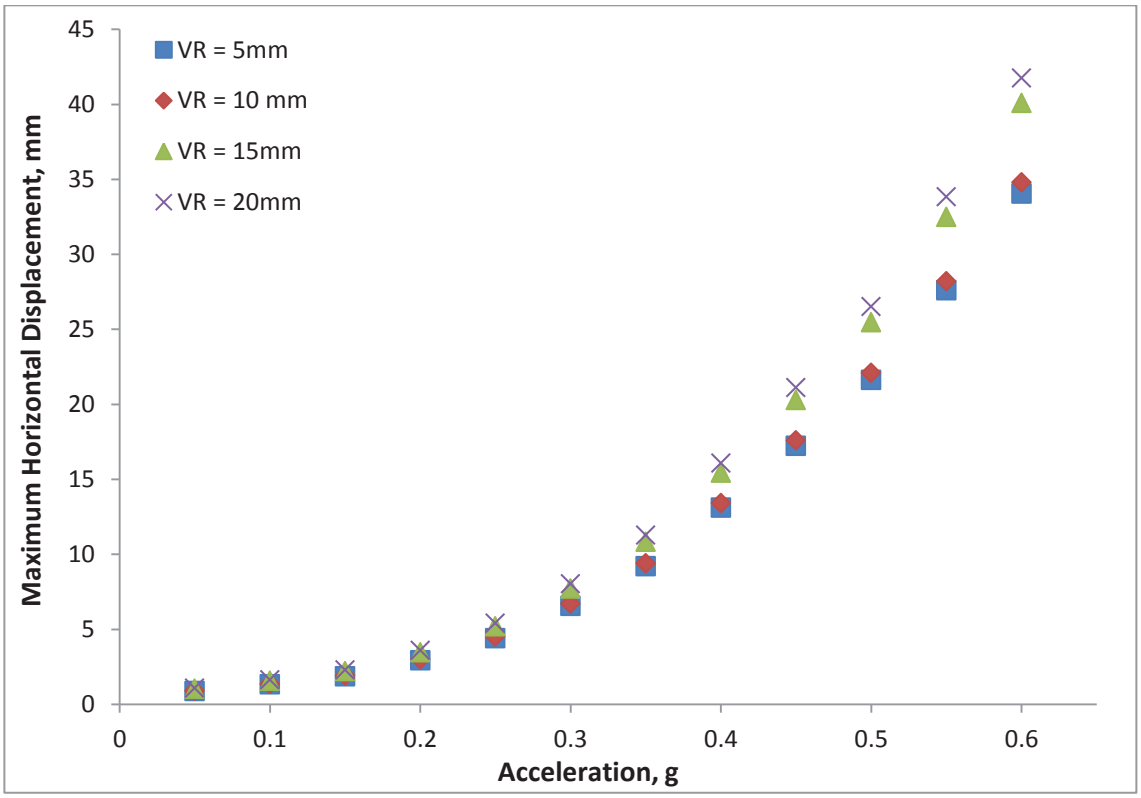

Figure 7.32 Effect of the spacing of vertical reinforcement on the maximum horizontal displacement

The finite element results indicate that maximum horizontal deflection with vertical reinforcement spaced at 5 mm and 10 mm were close to each other. Accordingly it can be concluded that closely packed vertical reinforcement (i.e. small spacing) may not add any benefits to a wall system and neither can large gaps between the reinforcement, and

hence it may be concluded that vertical reinforcement should be spaced more than twice that of the horizontal reinforcement. In addition, the spacing should be varied based on how the dynamic load accelerated.

7.5.3.3 Effect of Young's modulus of soil

Four Young's moduli of 5 MPa, 10 MPa, 15 MPa, and 20 MPa were assessed in the parametric study of soil wall vertical reinforcement. The dynamic responses of the maximum horizontal displacement of these moduli are illustrated in Figure 7.33, with the results showing that the magnitude of dynamic response decreased with an increase in Young's Modulus. The calculated displacements are in agreement with the concept that a reinforced soil wall built with a higher modulus of elasticity would be more stable than with backfill that was not as stiff.

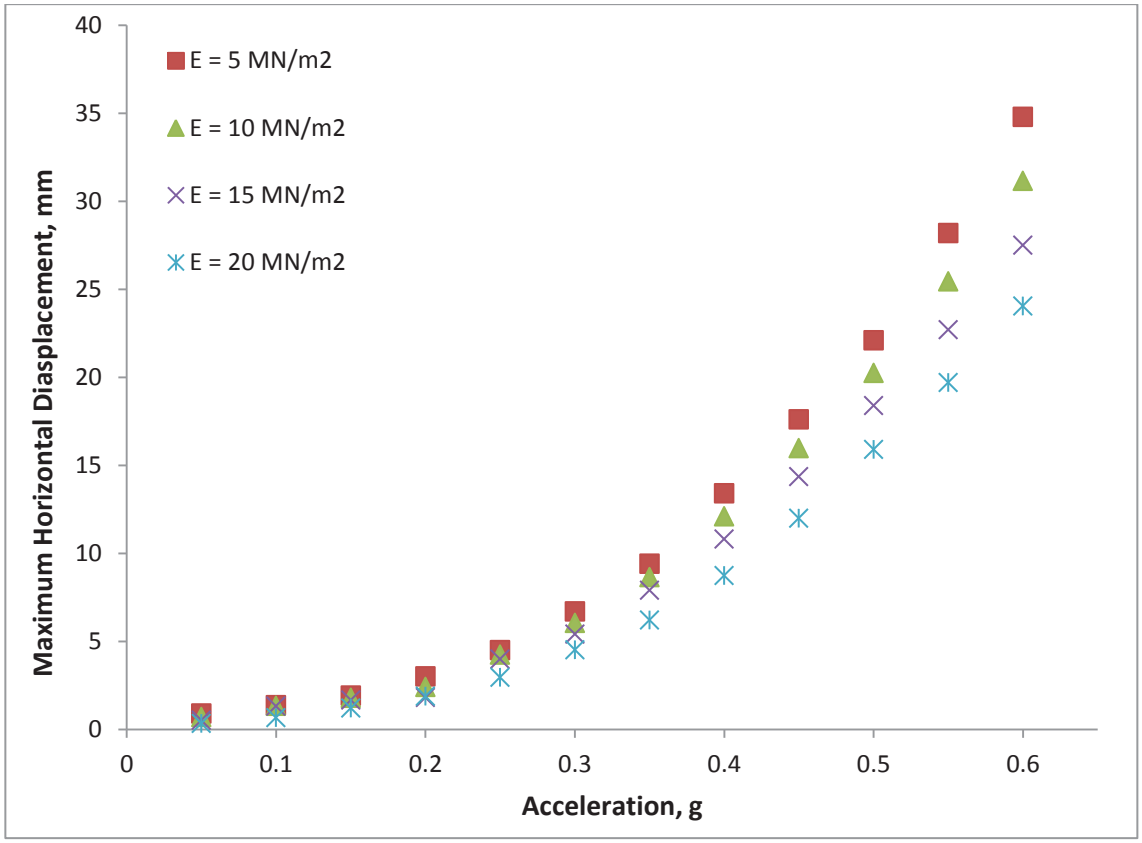

Figure 7.33 Effect of Young's modulus on the maximum horizontal displacement

7.6 Summary

The numerical models gave consistent results in evaluating the dynamic performance of the retaining walls used in the shake table experiments. The results of the numerical analysis harmonised with the results obtained from the shake table tests, although the simulation of shaking over estimated displacement in the wall compared to the shake table experiments. Overall the numerical analysis clearly indicated that an inclusion of vertical or angled (almost vertical) reinforcement in soil walls reduces lateral deformation compared to a reinforced wall without any vertical reinforcement. These outcomes generally verify the finite element procedures. Thus a series of parametric studies were carried out where the soil friction angles, the spacing of vertical reinforcement, and stiffness of the soil were varied.

The deformation of walls predicted by numerical model that included vertical reinforcement and slightly angled reinforcement were found to be almost similar to the experimental results. This finding is beneficial for the field implementation of vertical reinforcement because a minor change in the angle will not affect the performance of the wall. In addition, in a similar manner to the test results, the calculated amplification of acceleration increases with the height of the model, and the model with vertical or inclined reinforcement produced a less amplified acceleration compared to the wall without vertical reinforcement.

A validated finite element model was used to conduct a series of parametric studies to study the behaviour of a soil wall inserted with vertical reinforcement. The results of a parametric study were similar to the outcomes of previously published parametric analyses using common horizontal reinforcement. As expected, the results where the friction angles were varied, indicate that the dynamic response increased in magnitude as the friction angle decreased. Similarly, the dynamic response also decreased with an

increase in Young's Modulus. The results of varying the spacing of vertical reinforcement showed that vertical elements spaced less than two to three times the spacing of horizontal reinforcement, cannot add any extra benefits to a reinforced wall system.

Chapter 8

8. Conclusions and Recommendations

8.1 Introduction

Over the past several decades, retaining structures with reinforced backfill have been constructed far more frequently than their conventional counterparts due to its low material cost, short construction period, ease of construction, and aesthetic appearance. However, the stability and performance of reinforced soil retaining structures situated in earthquake prone areas is of great concern due to the potential failures that can create a significant threat to people and a wide range of natural and man-made earth structures. Much research has been carried out on the seismic response of a reinforced soil wall that considers a conventional approach using horizontal reinforcement. Very limited investigations have been conducted on the performance of soil walls reinforced with the partial inclusion of vertical elements, but have not considered the effects of dynamic loading.

This research presents a new concept of using vertical reinforcement that is designed to connect the layers of conventional horizontal reinforcement together. In this system the selected granular material is compacted over the horizontal reinforcement up to a given height and then another layer of horizontal reinforcement is laid down, after which the vertical reinforcement is inserted vertically or at an angle with vertical, as per the design requirements. Each layer is then tied with another and thus acts as one integrated wall system which reduces the total force at the back of the facing panels.

This thesis has focused on investigating the performance enhancement of reinforcing soil by inserting vertical reinforcement that is subject dynamic loading. For this purpose, shake table tests for four different models were carried out, following an extensive laboratory experiments for materials selection to construct the models. The results of the shake table experiments were then compared with the numerical models obtained from the finite element analysis conducted using PLAXIS software. In addition, meticulous parametric studies were conducted and predictions were made using a validated model.

8.2 Conclusions

The main conclusions drawn from this study are summarised as follows:

Before these extensive laboratory experiments commenced, a numerical study was carried out on a reinforced soil retaining wall 10 m high with an inclined facing of 1 in 20, under seismic loading, using the PLAXIS program. A load the same as the 1995 Kobe earthquake was implemented in the numerical model. The analyses were conducted on wall models without any vertical fortification and with the inclusion of vertical reinforcement. Various angles of inclination were also considered in the numerical analysis. The outcomes showed that connecting each subsequent layer and inserting vertical reinforcement resulted in a remarkable reduction in deformation of the facing panels and total vertical settlement.

Four reduced scale reinforced wall shake table tests were carried out using an advanced shake table facility. The results clearly indicated that the inclusion of vertical or near vertical reinforcement in reinforced soil walls reduced the lateral deformation, the backfill surface settlements, and the response to acceleration in different layers compared to the wall without any vertical fortification.

- It is observed that in all models, the lateral deflection increased with the height of the wall. The lateral deflection of the top layer was considered as a comparison for the measured horizontal deformation where 60 mm of horizontal displacement had been induced at 0.4g of peak acceleration in the reinforced soil model with no vertical reinforcement. The same amount of horizontal deformation was achieved in the model with vertical and inclined reinforcement when the peak amplitude reached 0.8g after 80 seconds. These values clearly indicate that the inclusion of vertical/inclined fortifications into a reinforced soil wall reduced its lateral deformation to less than half.

  The peak amplitude was 0.5g between 45-50 seconds from commencement of the tests, and the wall facing deformation increased up to 12 mm, 3 mm, and 3 mm with no vertical reinforcement, with vertical reinforcement, and with inclined reinforcement, respectively. When the results with the proposed scale factor of the prototype to the model for time and displacement were converted, it was found that 5 seconds is equivalent to 28.2 seconds, and 12 mm and 3 mm displacements were equivalent to 380 mm and 95 mm for the prototype, respectively. These results revealed that horizontal deformation was reduced by four times when vertical/horizontal reinforcement was introduced, for the targeted amplitude of acceleration and time.

- Settlement of the backfill surface in the wall without vertical reinforcement was very rapid compared to the other models with vertical fortification. Settlement behind the reinforced soil zone was the largest due to a horizontal movement of the entire reinforced soil zone. It is obvious that when there is more horizontal deflection, there is more settlement. Based on these

experimental results, the general trend of vertical deformation was similar to the horizontal deflection.

- These test results also reveal that the amplification of acceleration increases with the height of model, and the model wall with vertical or inclined reinforcement produced less amplification of acceleration than the wall without vertical reinforcement.

In this study a numerical analysis was carried out using PLAXIS 2D Version 9 to verify the shake table experiments. Four models were developed to the same dimensions and physical properties of the materials used in the experimental cases. Likewise, in the experimental program a stepped up sinusoidal base excitation was applied for a period of 60 seconds.

- The results of the lateral deflection of all four model walls without vertical reinforcement clearly showed that deformation was significantly higher than the models with a combination of horizontal and vertical reinforcement. For example, 40 seconds after the commencement of shaking (the base acceleration was 0.4g), the horizontal displacement was 48 mm for the wall without vertical reinforcement, while other walls only experienced about 24 mm, which was almost half. These findings were similar to the results of the shake table experiments.

- The calculated vertical deformation where there was no vertical reinforcement was higher than the other two models, and settlement behind the reinforced soil zone was greater than that close to the facing. The settlement values and variations between the models with the inclusion of vertical/inclined reinforcements were similar.

- The acceleration at different heights clearly indicated that it was amplified on the top of the wall compared to the bottom. Acceleration in the model without vertical reinforcement was amplified more than the other models, which shows that amplified acceleration is reduced when vertical reinforcement is inserted, and as a consequence, there is less deformation.

Displacement in the wall facing increased as the dynamic loads increased, both in the experimental measurements and numerical calculations. A similar settlement profile emerged from the numerical analysis and laboratory tests. More settlement took place between the reinforced and retained soil zones and less settlement took place towards the front and back of the wall. Even though the horizontal displacement profile and settlements between the calculated and measured responses were the same, the results showed that a simulation of shaking over estimated the displacement and settlement in the wall. It can be noted that a great variability existed in the profile of measured results taken from the shake table experiments, whereas the outputs of the numerical simulations were consistent. The cause of more displacement in numerical modelling can be due to the higher amplification of acceleration, as the shake table models may have a larger damping factor than the values in the numerical calculations.

A comparison between the peak horizontal acceleration and the calculated and measured results in the facing of the reinforced soil wall showed that the acceleration was less pronounced in the measured results, especially in the higher amplitude of input acceleration. The numerical simulations indeed demonstrated that displacement in the wall facing was proportional to the amplified acceleration. It was more apparent in the calculated results that the higher levels of the wall experience greater acceleration than the lower layers.

These results showed a good agreement between the measured and calculated displacements, settlement of the backfill surface and accelerations, albeit with some discrepancies. These minor disagreements may be due to the difference between the values of the physical properties of the models assumed in the numerical analysis and those real values associated with the experiments. Variability within the measured data could also contribute to some of these discrepancies. In addition, the inconsistent results could be due to limitations in the PLAXIS program to model small scale retaining walls. Although, some disagreement was found between the measured and calculated results due to variations in the assumed parameters, there was sufficient evidence to conclude that the seismic simulation of models clearly showed the positive impact of vertical fortification on the performance of a reinforced wall.

The results of the parametric studies are similar to the outcomes of parametric investigations for horizontally reinforced walls discovered by previous researchers. The results of variations in the friction angles indicate that the magnitude of dynamic response increases as the friction angle decreases. Similarly, the extent of dynamic response decreases with an increasing Young's Modulus. The results of varying the spacing between the vertical reinforcement shows that too close spacing did not add any benefit to the wall system.

As a result, the findings of this study indicate that the proposed inclusion of vertical components to reinforced soil walls provides better stability than conventional reinforced soil systems under earthquake loading. Each conventional layer of reinforcement connected by vertical reinforcement is enhanced by additional components of tensile forces and increased frictional resistance which raise the anisotropic cohesion and the friction angle. This is due to an increase in integrity of the

reinforced wall, creating block actions which consequently reduce deformations at both the wall facing and backfill surface. These outcomes notably point out the potential benefits of the inclusion of vertical elements into conventional soil reinforcement systems under dynamic loads.

8.3 Recommendations for Further Research

A reinforced soil wall represents a sophisticated soil-structure system that is complicated to simulate under dynamic loading. The accuracy of the results of the shake table experiments and numerical simulations depends on factors such as the scale, the properties of the materials used, soil-structure interaction modelling, and numerical procedures. Based on the findings of this study, the following recommendations are made for areas of further research into soil with the inclusion of vertical reinforcement:

1. Further research is needed to quantify the effect of vertical reinforcement with different types of reinforcement such as metal strips and different types of geogrids, using shake table tests. In addition, the properties of vertical reinforcement such as type, size, and spacing could be changed to optimise the effect in case of seismic loading.

2. Another study of interest would be to carry out the shake table tests to identify the effect of vertical reinforcement when altering the wall height, the spacing between two consecutive horizontal reinforcements, the backfill soil properties, the effect of surcharge, and the effect of foundation soil. The local and global strains of reinforcement can be measured using strain gauges and extensometers, respectively. The number and location of accelerometers could be increased to measure the acceleration during shaking. In addition, vertical and horizontal load

cells can be installed at the base of the facing panels to measure the forces transmitted to the footing.

3. It is of special interest to compare the results of the simulation obtained from the computer program PLAXIS with other commercial finite element codes such as FLAC and ABACUS. The extension of 2-D finite element method to 3-D may replicate more analogous results of the shake table experiments. An efficient numerical optimisation scheme may be further refined and implemented to calibrate the model parameters and help reduce computational costs.

4. A study should be carried out to consider varying the water table draining conditions. Such models may resemble real field problems and show a genuine response of reinforced soil walls with vertical reinforcement under dynamic loading.

5. As construction is a major challenge for the implementation of this concept, further research is required to develop the construction techniques briefly presented in this dissertation. A detailed cost analysis would be required to determine the extra expense of construction the proposed wall with the inclusion of vertical reinforcement compared to conventional reinforced soil walls.

6. A detailed study into the damping properties of reinforced soil walls and their simulation in finite element analysis can be another potential research topic.

7. It might be presumed that the same benefits can be achieved if longer horizontal layers are used in conventional reinforced soil walls instead of using vertical reinforcement. Hence, further dynamic shake table tests can be conducted to compare the response of conventional reinforced soil wall with longer horizontal layers to walls with shorter geogrids but including the vertical reinforcement.

References

AASHTO 2002, *Standard specifications for highway bridges, (17th Edition 2002), American Association of State Highway and Transportation Officials*, Washington, DC, USA.

Abu-Farsakh, M., Chen, Q. & Yoon, S. 2008, *Use of Reinforced Soil Foundation (RSF) to Support Shallow Foundation: Final Report*, Louisiana Transportation Research Center (LTRC), Louisiana Department of Transportation and Development (LADOTD), Baton Rouge, LA, Report No. FHWA/LA.07/424.

Anastasopoulos, I., Georgarakos, T., Georgiannou, V., Drosos, V. & Kourkoulis, R. 2010, 'Seismic performance of bar-mat reinforced-soil retaining wall: Shaking table testing versus numerical analysis with modified kinematic hardening constitutive model', *Soil Dynamics and Earthquake Engineering*, vol. 30, no. 10, pp. 1089-1105.

Aoki, H., Watanabe, K., Tateyama, M. & Yonezawa, T. 2003, 'Shaking table tests on earthquake resistant bridge abutment', *Proc. of 12th Asian Regional Conf. on Soil Mechanics and Geotechnical Engineering*, vol. 1, pp. 267-270.

Arenicz, R.M. & Choudhury, R.N. 1988, 'Laboratory investigation of earth walls simultaneously reinforced by strips and random reinforcement', *Geotechnical Testing Journal*, vol. 11, no. 4, pp. 241–247.

Aversa, S., Maiorano, R.M.S. & Tamagnini, C. 2007, 'Influence of damping and soil model on the computed seismic response of flexible retaining structures', *Geotechnical Aspects of EC8*, vol. 15, XIV European Conference on Soil Mechanics and Geotechnical Engineering, Madrid.

Bathurst, R.J. 1998, *NCMA segmental retaining wall seismic design procedure - supplement to design manual for segmental retaining walls*, second edn, The National Concrete Masonry Association, Herndon, VA.

Bathurst, R.J. & Alfaro, M.C. 1997, 'Review of seismic design, analysis and performance of geosynthetic reinforced walls, slopes and embankments', *Earth Reinforcement*, vol. 2, pp. 887-918.

Bathurst, R.J. & Cai, Z. 1995, ' Pseudo-static seismic analysis of geosynthetic-reinforced segmental retaining walls', *Geosynthetics International*, vol. 2, no. No. 5, pp. 787-830.

Bathurst, R.J. & Hatami, K. 1998, 'Seismic response analysis of a geosynthetic reinforced soil retaining wall', *Geosynthetics International*, vol. 5, no. 1-2, pp. 127–166.

Bathurst, R.J. & Hatami, K. 1999, 'Numerical study of the influence of base shaking on reinforced soil retaining walls', *Geosynthetics '99*, Industrial Fabrics Association International, Roseville, Mont, pp. 963-976.

Bathurst, R.J. & Hatami, K. 2001, 'Review of numerical modelling of geosynthetic reinforced soil walls', *10th International Conference on Computer Methods and Advances in Geomechanics*, pp. 1223-1232.

Bathurst, R.J., Hatami, K. & Alfaro, M.C. 2002, *Geosynthetic reinforced soil walls and slopes: seismic aspects*, Thomas Telford.

Bergado, D.T., Bukkanasuta, A. & Balasubramaniam, A.S. 1987, 'Laboratory pull-out tests using bamboo and polymer geogrids including a case study', *Geotextiles and Geomembranes*, vol. 5, no. 3, pp. 153-189.

Bergado, D.T., Youwai, S., Teerawattanasuk, C. & Visudmedanukul, P. 2003, 'The interaction mechanism and behavior of hexagonal wire mesh reinforced embankment with silty sand backfill on soft clay', *Computers and Geotechnics*, vol. 30, no. 6, pp. 517-534.

Binquet, J. & Lee, K.L. 1975a, 'Bearing capacity tests on reinforced earth slabs', *Journalof Geotechnical Engineering Division, ASCE*, vol. 101, no. (GT12), pp. 1241-1255.

Binquet, J. & Lee, K.L. 1975b, 'Bearing capacity analysis on reinforced earth slabs', *Journal of Geotechnical Engineering Division, ASCE*, vol. 101 (GT12), no. 1257-1276.

Bolton, M.O. 1986, 'The strength and dilatency of sands', *Geotechniques*, vol. 36, no. 1, pp. 75-78.

Bonaparte, R., Schmertmann, G.R. & Williams, N.D. 1986, 'Seismic designof slopes reinforced with geogrids and geotextiles. Proceedings of the 3rdInternational Conference on Geotextiles', Vienna, Austria, pp. 273-278.

Burke, C.B. 2004, 'Full-scale shaking table tests and finite element analysis of reinforced soil retaining walls', 3147214 thesis, Columbia University, New York, United States

Cai, Z. & Bathurst, R.J. 1995a, 'Seismic response analysis of geosynthetic reinforced soil segmental retaining walls by finite element method', *Computational Geotechniques*, vol. 17, pp. 523-546.

Cai, Z. & Bathurst, R.J. 1995b, 'Seismic response analysis of geosynthetic reinforced soil segmental retaining walls by finite element method', *Computers and Geotechnics*, vol. 17, no. 4, pp. 523-546.

Carrubba, P. & Colonna, P. 2000, 'A comparison of numerical methods for multi-tied walls', *Computers and Geotechnics*, vol. 27, no. 2, pp. 117-140.

Carter, J.P. & Balaam, N.P. 1990, 'Program AFENA, A general finite element algorithm', Centre for Geotechnical Research, University of Sydney, New South Wales, Australia.

Celebi, E., Goktepe, F. & Karahan, N. 2012, 'Non-linear finite element analysis for prediction of seismic response of buildings considering soil-structure interaction', *Natural Hazards and Earth System Sciences*, vol. 12, pp. 3495-3505.

CFEM 2006, *Foundation Engineering Manual*, Canadian Geotechnical Society, Richmond, BC, Canada.

Chen, H.T., Hung, W.Y., Chang, C.C., Chen, Y.J. & Lee, C.J. 2007, 'Centrifuge modeling test of a geotextile-reinforced wall with a very wet clayey backfill', *Geotextiles and Geomembranes*, vol. 25, no. 6, pp. 346-359.

Chen, Q. 2007, 'An experimental study on characteristics and behavior of reinforced soil foundation', PhD dissertation thesis, Louisiana State University, Baton Rouge, USA.

Chen, R.H. & Chiu, Y.M. 2008, 'Model tests of geocell retaining structures', *Geotextiles and Geomembranes*, vol. 26, no. 1, pp. 56-70.

Das, B.M. 1999, *Principal of Foundation Engineering*, 7 edn, CL Engineering, US.

Das, B.M. & Ramana, G.V. 1995, *Principal of Soil Dynamics*.

Das, B.M. & Ramana, G.V. 2009, *Principal of Soil Dynamics*, Cengage Learning, US.

Day, R.W. 2002, *Geotechnical Earthquake Engineering Handbook*, McGraw-Hill, New York.

El-Emam, M.M. & Bathurst, R.J. 2004, 'Experimental design, instrumentation and interpretation of reinforced soil wall response using a shake table', *International Journal of Physical Modelling in Geotechnics*, vol. 4, no. 4, pp. 13–32.

El-Emam, M.M. & Bathurst, R.J. 2005, 'Facing contribution to seismic response of reduced-scale reinforced soil walls', *Geosynthetics International*, vol. 12, no. 3, pp. 215–238.

El-Emam, M.M. & Bathurst, R.J. 2007, 'Influence of reinforcement parameters on the seismic response of reduced-scale reinforced soil retaining walls', *Geotextiles and Geomembranes*, vol. 25, no. 1, pp. 33-49.

El-Emam, M.M., Bathurst, R.J., Hatami, K. & Mashhour, M. 2001, 'Shaking table and numerical modelling of reinforced soil walls', *Proceedings of the International Symposium on Earth Reinforcement*, vol. 1, Kyushu, Japan, pp. 329-334.

Elias, V., Christopher, B.R. & Berg, R.R. 2001, *Mechanically Stabilized Earth Walls and Reinforced Soil Slopes*, NHI-FHWA.

Engineering Toolbox 2012, *Elastic Properties and Young Modulus for some Materials*, Young Modulus (Tensile Modulus) for common materials, http://www.engineeringtoolbox.com/young-modulus-d_417.html, viewed 15/11/2012.

Fakharian, K. & Attar, I.H. 2007, 'Static and seismic numerical modelling of geosynthetic-reinforced soil segmental bridge abutments', *Geosynthetics International*, vol. 14, no. 4, pp. 228-243.

Farrag, K., Acar, Y.B. & Juran, I. 1993, 'Pull-out resistance of geogrid reinforcements', *Geotextiles and Geomembranes*, vol. 12, no. 2, pp. 133-159.

FHWA 1996, *Mechanically stabilised earth walls and reinforced soil slopes design and construction guidelines*, FHWA Demonstration Project 82 (V. Elias and B. R. Christopher), Washington, DC, USA.

FHWA 2001, *Mechanically stabilized earth walls and reinforced soil slopes: design and construction guidelines*, Publication FHWA NHI-00-43, Federal Highway Administration and National Highway Institute, Washington, DC, USA.

Fredlund, D.G. & Krahn, J. 1976, 'Comparison of slope stability methods ofanalysis', *Canadian Geotechnical Journal*, vol. 14, pp. 429-439.

Fujii, T., Izawa, J., Kuwano, J., Ishihara, M. & Nakane, J. 2006, 'Prediction of deformation of retaining walls of geosynthetic- reinforced soil under large earthquakes', *Proc. of 8th International conference on Geosynthetics* pp. 1485-1489

Gray, D.H. & Lieser, A.T. 1982, *Biotechnical Slope Protection andErosion Control*, Van Nostrand Reinhold Co., New York.

Gray, D.H. & Ohashi, H. 1983, 'Mechanics of fiber reinforcement in sand', *Journal of Geotechnical Engineering, ASCE*, vol. 109, no. 3, pp. 335–353.

GRB 1990, 'Geogrid construction method guidelines', Fukuoka, Japan.

Gughes, T.J.R. 1987, *The finite element method, linear static and dynamic analyis*, Prentice Hall International.

Guler, E. & Bakalci, E. 2004, 'Parametric seismic analysis of tiered geosynthetic-reinforced segmental retaining walls', *Geotechnical engineering with geosynthetics, Proceedings of the Third European Geosynthetic Conference*, vol. 2, Munich, Germany, pp. 625-630.

Hardin, B.O. & Drnevich, V.P. 1972, 'Shear modulus and damping in soils: Measurement and parameter effects', *Journal of Soil Mechanics and Foundations Division, ASCE*, vol. 98, no. 6, pp. 603-624.

Hatami, K. & Bathurst, R.J. 2000, 'Effect of structural design on fundamental frequency of reinforced-soil retaining walls', *Soil Dynamics and Earthquake Engineering*, vol. 19, no. 3, pp. 137-157.

Helwany, S.M.B., Budhu, M. & McCallen, D. 2001, 'Seismic analysis of segmental retaining walls. I: model verification', *Journal of Geotechnical and Geoenvironmental Engineering, ASCE*, vol. 127, no. 9, pp. 741-748.

Hoe, I.L. & Dov, L. 2005, 'Failure Analysis of Modular-Block Reinforced-Soil Walls during Earthquakes', *Journal of Performance of Constructed Facilities*, vol. 19, no. 2, pp. 117-123.

Huang, C.C. 2000, 'Investigations of the damaged soil retaining structures during the Chi-Chi earthquake', *Journal of the Chinese Institute of Engineers*, vol. 23, no. 4, pp. 417-428.

Iai, S. 1989a, 'Similitude for shaking table tests on soil-structure-fluid model in 1g gravitational field', *International Journal of Rock Mechanics and Mining Sciences & Geomechanics Abstracts*, vol. 26, no. 6, pp. 343-343.

Iai, S. 1989b, 'Similitude for shaking table tests on soil-structure-fluid models in 1 g gravitational field', *Soils and Foundations*, vol. 29, no. 1, pp. 105–118.

Iai, S., Matsunaga, Y. & Kameoka, T. 1992, 'Strain space plasticity model for cyclic mobility', *Soils and Foundations*, vol. 32, no. 2, pp. 1-15.

Inglis, D., Macleod, G., Naesgaard, E. & Zergoun, M. 1996, 'Basement wall with seismic earth pressures and novel expanded polystyrene foam buffer layer', paper presented to the *Tenth Annual Symposium of the Vancouver Geotechnical Society*, Vancouver, BC, Canada.

Ito, H., Saito, T., Izawa, J. & Kuwano, J. 2006, ' In situ construction of the Geogrid reinforced soil wall combined with soil cement', *Proc. of 8th International conference on Geosynthetics* pp. 1181-1184

Izawa, J., Kuwano, J. & Takahashi, A. 2002, 'Centrifuge tilting and shaking table tests on reinforced soil wall,' *Proc. of 7th International Conference on Geosynthetics*, vol. 1, Nice, pp. 229-232.

Izawa, J., Kuwano, J. & Y., I. 2004, 'Centrifuge tilting and shaking table tests on the RSW with different soils,' *Proc. of 3rd Asian Regional Conference on Geosynthetics*, Seoul, pp. 803-810.

Jesmani, M. & Kamalzare, M. 2010, 'Comparison between Numerical and Analytical Solution of Dynamic Response of Circular Shallow Footing', *The Electronic Journal of Geotechnical Engineering*, vol. 15, no. Bund. P, pp. 1768-1781.

Jewell, R.A. 1996, 'Soil reinforcement with geotextiles', *CIRIA and Thomas Telford*.

JSCE 2006, 'Report on the 2004 Niigata Chuetsu earthquake, Japan Society of Civil Engineers'.

Kato, N., Huang, C.C., Tateyama, M., Watanabe, K., Koseki, J. & Tatsuoka, F. 2002, 'Seismic stability of several types of retaining walls on sand slope', *Proc. of 7th International Conference on Geosynthetics*, vol. 1, Nice, pp. 237-240.

Khedkar, M.S. & Mandal, J.N. 2007, 'Pullout response study for cellular reinforcement', *Proceedings of Fifth International Symposium on Earth Reinforcement, IS Kyushu '07*, Fukuoka, Japan, pp. 293-298.

Khedkar, M.S. & Mandal, J.N. 2008, 'Pullout response study for cellular reinforcemnt', paper presented to the *New Horizons in Earth Reinforcement*, Japan.

Khedkar, M.S. & Mandal, J.N. 2009, 'Pullout behaviour of cellular reinforcements', *Geotextiles and Geomembranes*, vol. 27, no. 4, pp. 262-271.

Koseki, J. 2012, 'Use of geosynthetics to improve seismic performance of earth structures', *Geotextiles and Geomembranes*, vol. 34, no. 0, pp. 51-68.

Koseki, J., Bathurst, R.J., Guler, E., Kuwano, J. & Maugeri, M. 2006, 'Seismic stability of reinforced soil walls', *Proc. of 8th International Conference on Geosynthetics*, vol. 1, Yokohama, pp. 51-77.

Koseki, J. & Hayano, K. 2000, 'Preliminary report on damage to retaining walls caused by the 1999 Chi-Chi earthquake,' *Bulletin of ERS, Institute of Industrial Science, Univ. of Tokyo*, vol. 33, pp. 23-34.

Koseki, J., Munaf, Y., Tatsuoka, F., Tateyama, M., Kojima, K. & Sato, T. 1998, 'Shake and tilt table tests of geosynthetic-reinforced soil and conventional-type retaining walls', *Geosynthetics International*, vol. 5, no. 1-2, pp. 73–96.

Koseki, J., Tatsuoka, F., Watanabe, K., Tateyama, M., Kojima, K. & Munaf, Y. 2003, 'Model tests on seismic stability of several types of soil retaining walls', *Reinforced Soil Engineering*, Dekker, pp. 317-358.

Krishna, A.M. & Latha, G.M. 2007, 'Seismic response of wrap-faced reinforced soil retaining wall models using shaking tabke tests.', *Geosynthetics International*, vol. 14, no. 6, pp. 355-364.

Kumar, A. & Saran, S. 2003, 'Bearing capacity of rectangular footing on reinforced soil', *Geotechnical and Geological Engineering*, vol. 21, pp. 201-224.

Kumar, A., Walia, B.S. & Mohan, J. 2006, 'Compressive strength of fiber reinforced highly compressible clay', *Construction and Building Materials*, vol. 20, no. 10, pp. 1063-1068.

Latha, G.M. & Krishna, A.M. 2008a, 'Seismic response of reinforced soil retaining wall models: Influence of backfill relative density', *Geotextiles and Geomembranes*, vol. 26, no. 4, pp. 335-349.

Latha, G.M. & Krishna, A.M. 2008b, 'Seismic Response of Rigid Faced Reinforced Soil Retaining Walls', vol. 310, ASCE, New Orleans, Louisiana, pp. 94-94.

Lee, K.Z.Z. & Chang, N.Y. 2012, 'Predictive modeling on seismic performances of geosynthetic-reinforced soil walls', *Geotextiles and Geomembranes*, vol. 35, no. 0, pp. 25-40.

Lee, K.Z.Z., Chang, N.Y. & Ko, H.Y. 2010, 'Numerical simulation of geosynthetic-reinforced soil walls under seismic shaking', *Geotextiles and Geomembranes*, vol. 28, no. 4, pp. 317-334.

Leshchinsky, D., Ling, H.I. & Hanks, G.A. 1995, 'Unified design approach to geosynthetic reinforced slopes and segmental walls', *Geosynthetics International*, vol. 2, no. 5, pp. 845-881.

Ling, H.I. & Leshchinsky, D. 1998, 'Effects of vertical acceleration on seismicdesign of geosynthetic-reinforced soil structures', *Geotechnique*, vol. 48, no. 3, pp. 347-373.

Ling, H.I. & Leshchinsky, D. 2003, 'Post-earthquake investigation of several geosynthetic reinforced soil retaining walls and slopes during Ji-Ji earthquake in Taiwan', *Reinforced Soil Engineering,* , Dekker, pp. 297-316.

Ling, H.I., Leshchinsky, D. & Perry, E.B. 1996, 'A new concept on seismicdesign of geosynthetic-reinforced soil structures: permanent-displacement limit.Earth Reinforcement',

Proceedings of the International Symposium on EarthReinforcement, IS-Kyushu '96, Fukuoka, Kyushu, Japan, pp. pp. 117-122.

Ling, H.I., Leshchinsky, D. & Perry, E.B. 1997, 'Seismic design and performance of geosynthetic-reinforced soil structures.', *Geotechnique*, vol. 47, no. 5, pp. 933- 952.

Ling, H.I., Liu, H., Kaliakin, V. & Leshchinsky, D. 2004, 'Analyzing dynamic behavior of geosynthetic-reinforced soil retaining walls', *Journal of Engineering Mechanics*, vol. 130, no. 8, pp. 911-920.

Ling, H.I., Liu, H. & Mohri, Y. 2005, 'Parametric Studies on the Behavior of Reinforced Soil Retaining Walls under Earthquake Loading', *Journal of Engineering Mechanics*, vol. 131, no. 10, pp. 1056-1065.

Ling, H.I., Liu, H. & Mohri, Y. 2005a, 'Parametric Studies on the Behavior of Reinforced Soil Retaining Walls under Earthquake Loading', *Journal of Engineering Mechanics*, vol. 131, no. 10, pp. 1056-1065.

Ling, H.I., Mohri, Y., Leshchinsky, D., Burke, C., Matsushima, K. & Liu, H. 2005, 'Large-Scale Shaking Table Tests on Modular-Block Reinforced Soil Retaining Walls', *Journal of Geotechnical and Geoenvironmental Engineering*, vol. 131, no. 4, pp. 465-476.

Lo, S.C.R. 2003, 'Practice and Research of Geosynthetic Reinforced Soil Walls in Australia', in H.I. Ling, D. Leshchinsky & F. Tatsuoka (eds), *Reinforced Soil Engineering Advances in Research and Practice*, CRC Press 2003.

Matsuo, O., Tsutsumi, T., Yokoyama, K. & Saito, Y. 1998, 'Shake table tests and analysis of geosynthetic-reinforced soil retaining walls', *Geosynthetics International*, vol. 1, no. 2, pp. 97–126.

Michalowski, R.L. 2004, 'Limit loads on reinforced foundation soils', *Journal of Geotechnical and Geoenviromental Engineering, ASCE*, vol. 130, no. 4, pp. 381-390.

Michalowski, R.L. & Cermak, J. 2003, 'Triaxial compression of sand reinforced with fibers', *Journal of Geotechnical and Geoenvironmental Engineering*, vol. 129, no. 2, pp. 125–136.

Mononobe, N. & Matsuo, H. 1929, 'On the determination of earth pressure during earthquake', *Proceedings of the World Engineering Congress*, Tokyo, Japan, pp. pp. 177-185.

Moraci, N. & Recalcati, P. 2006, 'Factors affecting the pullout behaviour of extruded geogrids embedded in a compacted granular soil', *Geotextiles and Geomembranes*, vol. 24, no. 4, pp. 220-242.

Murata, O. 2003, 'An outlook on recent research and development concerning long-term performance and extreme loading', *Landmarks in Earth Reinforcement*, vol. 2, Balkema, pp. 869-893.

Nakajima, S., Hong, K., Mulmi, S., Koseki, J., Watanabe, K. & Ateyama, M. 2007, 'Model tests on seismic performance of reinforced soil retaining walls by using different geo-grids', *International Workshop on Earthquake Hazards and Mitigations*, Guwahati, India, pp. 319-325.

Nakajima, T., Toriumi, N., Shintani, H., Miyataka, H. & Dobahi, K. 1996, 'Field performance of a geotextile reinforced soil wall withconcrete facing blocks', *Earth Reinforcement*, eds H. Ochiai, N. Yasufuku & K. Omine, Balkema, Rotterdam/Brookfield, pp. 427-432.

Nernheim, A. 2005, 'Design and test methods for geosynthetic reinforced structures', *Electronic Journal of Geotechnical Engineering*, vol. 10 Bundle F-2005.

Nova-Roessig, L. & Sitar, N. 2006, 'Centrifuge model studies of the seismic response of reinforced soil slopes', *Journal of Geotechnical and Geoenvironmental Engineering*, vol. 132, no. 3, pp. 388-400.

Ochiai, Y. & Fukuda, N. 1996, 'Experimental study on geotextile-reinforced soil walls with different facing', *Symposium on Geosynthetics: Application, Design and Construction*, eds M.B. de Groot, G. de Hoedt & R.J. Termaat, Balkema, Rotterdam/Brookfield, pp. 113-120.

Okabe, S. 1924, 'General theory on earth pressure and seismic stability ofretaining wall and dam. Doboku Gakkai.', *Journal of the Japan Society of Civil Engineers*, vol. 10, no. No. 6, pp. 1277-1323.

Palmeira, E.M. 2004, 'Bearing force mobilisation in pull-out tests on geogrids', *Geotextiles and Geomembranes*, vol. 22, no. 6, pp. 481-509.

Palmeira, E.M. & Milligan, G.W.E. 1989, 'Scale and other factors affecting the results of pull-out tests of grid buried in sand', *Geotechnique*, vol. 11, no. 3, pp. 511-524.

Prabakar, J. & Sridhar, R.S. 2002, 'Effect of random inclusion of sisal fiber on strength behaviour of soil. ', *Construction and Building Materials*, vol. 16, no. 2, pp. 123-131.

Public Works Research Institute (PWRI) 1997, *Observation of behaviour of full scale model test on reinforced retaining wall using geotextile*, PWRI, Japan, Report-3487.

PWRI. 1992, *Design and construction manualfor reinforced soil structures using geotextiles*, PublicWorks Research Institute, Ministry of Construction Tsukuba, Japan (in Japanese).

Racana, N., Grediac, M. & Gourves, R. 2003, 'Pull-out response of corrugated geotextile strips', *Geotextiles and Geomembranes*, vol. 21, no. 5, pp. 265-288.

Race, R. & Del Cid, H. 2001, 'Seismic performance of modular block retaining wall structures during the January 2001 El Salvador earthquake', paper presented to the *International Geosynthetics Engineering Forum 2001*, Taipei, Taiwan (CD-ROM).

Richardson, G.N. & Lee, K.L. 1975, 'Seismic design of reinforced earth walls', *ASCE Journal of the Geotechnical Engineering Division*, vol. 101, no. 2, pp. 167-188.

Rowe, R.K. & Ho, S.K. 1998, ' Horizontal deformation in reinforced soil walls', *Canadian Geotechnical Journal*, vol. 35, no. 2, pp. 312-327.

Rowe, R.K. & Skinner, G.D. 2001, 'Numerical analysis of geosynthetic reinforced retaining wall constructed on a layered soil foundation', *Geotextiles and Geomembranes*, vol. 19, no. 7, pp. 387-412.

Sabermahani, M., Ghalandarzadeh, A. & Fakher, A. 2009, 'Experimental study on seismic deformation modes of reinforced-soil walls', *Geotextiles and Geomembranes*, vol. 27, no. 2, pp. 121-136.

Saito, T., Ito, H., Izawa, J. & Kuwano, J. 2006, 'Seismic stability of the geogrid-reinforced soil wall combined with soil cement', *Proc. of 8th International conference on Geosynthetics*, pp. 1495-1499

Sakaguchi, M. 1996, 'A study of the seismic behaviour of geosynthetic reinforced walls in Japan', *Geosynthetics International*, vol. 3, no. 1, pp. 13-30.

Sandri, D. 1997, 'A performance summary of reinforced soil structures in the greater Los Angeles area after the Northridge earthquake', *Geotextiles and Geomembranes*, vol. 15, no. 4-6, pp. 235-253.

Saran, S. 2005, *Reinforced Soil and its Engineering Applications*, I.K. International Pvt. Ltd.

Seed, H.B. 1983, 'Earthquake-resistant design of earth dams', *Seismic Design of Embankments and Caverns*, ASCE, Philadelphia, Pennsylvania, pp. 41-64.

Segrestin, P. & Bastick, M.J. 1998, 'Seismic design of reinforced earth retaining walls-The contribution of finite element analysis', paper presented to the *Theory and practice of earth reinforcement*, Balkema, Rotterdam, The Netherlands.

Sharma, R., Chen, Q., Abu-Farsakh, M. & Yoon, S. 2009, 'Analytical modeling of geogrid reinforced soil foundation', *Geotextiles and Geomembranes*, vol. 27, no. 1, pp. 63-72.

Shekarian, S., Ghanbari, A. & Farhadi, A. 2008, 'New seismic parameters in the analysis of retaining walls with reinforced backfill', *Geotextiles and Geomembranes*, vol. 26, no. 4, pp. 350-356.

Shrestha, B., Khabbaz, H. & Fatahi, B. 2011, 'Performance analysis of reinforced soil foundation structures with vertical reinforcement', *Proceedings of the 3rd International Conference on Geotechnical Engineering for Disaster Mitigation and Rehabilitation*, eds S.P.R. Wardani, J. Chu, S.C.R. Lo, S. Iai & K.K. Phoon, World Scientific, pp. 443-448.

Sobhi, S. & Wu, J.T.H. 1996, 'An interface pullout formula for extensible sheet reinforcement', *Geosynthetics International*, vol. 3, no. 5, pp. 565-582.

Stewart, J.P., Bray, J.D., Seed, R.B. & Sitar, N. 1994, *Preliminary report on the principal geotechnical aspects of the January 17, 1994 Northridge earthquake.*, Earthquake Engineering Research Center, University of Californial at Berkeley, Report UCB/EERC-94/08.

Sugimoto, M., Alagiyawanna, A.M.N. & Kadoguchi, K. 2001, 'Influence of rigid and flexible face on geogrid pullout tests', *Geotextiles and Geomembranes*, vol. 19, no. 5, pp. 257-277.

Tatsuoka, F. 1993, 'Roles of facing rigidity in soil reinforcing, Keynote Lecture', *Proc. Int. Sym. on Earth Reinforcement Practice*, vol. 2, IS Kyushu '92, Balkema, pp. 831-870.

Tatsuoka, F., Koseki, J. & Tateyama, M. 1997, 'Performance of Earth Reinforcement Structures during the Great Hanshin Earthquake', *Special Lecture, Proc. Int. Sym. on Earth Reinforcement, IS Kyushu '96*, vol. 2, Balkema, pp. 973-1008.

Tatsuoka, F., Koseki, J., Tateyama, M., Munaf, Y. & Horii, K. 1998, 'Seismicstability against high seismic loads on geosynthetic-reinforced soil retaining structures', *Keynote Lecture. Proceedings of the 6th International Conference onGeosynthetics*, Atlanta, Georgia, pp. pp. 103-142.

Tatsuoka, F., Tateyama, M. & Koseki, J. 1996, 'Performance of soil retaining walls for railway embankments', *Soils and Foundations, Special Issue for the 1995 Hyogoken-Nambu Earthquake*, no. Special Issue, pp. 311-324.

Teixeira, S.H.C., Bueno, B.S. & Zornberg, J.G. 2007, 'Pullout resistance of individual longitudinal and transverse geogrid ribs', *Journal of Geotechnical and Geoenvironmental Engineering*, vol. 133, no. 1, pp. 37-50.

Tsukada, Y., Ochiai, Y., Miyataka, H. & Tajiri 1998, 'Field performance of a geosynthetic-reinforced soil wall with rigid facing', *Sixth International Conference on Geosynthetics*, Industrial Fabrics Association International, Atlanta, USA, pp. 577-580.

Vieira, C.S., Lopes, M.L. & Caldeira, L.M.M.S. 2006, 'Numerical modelling of a geosynthetic reinforced soil retaining wall subjected to seismic loading', paper presented to the *International Conference on Geosynthetics*.

Viswanadham, B.V.S. & Mahajan, R.R. 2007, 'Centrifuge model tests on geotextile reinforced slopes', *Geosynthetics International*, vol. 14, no. 6, pp. 365-379.

Vrymoed, J. 1989, 'Dynamic stability of soil-reinforced walls', *TransportationResearch Record*, vol. 1242, pp. 29-38.

Watanabe, K., Munaf, Y., Koseki, J., Tateyama, M. & Kojima, K. 2003, 'Behavior of several types of model retaining walls subjected to irregular excitation', *Soils and Foundations*, vol. 43 no. 5, pp. 13-27.

Wayne, M.H., Han, J. & Akins, K. 1998, 'The design of geosynthetic reinforced foundations', *In: Proceedings of ASCE's 1998 Annual Convention & Exposition*, ASCE Geotech Special Publication 76, pp. 1-18.

Wesseloo, J., Visser, A.T. & Rust, E. 2009, 'The stress-strain behaviour of multiple cell geocell packs', *Geotextiles and Geomembranes*, vol. 27, no. 1, pp. 31-38.

White, D. & Holtz, R.D. 1997, 'Performance of geosyntheticreinforced slopes and walls during the Northridge California earthquake of January 17, 1994', *Earth Reinforcement*, Balkema, Rotterdam, The Netherlands, pp. 965-972.

Whitman, R.V. 1990, 'Seismic design and behavior of gravity retaining walls', *ASCE Specialty Conference: Design and Performance of Earth Retaining Structures, ASCE Geotechnical Special Publication No. 25*, Cornell University,Ithaca, New York, USA, pp. 817-842.

Won, M.S. & Kim, Y.S. 2007, 'Internal deformation behavior of geosynthetic-reinforced soil walls', *Geotextiles and Geomembranes*, vol. 25, no. 1, pp. 10-22.

Wood, D.M. 2004, *Geotechnical Modelling*, 1 edn, Spons Architecture Price Book, London.

Woods, R.I. & Jewell, R.A. 1990, 'A computer design method for reinforced soil structures', *Geotextiles and Geomembranes,*, vol. 9, no. 3, pp. 233-259.

Xie, W. 2003, 'Consideration for modifying reinforced retaining wall', *Nonferrous Mines*, vol. 32, no. 3, pp. 46-48.

Yetimoglu, T. & Salbas, O. 2003, 'A study on shear strength of sands reinforced with randomly distributed discrete fibers', *Geotextiles and Geomembranes*, vol. 21, no. 2, pp. 103-110.

Yogendrakumar, M., Bathurst, R.J. & Finn, W.D.L. 1992, 'Dynamic response analysis of reinforced soil retaining wall', *Journal of Geotechical Engineering*, vol. 118, no. 8, pp. 1158-1167.

Yoo, C. & Kim, S.B. 2008, 'Performance of a two-tier geosynthetic reinforced segmental retaining wall under a surcharge load: full-scale load test and 3D finite element analysis', *Geotextiles and Geomembranes*, vol. 26, no. 6, pp. 460-472.

Zarnani, S., Bathurst, R.J. & Gaskin, A. 2005, 'Experimental investigation of geofoam seismic buffers using a shaking table', paper presented to the *2005 North American Geosynthetics Society Conference*, Las Vegas, Nevada, 14-16 December.

Zeienkiewicz, O.C. & Taylor, R.L. 1991, *The finite element method*, 4 edn, vol. 2, Mc Graw-Hill, U.K.

Zhang, M.X., Javadi, A.A. & Min, X. 2006, 'Triaxial tests of sand reinforced with 3D inclusions', *Geotextiles and Geomembranes*, vol. 24, no. 4, pp. 201-209.

Zhang, M.X., Zhou, H., Javadi, A.A. & Wang, Z.W. 2008, 'Experimental and theoretical investigation of strength of soil reinforced with multi-layer horizontal-vertical orthogonal elements', *Geotextiles and Geomembranes*, vol. 26, no. 1, pp. 1-13.

Zornberg, J.G. & Leshchinsky, D. 2003, 'Comparison of international design criteria for geosynthetic-reinforced soil structures', *Landmarks in Earth Reinforcement*, vol. 2, Balkema, pp. 1095-1106.